UNIVERSIDAD COMPLUTENSE DE MADRID

FACULTAD DE CIENCIAS BIOLÓGICAS

Departamento de Bioquímica y Biología Molecular I

TESIS DOCTORAL

Relaciones estructura-función en complejos de surfactante pulmonar intracelulares y secretados: desarrollo e implementación de modelos celulares

MEMORIA PARA OPTAR AL GRADO DE DOCTOR

PRESENTADA POR

Alejandro Cerrada de Dueñas

Directores

Jesús Pérez Gil

Ana Isabel Flores de la Cal

MENCIÓN “DOCTOR EUROPEUS”

Madrid, 2015

UNIVERSIDAD COMPLUTENSE DE MADRID

FACULTAD DE CIENCIAS BIOLÓGICAS

Departamento de Bioquímica y Biología Molecular I

Structure-function relationships in intracellular and secreted pulmonary surfactant complexes: development and implementation of cellular models

PhD THESIS

by

Alejandro Cerrada de Dueñas

Supervisors

Jesús Pérez Gil, PhD

Ana Isabel Flores de la Cal, PhD

"DOCTOR EUROPEUS" MENTION

Madrid, 2015

The present PhD Thesis has been accomplished at the Department of Biochemistry and Molecular Biology I of Complutense University, Madrid, under the supervision of Professor Jesús Pérez Gil and at 12 de Octubre Hospital Research Institute, under the supervision of Dr. Ana Isabel Flores de la Cal.

Part of the experimental work was performed at the National Center of Biotechnology (Madrid, Spain), in collaboration with the group of Dr. José María Valpuesta; at the Department of Physiology and Medical Physics of Innsbrück University (Innsbrück, Austria), in collaboration with Professor Thomas Haller; at the Department of Chemistry of Imperial College London (London, United Kingdom), in collaboration with Dr. Nicholas Brooks and in collaboration with Professor Claus-Michael Lehr at Helmholtz Institute for Pharmaceutical Research and Saarland University (Saarbrücken, Germany).

The financial support to carry out the present PhD Thesis was obtained from Instituto de Salud Carlos III (FI10/00869) and from research grants from Spanish Ministry of Economy (BIO2009-09694, BIO2012-30733) and the Regional Government of Madrid (S2009MAT-1507, P2013/MIT2807).

INDEX

Page

ACKNOWLEDGMENTS

First and foremost, I would like to express my sincere gratitude to my PhD supervisors Professor Dr. Jesús Pérez Gil and Dr. Ana Isabel Flores de la Cal. Thanks to Prof. Pérez Gil for his infectious optimism, for inspiring my research with stimulating discussions as well as for offering me so many precious opportunities to grow as a research scientist. Thanks to Dr. Flores for her dedicated involvement in my technical instruction, for her encouraging words and for her open mind, always ready to join new scientific adventures.

I would like to thank my international mentors for offering me a warm welcome in their groups, allowing me to participate in motivating and multicultural scientific environments.

Thanks to Dr. Nicholas Brooks from Imperial College London, for his kindness and for allowing me the access to cutting-edge technologies.

From Helmholtz Institute/Saarland University, I am deeply indebted to Prof. Dr. Claus-Michael Lehr, for the productive time and extraordinary experience I enjoyed in his laboratory and for his trust and support. Grateful thanks to Dr. Cristiane Carvalho for her involvement and supervision and to Dr. Frantiescoli Dimer, Marius Hittinger, Emad Malaeksefat and particularly to Dr. Xabier Murgia, for their kindly and helpful technical assistance as well as their hospitality and emotional support.

A very special thanks to Prof. Dr. Thomas Haller from Innsbrück University, for providing me with direction and technical support, for sharing his brilliant suggestions and experience with me and for being more of a generous mentor and friend, than a professor. Appreciation is also given to Dr. Andrea Ravasio, Dr. Nina Hobi, Gerlinde Siber and Irina Öttl for their valuable help, technical assistance and personal training.

Coming back to Spain, I must also thank Dr. José María Valpuesta, Dr. Javier Chichón, Dr. Rocío Arranz, and Javier Conesa from the National Center of Biotechnology for their appreciated scientific advice and technical support.

I am grateful to Dr. Isabel Macías and Dr. Paz de la Torre from Hospital 12 de Octubre for giving me all necessary assistance during my training. From Complutense University, I would like to express my sincere apreciation to Dr. Inmaculada Fernández from her priceless and generous help and scientific and personal support and to Mikel Conde for his valuable contribution to this work.

I cannot go without showing my warm gratitude to my past and present lab mates from my group of the Department of Biochemistry and Molecular Biology from Complutense University for all the friendship, camaraderie and support that I have enjoyed during the last years. At fault of missing some names, I would like to thank Olga Lucía, Beatriz, Victoria, Odalys, Suri, Elena L, Bárbara, Elisa J, Elisa P, Ángeles, Virginia, Nuria R, Alicia, Nuria P, Elena A, Sonia, Carolina, Marta, Alberto, Raquel and José Carlos. A very special thanks to Dr. Mercedes Echaide, Dr. Antonio Cruz and Dr. Begoña García for sharing their wisdom as well as for their scientific advice and personal support. I would like also to thank Cristina Casals' group members for their friendship and pleasant and enriching coexistence in the lab.

On a more personal note, I will be eternally grateful to my family and friends. My heartfelt gratitude especially to my parents, Rosa and Carlos, for their endless love and unconditional encouragement. My deepest appreciation to my life partner, Pilar, for her patience and for always supporting me in my academic pursuits.

Finally, I must acknowledge Spanish Government and Insituto de Salud Carlos III for their financial support.

LIST OF ABBREVIATIONS

3-D	3-dimensional
ABCA3	ATP-binding cassette transporter A3
AC	Alternating current
AFM	Atomic force microscopy
AgNP	Silver nanoparticle
ALI	Air-liquid interface
ALICE	Air-Liquid interface cell exposure system
ARDS	Acute respiratory distress syndrome
ATI	Alveolar type I
ATII	Alveolar type II
ATII-LCs	Alveolar type II-like cells
ATP	Adenosine triphosphate
ATR-FTIR	Attenuated Total Reflection Fourier Transform Infrared
BAL	Bronchoalveolar lavage
BB	Brilliant black
Bg	Background
BSA	Bovine serum albumin
cAMP	Cyclic adenosine monophosphate
CB	Composite bodies
CBS	Captive bubble surfactometer
CD	Collagenous domain
CDP	Cytidine diphosphate
Ch/Chol	Cholesterol
CRD	Carbohydrate recognition domain
Cryo-EM	Cryo electron microscopy
Cryo-ET	Cryo electron tomography
Cryo-SXT	Cryo soft X-ray tomography
CS	Chitosan
CTFR	Cystic fibrosis transmembrane conductance receptor
DAG	Dyacylglycerol

DMAP	1-ethyl-3-(3-Dimethylaminopropyl)-carbodiimide hydrochloride
DMEM	Dulbecco's Modified Eagle's Medium
DMSCs	Decidua-derived mesenchymal stem cells
DMSO	Dimethyl sulfoxide
dNTP	Deoxynucleoside triphosphate
DPPC	Dipalmitoylphosphatidylcholine
ECM	Extracellular matrix
EE	Early endosomes
EGTA	Ethylene glycol tetraacetic acid
ER	Endoplasmic reticulum
EVOM	Epithelial volt-ohm-meter
FA	Fluoresceinamine
FDA	Food and Drug Administration
FOXA1(A2)	Forkhead ortholog a1(a2)
ɣ	Surface tension
GA	Golgi apparatus
GAPDH	Glyceraldehyde-3-phosphate dehydrogenase
GPF	Generalized polarization function
GPR116	G-protein couple receptor 116
GUV	Giant unilamellar vesicle
H_I	Direct hexagonal lipid phase
HIF	Hypoxia inducible factor
H_{II}	Inverse hexagonal lipid phase
HMDS	3-hexamethyldisilazane
HPLC	High-performance liquid chromatography
HRP	Horseradish peroxydase
IgG	Immunoglobulin G
IP3	Inositol trisphosphate
KGF	Keratinocyte growth factor
KRB	Krebs-Ringer buffer
LA	Large aggregates
Laurdan	6-lauroyl, 1-2-dimethylamino naphthalene
LB	Lamellar bodies
LBPs	Lamellar body-like particles

L_c	Liquid condensed
L_d	Liquid disordered
LDH	Lactate dehydrogenase
L_e	Liquid expanded
L_o	Liquid ordered
LPCAT 1	LysoPC acyltransferase 1
LTG	LysoTracker green
Lys	Lysosomes
L_α	Liquid-crystalline phase
L_β	Gel phase
MAS	Meconium aspiration syndrome
MCT	Mercury cadmium telluride
MLVs	Multillamelar vesicles
MSC	Mesenchymal stem cell
MTT	3-(4, 5-dimethylthiazol-2-yl)-2,5-diphenyl tetrazolium bromide
MVBs	Multivesicular bodies
Nk	Neck domain
NL	Neutral Lipids
NMR	Nuclear magnetic resonance
NP	Nanoparticle
NRDS	Neonatal distress respiratory syndrome
NS	Native surfactant
OCT	Organic cation transporter
OE	Organic extract
P	Pressure
PA	Phosphatidic acid
P_{app}	Aparent permeability coefficient
PBS	Phosphate buffer saline
PC	Phosphatidylcholine
PCR	Polymerase chain reaction
PE	Phosphatidylethanolamine
PEG	Poly-ethylen-glycol
PG	Phosphatidylglycerol
PI	Phosphatidylinositol
PdI	Polydispersity index

PIP2	Phosphatidylinositol 4,5-bisphosphate
PKC	Protein kinase C
PLGA	Polylactic-co-glycolic acid
PMA	Phorbol 12-myristate 13-acetate
PMPC	Palmitoylmirystoyl-PC
POPC	Palmitoyloleoyl-PC
PPPC	Palmitoylpalmitoleoyl-PC
PS*	Phosphatidylserine
PS	Pulmonary surfactant
PVA	Poly-vinyl alcohol
PVDF	Polyvinylidene difluoride
r	Radius
RFU	Relative Fluorescence Units
Rpm	Revolutions per minute
RT	Room temperature
SA	Small aggregates
SAGM	Small airway growth medium
SAXS	Small Angle X-ray Scattering
SC	Submerged culture
SDS-PAGE	Sodium dodecyl sulfate- polyacrylamide agarose gel electrophoresis
SF	Surface film
SM	Sphingomyelin
S_o	Solid ordered
SP-A, B, C, D	Surfactant proteins A, B, C, D
TEER	Transepithelial electrical resistance
TEM	Transmission electron microscopy
TGN	Trans-Golgi network
TLC	Thin layer chromatography
T_m	Melting temperature
TM	Tubular myelin
TRP	Transient receptor potential
TTF-1	Thyroid transcription factor-1
VLDL	Very low density lipoproteins

THESIS ABSTRACT

MOTIVATIONAL CONTEXT

The respiratory epithelium of the lung lines the largest surface of contact with the external environment and it is comprised by alveolar type I (ATI) and type II (ATII) cells. ATI cells form the epithelial component of the air-blood barrier and their extremely thin thickness favors gas exchange between the alveoli and the bloodstream. Type II cells participate in a variety of functions, including ion transport, epithelial repair in response to lung injury and synthesis and secretion of surface-active material. Pulmonary surface-active material or pulmonary surfactant (PS), lowers surface tension at the air-liquid interface of the alveoli, preventing collapse of the lung on expiration and stabilizing the respiratory surface along compression-expansion breathing cycles. Besides its biophysical functions, PS is involved in lung host defense against inflammation and infection, exerting a direct antimicrobial activity as well as facilitating pathogen uptake and killing by immune cells.

Compositionally, PS is constituted by approximately 90 % lipids and 8-10 % of some specific proteins. Phospholipids (80 % surfactant mass) , mainly dipalmitoylphosphatidylcholine (40 %) and phosphatidylglycerol (10-15 %) are the main surface active agents, but the presence of hydrophobic surfactant proteins SP-B and SP-C is strictly required to facilitate phospholipid dynamics during surface film formation and stabilization. Complementarily, hydrophilic proteins SP-A and SP-D are mainly related to the defence functions of PS, enhancing bacterial clearance and the regulation of the inflammatory response of the lung. The integrated regulation of surfactant synthesis, secretion and metabolism is vital for air breathing and ultimately, survival. Indeed, pulmonary surfactant dysfunctions are associated with severe respiratory pathologies, such as neonatal respiratory distress syndrome in preterm infants or acute respiratory distress associated with lung injury.

During the process of PS biosynthesis in ATII cells, lipid and protein components are assembled into complexes that are stored as tightly packed membranes in intracellular vesicles called lamellar bodies (LBs). Upon physiological stimulation, PS is exocyted in the form of lamellar body-like particles (LBPs), which disintegrate in a very cooperative manner once reached the

air-water interface. The spontaneous and rapid adsorption and transfer of active material into the air-liquid interface to form the surface active film leads to the dramatic reduction in surface tension. Besides the interfacial film, other related membranous structures are also present in the alveolar hypophase, although their functions are still not fully understood.

Up to now, most of surfactant research has been carried out studying PS as isolated from animal bronchoalveolar lavages (BAL). Although this material has been taken as a reference for the elucidation of structural determinants and representative of optimal surfactant function, we hypothesize that it contains not only active structures but also a mixture of less functional membranes from extracellular already "spent" surfactant as well as non surface-related structures. Taking this into account, we postulate that the study of the components and properties of membranes and films originated from freshly secreted PS might more closely represent the real behaviour of surfactant in its native environment.

On the other hand, our current knowledge about PS biogenesis is still incomplete and important gaps in the understanding of protein processing and lipid traffic as well as in the packing and storage of PS complexes into LBs, still remain. To investigate these questions, much research has been performed taking advantage of primary cultures of ATII cells isolated from animal lungs. Primary cells are often the first choice since they represent a closer option for mimicking the *in vivo* conditions. However, primary cultures are heterogeneous and they require the use of animals. In this respect, *in vitro* models can be contemplated as a suitable alternative, considering that they are more stable and homogeneous, providing with a good reproducibility and potential to replace animal experimentation. However, at present, surfactant-producing established cell-lines are still unavailable. The development of a reliable *in vitro* model of ATII cells would permit to gain further insight into the biological mechanisms of PS that still remain as open questions. Additionally, this approach may also result in a prospective tool for the screening of novel drug formulations intended to be pulmonary administrated. For this purpose, the possibility of generating alveolar epithelial cells throughout the specific differentiation of stem cells looks promising. As a matter of fact, this strategy is currently being implemented for multiple applications, such as the study of lung development or in regenerative medicine.

GENERAL AIMS

In general terms, the goals of the present PhD Thesis are:

1. Study of the micro- and nanostructural organization of surfactant membranes stored in intracellular LBs as well as freshly secreted in the form of lamellar body-like particles (LBPs) in comparison with native surfactant (NS) complexes purified from BAL (**Chapter 1**).

2. Examination of the structural and functional diversity present in NS complexes isolated from BAL (**Chapter 2** and its **appendix**).

3. Development and characterization of a new cellular model based on the differentiation of human placental mesenchymal stem cells into ATII-like cells (ATII-LCs) (**Chapter 3**).

4. Optimization of ATII-LC cultures under physiological conditions mimicking the native alveolar microenvironment. Implementation of the cellular model for biopharmaceutical applications (**Chapter 4**).

MAIN OUTCOMES AND CONCLUSIONS

In the present PhD Thesis, we have investigated the organization of lipids and proteins in PS membranes as intracellularly assembled in LBs as well as freshly secreted as LBPs from primary ATII cells upon induction of exocytosis with secretagoges, in comparison with NS purified from BAL (**Chapter 1**). First, we have analyzed phospholipid packing and hydration by means of fluorescence, polarization and infrared spectroscopy/microscopy. As previously proposed, PS membranes either in the form of LBs or as LBPs exhibit properties that are very different from those of membranes from NS material. LBs display a distinctive structural organization manifested in a highly packed and dehydrated state of the surfactant phospholipids at the head group level, which is preserved when LBs are exocyted to the extracellular medium. Furthermore, when LBPs are subjected to high temperatures, they still maintain a considerable packed/dehydrated state, whereas membranes from NS are totally unpacked and hydrated. In addition, analysis with polarized-light microscopy also corroborate this particular organization demonstrated

by crystalline-like highly ordered structures in LBs/LBPs, also resistant to supraphysiological temperatures.

On the other hand, the information provided by infrared spectroscopy about phospholipid acyl chains order and dynamics suggests that, despite the highly dehydrated state at the polar heads, acyl chains are relatively disordered in LBPs, pointing to the existence of geometrical phospholipid organizations different from lamellar phases. In general, the remarkable differences in the thermotropic profiles of NS and LBPs suggest the presence of additional levels of structural complexity in LBPs that could impose restrictions to temperature-dependent hydration as associated with potential phase transitions in membranes.

Additionally, the peculiar micro- and nanometer scale organization of membranes derived from LBPs has been further confirmed in terms of lateral phase structure by means of the generation of giant unilamellar vesicles and the detection of particular lipid domain segregation patterns. Direct observation of spread LBPs under atomic force microscopy also points to the existence of a remarkable internal complexity present in the membranes of these corpuscles. From a functional point of view, freshly secreted LBPs display a superior adsorption efficiency and a significantly higher resistance to inhibitory agents, even at high concentrations of those, in comparison with NS complexes. In view of these results, we conclude that the particular complex internal organization of lipids and proteins in LBPs likely confers them critical properties for the maximum efficacy in the formation of interfacial films and therefore for surfactant function. At present, the extremely low amount of freshly secreted surfactant material yielded by primary cell cultures is a challenging limitation that precludes the application of additional techniques to address some of the unanswered questions and thus, alternative sources of material have to be explored.

On the other hand, as we had initially hypothesized, a more detailed examination of NS complexes corroborated the heterogeneous nature of the preparations purified from BAL (**Chapter 2**). By means of density gradient centrifugation, different subfractions have been further purified from NS lipid-protein complexes and analyzed from a morphological, biochemical and functional point of view. We have confirmed that despite the fact that NS contains a major part

of highly active structures, morphologically consistent with LBPs, it also comprises fractions of less efficient material, with a marked diminished biophysical performance correlated with a different ultrastructure and biochemical composition. The less dense portions, presumably corresponding with different populations of LBPs, would be related to the traditionally termed "large aggregates" (LA) or "heavy fractions", the most active structures in PS. However, in view of our results, we postulate that LA are not homogeneous in nature but a collection of different structures that can be further subfractioned.

The less active part of NS has been found in the heaviest fractions, and its content in surfactant proteins and cholesterol is significantly different from that of the most efficient structures, exhibiting a reduced amount in SP-B whereas its levels of SP-A, aggregated forms of SP-C and cholesterol are particularly high. The interpretation of these results is not totally clear, although it is tempting to think that the less active material corresponds to already "spent" or "deactivated" surfactant which might coexist in the alveolus with surfactant-like structures. Furthermore, the co-existence in NS of structures with roles different than surface tension reduction, like surfactant regulation or alveolar homeostasis, should not be discarded. Obviously, we have to take also into consideration that BAL might contain not only alveolar material, but also structures extracted from other locations of the airways, likely participating in other functions.

We have taken advantage of cryo-preservation techniques to examine the ultrastructure of the morphological diversity contained in NS material under close-to-native conditions, avoiding the potential influence of artifacts resultant from sample preparation (**Chapter 2: appendix**). We have imaged NS under cryo-electron and cryo-soft x-ray tomography, unveiling unprecedented structural details in tomographic reconstructions, particularly from LBPs. This structural analysis has allowed us to propose a model for the process of progressive unravelling of LBPs, from the intact highly condensed state to unpacked forms.

In spite of the usefulness and reliability demonstrated by primary ATII cells, they fail to sustain a differentiated phenotype in culture as they progressively transform into ATI cells and they are unable to synthesize surfactant de novo, precluding their use for the study of surfactant biogenesis. In view of the necessity of a well-established ATII cell model, we have developed and

characterized a new cellular model of ATII cell based on the differentiation of Decidua-derived Mesenchymal Stem Cells (DMSCs) isolated from human placenta into cells with phenotypical features of ATII cells, that we have termed ATII-like cells (ATII-LCs) (**Chapter 3**). ATII-LCs display membranous cytoplasmic organelles resembling LBs, and accumulate disaturated phospholipid species, a surfactant hallmark. Importantly, we have demonstrated that throughout their differentiation process, ATII-LCs increase their content in mRNAs involved in pulmonary development (TTF1, FOXA1 and FOXA2), alveolar homeostasis (GPR116, CFTR) or those encoding for surfactant-related proteins (SPA-D, ABCA3) and for their processing enzymes (Cathepsin H, Napsin A). At a protein level, the expression of SP-A, SP-B and SP-C is also manifestly enhanced in ATII-LCs. Mimicking the response of ATII cells to secretagoges, ATII-LCs are able to exocytose lipid-rich assemblies, which exhibit faster interfacial adsorption kinetics than standard NS, even in the presence of inhibitory agents.

However, despite of these interesting properties, we presume that ATII-LCs are still in a less differentiated state than “true” ATII cells as seen in vivo in the alveolar epithelium or in isolated primary cultures. We speculate that subjecting DMSCs to differentiation under a more complete lung environment mimicking the native situation may facilitate further progress in pneumocyte phenotypes (**Chapter 4**). For instance, we assume that in the real situation, alveolar cells are exposed to the close proximity of an air-liquid interface (ALI) or in direct contact with components of the extracellular matrix (ECM). Bearing this in mind, we have implemented advanced culture techniques, differentiating DMSCs under the influence of an ALI taking advantage of the Transwell systems technology. In addition, we have also tested the possible enhancive effect of components of the alveolar ECM, incorporating collagen and fibronectin in culture substrates. Unfortunately, the implementation of these factors does not significantly promote further differentiation in ATII-LCs, at least in terms of morphology, expression of surfactant proteins or barrier properties. Our results suggest that whole cell differentiation may still require of a complex synergistic signaling, integrating not only physical and/or chemical factors, but also the active interaction with other cell types naturally present in the alveolar epithelium. Nevertheless, we consider that our cellular model of ATII-LCs, as it currently stands, may constitute a valuable tool, not only for the study of surfactant biosynthesis but also for toxicological or metabolic studies. As a proof of concept,

we have exposed differentiated ATII-LCs to different engineered nanostructured materials intended to be used in biopharmaceutical applications, to evaluate their potential cytotoxic effects. In addition, the uptake behaviour of ATII-LCs has been also tested upon exposure of nanoparticles by means of an innovative ALI system optimized to provide a simulated *in vivo* drug-delivery scenario, and subsequently subjected to microscopical examination. Considering the wide interest raised by lung administration of therapeutical nanoparticles, ATII-LCs could be implemented as a drug screening tool to detect potential hazards of nanopreparations in their first stages of their development.

RESUMEN DE LA TESIS

CONTEXTO MOTIVACIONAL

El epitelio respiratorio del pulmón recubre la mayor superficie del organismo expuesta al medio externo y está formado principalmente por células alveolares de tipo I (ATI) y de tipo II (ATII). Las células ATI constituyen el componente epitelial de la barrera aire-sangre y su reducido grosor favorece el intercambio gaseoso entre el alvéolo y el torrente sanguíneo. Las células ATII participan en varias funciones, incluyendo el transporte de iones, la reparación del epitelio en respuesta a daño pulmonar así como la síntesis de material tensioactivo. El material tensioactivo del pulmón, conocido como surfactante pulmonar (*pulmonary surfactant,* PS), reduce la tensión superficial en la interfase aire-líquido (*air-liquid interface,* ALI) de los alvéolos, previniendo el colapso del pulmón durante la espiración y estabilizando la superficie respiratoria a lo largo de los ciclos respiratorios de compresión-expansión. Además de sus funciones biofísicas, el PS está implicado en la defensa del pulmón frente a procesos de inflamación e infección, ejerciendo una acción antimicrobiana directa, así como facilitando la eliminación de patógenos por las células del sistema inmunitario.

Desde un punto de vista composicional, el PS está constituido por un 90 % de lípidos y un 8-10 % de proteínas específicas. Los fosfolípidos (80 % de la masa del surfactante), particularmente dipalmitoilfosfatidilcolina (40 %) y fosfatidilglicerol (10-15 %), son los principales agentes tensioactivos, pero la presencia de las proteínas hidrofóbicas SP-B y SP-C es estrictamente necesaria para facilitar la acción dinámica de los fosfolípidos durante la formación y estabilización de la película tensioactiva interfacial. Complementariamente, las proteínas hidrofílicas SP-A y SP-D están relacionadas esencialmente con las funciones de defensa del PS, promoviendo la eliminación de bacterias y la regulación de la respuesta inflamatoria del pulmón, entre otras funciones. La regulación integrada de la síntesis, secreción y metabolismo del PS es vital para la respiración y en último término, para la supervivencia del individuo. De hecho, deficiencias en el sistema PS están asociadas con patologías respiratorias severas, tales como el síndrome de dificultad respiratoria neonatal o el síndrome de dificultad respiratoria aguda asociado a daño pulmonar en adultos.

Durante el proceso de biosíntesis del PS en las células ATII, los componentes lipídicos y proteicos del surfactante son ensamblados en complejos que son almacenados en forma de membranas densamente empaquetadas en vesículas intracelulares llamadas cuerpos lamelares (*lamellar bodies,* LBs). Como resultado de cierta estimulación fisiológica, el PS es exocitado en forma de cuerpos lamelares particulados (lamellar body-like particles, LBPs), los cuales sufren un proceso de desintegración cooperativa una vez alcanzan la ALI. La adsorción espontánea y rápida de los LBPs conduce a la transferencia de material activo hacia la ALI para formar la película tensioactiva, generando una marcada reducción de la tensión superficial. Además de la película interfacial, otras estructuras relacionadas con carácter membranoso están también presentes en la hipofase alveolar, aunque sus funciones aún no son completamente comprendidas.

Hasta la fecha, gran parte de la investigación en el campo del surfactante se ha llevado a cabo estudiando el PS aislado a partir de lavados broncoalveolares (*bronchoalveolar lavage,* BAL) de animales. Si bien es cierto que este material ha sido tomado como referencia para la elucidación de determinantes estructurales y como representante de una óptima función tensioactiva, sospechamos que contiene no solo estructuras activas sino también una mezcla de membranas menos funcionales procedentes de material extracelular ya gastado o no relacionado con funciones surfactantes. Teniendo esto en consideración, postulamos que el estudio de los componentes y películas originadas a partir de PS recién secretado podría representar más fielmente el comportamiento del PS en su ambiente nativo.

Por otra parte, el conocimiento actual acerca de la biogénesis del PS es aún incompleto y existen importantes lagunas en la comprensión de diversos procesos como el procesamiento proteico y el tráfico lipídico de los componentes del PS así como su empaquetamiento y almacenamiento en los LBs. Para abordar esta clase de estudios, el empleo de cultivos primarios de células ATII aisladas de pulmones animales ha tenido una gran importancia. De hecho, las células primarias son a menudo la elección de referencia, puesto que representan una opción más próxima a simular las condiciones *in vivo*. Sin embargo, los cultivos primarios son heterogéneos y requieren del uso de animales para su obtención. A este respecto, los modelos *in vitro* pueden ser contemplados como una adecuada alternativa, teniendo en cuenta su mayor reproducibilidad y estabilidad fenotípica así como su potencial para reemplazar el uso de animales. Sin embargo,

actualmente no existen líneas celulares establecidas productoras de surfactante. Es por ello que el desarrollo de un modelo *in vitro* fiable de células ATII permitiría profundizar en el estudio de ciertos mecanismos biológicos del PS aún desconocidos. Además, esta aproximación podría ser de interés para su utilización en el *screening* o cribado de nuevas formulaciones farmacéuticas diseñadas para ser administradas por la vía pulmonar, una estrategia en pleno desarrollo en la actualidad. Con este propósito, la posibilidad de generar células epiteliales alveolares a partir de la diferenciación específica de células madre parece prometedora, y dicha estrategia está siendo ya actualmente aplicada en diversos campos como el estudio del desarrollo pulmonar o en medicina regenerativa.

OBJETIVOS GENERALES

En términos generales, la presente Tesis Doctoral está enfocada hacia la consecución de los siguientes objetivos:

1. Estudio de la organización estructural micro- y nanoscópica de las membranas de PS almacenadas intracelularmente como LBs así como secretadas en forma de LBPs, en comparación con el surfactante nativo (*native surfactant,* NS) purificado de BAL (**Capítulo 1**).

2. Análisis de la diversidad estructural y funcional presente en los complejos de NS aislados de BAL (**Capítulo 2** y su **apéndice**).

3. Desarrollo y caracterización de un nuevo modelo celular basado en la diferenciación de células madre mesenquimales aisladas de placenta humana hacia células con un fenotipo similar a la de las células ATII o ATII-LCs (*alveolar type II-like cells*) (**Capítulo 3**).

4. Optimización de cultivos de ATII-LCs simulando las condiciones fisiológicas que tienen lugar en el ambiente nativo alveolar. Implementación del nuevo modelo celular para aplicaciones de interés biofarmacéutico (**Capítulo 4**).

PRINCIPALES RESULTADOS Y CONCLUSIONES

En la presente Tesis Doctoral se ha investigado la organización de los lípidos y proteínas presentes en las membranas de PS, tanto almacenadas intracelularmente como LBs así como secretadas como LBPs, tras la inducción de exocitosis mediante secretagogos, en comparación con el NS aislado de BAL (**Capítulo 1**). En primer lugar, se ha analizado el grado de empaquetamiento e hidratación de los fosfolípidos del PS mediante espectroscopía/microscopía de fluorescencia y de polarización. Como se había hipotetizado inicialmente, las membranas de PS tanto en forma de LB como de LBP presentan propiedades muy diferentes de las presentes en el NS. Los resultados de esta Tesis han revelado que los LBs presentan una característica organización estructural manifestada en un estado altamente empaquetado y deshidratado al nivel de la cabeza polar de los fosfolípidos, que se mantiene cuando los LBs son secretados al medio extracelular. Además, cuando los LBPs son sometidos a altas temperaturas, éstos mantienen un considerable estado empaquetado/deshidratado, mientras que las membranas de NS están totalmente desempaquetadas/hidratadas. Un análisis mediante microscopía de luz polarizada también ha corroborado esta particular organización, revelando estructuras de tipo cristalino altamente ordenadas en los LBs/LBPs, que también resultan ser altamente resistente a temperaturas elevadas. Por otro lado, la información aportada por espectroscopía de infrarrojos sobre el grado de orden de las cadenas de acilo de los fosfolípidos sugiere que, a pesar del estado altamente deshidratado al nivel de la cabeza polar, las cadenas de ácidos grasos están relativamente desordenadas en los LBPs, apuntando a la existencia de organizaciones geométricas de los fosfolípidos distintas a las típicas de fases lamelares. En general, las acentuadas diferencias en los perfiles termotrópicos del NS y de los LBPs sugiere la presencia de niveles adicionales de complejidad estructural en los segundos, que serían responsables de las restricciones en el proceso de hidratación asociado a potenciales transiciones de fase de las membranas. Asimismo, la peculiar organización de las membranas derivadas de los LBPs ha sido también confirmada en términos de estructura lateral de fase mediante la generación de vesículas unilamelares gigantes, lo que ha permitido detectar un particular patrón de segregación de dominios lipídicos. Además, la observación directa mediante microscopía de fuerza atómica de LBPs desplegados también apunta a la existencia de una notable complejidad interna presente en las membranas

de estos corpúsculos. Desde un punto de vista funcional, los LBPs recién secretados demuestran una superior eficiencia en términos de adsorción así como una significativa resistencia a agentes inhibitorios, incluso a altas concentraciones de éstos, en comparación con los complejos de NS. En vista de estos resultados, se concluye que la particular complejidad interna que adoptan los lípidos y proteínas dentro de los LBPs podría conferirles propiedades críticas para una eficacia máxima en la formación de películas interfaciales y por tanto para la función surfactante. Actualmente, la extremadamente reducida cantidad de PS que puede ser obtenido recién secretado por cultivos primarios es una importante limitación que dificulta e impide la utilización de las técnicas adicionales necesarias para abordar ciertas preguntas aún sin respuesta, lo que plantea por tanto la exploración de fuentes alternativas de material.

Por otro lado y como también se había hipotetizado, un detallado análisis de los complejos de NS ha corroborado la naturaleza heterogénea de las preparaciones purificadas a partir de BAL (**Capítulo 2**). Mediante centrifugación en gradiente de densidad, los complejos lipoproteicos de NS han sido subfraccionados y analizados desde un punto de vista morfológico, bioquímico y funcional. Se ha confirmado que a pesar de que el NS contiene una parte mayoritaria de estructuras altamente activas, consistentes morfológicamente con la presencia de LBPs, también recoge material menos eficiente, que muestra una reducida actividad biofísica correlacionada con una diferente ultraestructura y composición bioquímica. Las porciones menos densas del gradiente, posiblemente distintas poblaciones de LBPs, estarían relacionadas con los denominados agregados grandes o fracciones pesadas, las estructuras más activas del PS. Sin embargo, a la luz de estos resultados, se postula que los agregados grandes no son tampoco entidades homogéneas, sino una recopilación de diversas estructuras que pueden ser a su vez subfraccionadas.

La fracción menos activa del NS ha sido encontrada en el material más denso, y su contenido en proteínas del surfactante y colesterol es significativamente diferente de la de las estructuras más eficientes, exhibiendo una cantidad reducida de SP-B y unos niveles incrementados de SP-A, de formas agregadas de SP-C y de colesterol. La interpretación de estos resultados no está totalmente clara, aunque es posible que el material menos activo corresponda a surfactante ya “gastado” o “desactivado” que podría coexistir en el alvéolo con material surfactante funcional.

Asimismo, tampoco se descarta la existencia de funciones alternativas en el material contenido en el NS más allá de la reducción de la tensión superficial, como puede ser lo relacionado con la regulación de los niveles de surfactante o la homeostasis alveolar. Obviamente, también ha de tenerse en cuenta que el BAL no solo contiene material alveolar, sino también procedente de otras localizaciones del sistema respiratorio, posiblemente participando en otras funciones.

Adicionalmente, se han implementado las más recientes técnicas de crio-preservación para examinar la ultraestructura de la diversidad morfológica contenida en el NS, en condiciones similares a las nativas y evitando la potencial influencia de artefactos resultantes de la preparación de las muestras (**apéndice** del **Capítulo 2**). Así, se ha visualizado el NS mediante crio-tomografía electrónica y de rayos X, desvelando detalles estructurales mediante reconstrucciones tomográficas, particularmente de los LBPs. Esta estrategia ha permitido proponer un modelo del proceso de desempaquetamiento de los LBPs, desde estados altamente condensados hasta formas desempaquetadas.

Sin embargo, a pesar de la utilidad y fiabilidad demostradas por los cultivos primarios de células ATII, éstas tienen la desventaja de perder su fenotipo diferenciado en cultivo y progresivamente desdiferenciarse dando lugar a células tipo I. Además, las células ATII primarias son incapaces de sintetizar surfactante *de novo* una vez son extraídas del pulmón, lo cual impide llevar a cabo estudios sobre la biogénesis del PS. En vista de la necesidad de un modelo bien establecido de célula ATII, en esta Tesis se ha desarrollado y caracterizado un nuevo modelo celular basado en la diferenciación de células madre humanas mesenquimales derivadas de la decidua placentaria (*Decidua-derived mesenchymal stem cells*, DMSCs), hasta dar lugar a unas células que hemos denominado ATII-LCs (**Capítulo 3**). Las ATII-LCs exhiben orgánulos citoplasmáticos membranosos que recuerdan a los LBs, y acumulan especies fosfolipídicas disaturadas, un rasgo distintivo del surfactante. Se ha demostrado que a través del proceso de diferenciación, las ATII-LCs incrementan su contenido en mRNAs implicados en desarrollo pulmonar (TTF1, FOXA1, FOXA2), homeostasis alveolar (GPR116, CFTR) o codificantes para proteínas relacionadas directamente con el PS (SPA-D, ABCA3) o las enzimas que catalizan su procesamiento (Cathepsin H, Napsin A). A nivel de proteína, la expresión de SP-A, SP-B y SP-C está incrementada de manera patente en las ATII-LCs. Del mismo modo, simulando la respuesta de las células ATII a los secretagogos, las

ATII-LCs son capaces de exocitar complejos ricos en lípido, los cuáles exhiben una rápida cinética de adsorción interfacial superior a la de los complejos de NS, incluso en presencia de agentes inhibitorios.

Sin embargo, a pesar de estas interesantes propiedades, se presume que las ATII-LCs se encuentran en un estado no totalmente diferenciado en comparación con las "verdaderas" células ATII que se encuentran *in vivo* en el epitelio pulmonar o aisladas como cultivos primarios. En este contexto, se ha planteado exponer las células a un ambiente que simule el entorno pulmonar nativo, como posibilidad de aumentar el grado de diferenciación (**Capítulo 4**). Por ejemplo, se propone que en la situación real, las células alveolares están próximas a una interfase aire-líquido (*air-liquid interface*, ALI) o en contacto directo con componentes de la matriz extracelular (*extracellular matrix,* ECM). Se han implementado así técnicas avanzadas de cultivo, diferenciando las DMSCs bajo la influencia de una ALI, aprovechando la tecnología de los sistemas Transwell. Además, se ha examinado el posible efecto potenciador de componentes de la ECM alveolar, incorporando colágeno y fibronectina en los sustratos de cultivo. No obstante, la implementación de estos factores no parece aumentar el nivel de diferenciación de las ATII-LCs, al menos en términos de morfología, expresión de proteínas del surfactante o propiedades de barrera. Los resultados sugieren que la diferenciación celular completa podría requerir de una compleja señalización sinérgica, que integre no sólo factores químicos y físicos, sino también posiblemente la interacción activa con otros tipos celulares presentes en el epitelio alveolar de manera natural. No obstante, el modelo celular de ATII-LCs, en su actual estado, podría ser aún una herramienta útil, no sólo para el estudio de la biosíntesis del PS sino también como herramienta para estudios toxicológicos o metabólicos. Como prueba de concepto, se han expuesto ATII-LCs a diferentes materiales nanoestructurados de interés biofarmacéutico, con objeto de evaluar sus potenciales efectos citotóxicos. Además también se ha analizado la capacidad de las ATII-LCs para interaccionar e internalizar nanopartículas empleando un nuevo sistema de exposición que simula la situación *in vivo* y un posterior examen mediante microscopía confocal. Teniendo en consideración el interés creciente en la administración pulmonar de nanopartículas terapéuticas, las ATII-LCs podrían ser implementadas como herramienta de cribado para detectar potenciales riesgos de nanofármacos en sus primeras etapas de desarrollo.

Introduction

1. Physiology of the lung

Most of living cells obtain their energy from chemical reactions involving oxygen. Just as crucial is the elimination of carbon dioxide, the major end product of an oxidative metabolism. The process of **exchange of oxygen and carbon dioxide** between an organism and the external environment known as respiration can be directly performed by a unicellular organism. However, this is impossible for most cells of a complex organism like a vertebrate. Consequently, the evolution of large animals has required the development of a specialized respiratory system, although it substantially differs in structure, embryological origin and function between vertebrate groups (Daniels and Orgeig 2003). In humans, the **respiratory system** is principally constituted by **lungs**, **airways** and the **muscles of breathing**. Lungs consist of the three lobes of the right lung and two lobes of the left lung. The bronchi, blood vessels, and nerves leave and enter at the hilum of each lung. The airways comprise the trachea, right and left main bronchi, smaller bronchi, bronchioles and alveoli. Also part of the respiratory system are the pleural membranes and the respiratory muscles that form the chest cavity, diaphragm and intercostal muscles, which are key in the generation of the forces that control the inflation and deflation of the lung and so the flow of air between them and the atmosphere. Within the lungs, there are more than 20 **branching** generations, each resulting in narrower, shorter and more numerous tubes to finally reach the tiny air-containing sacs called **alveoli**, where gas exchange occurs **(Figure 1)**.

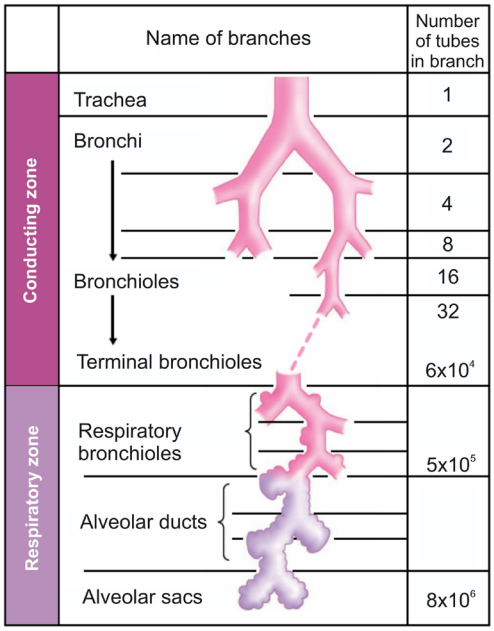

Figure 1. **Airway branching in humans**. Scheme of the more than 20 generations of branching in the human respiratory system divided in two zones: a conductive zone from where air flows towards the respiratory zone which contains alveoli and where the exchange of gases with the blood takes places. Diameters are not drawn to scale. Modified from (Widmaier, Raff et al. 2014).

The alveolar number is closely related to total lung volume, with larger lungs having considerably more alveoli, although mean values are about 300-500 million and 200 µm of diameter (Daniels and Orgeig 2001; Ochs, Nyengaard et al. 2004) exposing an exchange area of 50 to 100 m^2, roughly the size of a tennis court (Coxson and Hogg 2001). The thickness of the alveolar capillary barrier (500 nm thick) coupled to the extensive surface area permit the rapid exchange of large quantities of oxygen and carbon dioxide by diffusion. Gas exchange takes place through a complex physical barrier composed by a thin aqueous film lining the alveolus, alveolar epithelial cells, the interstitial layer, endothelial cells forming the blood capillaries, the blood plasma and finally the erythrocyte membrane **(Figure 2)**.

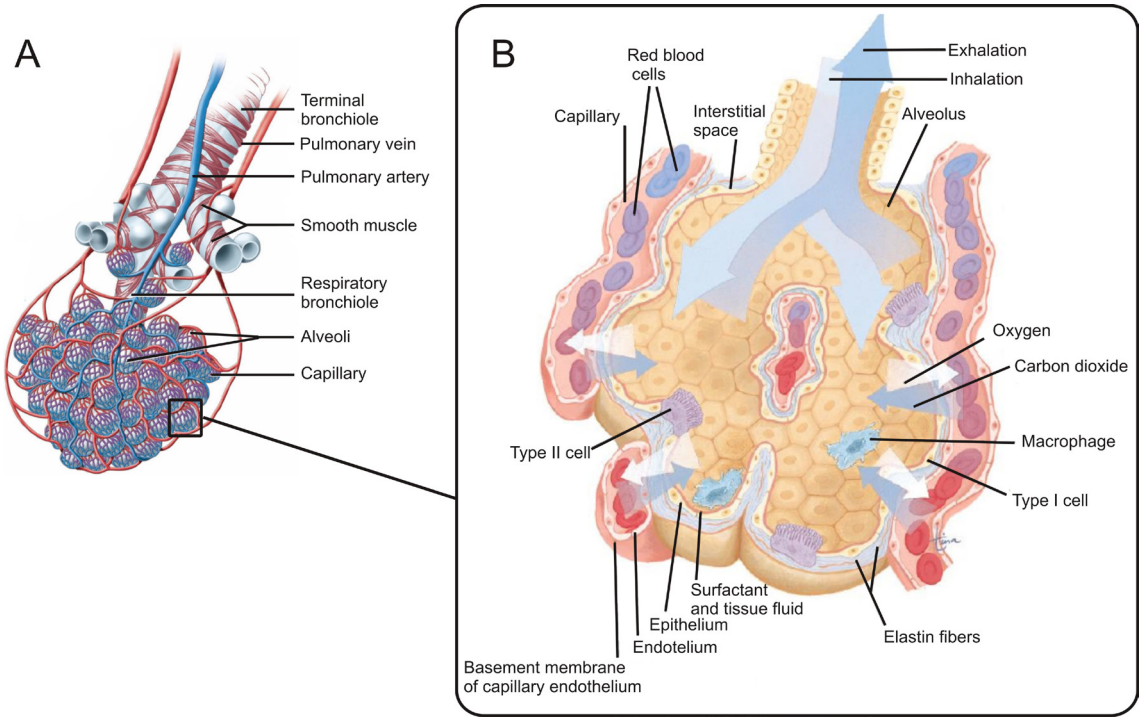

Figure 2. **Structure of the alveolar respiratory units**. **A.** Relationship between blood vessels and the clusters of alveoli at their end. Red represents oxygenated blood; blue represents deoxygenated blood. **B.** An enlargement of a small section of A (square) representing the alveolar structure showing type I-II cells and macrophages as well as the alveolar-capillary barrier through which gases must pass as they diffuse from air to blood (oxygen) or from blood to air (carbon dioxide). Adapted from (Scanlon V.C. and T. 2015) and (Widmaier, Raff et al. 2014).

With respect to the **epithelial cells**, most of the air-facing surfaces of the alveolar walls are lined by a continuous layer, one cell thick, of flat cells termed **alveolar type I** (ATI) cells, which comprise around 90 % of the respiratory surface area (Crapo, Barry et al. 1982). Interspersed between these

cells are thicker, specialized cells termed **alveolar type II** (ATII) cells. These are more abundant but, because of their cuboidal shape, only account for around 10 % of the alveolar surface area (Mason and Williams 1977) and secrete the so called **pulmonary surfactant** (PS), a lipid protein complex that lines the surface of alveoli and reduces their **surface tension**, increasing lung compliance, thereby making easier for the lungs to expand. Besides, alveolar macrophages are the third cellular type present inside alveoli, involved in preserving a clean and pathogen-free respiratory surface.

2. Surface tension at the alveoli and pulmonary surfactant

The surface of these alveolar cells is moist, so the alveoli can be pictured as air-filled sacs lined with an aqueous fluid consequence of cell metabolism. A typical molecule in the bulk of a liquid is attracted equally in all directions by its nearest neighbors. However, a molecule in the interfacial region has a relative lack of attraction from the dilute gas phase and thus, there is an unbalanced attraction on surface molecules toward the bulk of the liquid **(Figure 3)**. This causes the surface to minimize its area generating the energetically-optimized spherical shape, as a result of the force called **surface tension** (ɣ). This force makes the alveolar water lining like a stretched balloon that constantly lends to shrink and resists further stretching. Thus, expansion of the lung requires energy not only to stretch the connective tissue of the lung but also to overcome the surface tension of the water layer lining the alveoli. In fact, the surface tension of pure water, which is around 70 mN/m at 37 °C, is so high that if the alveoli were lined with pure water, lungs would

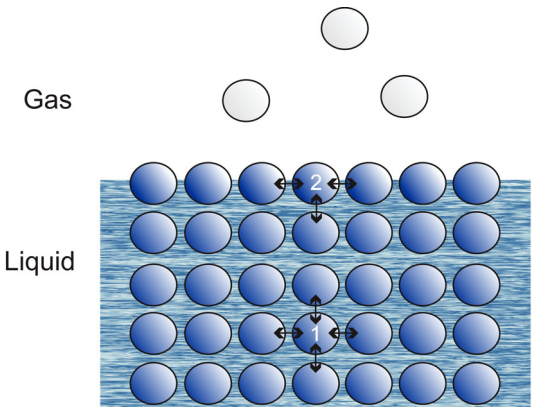

Figure 3. **Molecular forces leading to surface tension**. A bulk liquid molecule 1 is equally attracted by its neighbors being all the forces compensated in all space directions. However, molecule 2 is located at an interfacial region in contact with the gas phase, which is much more diluted than the liquid. Gas molecules exert a negligible attraction on interfacial molecules and this unbalanced inward attractive force on interfacial molecules causes the surface to seek a minimal area as a result of surface tension.

require exhausting muscular effort and they would tend to collapse.

Idealizing the alveoli shape as spherical cavities, the **law of Laplace-Young** ($\Delta P = 2\ \gamma / r$), which enounces that the pressure (P) inside an alveolus is directly proportional to surface tension (γ) and inversely proportional to the alveolar radius (r), can be applied. Lung alveoli can be considered as very small and interconnected bubbles and given their heterogeneous size, the smaller ones would be subjected to higher pressures and would tend to collapse earlier into large alveoli, especially at the end of expiration **(Figure 4)**.

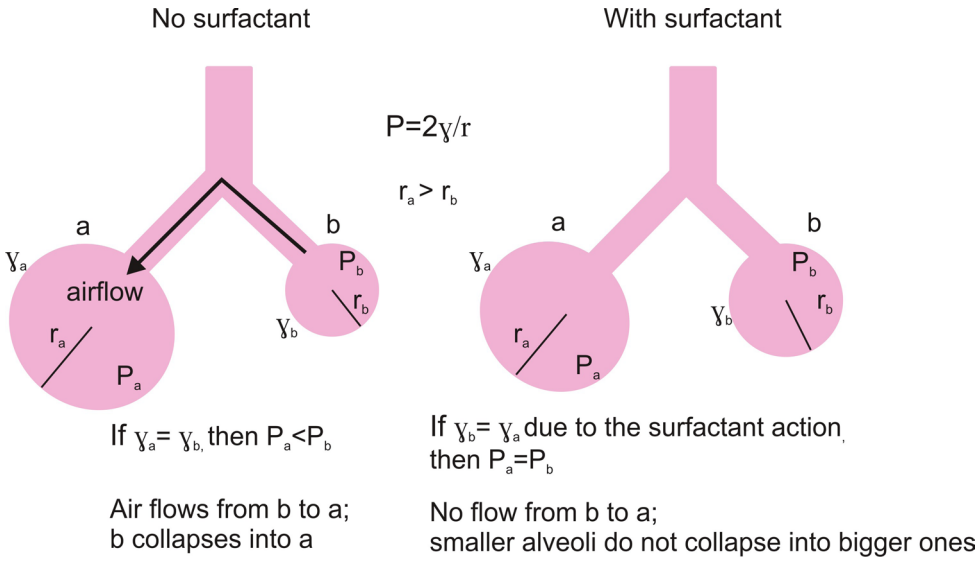

Figure 4. Stabilizing effect of surfactant. Application of the Law of Laplace to two alveoli (*a* and *b*) next to each other sharing an alveolar duct, being the radius of *a* greater than the radius of *b*. *P* is pressure inside the alveoli, *γ* is the surface tension and *r* is the radius of the alveolus. Adapted from (Widmaier, Raff et al. 2014).

However, the presence of PS molecules interposed between water molecules at the alveolar surface permits maintaining an opened interface compensating the water-water interactions that cannot be established at the interface. The reduction in surface tension helps to maintain a pressure in smaller alveoli approximately equivalent to that in the larger ones, providing stability to alveoli of different sizes. This specialized function of PS comes from its particular biochemical composition, which has been evolutionarily tuned to optimize the surfactant activity (Daniels and Orgeig 2003).

As stated above, the optimized complex mixture of lipids and proteins constituting PS is key to understand the basic molecular mechanisms that underlie its singular properties. **Lipids** account for more than 90 % of surfactant by mass and its qualitative and quantitative composition varies among different species (Lang, Postle et al. 2005), exhibits particular adaptations to environmental conditions, such as body temperature (Suri, McCaig et al. 2012), and varies in response to physiological constraints or pathological situations (Gunther, Schmidt et al. 1999). On the other hand, approximately 10 % of surfactant in mass is constituted by **proteins**, including specific surfactant proteins, which can be classified with respect to their water affinity: **hydrophilic** proteins (SP-A and SP-D) and **hydrophobic** proteins (SP-B and SP-C). SP-A and SP-D belong to the collectin protein family and they are involved in immune innate defense and inflammatory responses in the lung as well as in the maintenance of alveolar homeostasis, whereas SP-B and SP-C are crucial for the biophysical function of surfactant (Crouch and Wright 2001; Weaver and Conkright 2001).

3. Pulmonary surfactant: components and functions

3.1. Lipids

3.1.1. Lipid structure

Lipids, and predominantly **phospholipids**, make up the bulk of PS. These are amphipathic molecules formed by a polar hydrophilic head and a non-polar or hydrophobic acyl chains **(Figure 5)**. Glycerol-based phospholipids are the principal lipid species and they are characterized for containing a glycerol molecule and a negatively charged phosphate group bonded to a variable polar group. Phospholipids classes are defined by the structure of the polar group which comprise: zwitterionic groups (with zero overall net charge at physiological pH), such as phosphatidylcholine (PC) and phosphatidylethanolamine (PE) and anionic groups (with negative net charge) including phosphatidylglycerol (PG), phosphatidylserine (PS*) and phosphatidylinositol (PI). The glycerol molecule is esterified by two fatty acids, which are hydrocarbon chains of different length and saturation (number of double bonds).

Lysophospholipids have the same structure but have only one fatty chain. An additional class of phospholipid is sphingomyelin (SM), which possess a PC head group, sphingosine, and a fatty acid.

The **amphipathic character** of phospholipids make them to adopt an energetically favorable orientation at the air-liquid interface, with the polar heads pointing toward the aqueous phase whereas the apolar chains are oriented toward the air, minimizing the contact between the hydrophobic region and water molecules (Marsh 2012).

A

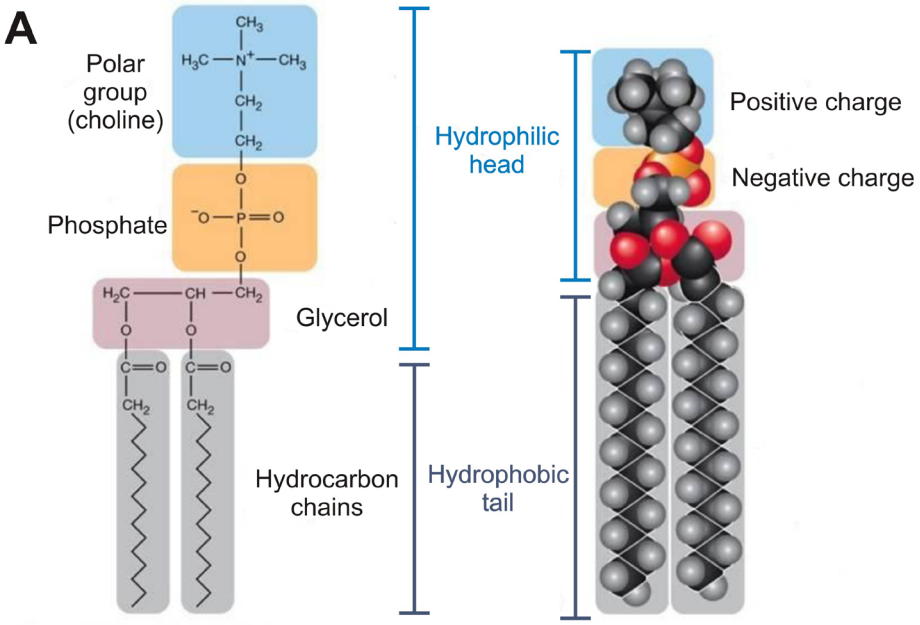

B

Phospholipid	Polar group	Charge
PC	-O-CH_2-CH_2-$N_+(CH_3)_3$	0
PG	-O-CH_2-CHOH-CH_2OH	-
PI	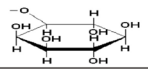	-
PE	-O-CH_2-CH_2-N_+H_3	0
PS	-O-CH_2-CH-COOH NH^+_3	-

Figure 5. Structure of glycerophospholipids. **A**. Representation of the molecular structure of phosphatidylcholine, including the hydrophilic moiety constituted by the polar head group and the hydrophobic acyl chains. Modified from (Sadava, Heller et al. 2012). **B**. Presentation of the most common phospholipids in pulmonary surfactant: phosphatidylcholine (PC), phosphatidylglycerol (PG), phosphatidylinositol (PI), phosphatidylserine (PS), phosphatidylethanolamine (PE); chemical formula of their head groups and net electric charge at a neutral pH.

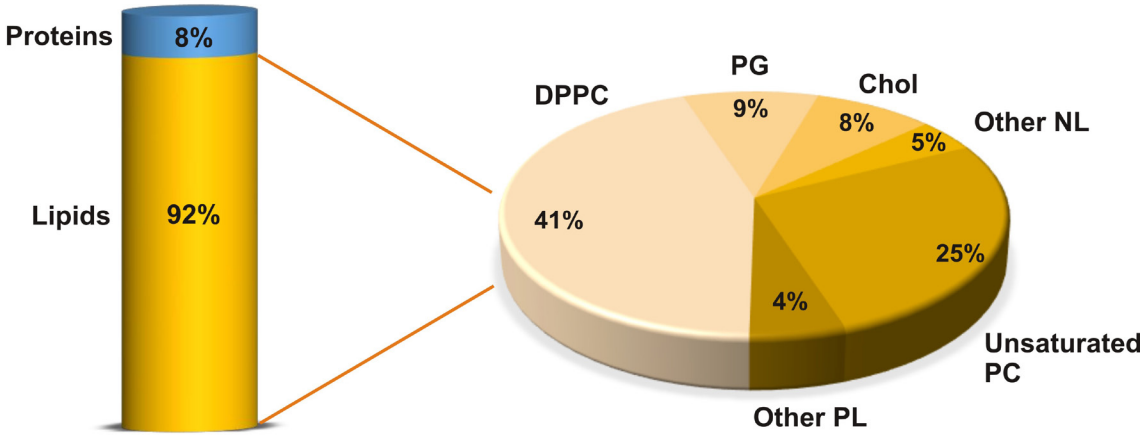

Figure 6. **Lipid composition of pulmonary surfactant**. Pulmonary surfactant obtained from bronchoalveolar lavages of mammalian lungs typically comprises around 8-10 % of proteins and 90-92 % of lipids: dipalmitoylphosphatidylcholine (DPPC), unsaturated phosphatidylcholine (PC), phosphatidylglycerol (PG) as well as a minor proportion of other phospholipids (PL). Besides phospholipids, other lipid constituents are cholesterol (Chol) and other neutral lipids (NL).

Despite the fact that PS composition differs among animal species, as mentioned above, similarities are more perceptible than differences and in general it is considered to be highly conserved among mammals (Veldhuizen, Nag et al. 1998; Agassandian and Mallampalli 2013). A typical lipid surfactant composition mainly contains PC (around 60-70 %) and PG (approximately 9 %) species **(Figure 6)**. Among PC species, **dipalmitoylphosphatidylcholine** (**DPPC**, 16:0/16:0) represents 40 % of the total surfactant mass and it is essential for producing the extremely low surface tensions observed during expiration; its saturated acyl chains can adopt a highly lateral packed state occupying smaller area per molecule compared to unsaturated phospholipids (Hawco, Davis et al. 1981; Batenburg 1992). Besides DPPC, other saturated PC species can be found in PS such as palmitoylmirystoyl-PC (PMPC, 16:0/14:0), and unsaturated PCs, such as palmitoyloleoyl-PC (POPC, 16:0/18:1) or palmitoylpalmitoleoyl-PC (PPPC, 16:0/16:1). Anionic phospholipids such as **PG** and **PI** are thought to take part in selective interactions with the cationic hydrophobic proteins (Pérez-Gil, Tucker et al. 1992; Pérez-Gil, Casals et al. 1995). The other minor phospholipids such as PE, PI, SM, as well as lysophosphatidylcholine comprise the remainder of the phospholipid pool. Additionally, neutral lipids are also present in PS membranes and account for approximately 13 % by mass, being cholesterol the most abundant (around 8 % by mass). Other neutral lipids such as cholesterol esters, triglycerides, diglycerides and free fatty acids exist in small quantities (Goerke 1998).

3.1.2. Lipid polymorphism

The ability of lipids to adopt distinctive structural configurations from one shape to another, or **lipid polymorphism**, becomes key to understand the interactions and properties exhibited by PS membranes. As we explained before, lipids display a self-assembly capacity when they are exposed to an aqueous environment due to a hydrophobic effect, giving rise to aggregates and organizations of high complexity levels (**Figure 7**). Additionally, the generation of these

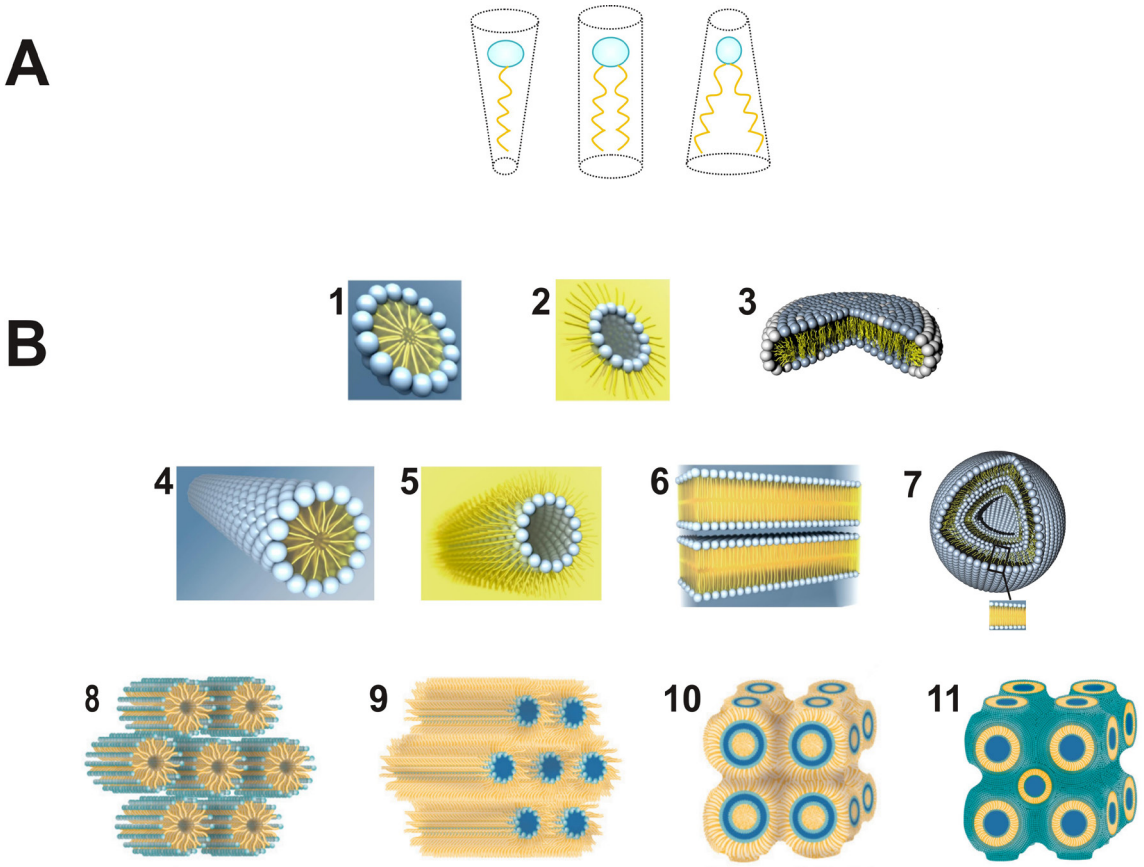

Figure 7. Lipid polymorphism. **A**. Overall shape that lipid molecules exhibit according to the relationship between the cross-sectional areas of the head group and the acyl chains: inverted cone (left), cylindrical (middle), and cone (right). **B**. Schematic illustration of the large variety of mutually related structures that lipids adopt as a function of their chemical structure and of external variables such as water content, temperature, pressure and aqueous phase composition. Phospholipids typically assemble as bilayers forming planar lamellar structures (6), liposomes (7) or disks (3). Non lamellar structures such as micelles (1) and inverted micelles (2) give rise to bidimensional cylinders in which the lipid acyl chains are oriented inward (4) or outward (5), respectively. These cylinders configure hexagonally coordinated macromolecular HI (8) or inverted HII (9) phases. Upon certain conditions, lipids can be also organized as inverted (10) and bicontinuous (11) cubic phases. Adapted from (Lee, Jamgotchian et al. 2008), www.particlesciences.com and www.cbmn.u-bordeaux.fr.

structures is also defined by the geometrical shape of the molecules constituting the lipid system (van den Brink-van der Laan, Killian et al. 2004). Most of the phospholipid species, such as PCs, are considered to have a rather cylindrical shape, since the cross-sectional area of the head group and the acyl chains are equivalent. These lipids dominating in biological membranes are arranged primarily as bilayer structures, the so-called **lamellar phases**, whose curvature is close to zero. Phospholipids that form flat bilayers spontaneously stack when hydrated, and form repeating spherical lamellae or multillamelar vesicles (MLVs) to avoid edges exposed to water. When the cross-sectional areas of the lipid head group and acyl chains differ, other aggregate structures are preferred constituting **non-lamellar phases**. If the cross-sectional area of the head group is larger than that of the acyl chains (type I lipids such as detergents or lysophospholipids), structures with a positive curvature, such as micelles, are favored, giving rise to **hexagonal phases H_I**. On the other hand, when the cross-sectional area of the head group is smaller, it results in an overall conical shape (type II lipids, such as diacylglycerol or PE) forming negatively-curved structures termed **inverted hexagonal phases H_{II}** and **cubic phases**. In the hexagonal phases, lipids are packed together to form hollow cylinders. The most common kind of hexagonal phase formed in water is the H_{II} phase, where the methyl ends of the acyl chains form the exterior of a lipid cylinder filled with water. These cylinders are packed together with hexagonal symmetry in which each cylinder is surrounded by six other cylinders, hence the name hexagonal phase. With respect to cubic phases, these can be divided in two general classes: inverted micellar and bicontinuous. In the first case, lipids are packed into spherical aggregates, with each sphere representing a unit cell that packs together with other unit cells in a cubic array. In bicontinuous cubic phases, both lipid and water channels are continuous in space and the arrangement is accomplished with several different morphologies, all of which have cubic symmetry but belong to different space groups (Luzzati 1997).

However, within the shape-structure concept of lipid polymorphism, the overall shape of the lipid is not only function of its chemical structure but also of external parameters like temperature, pH, salt concentration, presence of divalent cations, pressure or hydration (Cullis and de Kruijff 1979; Tate, Eikenberry et al. 1991). The lipid phases shown in **Figure 7** are mutually related and

transform into each other via phase transitions driven by temperature, pressure, lipid composition and so on (Koynova and Tenchov 2013). Besides environmental conditions, particular interactions of lipids with proteins (i.e.: amphiphilic or membrane-lytic peptides) can also lead to the promotion of non-lamellar phases modulating the activity of diverse biological systems (Epand 1998).

3.1.3. Lateral organization

When assembled in bilayers, phospholipids present different levels of molecular ordering and mobility as a function of temperature. At temperatures above a threshold, known as the **gel-to-fluid transition temperature** or T_m (**melting temperature**), the bilayers melt from an ordered state (**gel phase** or L_β) to a disordered, more fluid state (**liquid-crystalline phase**, L_α). In the gel phase, molecules have little rotational or translational mobility and adopt quasi-crystalline order with homogeneous well-defined intermolecular distances and extensive packing of their acyl chains. However, in the liquid-crystalline phase, lipid molecules are relatively disordered as a result of the trans-gauche isomerization which takes place at their C-C bonds (Pérez-Gil 2008). The melting temperature of a given phospholipid depends on the number of double bonds and length of its acyl chains, with long, fully saturated chains undergoing ordered-to-disordered transitions at much higher temperatures than shorter or unsaturated chains. In the particular case of PS, it seems to have evolved to contain around 50 % saturated and 50 % unsaturated species as a result of a particular modulation in the lipid biosynthesis pathways in ATII cells (Pérez-Gil and Weaver 2010). Saturated species such as DPPC, the main component of PS, melt from ordered to disordered phase at 41 °C, whereas POPC, one of the most abundant unsaturated species, melts at -2 °C. The coexistence of ordered and disordered phases at a wide range of temperatures, including physiological values, manifests in a high stability of surfactant layers at high compression sustained by saturated molecules (mainly DPPC) and enough fluidity and dynamics, which are facilitated by unsaturated species.

The gel and fluid phases in bilayers have some correspondence with the order and packing of phospholipids in interfacial monolayers. In fact, in addition to temperature, changes in lateral compression can define lipid packing at the air-liquid interface. At low compression

levels, areas per lipid molecule are large and the configurational freedom of the acyl chains is also high and monolayers constitute what is called a **liquid-expanded** (L_e) phase, qualitatively equivalent to the L_α in bilayers (Nag, Boland et al. 1991). When compressed enough at the interface, phospholipid can reach a highly packed state, the **liquid condensed** (L_c) phase, whose low mobility is comparable to that of L_β in bilayers (MacDonald and Simon 1987). Beyond this, an extreme packing state can be achieved producing **solid-ordered** (S_o) phases which are not compressible any further and behave as real two-dimensional solids. Molecules in S_o phases have no translational mobility and if the compression exceeds a certain threshold the film collapses and the material present in the interface is expulsed into the air or water bulk phases (Discher, Maloney et al. 1996).

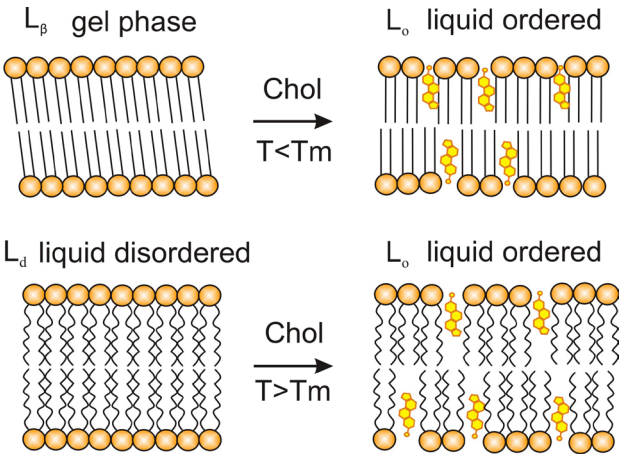

Figure 8. Cholesterol-induced liquid ordered phase. When added to lipids in the gel phase (L_β) at temperatures below T_m, cholesterol tends to liquefy the membrane structure by disrupting the highly ordered tilted structure of the hydrocarbon chains and inducing them to be fully extended, but not tilted. At temperatures above Tm, cholesterol tends to rigidify lipids in the liquid disordered (L_d) phase also leading to the formation of the intermediate phase Lo, where the lipid tails are more ordered similarly to the L_β phase, but maintain lateral fluidity similar to the L_d.

Besides temperature and compression, the incorporation of **cholesterol** has a profound effect in the modulation of the lateral organization and dynamics of surfactant membranes (**Figure 8**). Intercalation of enough cholesterol molecules into phospholipid bilayers and interfacial monolayers reduces packing and increases mobility of phospholipids in the ordered phases (L_β, L_c) giving rise to phases with a certain molecular order but maintaining a relatively fluid state. On the other hand, disordered phases gain order when cholesterol molecules are inserted reducing the conformational freedom of the acyl chains. Presence of cholesterol defines an organization of a particular phase termed liquid-ordered (L_o), where phospholipids may retain ordered states with high packing and low hydration, as occurs in L_β phases, but associated with significantly higher lateral and rotational mobility (Casals and Cañadas 2012; López-Rodríguez and Pérez-Gil 2014).

The L_o phase transforms into a **liquid-disordered** (L_d) phase at temperatures above the T_m. This coexistence of ordered and disordered phases in PS, which have been confirmed by a number of evidences (Bernardino de la Serna, Oradd et al. 2009; Bernardino de la Serna, Vargas et al. 2013) results in the segregation of lipid membrane domains. This lateral heterogeneity, which takes place in both surfactant bilayers and monolayers, might imply changes in surfactant macroscopic properties and in addition to its compositional complexity, would contribute to maintain PS membranes at the critical point between two fluid states permitting fluctuations and interactions that are essential for its function (Parra and Pérez-Gil 2015).

3.2. Proteins

Besides lipids, to accomplish its biophysical function as well as to participate in the alveolar homeostasis and the lung defense against pathogens, pulmonary surfactant requires the presence of four specific proteins in the alveolar hypophase: **SP-A**, **SP-B**, **SP-C** and **SP-D** (**Figure 9**). SP-A, SP-B and SP-C, but not SP-D, are membrane-associated proteins and occur in surfactant in small amounts (3-5 % by mass in the case of SP-A, 0.5-1 % by mass for SP-B and SP-C). SP-D is not usually associated with surfactant membranes and it constitutes less than 0.5 % by mass (Serrano and Pérez-Gil 2006).

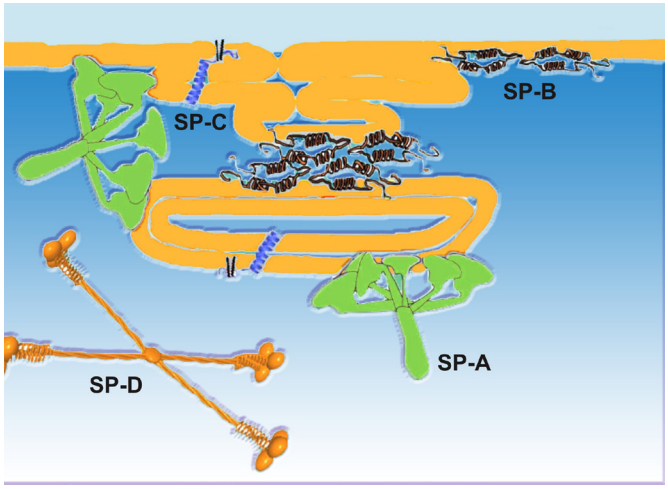

Figure 9. Surfactant proteins associated with lipid multilayers. Schematic representation of the structural models of octadecameric SP-A and dimeric SP-B, the resolved structure in organic solvent of SP-C and a structural model of a dodecameric SP-D. Orange bands represent monolayer/leaflets. Modified from (López-Rodríguez and Pérez-Gil 2014).

3.2.1. Hydrophobic proteins: SP-B and SP-C

SP-B is a 17.4 kDa homodimer containing around 52 % of hydrophobic amino acids and a mainly α-helical secondary structure (40-50 %) oriented parallel to the membrane surface, establishing hydrophobic interactions between the helical segments and the membrane surface (Pérez-Gil, Cruz et al. 1993; Johansson and Curstedt 1997). SP-B belongs to the saposine-like family of proteins, characterized by containing 6 cysteines in strictly conserved positions that establish 3 intrachain disulphide bonds (Olmeda, García-Álvarez et al. 2013). An additional cysteine is involved in an intermolecular disulphide bond, which is responsible for the covalent dimerization of the protein (Johansson, Curstedt et al. 1991). SP-B sequence possesses eight conserved positively-charged residues and one conserved negatively-charge residue, which confer to the protein a **net positive charge** that enhances its interactions with anionic phospholipids, primarily PG (Pérez-Gil, Casals et al. 1995). SP-B has been proposed to favor the promotion of **membrane interconnections** through supradimeric oligomerization of the protein (Baoukina and Tieleman 2011; Olmeda, García-Álvarez et al. 2013) as well as to induce **permeability and aggregation of lipid membranes** (Ryan, Qi et al. 2005; Parra, Moleiro et al. 2011; Parra, Alcaraz et al. 2013). These processes are thought to be related with the canonical properties exhibited by an operative surfactant including **1**) promoting a rapid adsorption of phospholipids into the air-liquid interface and **2**) facilitating the refinement of the interfacial film during compression and **3**) an efficient re-extension of the material from the reservoirs during expansion (Serrano and Pérez-Gil 2006; López-Rodríguez and Pérez-Gil 2014). Moreover, it has been recently proposed that the interconnection of membranes mediated by SP-B might permit the formation of a continuous network highly conductive for hydrophobic molecules, such as oxygen, facilitating oxygen diffusion though the alveolar barrier (Olmeda, Villén et al. 2010).

SP-C is another small (3.7 kDa) hydrophobic peptide of 35 residues and it appears to be the only constituent which is almost unique to PS, indicating important and specific functions (Weaver and Whitsett 1991; Johansson 1998). SP-C forms a single α-helix rich in branched aliphatic residues, mostly valine, which upon insertion in phospholipid membranes adopts a transmembrane orientation with a ~70° tilt relative to the plane of the membrane (Vandenbussche, Clercx et

al. 1992; Johansson, Szyperski et al. 1994). The SP-C N-terminal tail includes two palmitoylated cysteine residues and 3 positive charges that favor a preferential interaction with anionic phospholipids (Pérez-Gil, Casals et al. 1995). The palmitic chains seem to play an important role by anchoring the N-terminal segment to the membrane, strengthening the association of the protein to the interfacial film preventing its exclusion during compression (Bi, Flach et al. 2002) and being key in the modulation of SP-C-lipid interactions in lung surfactant multilayers (Roldán, Goormaghtigh et al. 2015). Although palmitoylation is not essential to promote a rapid interfacial adsorption of phospholipids, it has been proved to be required to reach and maintain the lowest surface tensions of the films at high compression rates, in the presence of SP-B and cholesterol (Baumgart, Ospina et al. 2010). SP-C is thought to **promote and stabilize membrane-membrane and membrane-interface contacts** (Ross, Krol et al. 2002), facilitating lipid exchange between bilayers or between bilayers and monolayers, particularly at highly compressed states (Klenz, Saleem et al. 2008). Additionally, recent investigations suggest that SP-C might have a protective role specifically interacting with cholesterol through its palmitoylated segment, preventing its deleterious effect in surfactant activity (Gómez-Gil, Schürch et al. 2009).

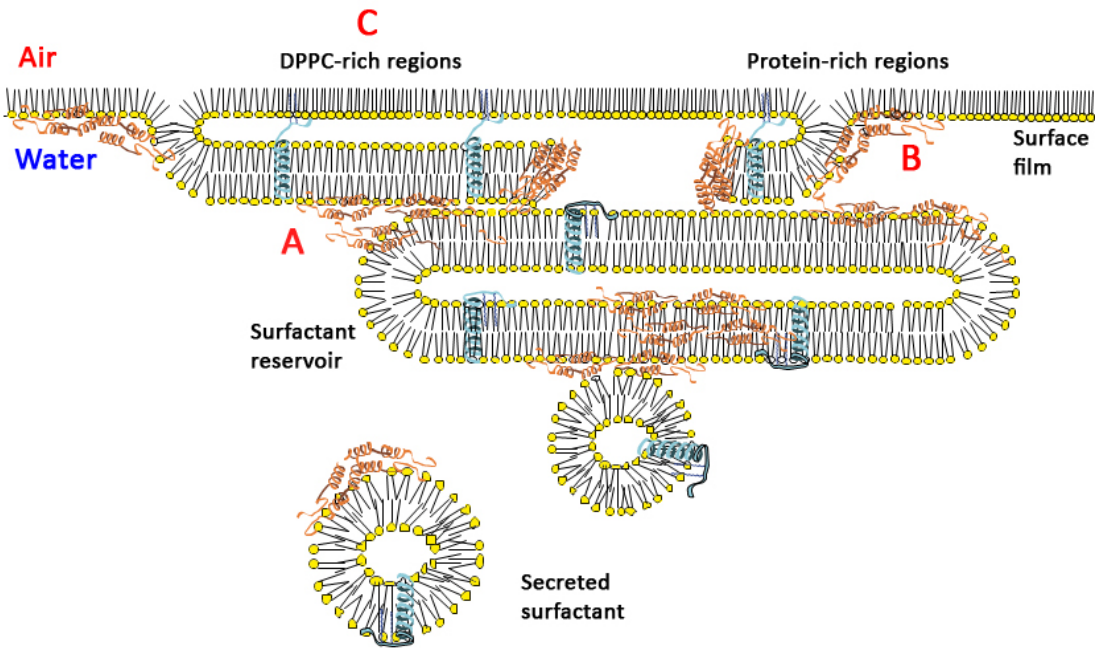

Figure 10. **Functions of hydrophobic proteins**. Graphic representation of the main functions related to SP-B and SP-C: promotion of molecular interactions between the membranes associated to the surface and the reservoir (**A**), perturbation of bilayered structures to favour transfer of surface active molecules into the air-water interface (**B**), facilitate the enrichment of the surface films in DPPC (**C**) and permit the re-extension of the interfacial film during inspiration. Modified from (Pérez-Gil 2010).

In general, the hydrophobic proteins SP-B and SP-C are considered mainly responsible for the **biophysical activity of PS** and their presence is vital for an efficient interfacial adsorption, film stability and re-spreading processes of surfactant along the multiple compression-expansion breathing cycles (Serrano and Pérez-Gil 2006) (**Figure 10**). Currently, their concerted action is thought to be key to create and stabilize the structure of multilayered film that PS adopts at the air-liquid interface (Pérez-Gil and Weaver 2010).

3.2.2. Hydrophilic proteins: SP-A and SP-D

SP-A is the most abundant surfactant-associated protein synthesized by ATII cells. The protein monomer has a molecular mass of ~ 28-36 kDa, although in lung lavage this protein exists as a 650 kDa oligomeric glycoprotein constituted by 18 subunits (Hawgood and Shiffer 1991). **SP-D** is a 43 kDa glycoprotein and it is assembled as homotrimeric subunits which form a cruciform structure in which four trimeric subunits self-associate to form highly ordered SP-D dodecamers (~ 520 kDa) (Crouch 2000). Both hydrophilic proteins belong to the **collectin family of proteins** and present a common structural pattern particularly optimized for their function, including a N-terminal collagen-like region and a C-terminal globular lectin domain. The globular domains are able to recognize and bind carbohydrates (CRDs, carbohydrate recognition domains) present at the surface of numerous types of microorganisms, including viruses, bacteria and fungi.

Thus, these proteins are in charge of **recognizing** and **opsonising pathogens**, presenting them to immune cells such as alveolar macrophages and monocytes (Wright 2003). However, in the absence of immune cells, they still exhibit **intrinsic antimicrobial activity** by increasing the permeability of the microbial cell membrane (Wu, Kuzmenko et al. 2003). In particular, SP-A binds lipopolysaccharides preferentially from Gram-negative bacteria, whereas SP-D binds also to peptidoglycans and lipoteichoic acid (Kingma and Whitsett 2006). Additionally, SP-A has been shown to specifically bind DPPC via the CRD domain (Kuroki and Akino 1991) and it can also promote vesicle aggregation in the presence of calcium (Casals 2001). This feature might be related to the action of the protein of enhancing the adsorption of surfactant complexes into

the alveolar air-water interface (Poulain, Allen et al. 1992; Sáenz, Cañadas et al. 2007) and to the generation of tubular myelin, an intermediary structure in surfactant metabolism (see page 52 for further details). In addition, the interaction of SP-A trough CRDs with phospholipids can also lead to the recycling and clearance of surfactant by ATII cells and alveolar macrophages.

On the other hand, SP-D is also involved in **surfactant homeostasis** by regulating the surfactant pool in the alveolar spaces, although the mechanisms underlying this function remain still unclear (Wert, Yoshida et al. 2000). In general terms, the hydrophilic section of surfactant proteins is specialized in the clearance of pathogens from the alveolar spaces by binding and agglutinating microorganisms and molecules such as allergens or environmental inorganic particles as well as in the modulation of the inflammatory cellular response in the lung (**Figure 11**). As a matter of fact, the interaction of the surfactant collectins with macrophages has a profound effect in the regulation of a variety of processes such as phagocytosis, the production of reactive oxygen species or the release of proinflammatory cytokines (Sano and Kuroki 2005). Besides the presence of SP-A and SP-D in the lung environment, both proteins have been detected in a

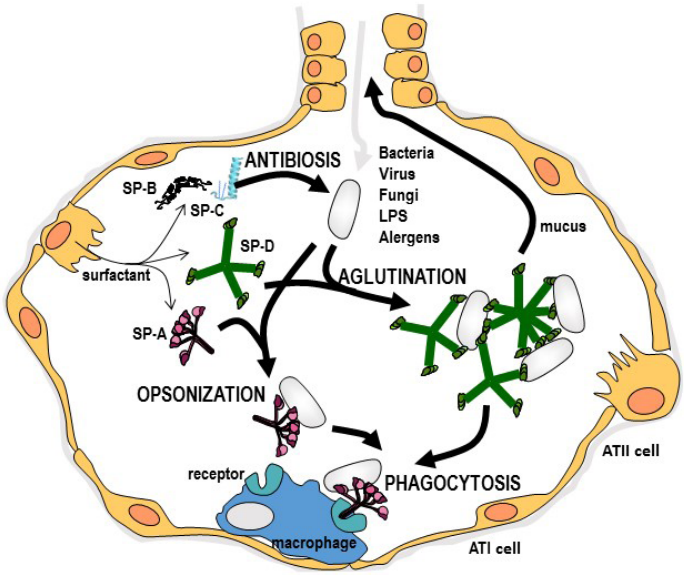

Figure 11. **Functions of hydrophilic proteins**. Pulmonary surfactant collectins SP-A and SP-D bind to a variety of bacteria, viruses, fungi or allergens and thereby function as opsonins to enhance the phagocytosis of cells and particles by alveolar macrophages via interaction with specific receptors for the collagenous parts of SP-A and SP-D. Some pathogens can be agglutinated by SP-A and/or SP-D to favour their removal by macrophages or their elimination through the upper airways. SP-B and SP-C also possess intrinsic antibiotic activity and they also participate in host-defense functions. Modified from (Pérez-Gil 2010).

number of non-pulmonary contexts, such as uterus, ovary, lacrimal gland (Akiyama, Hoffman et al. 2002), ear mucosa (Dutton, Goss et al. 1999) or in amniotic fluid (Miyamura, Malhotra et al. 1994) and placental membranes (Sun, Brockman et al. 2006), principally involved in immune regulatory responses.

4. Pulmonary surfactant biology: biogenesis and metabolism

In the alveolar epithelium, ATII cells are in charge of synthesizing and assembling the lipid and protein constituents of PS into structures that are stored as tightly packed membranous complexes called **lamellar bodies** (LBs) until they are exocyted into the airspaces (Goerke 1998). After a number of respiratory cycles, the "spent" secreted surfactant material is internalized by ATII cells and other cell types to avoid accumulation in the alveolar spaces. These processes are subjected to a strict modulation and defects in their regulation lead to pathophysiological manifestations, being some of them lethal.

4.1. Biosynthesis of PS components

4.1.1. Surfactant lipids

Lipids constituting PS are synthesized in the **endoplasmic reticulum** (ER) of ATII cells (**Figure 12**). *De novo* synthesis of PC predominantly occurs by the choline pathway and is catalyzed by the sequential activities of choline kinase, cholinephosphate cytidyltransferase and cholinephosphotransferase (Goss, Hunt et al. 2013). Although DPPC can be also formed by *de novo* synthesis, this is predominantly produced (75 %) via deacylation-reacylation of existing PC species, participating a calcium-dependent phospholipase A2 and lysoPC acyltransferase 1 (LPCAT 1) (Bridges, Ikegami et al. 2010). PG and PI are obtained from the common precursor CDP-diacylglycerol and cholesterol is mostly supplemented by serum lipoproteins, particularly VLDL (Guthmann, Harrach-Ruprecht et al. 1997).

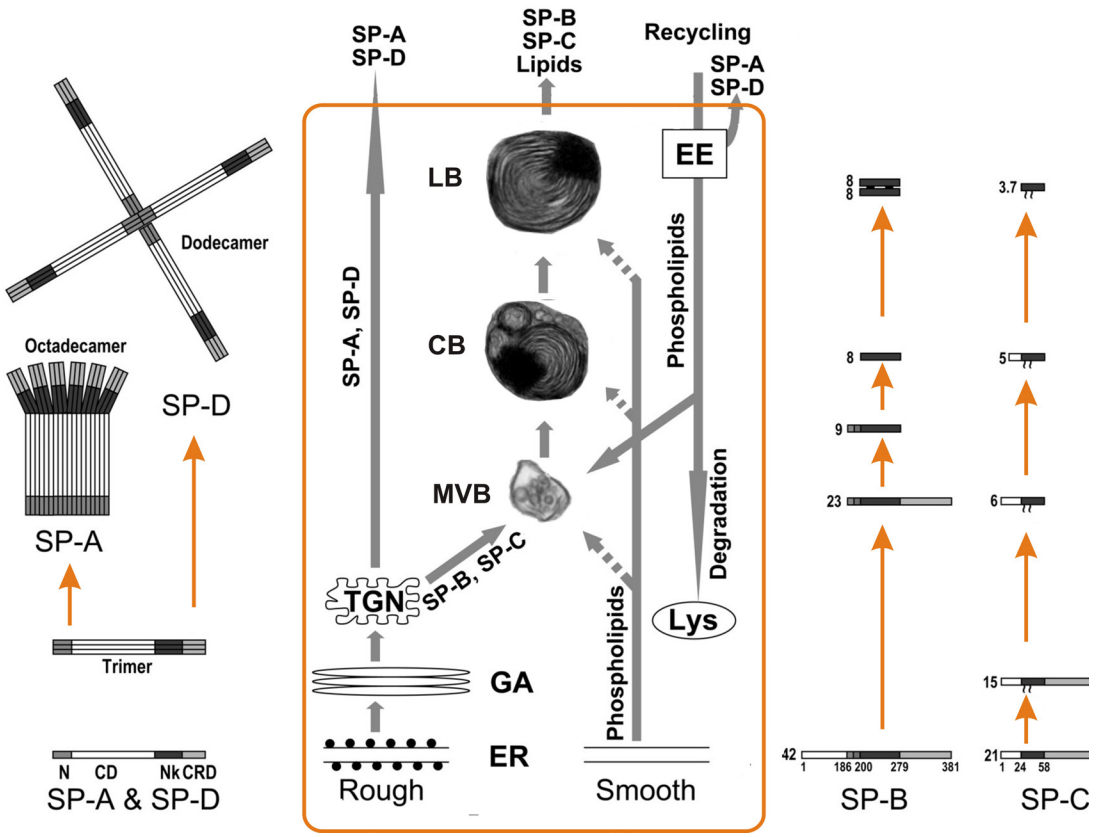

Figure 12. **Biosynthesis and trafficking of surfactant components**. Scheme illustrating the processing and secretion of the main constituents of PS. Left: Domain structure and assembly of the hydrophilic proteins SP-A and SP-D. N, NH2-terminal domain; CD, collagenous domain; Nk, neck domain; CRD, carbohydrate recognition domain. Middle: Lamellar body (LB)-independent (SP-A and SP-D) and LB-dependent (SP-B, SP-C, and phospholipids) secretion. *The secretion of SP-A via LB-dependent is still under debate. Recycling of surfactant components is also shown, followed by either degradation or recycling to multivesicular bodies (MVBs) and eventually re-secretion. ER, endoplasmic reticulum; GA, Golgi apparatus; TGN, trans-Golgi network; EE, early endosomes; Lys, lysosomes; CB, composite bodies. Right: Domain structure and processing of the hydrophobic proteins SP-B and SP-C. Processing products are shown at the level of their presumed locations in the organelles of secretory pathways. Modified from (Andreeva, Kutuzov et al. 2007) and (Ochs 2010).

Upon their biosynthesis in the ER, surfactant lipids are thought to be transported via different pathways, including vesicular tranport, non-vesicular transport and diffusion at membrane contact sites, although the specific weight of either of the routes is still unclear (van Meer, Voelker et al. 2008; Pérez-Gil and Weaver 2010). Vesicular transport through **Golgi apparatus** and **multivesicular bodies** (MVBs) is believed to play an important role. MVBs are organelles containing numerous internal unilamellar vesicles and are supposed to be the organelles preceding the final assembly and storage of surfactant (Pérez-Gil 2008). Besides the vesicular route, a direct traffic from ER to the LBs is also plausible, being involved the participation of transport proteins to facilitate the connection between both structures.

4.1.2. Surfactant proteins

Whereas secretion of phospholipids is mediated solely by LBs, secretion of surfactant proteins is more complex (**Figure 12**).

SP-A and **SP-D** are translated from their mRNA as propeptides that contain a signal peptide which leads them to the ER, where they are subjected to postranslational modifications such as glycosilations and hydroxilations before secretion to the alveolus. Whether the secretion occurs either as a regulated process via LBs or as a constitutive release by a different pathway has been a matter of debate for many years. Indeed, it has been previously assumed that SP-A is exocyted to the extracellular media not associated to LBs, probably joining and interacting with surfactant membranes once in the alveolar spaces (Ochs, Johnen et al. 2002). However, recent evidences seem to indicate that newly synthesized SP-A can be targeted to LBs for storage and subsequent secretion by controlled exocytosis (Fisher, Dodia et al. 2010).

SP-B and **SP-C** are produced as soluble proproteins with N- and C- flanking domains (proSP-B and proSP-C) that are subjected to multiple proteolytic cleveage steps before reaching their mature forms probably sharing processing enzymes (napsin A, cathepsin H, pepsinogen C) in a progressive acidificated environment along the exocytic pathway. SP-B initally contains a signal peptide that mediates the translocation of the protein to the ER (Brasch, Johnen et al. 2004), whereas SP-C does not contain a classic cleavable signal sequence, acting the mature SP-C domain itself as an anchoring motif sufficient for translocation (Russo, Wang et al. 1999). Both proteins follow a parallel pathwaty from the ER, reaching MVBs through the Golgi apparatus. Before entering to the LBs, they are transferred through different endosomal compartments as **composite bodies** (Weaver 1998). In human ATII cells there have been identified not only proSP-B, processing intermediates of proSP-B, and mature SP-B, but also fragments of the N-terminal propeptide. In fact, both mature SP-B and the N-terminal propeptide seem to be transported together to the LBs (Brasch, Johnen et al. 2004). ProSP-C is translocated to the ER for a proper folding and post-translational addition of covalent palmitic acid. Once released from the Golgi, the proprotein suffers the cleavage of the flanking domains to yield the mature SP-C module that is subsequently transferred to the lumen of LBs (Beers and Mulugeta 2005). The processing of SP-C to its mature form strictly needs the correct expression of SP-B, probably

related to the SP-B lytic and fusogenic activities, which might facilitate the access of proteases to the lumen of MVBs (Weaver and Conkright 2001).

4.2. Biogenesis of LBs

The LBs are the specialized organelles where PS is packed and stored in ATII cells, and their biogenesis is tightly reliant on the involvement of two proteins: SP-B and the recently described specific ATP-binding cassette transporter A3 (ABCA3).

On the one hand, **SP-B** seems to be key for the accumulation and packing of membranes in LBs, and its absence results in a deficit of LBs and a subsequent accumulation of their precursors, the MVBs (Stahlman, Gray et al. 2000). Furthermore, the membrane-membrane interactions that SP-B promotes *in vitro* (Cruz, Casals et al. 1997; Cruz, Worthman et al. 2000), might be responsible for the tight packing of membranes observed in LBs since, when SP-B is not present, LBs result loosely packed. Concerted with SP-B action, the acidic pH present in LBs has been also proposed as a complementary force to trigger full membrane packing, by permiting the proper conformation and state of charge of surfactant lipids and proteins (Ruano, Pérez-Gil et al. 1998).

On the other hand, the relevance of the role that **ABCA3** plays on the LB biogenesis has been extensively discussed in the latest years. This protein belongs to the family of ABC transporters, which bind and hydrolise ATP coupled to the transport of different molecules, like phospholipids, through membranes. Recent evidences suggest that DPPC and PG are directly transferred to the LB through a vesicle independent mechanism in wich ABCA3 is involved. ABCA3 would act as a flippase, significantly enhancing the catalysis of the transmembrane movement of saturated phospholipid species, originating an asymmetric character of the LB limiting membrane (Pérez-Gil 2008). Indeed, other ABC-type flippases have been previously described to maintain the assymetry of most cellular membranes, performing a selective pumping of certain lipid species from one leaflet of membranes to the other (Pomorski and Menon 2006). The progressive accumulation of phospholipids into the inner leaflet could only be relaxed upon the creation of membrane folds, generating a driving force to produce and accumulate membrane structures into the lumen of MVBs, which in a later stage would be tightly packed as LBs, thanks to the action of SP-B and the fluidizing effects of cholesterol/minor phospholipids (Pérez-Gil 2008;

Pérez-Gil and Weaver 2010). Furthermore, a putative location of ABCA3 in inner membranes could promote additional membrane vesiculation at different levels, what could explain the onion-like morphology typical of LBs. In addition, it has been proposed that most of these membranes could form a single interconnected structure that might facilitate its rapid and cooperative unravelling observed upon secretion (Pérez-Gil 2008; Ravasio, Olmeda et al. 2010).

4.3. Secretion and unpacking of LBs

A burst in secretion of surfactant occurs at birth with the first breath, and afterwards, the requirement for synthesis becomes lower (Agassandian and Mallampalli 2013). Surfactant turnover is considerably low, between about 4 and 11 hours (Wright and Clements 1987), but it is accelerated under conditions of physical exercise, even though a single deep breath or a yaw is sufficient to trigger the process (Dietl, Haller et al. 2012). Surfactant secretion is a highly regulated event and it involves the concerted action of a number of proteins and other constituents throughout the exocytotic pathway (Dietl and Haller 2005).

4.3.1. Stimuli of surfactant secretion

Presumably because this process is vital for the survival of the organism, there are several independent pathways for stimulating secretion, which work through different cell surface receptors and signalling mechanisms (Mason and Voelker 1998). Indeed, surfactant exocytosis can be triggered by numerous **chemical** and **physical stimuli**, although the two probably most potent and physiologically important are **alveolar stretch** and **extracellular ATP** (Dietl, Liss et al. 2010). A number of agonists have been reported to activate ATII cells, including β2-mimetic drugs (Dobbs and Mason 1979), ATP and other purinergic receptor agonists (Gilfillan and Rooney 1987) as well as para- or endocrine mediators such as gastrin-realising peptide, prostaglandin derivatives, vasopressin and endothelin-1 (Dietl and Haller 2005). However, under experimental conditions, lung distension or ATII cell stretch have been considered so far to be the most physiologically relevant factor and it is likely that the increase of surfactant release, which is detected after only a single inflation of isolated perfused lungs, is the result of a related epithelial cell mechanical stretch (Nicholas, Power et al. 1982).

4.3.2. Fusion of LBs with plasma membrane

Numerous evidences indicate that **Ca^{2+}** is a pivotal factor to trigger the LB fusion event in the ATII cell. It is known that β2-adrenergic stimulation induces the formation of cAMP, but also elicits a transient increase of intracellular calcium, whereas **ATP** involves P_1receptor-dependent cAMP formation as well as P_2receptor-dependent phosphoinositide hydrolysis and subsequent Ca^{2+} mobilization (Haller, Ortmayr et al. 1998). The actions of Ca^{2+} and those of cAMP are additive, consistently with the concept that surfactant exocytosis is independently regulated at various sites (Gobran, Xu et al. 1994). A model can be conceptualized from analyses of secretion stimulated by ATP and use the P2Y2 purionoreceptor as an example of a seven membrane spanning G-protein coupled receptor (see **Figure 13** for details). Additionally, among Ca^{2+} permeable channels, which might be involved in stretch-induced Ca^{2+} entry in ATII cells, mechanosensitive channels like those from the **transient receptor potential** (TRP) channel family have been proposed to play a potential role (Dietl, Liss et al. 2010). On the other hand, besides calcium signaling pathways, other powerful stimulus is the treatment with **phorbol esters**, which activate protein kinase C (PKC) and does not cause increments in intracellular Ca^{2+}, althougt the process seems to be not completely Ca^{2+} independent (Frick, Eschertzhuber et al. 2001).

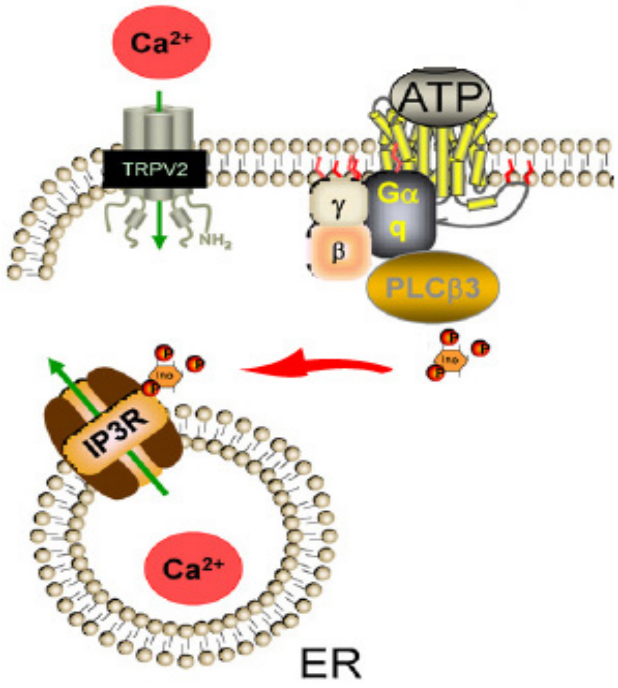

Figure 13. **Physical/chemical stimulation of surfactant exocytosis**. Schematic representation of purinergic and mechanosensitive signaling, which trigger surfactant exocytosis in ATII cells. ATP binds P2Y2 receptor, leading to activation of phospholipase C. Cleavage of PIP_2 by phospholipase C yields IP_3 and DAG. After diffusion through the cytosol, IP_3 interacts with and opens Ca^{2+} channels in the membrane of endoplasmic reticulum, causing release of stored Ca^{2+} ions into the cytosol. Rapid, cell stretch-induced Ca^{2+} entry can take place via the transient receptor potential (TRP) channel. Adapted from (Dietl, Haller et al. 2012).

In general, an elevated concentration of calcium is assumed to facilitate LB transfer to and docking with the plasma membrane by cytoeskeletal elements and molecular motors (Dietl and Haller 2005; Dietl, Haller et al. 2012).

When LBs are close to the plasma membrane, they connect with the extracellular space through a single pore, formed by the limiting membrane of the vesicles and the plasma membrane. Among the bioactive lipid metabolites result of the purinergic stimulation that might promote LB fusion, phosphatidic acid (PA) appears specially promising thanks to its ability to change lipid topology. PA is known to induce negative plasma membrane curvature thanks to its small head group combined to two fatty-acyl side chains, likely promoting lipid merging with the vesicle membrane and hemi-fusion (Zeniou-Meyer, Zabari et al. 2007).

The **fusion pores** generated during surfactant exocytosis are about half of the average diameter of the associated LBs, and this imposes a deformation of LBs during secretion, which might be significant for unraveling of LB material, or even for the transformation into its active forms (Haller, Dietl et al. 2001). This restriction could be also responsible for the slowered kinetics observed in LB exocytosis, since once the fusion pore is formed, it still takes some time for the packed membranes to be completely expelled out of the cell (Singer, Frick et al. 2003).

4.3.3. Postfusion and unravelling of LBs

The contact of the internal medium of LBs with the extracellular environment via the fusion pore is thought to prompt modifications in membrane packing, due perhaps in part to re-hydration but also likely to pH neutralization and other potential changes in the ionic environment (Pérez-Gil 2008), including a decrease in the levels of Cl^- or Ca^{2+}, which are known to be considerably higher inside LBs (Eckenhoff and Somlyo 1988).

The unpacking of LBs is a cooperative and almost instantaneous event and frequently, it seems to be originated from a defined peripheric point of the secreted structure, with inner layers being expelled out of the LB preceding the more external ones (Haller, Dietl et al. 2004). The presence of a pressure gradient towards the center of the LB result of the progressive pumping activity of ABCA3 might be a tentative explanation to this observation, although the possibility of local protein-protein interactions forming valve-operating structures to favor a cooperative unravelling could not be discarded either (Pérez-Gil 2008).

4.4. Extracellular surfactant

4.4.1. Membrane organization in tubular myelin

In the alveolus, a number of potential elements are believed to participate in the unravelling of LBs, to give rise to the definitive lipid-protein networks in charge of accomplishing the multiple activities of PS. On the one hand, strong evidences suggest that the highly packed membranes constituting secreted LBs are adsorbed spontaneously to the interface whithout passing through any unpacked intermediary (Haller, Dietl et al. 2004). However, on the other hand, some extracellular structures have been found in the alveolar hypophase, rearranged in a lattice-like structure of elongated proteolipid tubes termed **tubular myelin** (TM) and electron micrographs have shown a continuity between LB and these structures (Williams 1977). In the aqueous hypophase, SP-A is thought to contribute to LB unpacking mainly through the conversion of multillamelar arrays into TM. According to this, the square membrane lattices typical of TM are proposed to be sustained by SP-A/SP-A interactions via their headgroups, since the molecular size of the SP-A complexes coincide with that of the periodic lattice, around 40 nm (Nag, Munro et al. 1999) and their presence at the corners of the lattice has been confirmed by immunolabeling (Voorhout, Veenendaal et al. 1991). In the current model, besides SP-A, the presence of SP-B/SP-B interactions would be crucial in the TM architecture by favoring membrane-membrane interactions, probably followed by membrane fusion (Pérez-Gil 2008) (**Figure 14**). Furthermore, lipids are not considered passive structures but instead can play an important role in determining the three-dimensional organization of TM (Palaniyar, Ridsdale et al. 1999). Interestingly, it is possible to reconstruct TM *in vitro* by combining synthetic lipids (DPPC and PG), SP-A, SP-B and calcium (Suzuki, Fujita et al. 1989), although the manner in which this structure is formed is still not clearly understood, neither its specific function in surfactant activities. In this regard, some authours interprete TM as the major reservoir of surfactant material in the alveoli whereas others support an antimicrobial function, in which TM would act as a high density SP-A lipid network in the first line of defense against pathogens (McCormack and Whitsett 2002).

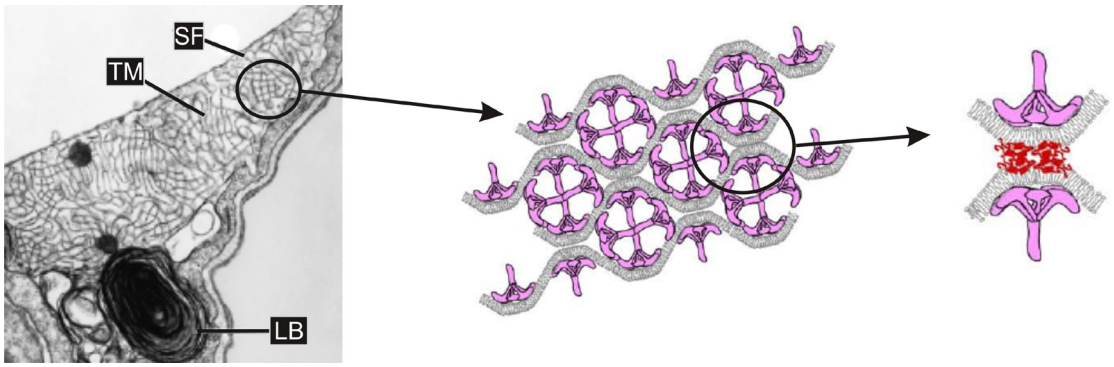

Figure 14. **Extracellular surfactant structures**. A freshly secreted lamellar body (LB) on top of the alveolar epithelium is partially unravelling to form tubular myelin (TM), which transfers surfactant to the air-liquid interface to generate the surface film (SF) (left). Model to explain the possible role of SP-A (middle and right) and SP-B (right) in the assembly of tubular myelin network (see text for discussion). Adapted from (Ochs 2010) and (Pérez-Gil 2008).

4.4.2. Surfactant at the air-liquid interface

Once the surfactant material is secreted and unpacked in the aqueous hypophase, it adsorbs onto the air-liquid interface to form the active **surface film**. The adsorption process occurs very rapidly in order to stabilize the interface against the mechanical forces that tend to collapse the alveolus. The surface film consists of a monolayer highly enriched in DPPC and lipid-protein stuctures attached to it. The further **enrichment in DPPC** is believed to be achieved by selective desorption of non-DPPC lipids during repetitive breathing cycles (Veldhuizen and Haagsman 2000). With regard to the **multilayered stacks** associated to the monolayer, they are thought to be a reservoir of surface active molecules involved in the respiratory dynamics, including the contribution of SP-B and SP-C in its formation, stability and recycling (Pérez-Gil and Keough 1998). Additionally, and as we stated above, TM could also feed the monolayer and can be part of the surface film.

A number of evidences support the notion that both SP-B and SP-C favor reversible compression-driven transitions from bilayers to interfacial films, prompting the generation of the multilayered films at the interface. Therefore, SP-C would facilitate the formation of multilayers associated to the surface monolayer, which would contribute to the lipid pool for the compression-expansion cycles (Kramer, Wintergalen et al. 2000). In parallel, SP-B would promote the creation of bilayer patches connected to the interface (Krol, Ross et al. 2000) as well as large membrane-membrane interactions in multilayered structures that, in the presence of phase

segregation, exhibit a considerable cohesivity (Bernardino de la Serna, Vargas et al. 2013). In general, the combined effect of both proteins supports the required tension reduction and a proper film stability whithout compromising the dynamic character of the lipid multilayers.

4.5. Surfactant recycling and homeostasis

Sucessive compression-expansion cyling of PS provokes a progressive appearance of less active fractions, result of the detachment of small particulate entities from the interface, changes in lipid/protein organization, and oxidation of lipid and protein species due to a repetitive exposure to air (Ueda, Ikegami et al. 1994; Pérez-Gil and Weaver 2010). Thus, to maintain a fully functional surface film, a proper refinement via efficient **removal** and **clearance of spent surfactant** and incorporation of fresh material is required. Surfactant components can be **recycled** by ATII cells that uptake them to be reincorporated into LBs, for new secretion. This recycling is promoted by SP-A via specific interaction with a receptor present in the cell surface, although its identity is still unknown (Agassandian and Mallampalli 2013). Phospholipids and SP-A are internalized together and sorted to early endosomes. However, some uptaked surfactant is directly degraded, largely by alveolar macrophages (Abe, Hiraoka et al. 2004) and the degradation products are reutilized to synthesize new components. Additionally, a small amount of surfactant moves up the airways through the mucociliary scalator and it is also removed through the epithelium-endothelium barrier into the blood (Wright 1990). To maintain the intracellular pool size, new synthesis of surfactant must be coupled to its depletion. Surfactant proteins may be involved in regulating pool size by modulating both secretion and uptake rates (Wright and Dobbs 1991). In this regard, SP-D seems to be particularly involved in the regulation of surfactant homeostasis altering surfactant structure by unknown mechanisms. SP-D preferentially binds PI, causing lysis of surfactant membranes and converting the lipid forms into simpler structures that seem to be critical for surfactant uptake by ATII cells and normal surfactant homeostasis (Ikegami, Grant et al. 2009).

5. Surfactant deficiencies and inactivation

PS is an essential complex for life and its absence, deficiency or inactivation affects lung compliance and gas exchange and contributes to the development and outcome of severe respiratory disorders in neonates and adults. Surfactant inactivation can be arosen from endogenous defects like genetic disorders associated to mutations at genes related to surfactant or from the deleterious action of exogenous effectors.

5. 1. Endogenous defects

The presence of SP-B is absolutely essential for breathing and certain mutations in the gene codifying SP-B (SFTPB) are lethal in newborn infants, which develop **neonatal distress respiratory syndrome** (NRDS) and other severe respiratory diseases such as congenital alveolar proteinosis (Nogee, Garnier et al. 1994; Williams, Christodoulou et al. 1999). Partial SP-B deficiencies also leads to a dysfunctional surfactant that exhibits a poor interfacial adsorption, inability to reach minimal surface tensions and to sustain proper dynamics upon the expansion-compression cycles as well as an intrinsic mechanical instability of the surface films (Schürch, Ospina et al. 2010; López-Rodríguez and Pérez-Gil 2014).

With respect to SP-C, although its deficiency is apparently compatible with an operative surfactant, mutations in its coding gene (SFTPC) seem to have more subtle long term effects, related to the appearance of **interstitial lug diseases** (Brasch, Griese et al. 2004) and chronic pathologies such as **idiopathic pulmonary fibrosis** (Korfei, Ruppert et al. 2008).

As expected, given the role of the pulmonary collectins in the alveolar spaces, their partial or total absence mainly results in lungs with a diminished innate immune response. SP-A null mice exhibit a defective clearance of pathogens and increased susceptibility to infections (LeVine, Gwozdz et al. 1999). Besides the immunological impairment, absence of SP-D also leads to accumulation of lipids, acute **pulmonary alveolar proteinosis**, foamy alveolar macrophages and emphysema (LeVine, Gwozdz et al. 1999; Guo, Lin et al. 2001).

In addition to deleterious mutations in surfactant proteins, deficiencies in other related proteins have been also associated to lung pathologies; i.e fatal surfactant deficiency related to mutations in ABCA3 (Shulenin, Nogee et al. 2004).

5.2. Inactivation by external agents

Under pathological conditions, PS may encounter exogenous substances with a potential capacity to impair its surface activity. In general terms, the **exogenous inactivation** of PS relies on two distinct mechanisms: **competition** with other surface-active molecules for the air-liquid interface or insertion of **membrane-perturbing molecules** that disrupt the structure of surfactant (Zuo, Veldhuizen et al. 2008).

The first case may result of leakage from the vascular endothelium and the subsequent release of serum proteins (i.e.: albumin) into the alveolar lumen, as a consequence of lung injury or edema. In this situation, the rate of surfactant adsorption is strongly affected by both the presence of the serum proteins at the surface (steric impediment) and the competitive adsorption of serum proteins (Fernsler and Zasadzinski 2009). **Acute respiratory distress syndrome** (ARDS), is a worldwide public health problem with a baseline mortality risk of 40-45 % (Phua, Badia et al. 2009), where serum and plasmatic surface-active proteins reach the interface provoking surfactant inactivation as well as alveolar collapse and alterations in gas exchange, yielding to hipoxemia and organ failure (Dushianthan, Grocott et al. 2011).

An example of the second mechanism is the direct exposition of surfactant complexes to meconium that occurs during **meconium aspiration syndrome** (MAS), in which a newborn inhales his first stool before or during delivery due to prenatal stress. Meconium is basically constituted by bile acids and cholesterol, which, once incorporated in excess into surfactant membranes induces important alterations in their structure and dynamics (López-Rodríguez, Echaide et al. 2011).

Supplementation with **exogenous surfactant preparations**, obtained from animal sources, have proved to be highly efficient in preterm newborns affected by neonatal respiratory distress syndrome (Blanco and Pérez-Gil 2007). Surfactant administration may also partially reduce the

severity of the respiratory illnesses such as ARDS or MAS although the relative efficacy and clinical benefit is insufficient in cases of critical lung injury (Spragg, Taut et al. 2011). In this context, recent investigations have shown that exposure of PS complexes to **hyaluronan** results in an improved resistance to inactivation by serum or cholesterol (López-Rodríguez, Cruz et al. 2013). Interestingly, even after removal of the polymer, PS membranes persist in a highly activated and resilient state, suggesting that transient exposure to hyaluronan or similar polymers could constitute a potential strategy for the production of more efficient clinical surfactant materials (López-Rodríguez and Pérez-Gil 2014).

6. Modeling the alveolar type II cell

In the previous sections we have briefly introduced the most important hallmarks of the biogenesis of pulmonary surfactant in ATII cells, including the biosynthesis and intracellular traficking of its constituents as well as its assembly and secretion into the alveolar airspaces to accomplish its different functions. However, despite the fact that ATII cells have been object of extensive investigation over the years, understanding of the alveolar epithelial phenotypic expression and surfactant metabolism in vivo in either healthy or diseased lungs is not completely fulfilled. Thus, given their importance, a large number of different animal models have been used to study ATII cell phenotype *in vivo* and *ex vivo*.

6.1. Primary cultures

Since the first method of isolating ATII cells was published in 1974 (Kikkawa and Yoneda 1974), much light has been shed on ATII cell characteristics upon their isolation from a variety of species, mainly adult **rodents** and **rabbit**. As with all primary cell isolations, either viability and purity can vary substantially among different purifications. Nevertheless, optimization of the isolation protocols has been pursued over the last years, and recent protocols report purities > 90 % (Roper, Staversky et al. 2003) or even > 99 % (Vanderbilt, González et al. 2015). Despite they represent the closer option for mimicking the *in vivo* condition, the primary culture of ATII cells

has disadvantages in that it requires recurring cell isolations or in that cells undergo different extents of phenotipic drift in culture, acquiring some characteristics of type I cell (Fuchs, Hollins et al. 2003; González, Yang et al. 2005; González and Dobbs 2013). As an alternative, for example, human primary ATII cells obtained from lung resection have been subjected to immortalization, but the produced cells show a phenotype similar to that of ATI cells (Kemp, Thorley et al. 2008). In spite of their handicaps, cultivation of primary cells is still the preferred approach for a number of researchers to investigate molecular biology, biochemistry and genetics of ATII cells.

6.2. Cell lines

There have been many attempts to establish passaged cell lines as ATII cell models but none display the full range of morphologic, biochemical and molecular characteristics of freshly isolated alveolar epithelial cells (González and Dobbs 2013).

To date, the **A549 cell line** is probably the most extensively used cell model for ATII cells. This tumor-cell line was initiated in 1972 from a human alveolar cell carcinoma (Giard, Aaronson et al. 1973) and it was reported to have morphologic and biochemical features of ATII cells, including multillamelar cytoplasmatic inclusion bodies as well as secretion of disaturated PC in response to secretagoges (Lieber, Smith et al. 1976; Smith 1977; Shapiro, Nardone et al. 1978). A549 cells have been used as a in vitro model for ATII cell dysfunction (Balis, Bumgarner et al. 1984) and drug metabolism (Ning, Yu et al. 2015) as well as to study surfactant production and regulation (Salmona, Donnini et al. 1992) and as a transfection host (Giavedoni and Yilma 1996).

However, the suitability of the A549 cell line as a model for ATII cells has been questioned by researchers since, for example, the surfactant produced by A549 cell cultures differ significantly from that of primary cells (Mason and Williams 1980). In addition, recent findings suggest that A549 are more similar to differentiated ATI than to undifferentiated ATII cells, casting furter doubt on the use of A549 cells to represent ATII cells (Swain, Kemp et al. 2010).

Besides A549 and with a minor significance, other cell lines like **L2** have been also used to model ATII cells. L2 is a permanent non tumor-derived epithelial cell line and it was first described in 1974 (Douglas and Kaighn 1974). L2 cells have been shown to enclose osmiophilic lamellar inclusions in both early and later passages (Hoffmann, Grote et al. 1995).

Interestingly, L2 cells have been described to express inducible nitric oxide synthase and thus, to generate nitric oxide (Hoffmann, Grote et al. 1995; Su, Day et al. 1996). This fact has been related to a putative contribution of distal airway epithelial cells to pulmonary host defense mechanisms and to pulmonary vasoregulation.

Objectives

Pulmonary surfactant (PS) membranes, as defined from their biogenesis in the alveolar type II (ATII) cells, are assembled into lamellar bodies (LBs) as a particularly dense structure which is preserved upon secretion but is rapid and cooperatively unpacked once in contact with the air-liquid interface. We presume that interfacial films formed by freshly secreted surfactant have structural features and surface properties that are different from those originated from partially "spent" surfactant as purified from animal lungs. In fact, we hypothesize that in whole native surfactant (NS) purified from bronchoalveolar lavage (BAL), considered so far as the "gold standard" of an optimized biophysical surface behaviour, coexist active membrane fractions with deactivated surfactant or other surfactant-like structures playing different roles in other locations of the respiratory airways different than alveoli.

To get deeper insight in the way in which PS is packed into lamellar bodies as well as to collect freshly secreted material for its structural and functional assessment, the use of *in vitro* models representing ATII cells become indispensable. Considering the lack of reliable surfactant-producing cell lines, we have taken advantage of primary cells isolated from animal sources. However, as mentioned in the introduction, primary ATII cells have important handicaps, including the necessity of an extensive use of animals and the progressive lack of type II features. In this context, we have also explored the potential of differentiation of mesenchymal stem cells isolated from human placenta into cells with a phenotype consistent with ATII-cells, to be useful not only for the study of surfactant biogenesis but also as an in vitro model for drug metabolism and other biopharmaceutical applications.

Taking all this into consideration, the specific objectives addressed in the present Thesis include:

1. Study of the **micro- and nanostructural organization of surfactant membranes stored in intracellular LBs as well as freshly secreted in the form of lamellar body-like particles (LBPs)** in comparison with native surfactant complexes purified from BAL. This includes the analysis of phospholipid packing/hydration and acyl chain order/dynamics, and the characterization of temperature-dependent packing, order, phase and lipid polymorphism (**Chapter 1**).

2. Examination of the **structural and functional diversity present in NS complexes isolated from BAL.** This will be possible upon fractionation of NS into discrete subtypes for morphological, biochemical and functional characterization (**Chapter 2**).

3. **Differentiation of human placental mesenchymal stem cells into ATII-like cells** (ATII-LCs). The characterization of this process will include the determination of expression of ATII cell markers at a gene and protein levels, the investigation of the capacity of ATII-LCs to generate surfactant-like assemblies and exocyte them upon physiological stimulation, and the assessment of the biophysical properties of material freshly secreted to the extracellular medium (**Chapter 3**).

4. **Optimization of ATII-LC cultures under physiological conditions mimicking the native alveolar microenvironment**. This will include the characterization of surfactant-related markers, barrier function and type II morphological features after differentiation in advanced cultures. The utility of this model will be explored in cytotoxicity studies and by evaluation of the responsiveness of ATII-LCs to nanoparticle preparations and molecule uptaking (**Chapter 4**).

Materials and methods

MATERIALS

Cell cultures

Isolation and culture of rat alveolar type II cells

Alveolar type II cells (ATII cells) were isolated from the lungs of anesthetized male Sprague-Dawley rats based on a protocol previously described (Dobbs, González et al. 1986) with minor modifications (**Figure 15**). Anaesthesia consisted on a mixture of 110 mg/kg ketamine (Ketamidor 10 %; Merial, France) and 12 mg/kg xylazin (Rompun 2 %; Bayer, Germany) and was administered intraperitoneally to rats weighting about 200 g (**Fig. 15A**). The abdominal cavity was opened and a heparin solution (400 IU/kg body weight) (Chiesi, Italy) was injected into the vena cava inferior with a 0.30x12 mm BL/LB needle (**Fig. 15B**). Then, before opening the thoracic cage, a small hole in the diaphragm was made in order to deflate the lungs. After incising the neck, the submandibular tissue and the thyroid gland were removed, passing a suture under the trachea, nicking it and cannulating it with a tracheal catheter, fixing it tightly with the suture (**Fig. 15C**). The chest wall was then incised along the entire length of the sternum and the anterior portions of the diaphragm so that the chest was opened. Once exposed the heart and the lungs, the auriculum of the right atrium of the heart was cut off and an additional catheter was placed into the pulmonary artery (**Fig. 15D**) connected to a perfusion bottle containing phosphate buffered saline. At this point, the perfusion system was opened to get the lungs free of blood and concomitantly, air was injected through the tracheal catheter to inflate the lungs. The lungs were inflated several times to total lung capacity (7-10 mL) using a 10 mL syringe in order to expand them and allowing perfusion to clear the lungs completely of blood (**Fig.15E**). In this step, the heart should still be spontaneously beating for a proper clearance of blood from the lungs. A successful perfusion can be noted when the lungs look completely white, without red or pink areas. Then, lungs were excised and washed via the trachea 8 times with solution “B” containing 1 M NaCl, 40 mM KCl, 0.1 M phosphate buffer, 75 mM HEPES, 8 mg/mL glucose and 0.6 mg/mL EGTA, 2 times with solution “A” containing 0.14 M NaCl, 5 mM KCl, 0.1 M phosphate buffer, 10 mM HEPES, 2 mM $CaCl_2$, 2.5 mM $MgCl_2$, 1 mg/mL glucose, pH 7.4 and 1 time with solution “C” containing 0.25 mg/mL elastase (Elastin, USA) and 0.05 mg/mL trypsin (Sigma-Aldrich, Germany) in solution “A”.

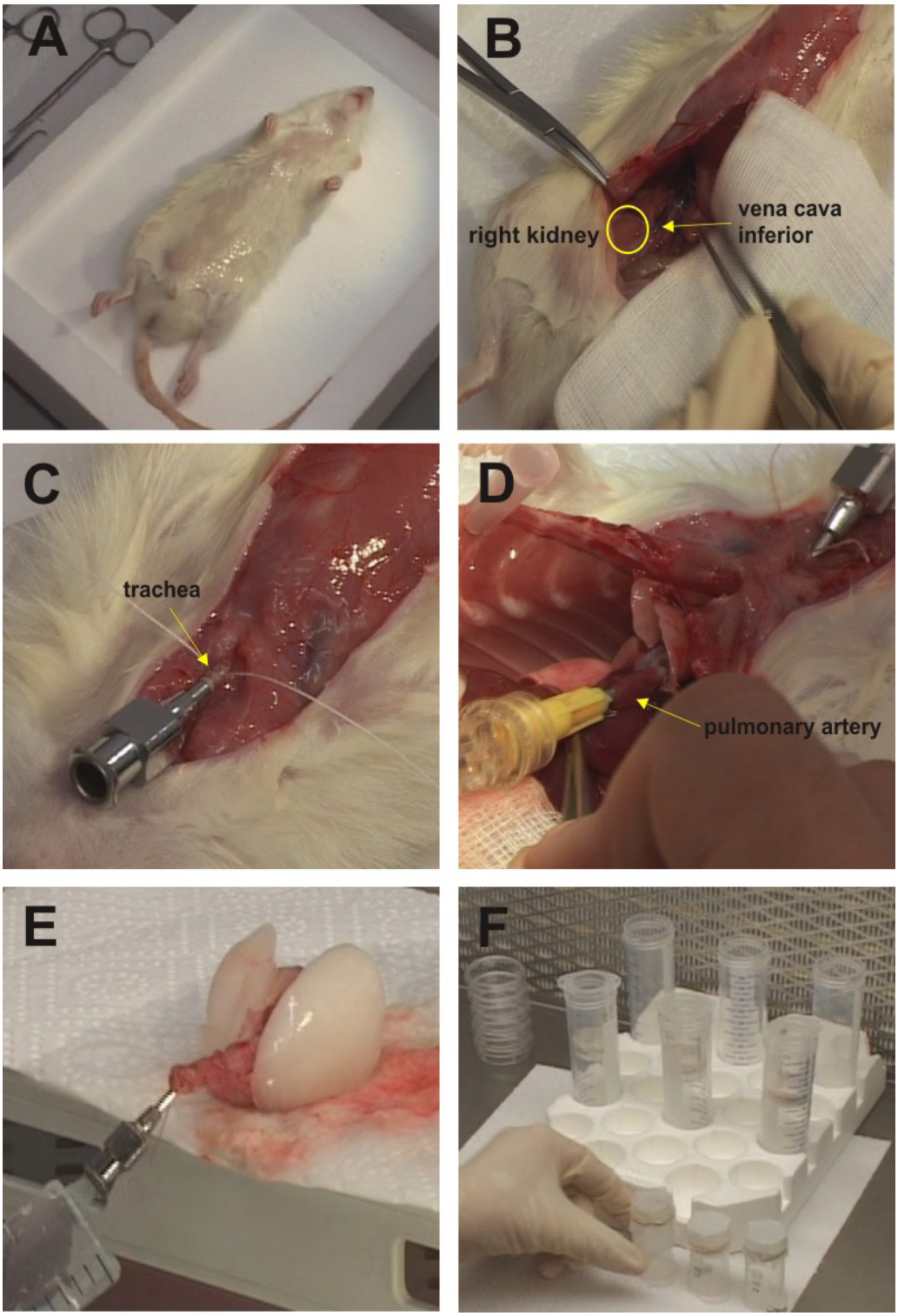

Figure 15. **Critical steps in the surgical procedure for the isolation of rat alveolar type II cells**. **A**. Male Sprague-Dawley rat anesthetized with ketamine/xylacine. **B**. Injection of heparin through vena cava. **C**. Placement and fixation of the tracheal catheter. **D**. Insertion of the heart catheter into the pulmonary artery to initiate the perfusion. **E**. Filling of the lungs with washing and enzymatic solutions through the tracheal catheter. **F**. Filtering of the homogenized lung tissue with gauze and nylon meshes. Photographs have been extracted with permission from a video recorded by Dr. Thomas Haller (Innsbrück University).

During the incubation with solution "C", the excised lungs were immersed in physiological NaCl solution, in a water bath maintained at 37 °C during 15-20 min. The elastase solution was added continuously at 5 cm H_2O pressure. The timed intratracheal instillation of elastase results in an enrichment of alveolar epithelial cells since they are effectively liberated from the underlying basement membrane, leaving most of the interstitial and vascular compartments intact. After enzymatic digestion, trachea and large airways were cut away and discarded. The lungs were minced with sharp scissors to tissue cubes of a final size of approx. 1 mm, in the presence of solution "D" containing 1.3 mg/mL DNAse I (Roche, Germany) in solution "A". After mincing, 5 mL fetal bovine serum (FBS) (Lonza, Germany) were added to stop the Dnase reaction. At this point, the cell suspension was filtered sequentially through meshes of different diameters coupled to falcons: 2 layers of gauze, 1 layer of gauze, and then nylon meshes of 150, 20 and 7 µm (**Fig. 15F**). Filtering occurred by gravity, and additional filters were used as needed when flow decreased due to filter clogging. Then, the suspension was centrifuged at 130 x g for 8 minutes, the supernatant was discarded and the pellet containing the cells was resuspended in 30 mL Dulbecco's Modified Eagle's Medium (DMEM) (Lonza, Germany) without FBS. The cells were put in an IgG-coated plate and maintained for 15 min in an incubator, to separate ATII cells by negative selection from most of the rest of cell types which interact with IgG molecules attached to the bottom of the plate. After shaking the plates gently, the cell suspension was returned to a Falcon tube and was centrifuged again. Cells were resuspended in DMEM with 10 % FBS and 1 % penicillin/streptomycin and seeded in culture plates for cultivation.

Isolation and culture of human alveolar type II cells

Human alveolar type II epithelial cells were freshly isolated from non-tumor lung resections under approval by the Saarland State Medical Board (Germany) according to an adapted protocol (Fuchs, Hollins et al. 2003; Ehrhardt, Kim et al. 2005; Daum, Kuehn et al. 2012) and with the generous technical assistance of Marius Hittinger, from Saarland University. Lung tissue was digested after chopping with trypsin type I (Sigma) and elastase (CellSystems, St Katharinen, Germany) in balanced salt solution for 40 min at 37°C. Purification of ATII cells was performed by consecutive steps of differential cell attachment, Percoll density gradient and magnetic cell

sorting. Purified ATII cells were seeded at a density of 6 x 10^5 cells/cm^2 on collagen (Sigma-Aldrich) and fibronectin (BDBioscicences, Belgium) coated plastics and cultured in SAGM (Lonza, Belgium). ATII cells were used 24 h post-seeding.

Isolation and culture of human Decidua-derived Mesenchymal Stem Cells (DMSCs)

Human placentas were provided by the Department of Obstetrics and Gynecology from healthy mothers under written consent approved by the Ethics Committee from Hospital Universitario 12 de Octubre. DMSCs were isolated and cultured from extraembryonic membranes as described previously (Macías, Grande et al. 2010). First, placental membranes were dissected and washed in phosphate-buffered saline (PBS) including 100 IU penicillin and 100 µg/mL streptomycin in order to remove red blood cells. Afterwards, tissue was digested with trypsin-versene (Lonza, Spain), twice and cells suspensions were centrifuged at 400 x g for 10 minutes, resuspended in PBS plus 2 mM EDTA and 0.5 % human serum albumin, and subsequently lysed in 0.8 % ammonium chloride solution for 15 minutes to further eliminate any remanent erythrocytes. Finally, cells were seeded at a density of 1.16 x 10 5 cells/cm^2 and cultured at 37 °C, 5 % CO_2 and 95 % humidity in Dulbecco's modified Eagle Medium (Lonza) supplemented with 2 mM L-glutamine, 0.1 mM sodium pyruvate, 55 µM of β-mercaptoethanol, 1 % non-essential amino acids, 1 % penicillin/streptomycin, 10 % fetal bovine serum and 10 ng/ml of Epidermal Growth Factor (Sigma-Aldrich Química, Spain). Non-adherent cells were washed off and adherent cells were grown to confluence and passaged at a density of 4-5 x 10^4 cells/cm^2.

Differentiation of DMSCs into ATII-Like Cells (ATII-LCs)

DMSCs grown at confluence were differentiated in Small Airway Epithelial Cell Growth Medium bullet kit (Lonza) for 4-5 days. This media was supplemented with the following factors: bovine pituitary extract, hydrocortisone, human epidermal growth factor, epinephrine, transferrin, insulin, retinoic acid, triiodothyronine, gentamycin and bovine serum albumin, as indicated by the manufacturer. Fresh medium was carefully added to prevent cell detachment every 3 days. Differentiation was assessed analyzing the morphological changes of the cells by

phase-contrast microscopy using a Leica DMIL microscope (Leica Microsistemas SLU, Barcelona, Spain).

In addition to the use of the conventional submerged cultures (SC), DMSCs were also differentiated under the influence of an air-liquid interface (ALI) exposing their apical part to the air. For cultures at the ALI, cells were grown on Transwell Clear Inserts (6.5, 12 or 24 mm in diameter, pore size 0.4 µm; Corning, VWR, Dublin, Ireland). Transwell inserts are permeable supports with independent access to both sides of a monolayer and in which the cells are fed only from the basolateral side, keeping the apical part exposed to the air (**Figure 16**). Apical and basolateral fluid volumes were 500 and 1500 µL to grow undifferentiated DMSCs and for differentiation in SC (**Fig. 16B**). For differentiation under the ALI, the apical fluid volume was removed maintaining the initial fluid volume in the basolateral compartment.

Additionally, transwell filters were precoated with a mixture of fibronectin and collagen in order to at least partially mimic the extracellular matrix. To this end, 100 µL of fibronectin (Becton Dickinson, Heidelberg, Germany) at a concentration of 1 mg/mL and 100 µL of a 3 mg/ml collagen (Sigma) solution were added to 10 mL of sterile water. The final concentration was 10 µg/mL and 30 µg/mL for fibronectin and collagen, respectively. 200 µL of this coating solution was deposited onto each insert (0.33 cm^2 growth area) and incubated for 2 h at 37 °C.

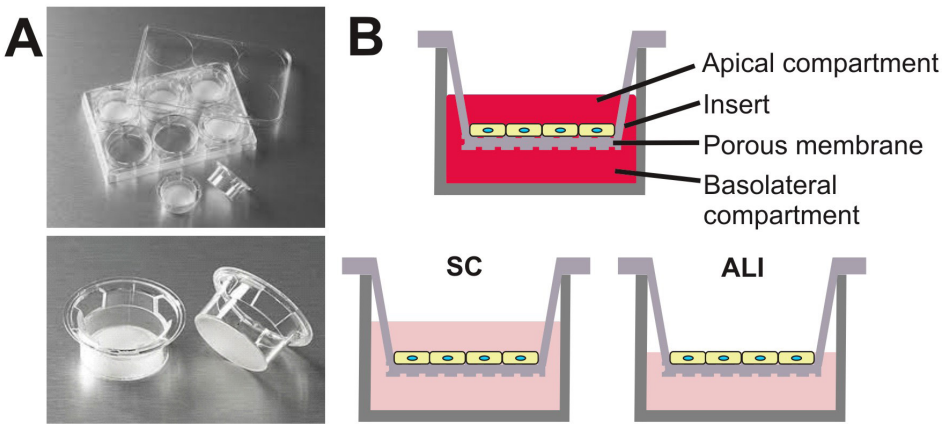

Figure 16. **Transwell systems for cell culturing**. **A**, Top. 6 well-plate for holding tranwell inserts (taken from "www.e-shop.vitaris.com"). **A**, Bottom. 24 mm Transwell inserts containing PTFE membrane with pore size of 0.4 µm (taken from "www.eandkscientific.com"). **B**, Top. Schematic view of DMSCs under submerged culture conditions prior to differentiation. B, Bottom. Derivation of DMSCs into ATII-LCs under SC conditions, with differentiation SAGM in both basolateral and apical compartments (left) and under ALI culture conditions, with SAGM exclusively in the basolateral compartment (right).

Afterwards, the coating solution was removed from the cell culture plastic and coated surfaces were allowed to dry in the sterile bench.

A549 cells

Human lung epithelial A549 cells, derived from lung adenocarcinoma, were generously provided by Dr. Claus-Michael Lehr and were used between passages 15 and 30. A549 cells were cultured in RPMI-1640 medium (PAA Laboratories GmbH, Pasching Austria) supplemented with 5 % fetal bovine serum, 100 U/mL penicillin and 100 µg/mL streptomycin (all from Sigma-Aldrich Chemie GmbH, Steinheim, Germany).

Surfactant preparations

Native surfactant purified from bronchoalveolar lavages

Native surfactant from bronchoalveolar lavages (BALs) of slaughtered porcine adult fresh lungs was purified and separated from blood components by NaBr density-gradient centrifugation as reported (Taeusch, Bernardino de la Serna et al. 2005). Porcine lungs were filled several times with a NaCl 0.9 % solution until completing total lung volume, and then the resultant lavage was collected, filtered with a gauze and centrifuged at 1000 x g for 5 min in order to remove cell debris. For total surfactant isolation, BALs were ultracentrifuged at 100000 x g for 1 h at 4 °C to pellet the membrane fraction and then this was centrifuged in a discontinuous density gradient at 120000 x g for 2 h at 4 °C. Three solutions to generate the gradient were used containing 16 % NaBr 0.9 % NaCl , 13 % NaBr 0.9 % NaCl and 0.9% NaCl. The material concentrated between the last two density solutions is the so called “native surfactant” consisting of lipids and associated proteins described in the composition of the lung surfactant system, including phospholipids, neutral lipids and surfactant proteins A, B and C, and some others eventually associated to surfactant such as hemoglobin or immunoglobulins.

Organic extraction of NS

The organic extract (OE) of native surfactant was obtained by chloroform/methanol extraction (Bligh and Dyer 1959). In this procedure, 1 volume of the aqueous native surfactant was mixed with 2 volumes of methanol and 1 volume of chloroform, homogenizing the mixture with vortex for 30 s. For precipitation of the water soluble proteins, the mixture was incubated for 30 min at 37 °C. Then, 1 volume of chloroform and 1 volume of distilled water were added resulting in the formation of two phases, which were separated by centrifugation at 2000 g for 5 min at 4 °C. The aqueous phase was subsequently extracted by addition of 1 volume of chloroform as many times as needed (normally two more times) to improve the yield of the lipid extraction, collecting the resultant organic phases. To obtain aqueous suspensions of OE, the required volume of the extract was first dried under nitrogen and then under vaccum in UNIVAP for 2 h to remove traces of solvent, and then hydrated in buffer 5 mM Tris pH 7, 150 mM NaCl for 1 h at 45 °C.

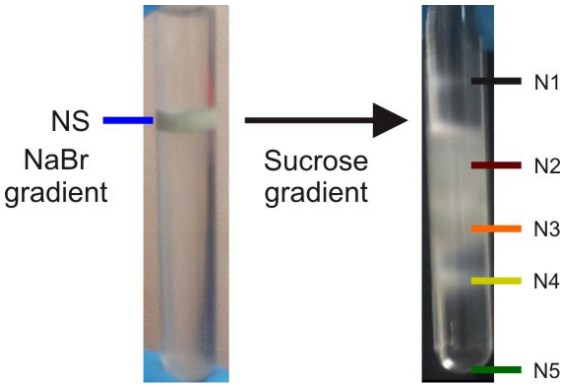

Figure 17. Isolation of native surfactant subfractions. Image depicting the result of subjecting the band of native surfactant isolated with the standardized NaBr gradient (left) to further purification by a discontinuous sucrose density gradient centrifugation (right) yielding five discrete subfractions termed from N1 to N5 in order of increasing density.

Isolation of subfractions from NS

Native surfactant (NS) complexes purified from bronchoalveolar lavage were subjected to subfractioning by a method adapted from an unpublished protocol generously provided by Dr. Andrea Ravasio. This method was based on the principle of upward flotation on a discontinuous sucrose gradient consisting of 3 mL of 0.32 M, 5 mL of 0.55 M, 3mL of 0.7 M layered above a mixture of 2 mL of 2 M and 0.25 M (1:1) containing 500 µL of NS. Each sucrose solution was prepared with a buffer containing 10 mM Tris-HCl, 1 mM $CaCl_2$, 2 mM $MgCl_2$, 150 mM NaCl, pH 7.4. Prior to centrifugation, a fine layer of buffered solution without sucrose was deposited on top of each gradient.

Then, the gradients were spun in a Beckman SW 40Ti rotor at 116000 x g for 2 h at 4 °C without brake. After centrifugation, five different fractions could be distinguished (termed N1, N2, N3, N4 and N5; **Figure 17**) and they were collected manually and stored separately, discarding the interfaces. Each fraction was concentrated by centrifugation for 1 h at 100000 x g at 4 °C, diluting the samples with buffer to diminish the percentage of sucrose in order to avoid the formation of additional density gradients and potential interferences. Finally, the pellets were suspended in buffer composed by 5 mM Tris-HCl, 150 mM NaCl pH 7.4, aliquoted in plastic tubes and then frozen in liquid nitrogen and stored at -80 °C until use. The band corresponding to N1 did not yield sufficient material hampering a proper analysis and it was not included in the experiments.

Surfactant harvested from cell cultures

Exocytosis of surfactant was stimulated by incubation of rat ATII cells or 4 day-differentiated ATII-LCs with 100 µM ATP and 100 nM phorbol 12-myristate 13-acetate (PMA) (both from Sigma, Spain) for 6 h at 37 °C, in buffered solution (containing, in mM: 140 NaCl, 5 KCl, 1 $MgCl_2$, 2 $CaCl_2$, 10 HEPES, pH 7.4 supplemented with 1 % penicillin/streptomycin) as previously described (Haller, Dietl et al. 2004). Supernatants containing freshly secreted surfactant were harvested, aliquoted and stored at -20 °C until use. Supernatants of DMSCs treated in the same manner, were also collected and used as negative controls. Before use, supernatants were concentrated by ultracentrifugation at 100000 x g.

Preparation of nanoparticles

Anionic fluorescent PLGA nanospheres

Fluorescent poly(d,l-lactide-co-glycolide) (PLGA) nanospheres were prepared using a technique of emulsion-diffusion-evaporation adapted from a protocol previously described (Horisawa, Kubota et al. 2002; Ravi Kumar, Bakowsky et al. 2004; Weiss, Schaefer et al. 2006) (see **figure 18**). PLGA (75:25, lactide:glicolide), Fluoresceinamine isomer I (FA) and poly(vinyl alcohol) (PVA)

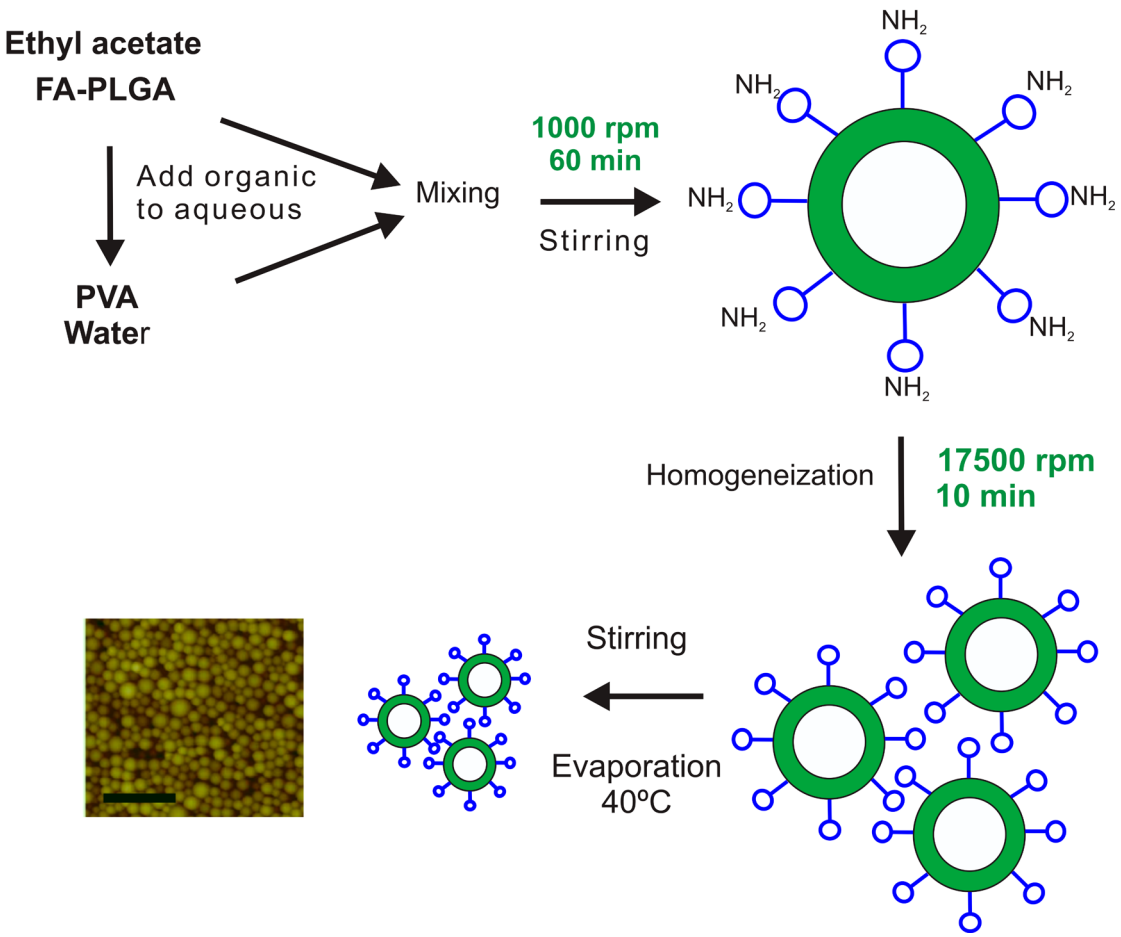

Figure 18. Scheme representing the different steps in the emmulsion-diffusion-evaporation method to prepare fluorescent PLGA nanospheres. An AFM image of PLGA nanospheres is shown (left bottom). Scale bar in image represents 500 nm. Modified from (Kumar et al. 2004).

were purchased from Wako Pure Chemicals Ind. (Osaka, Japan), MoWiol (Germany) and Sigma, respectively. For preparation of fluorescently labeled PLGA, PLGA (3.07 g) and FA (0.0583 g) were dissolved completely in 30 mL of acetonitrile with 0.0408 g of 1-ethyl-3-(3-Dimethylaminopropyl)-carbodiimide hydrochloride (DMAP), and incubated at room temperature for 24 h. The resultant FA-PLGA was washed with distilled water and separated by centrifugation. Then, the compound was dissolved in acetone and precipitated with ethanol (1 min, twice), followed by lyophilization. For the preparation of nanoparticles, 100 mg of FA-PLGA was dissolved in 10 mL of ethyl acetate at room temperature. This organic phase was added dropwise (aprox. 150 µL/min) to 5 ml water phase containing 125 mg PVA under stirring. This primary emulsion was stirred at room temperature for 1 h at 1000 rpm before homogenizing in a Ultrathurax T25 homogeneizer (Janke and Kunkel GmbH KG, Staufen, Germany) at 17500 rpm for 10 min for nano-precipitation. The homogeneized emulsion was transferred into a glass beaker and the volume was expanded to

45 mL by adding purified water. Stirring was continued at 40°C in a hood to evaporate the organic solvent.

Cationic chitosan modifed-PLGA nanospheres

Cationic nanoparticles were prepared using a self-asembling mechanism previously reported (Jornada and Beck 2012; Dimer, Pohlmann et al. 2013). The preparation consisted of the interfacial deposition of preformed polymer by adding 100 mg of PLGA (50:50), 170 µL of caprylic/capric trigliceride and 60 mg of Lipoid S-75® dissolved in 22 mL of acetone and 3 mL of ethanol. This organic phase was injected into 50 mL of a water phase containing 80 mg of Tween 80 and 10 mg of chitosan under magnetic stirring at 40°C. Then, the suspension was concentrated under reduced pressure to a final volume of 10 mL. Nanoparticles containing clarithromycin were prepared following the same methodoly and incorporating 10 mg of the antibiotic in the organic phase (at a final drug concentration of 1 mg/ml). Cationic PLGA nanoparticles containing clarithromycin were shown to have a drug content of 0.99 mg/mL with an encapsulation efficiency of 67 % as assessed by LC/MS-MS.

Silver nanoparticles

Silver nanoparticles (NM-300) were supplied by the Joint Research Centre Nanomaterials Repository. These particles consist of a colloidal 10 % w/w dispersion of silver NPs (average size of 15 nm) in water containing 4 % (w/w) polyoxyethylene glycerol trioleate and Tween 20 as stabilizing agents.

METHODS

ANALYTICAL TECHNIQUES

Lipid analysis

Phospholipid quantitation

Phospholipid content was measured by phosphorous quantitation (Rouser, Siakotos et al. 1966) or by enzymatic assay (García-Verdugo, Ravasio et al. 2008). For phosphorous determination, samples (surfactant preparations) and standards were dried in a sand bath and then, percloric acid (37 %) was added for organic phosphorous mineralization, incubating the samples at 260 °C for 30 min. Afterwards, the samples were incubated 7 min at 100 °C in the presence of ammonium molibdate 2.5 % and ascorbic acid 10 % solutions, generating a colorimetric reaction based on the formation of phosphomolibdic acid first and then, its reduction to a blue-coloured phosphomolybdate after being reduced by the ascorbic acid. Absorbance at 820 nm was measured and correlated to phosphorous concentration upon interpolation into a calibration curve built with standards of known concentrations of phosphate. Finally, values were transformed to concentration considering 734 Da as the average molecular weight of surfactant phospholipids.

For the quantitation of the phospholipid (particularly phosphatidylcholine, PC) content by the enzymatic colorimetric assay, a commercial kit was used (Spinreact, Spain). Despite the fact that this assay only detects and quantitates PC species, consistently with the major proportion of these in surfactant samples, final values were observed to be similar to those obtained by phosphorus mineralization, with the advantage of a requirement of much lower sample volumes due to the high sensitivity of the method. In this method, PC is hydrolyzed by phospholipase D and the liberated choline is then oxidized by choline oxidase to betaine with the simultaneous generation of hydrogen peroxide. In the presence of peroxidase, the hydrogen peroxide couples oxidatively the 4-aminophenazone and dichlorophenol to form a coloured quinone, proportionally to the PC concentration. For the experimental procedure, 5 µL of sample were mixed with 1 mL of the

working reagent and incubated for 5 min at 37 °C. Absorbance of the sample was measured at 505 nm and related to the absorbance of a standard of known PC concentration to calculate the final concentration.

Cholesterol quantitation

The determination of the amount of cholesterol present in the isolated subfractions of NS was performed following the protocol of a commercial kit based on enzymatic reactions (Spinreact, Spain). First, after 15 min of incubation of the samples and standards with the kit reagents, cholesterol esters are broken down into cholesterol and fatty acids by cholesterol esterase. Then, the free cholesterol is subsequently oxidized by cholesterol oxidase into 4-cholestenone and hydrogen peroxide. Then, a colorimetric reaction is developed between hydrogen peroxide, phenol and 4-aminophenazone to produce a colored quinonimine. Finally, measurements of the absorbance at 505 nm were carried out and interpolated into a calibrate curve built with known amounts of cholesterol, to determine the cholesterol concentration of the samples.

Thin Layer Chromatography (TLC)

The lipid composition of the different subfractions of NS was analyzed and compared by TLC using silica gel 60 plates (Merck, Germany) as stationary phase and a mobile phase composed by chloroform, methanol and water (65:25:4, vol/vol/vol). 100 µg of each sample and 50 µg of phosphatidylcholine (PC), phosphatidylglycerol (PG), phosphatidylethanolamine (PE), phosphatidylinositol (PI), sphingomyelin (Sm) and cholesterol (Ch) used as reference standards were applied in the same plates and the mobile phase was drawn up the plate via capillary action, permitting the separation of the different lipid species. Finally, the lipid bands in the TLC plates were visualized under development with iodine vapors. Regions corresponding to PC and PG bands of the samples were scratched from the plates and subjected to organic extraction with chloroform/methanol, determining their molar proportion with respect to total phospholipid by phosphorus quantitation.

High-performance liquid cromatography (HPLC) coupled to mass spectrometry

The molecular species of the phosphatidylcholine (PC) fraction present in pellets of DMSCs, rat ATII cells and ATII-LCs differentiated under SC conditions were analyzed quantitatively by HPLC coupled to mass spectrometry (Canals, Mormeneo et al. 2009) with the technical assistance of Drs. Gemma Fabriàs and Josefina Casas, from the Institute of Advanced Chemistry of Catalonia (CSIC). The liquid chromatography–mass spectrometer consisted of a Waters Aquity UPLC system connected to a Waters LCT Premier orthogonal accelerated time of flight mass spectrometer (Waters, Millford, MA), operated in positive electrospray ionization mode. Full scan spectra from 50 to 1500 Da were acquired and individual spectra were summed to produce data points each 0.2 s. Mass accuracy and reproducibility were maintained by using an independent reference spray via the LockSpray interference.

Nucleic acid analysis

End-point reverse transcription-polymerase chain reaction (PCR)

Total RNA extraction from DMSCs as well as ATII-LCs differentiated for 24, 48 or 96 h under SC conditions was performed using RNeasy mini kit (Qiagen, IZASA Distribuciones Tecnicas SA, Madrid, Spain). First, cells were lysed and homogenized in the presence of a denaturing buffer containing guanidine-isothiocyanate for inactivation of Rnases ensuring the isolation of intact RNA. Cell lysates were passed through a genomic DNA eliminating spin column. Ethanol was added to the lysates in order to provide ideal binding conditions for RNA, facilitating the elimination of contaminants. RNA was then eluted in ultrapure water and quantified by absorbance at 260 nm using a Nanodrop spectrophotometer (ThermoScientific, Madrid, Spain). Integrity of RNA was determined by SYBR gold staining of a small aliquot of each sample on a 1.5 % agarose gel. To reverse transcribe the RNA, the Transcriptor High Fidelity cDNA Synthesis kit was used (Roche, Roche España, Madrid, Spain). Reverse transcriptase (22 U) was mixed with dNTPs (1 mM each), random hexamer primers (60 µM), Rnase inhibitor (20 U), the appropriate volume of buffer, and with the template RNA (1 µg). Amplification was carried out in a TC3000

thermocycler (Techne, Staffordshire, UK) at 25°C for 10 min, followed by 37°C for 120 min and 85°C for 5 min. Complementary DNA (cDNA) was then amplified using MBL Taq DNA polymerase (Dominion MBL) and the specific primers for genes encoding for SP-A, SP-B, SP-C, SP-D, ABCA3, Thyroid transcription factor 1 (TTF1), Forkhead box protein A1 and A2 (FOXA1 and FOXA2, respectively), Cathepsin H, Napsin A, G-protein coupled receptor 116 (GPR116) and Cystic fibrosis transmembrane conductance regulator (CFTR) (**Table 1**). GAPDH was used as a loading control. Primers (Sigma-Aldrich) were designed using the public online software Primer-BLAST software (NCBI). PCR was carried out at 94 °C for 4 minutes (enzyme activation), followed by 30 cycles of 94°C for 30 seconds (denaturation of the DNA molecule), specific annealing temperature (55-60 °C) for 30 seconds, and 72°C for 30 seconds (extension of the nascent DNA chain). PCR set up contained the following components: dNTPs (0.2 mM), Taq polimerase (2.5 U), forward and reverse specific primers (5 µM), buffer solution that contains Mg^{2+} (1.5 mM), and the template cDNA (200 ng). The amplified DNA was kept at 4 °C until use. PCR products were separated on 2 % agarose gel and visualized by SYBR Gold staining.

Protein	Forward primer	Reverse primer
SP-A	AGACGGGACCCCTGTAAACT	TTCCACTGCCCATCTGTGTA
SP-B	CCAGGACACGATGAGGAAGT	GGGGAAGTAGTCGTCAAGCA
SP-C	ACACGGAGATGGTTCTGGAG	GGAGAAGGTGGCAGTGGTAA
SP-D	TGTGGTCTGCGAGTTCTGAG	GCATGAGGGTCTAAGCCTTG
ABCA3	GCCAGTTCCCCAGTAGTCCT	TTGCTCAGCTCCACACTCAT
Napsin A	TCCACATGGAGCGTGTGAAG	GCCACATACGTCCCCAAGAA
Cathespin H	CCTGTAAAAATCAGGGTGCC	CATGCTCCATCTGGGGAGGT
GPR116	CTCGAGGTTCACCTCACCTG	CTTTTTGTGGCAACGGCTCG
CTFR	GGAGGGATTTGGGGAATTATTTGAGAAAGC	CTATATTCATCATAGGAAACACCAAAGATG
TTF1	GCGCTTTCGGAGGGAATAAAA	GCATATCAGCCCCAACCTCA
FOXA1	ACTGTGAAGATGGAAGGGCA	AGTAGGCCTCCTGCGTGT
FOXA2	CTGGTCGTTTGTTGTGGCTG	GGAGGAGTAGCCCTCGG
GAPDH	AGCCACATCGCTCAGACAC	GCCCAATACGACCAAATCC

Table 1. Primers used for endpoint RT-PCRSequences of the forward and reverse primers used for amplification of the genes of interest by endpoint RT-PCR.

Quantitative real-time PCR

Whereas in traditional end-point PCR, detection of the amplified sequences are perfomed at the end of the reaction after the last PCR cycle, in real-time PCR, products are measured at each

cycle. By monitoring reactions during the exponential amplification phase of the reactions, it is possible to precisely determine the initial amount of target. In real-time PCR, the quantity of DNA is measured after each cycle via fluorescent dyes that yield increasing fluorescent signal in direct proportion of the number of PCR amplicons generated.

RNA isolation and reverse transcription into cDNA from DMSCs and ATII-LCs differentiated for 24, 48 or 96 h under SC conditions was performed as described for RT-PCR. Real-time PCR was carried out using an ABI 7,500 sequence detection system (Applied Biosystems, Life Technologies SA, Madrid, Spain). As fluorescent reporters, we used inventoried Taqman-specific probes (Applied Biosystems) for SP-A (Hs00831305_s1), SP-B (Hs01090658_g1), SP-C (Hs00161628_m1), SP-D (Hs01108490_m1) and ABCA3 (Hs00975530_m1) genes. Taqman probes have specific gene sequences and are designed to bind the target between the two PCR primers. Attached to the 5' end of the Taqman probe is the "reporter", which is a fluorescent dye that reports the amplification of the target. On the 3' end of the probe is a quencher, which quenches fluorescence from the reporter in intact probes. In the early PCR products, only the low, quenched reporter signal is detected, permitting to set a baseline. If the sample contains target, enough accumulated cleaved probe by the 5' nuclease activity of the polymerase is produced allowing the amplification signal to emerge from the baseline.

The point at which amplification signal becomes visible (threshold) is inversely related to the initial target quantity. Thus, by plotting fluorescence against the cycle number, amplification plots representing the accumulation of product over the duration of the entire PCR reaction were generated. Thermal cycling conditions were: 2 min at 50 °C, 10 min at 95 °C, 40 cycles of 15 s at 95 °C and 1 min at 60 °C. Dilution series of known template concentrations were used to establish a standard curve for confirmation of proper reaction efficiencies. Then, to perform the relative quantification of the genes, their expression in ATII-LCs at various differentiation time points was compared to their expression in undifferentiated cells. Data were analyzed using the $2^{-\Delta\Delta}$Ct method (Livak and Schmittgen 2001) in which $2^{-\Delta\Delta}$Ct is the amount of target normalized to an endogenous reference gene (TATA Box Protein, as a control for experimental variability) and relative to the positive control (adult lung tissue) (ΔCt = Ct (test gene)-Ct (housekeeping

gene); ΔΔCt = ΔCt (sample) – ΔCt (positive control). The results were expressed as fold change in expression of the differentiated cells in relation to the DMSCs.

Protein analysis

Cell protein extraction

Total cell protein was extracted from undifferentiated DMSCs, differentiated ATII-LCs under SC or ALI conditions, A549 cells and primary human ATII cells. Cell lysis was carried out in cell extraction buffer containing 10 mM Tris pH 7.4, 100 mM NaCl, 1 mM EDTA, 1 mM EGTA, 1 mM NaF, 20 mM Na4P2O7, 2 mM Na3VO4, 1 % Triton X-100, 10 % glycerol, 0.1 % SDS and 0.5 % deoxycholate (Invitrogen, Karlsruhe, Germany) and supplemented with 1 % protease inhibitors composed by aprotinin, bestatin, leupeptin and pepstain A (Sigma). Cells were detached by trypsin and centrifuged at 1200 rpm. Cell pellets were washed with PBS, centrifuged and the supernatants were removed to eliminate medium remanents. After lysis buffer addition, samples were kept on ice and vortexed each 30 min. Then, samples were centrifuged at 13000 rpm 4 °C for 10 min and pellets were discarded. Extracellular medium of the cultured DMSCs and differentiated ATII-LCs under SC conditions was also collected and concentrated by centrifugation using a Centripep system (Millipore Iberica SAU, Madrid, Spain) at 3000 x g and 25 °C.

Total protein quantitation

Protein content was determined with the widely used method developed by Lowry (Lowry, Rosebrough et al. 1951), based on a colorimetric reaction result of the reduction of the Folin-Ciocalteu reagent (phosphotungstic and phosphomolibdic acids) by the phenol groups of the tyrosine residues of proteins. Under alkaline conditions, the nitrogen of the peptide bonds reacts with cupper ions making the tyrosine lateral chains accessible to the Folin reactive. First, samples and standards (albumin) were incubated with 0.5 % SDS, 0.017 % Na-K tartrate, 0.008 % $CuSO_4$ and 1.6 % Na_2CO_3 0.08 M NaOH for 15 min at room temperature. After subsequent incubation

with the Folin reagent for 30 min, the absorbance at 700 nm was measured and directly related to the protein concentration from a standard curve.

Electrophoresis and Western blot analysis

Prior to electrophoresis, total protein content was determined using the Lowry method, as described above, to load samples at equal concentrations in the gels. SDS-Polyacrylamide Gel Electrophoresis (SDS-PAGE) was carried out using 10 % acrylamide (for SP-A, SP-D and OCT-1) or 16 % acrylamide (for SP-B and SP-C) gels under reducing conditions in the presence of 5 % β-mercaptoethanol. After electrophoresis, proteins were transferred to PVDF membranes using a semidry transfer system at 280 mA for 1 h. Blocking was performed by incubation with PBS/Casein blocker (Bio-Rad Laboratories SA., Alcobendas, España) for 1 h at room temperature. Afterwards, membranes were incubated with primary antibodies at 4 °C overnight with gentle orbital shaking. The primary antibodies used were: rabbit anti-SP-A (1:500) (Santa Cruz Biotechnology, Inc., Heidelberg, Germany), rabbit anti-SP-B and anti-SP-C (1:1000), mouse anti-SP-D (1:1000) all from Seven Hills Bioreagents (Cincinnati, Ohio, USA) and rabbit anti-OCT-1 (1:200) from (Aviva, San Diego, USA). After incubation with primary antibodies, three washes with PBS-Tween for 10 min each were performed and then, membranes were incubated with secondary antibodies for 1 h at RT. Secondary antibodies were swine anti-rabbit HRP conjugated (1:1000 for anti-SP-A and 1:2000 for anti-SP-B, anti-SP-C and anti-OCT-1 (Dako Diagnósticos, S.A., Sant Cugat del Vallés, Barcelona, Spain) and anti-mouse peroxidase conjugated (1:5000; Cell Signalling Technology, IZASA, S. A., L'Hospitalet de Llobregat, Barcelona, Spain). Anti-α-tubulin (1:10000; Cell Signaling) or anti-β-actin (1:10000; Invitrogen) were used as loading controls. After 3 washes with PBS-Tween, membranes were developed with Immobilon Western Chemiluminiscent HRP substrate (Millipore, Darmstadt, Germany).

Measurement of colloidal characteristics from NPs

Anionic and cationic PLGA nanoparticles were characterized with respect to mean diameter, polydispersity index (PdI) and zeta-potential using the ZetaSizer Nano ZS (Malvern Instruments Ltd.,Worcestershire, UK), based on a dynamic light scattering technology. All measurements were performed in triplicates.

SPECTROSCOPICAL TECHNIQUES

Infrared spectroscopy

Attenuated Total Reflection Fourier Transform Infrared (ATR-FTIR) spectroscopy is a powerful vibrational technique that provides information from a wide range of liquids, solids and gases, and from biological samples and biomembranes in particular, specially with respect to the structure and organization of membranes lipids in their various polymorphic phases (Lewis and McElhaney 2013) (**Figure 19**). It is fast and yields a strong signal with few micrograms of sample and it does not require the introduction of potentially disturbing extrinsic probes. Additionally, because of the long IR wavelength, light scattering problems are negligible permitting the investigation of aggregated materials or large membranous fragments (Goormaghtigh, Raussens et al. 1999). In an ATR-FTIR experiment, an infrared beam is directed onto an optically dense crystal (generally made of germanium, zinc selenide or diamond) with a high refractive index at a certain angle, covered with the sample (**Fig. 19A**). This internal reflectance creates an exponentially decaying evanescent wave that extends beyond the surface of the crystal into the sample held in contact with the crystal. In regions of the infrared spectrum where the sample absorbs energy, the evanescent wave is attenuated or altered. The attenuated energy from each evanescent wave is passed back to the infrared beam, which then exits the opposite end of the crystal and is passed to the detector in the spectrometer. The different regions or bands of the infrared spectrum contain the frequencies corresponding to the various vibrational modes of the covalent bonds of the organic molecules present in the sample and are often given descriptive names, such as stretching, bending or rocking (**Fig. 19B**). Thus, the absorption of the energy of

the evanescent field by the sample at certain regions generates an infrared spectra that contains valuable information about the structure of the system.

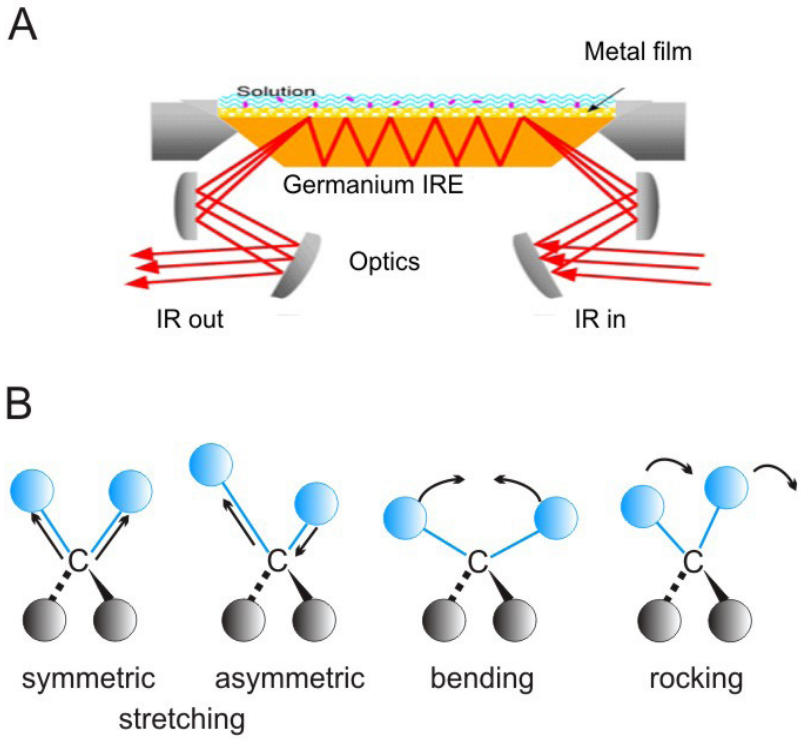

Figure 19. **ATR-FTIR spectroscopy**. **A**. ATR system representing a sample deposited in direct contact with a trapezoidal germanium crystal and the multiple reflections of the evanescent wave. **B**. Vibrational modes of the CH_2 molecule absorbing in the IR spectrum.

Oriented multilayers were formed by slow evaporation of 100 µg of NS, OE or LBPs suspensions, yielding a semi-dry film bearing residual water molecules onto the ATR crystal. Spectra were recorded in the double-sided, forward-backward mode on a FTIR Bruker IFS 66/R spectrophotometer (Ettlingen, Germany) equipped with a liquid nitrogen cooled mercury cadmium telluride (MCT) detector at a resolution of 2 cm^{-1} and with an aperture of 3.5 mm. The spectrometer was continuously purged with dry air (15 l/min) to minimize the contribution of atmospheric water. The internal reflection element was a trapezoidal germanium ATR plate (52×20×2mm, ACM, Villiers St Frédéric, France) with an aperture angle of 45° yielding 25 internal reflections. To improve the signal/noise ratio 256 accumulations were collected for each measurement. Thermotropic behavior of the samples within a range from 15 to 50 °C was characterized analyzing the asymmetric stretching of CH_2 vibration region, which is sensitive to

trans-gauche isomerization of the lipid chains. To investigate the potential lyotropic polymorphism present in the samples, the region corresponding to CH_2 bending vibration, sensitive to the presence of non-lamellar phases, was also analyzed. Data processing was performed with the software MATLAB® R12 Kinetics, generously provided by Dr. Erik Goormaghtigh, from Université Libre de Bruxelles. Baseline corresponding with the crystal absorption in the absence of sample and the atmospheric water contribution were subtracted as described (Alegre-Cebollada, Martínez del Pozo et al. 2007). The corrected spectra were smoothed by apodization of its Fourier transform by the Fourier transform of a 4 cm^{-1} Gaussian line shape.

Fluorescence spectroscopy

Laurdan fluorescence

Laurdan (6-lauroyl, 1-2-dimethylamino naphthalene) is a fluorescent probe that detects changes in membrane phase properties due to its sensitivity to the polarity of the environment in the lipid bilayer (**Figure 20**). This molecule was originally designed and synthesized in 1979 by Gregorio Weber (Weber and Farris 1979) to study dipolar relaxation. The fluorescent naphthalene moiety of the Laurdan molecule possesses a dipole moment due to a partial charge separation between the 2-dimethylamino and the 6-carbonyl residues. This dipole moment increases upon excitation and may cause reorientation of the surrounding solvent dipoles. The energy required for solvent reorientation decreases the excited state energy of the probe, which is reflected in a continuous red shift of the probe's emission spectrum. The consequence is that the emission spectrum of Laurdan is sensitive to the hydration level of the lipid headgroup region and so detects changes in membrane phase properties (De Vequi-Suplicy, Benatti et al. 2006). The hydrophobic tail of the lauric fatty acid allows solubilization of the dye within phospholipid membranes, locating the fluorescent moiety toward the aqueous environment. Thus, the fluorescence emission of Laurdan is blue in ordered, packed and highly dehydrated phases (gel, liquid ordered) while it shifts to green in more hydrated disordered phases (liquid-crystalline, liquid disordered) (Parasassi, De Stasio et al. 1990; Parasassi, De Stasio et al. 1991). This shift of the emission spectrum has been attributed to dipolar relaxation processes taking place in

the phospholipid liquid crystalline phase but not in the gel phase. These polarity changes are quantified by calculating the generalized polarization function, GPF (GPF= $(I_{440}-I_{490})/(I_{440}+I_{490})$).

NS, OE and suspensions of secreted LBPs were stained with the fluorescent probe Laurdan (Molecular Probes, USA) for 1h at 37 °C in a proportion of 1 % (mol/mol) with respect to phospholipids as previously described (Picardi, Cruz et al. 2011; Blanco, Cruz et al. 2012). The fluorescence spectra of surfactant suspensions were recorded in a thermostatized Aminco-Bowman Series 2 luminescence spectrometer, using an excitation wavelength of 370 nm and recording the emission spectrum between 400 and 550 nm, within a temperature range of 10 to 60 °C.

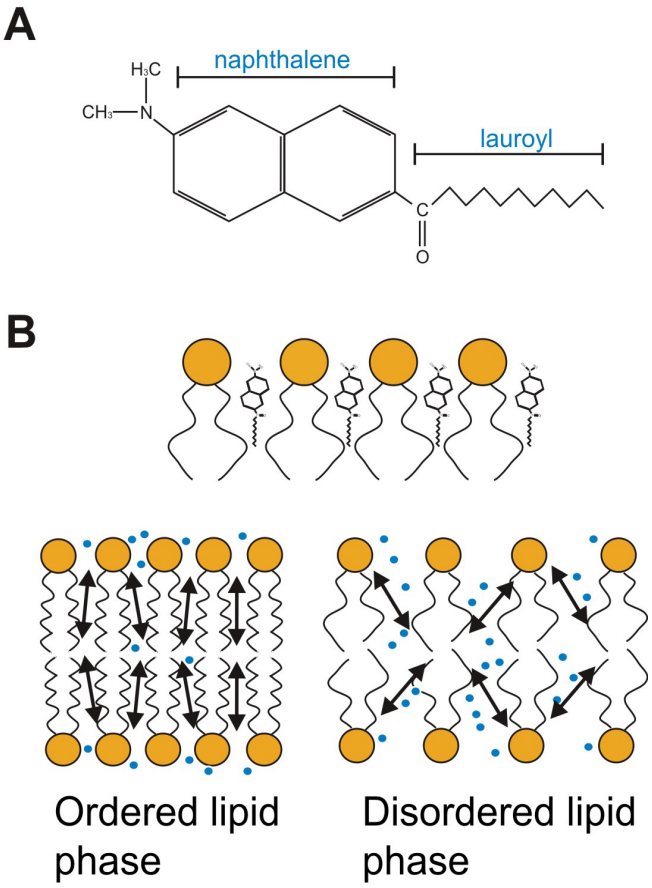

Figure 20. **Laurdan fluorescence in membranes**. **A**. Chemical structure of Laurdan, underlining the two main components of the fluorescent probe, the naphthalene and lauroyl moieties. **B**. Representation of the probe located at the head group level of phospholipid (top). Upon excitation, the Laurdan dipoles (arrows) provoke reorientation of the surrounding water molecules (blue dots) leading the red shift observed in the transition from ordered to disordered states (bottom) (adapted from (Sánchez, Tricerri et al. 2007)).

IMAGING TECHNIQUES

Fluorescence microscopy

Laurdan microscopy

For the staining of intracellular LBs with Laurdan, rat ATII cells grown on glass coverslips were incubated with 100 µM Laurdan in DMEM for 1 h at 37 °C. Fluorescence of intracellular LBs was measured with an inverted microscope (Zeiss 35, Germany) equipped with a Polychrome V Monochromator (TILL Photonics, Germany) and a microscopic stage T-controller (Tempcontrol 37, Zeiss). Excitation light (370 nm) was directed through a 420 nm dichroic mirror into a Zeiss Plan-Apochromat 100× NA 1.4 oil objective. Fluorescence images were taken separately by using two bandpass filters centered at 435 and 488 nm, respectively and a cooled 12-bit CCD-camera (PCO-Sensicam, Germany) operated at an acquisition rate of 1 frame/3 sec and a binning factor of 4. The optical properties of the microscope including the filter sets were cross-calibrated against the spectral output of a multiplate-spectrophotometer (Tecan M200pro, Switzerland) using Laurdan and DMSO as a reference. Thus, after subtraction of image background, GP formula was modified to be GPF = $(I_{440} - 0.25 \times I_{490})/ (I_{440} + 0.25 \times I_{490})$. Image and data analysis from fluorescence measurements obtained from individual LBs were performed with Image J and Microsoft Excel. For the Laurdan image presentation in Fig. 2 (lower panel), the GFP function was calculated from the intensity corrected images using the mathematical image functions in ImageJ.

Observation of Giant Unilamellar Vesicles (GUVs)

Aliquots of suspended LBPs were incubated with the fluorescent probes BodipyPC and DiIC18 (Molecular Probes Inc. (Eugene, OR) for 1h at 45 °C (probe/surfactant = 1 mol/mol %). GUVs composed of labeled- LBPs were prepared by electroformation following a method previously developed by Angelova and widely used for others (Puff and Angelova 2006). 5 µl of the aqueous suspension were spread on the surface of a the conductive side of two indium-tin oxide coated glasses as small drops and dried under a stream of N_2 avoiding a complete dehydration of the sample to maintain membrane integrity. Afterwards, the two slides were mounted to build

an electroformation chamber, with the conducting sides face to face, separated by a 2 mm thick Teflon spacer pre-coated with vacuum grease. Sufficient volume of a buffered solution containing Tris 5 mM NaCl 20 mM was added to fill the chamber and then this was completely sealed at both sides with moldable vinyl paste (CritoSeal, from Leica BioSystems). The chamber was connected to a function generator (Digimess® FG 100, Germany) and a low frequency AC field was applied using the following sequence: 1) From 0 to 1.5 V, increasing 250 mV every 5 min, with a frequency of 500 Hz 2) 1.5 V for 1 h, at 500 Hz and 3) From 500 Hz to 0 Hz, reducing 100 Hz every 10 min. After vesicle formation, the AC field was turned off, and the vesicles were collected with a pipette and transferred to a plastic tube. GUV preparations were observed in a fluorescence upright microscope Leica DM-4000B equipped with the appropriate fluorescence filters for observation of BodipyPC and DiIC18 fluorescence (maximum fluorescence emission at 488 and 543 nm, respectively) and connected to a cooled digital camera (Model C10600-10B ORCA-R2, Hammamatsu).

Polarization microscopy

Polarized light microscopy is a contrast-enhancing technique with high degree of sensitivity and can be used for both quantitative and qualitative studies targeted at a wide range of anisotropic samples. The electric field vectors of the light vibrate in all planes that are perpendicular with respect to the direction of propagation. If the electric field vectors are restricted to a single plane by filtration of the beam with specialized materials, then the light is referred to as plane or linearly polarized with respect to the direction of propagation, and all waves vibrating in a single plane are termed plane-polarized. A polarized light microscope (**Figure 21**) is equipped with a polarizer, positioned in the light path before the sample, and a second polarizer (analyzer), located in the optical pathway between the objective rear aperture and the camera port. Image contrast arises from the interaction of plane-polarized light with a birrefringent sample generating two individual wave components that are each polarized in mutually perpendicular planes. Thus, anisotropic materials act as beamsplitters dividing light rays into two orthogonal components which are subsequently re-united along the same optical path providing structural information.

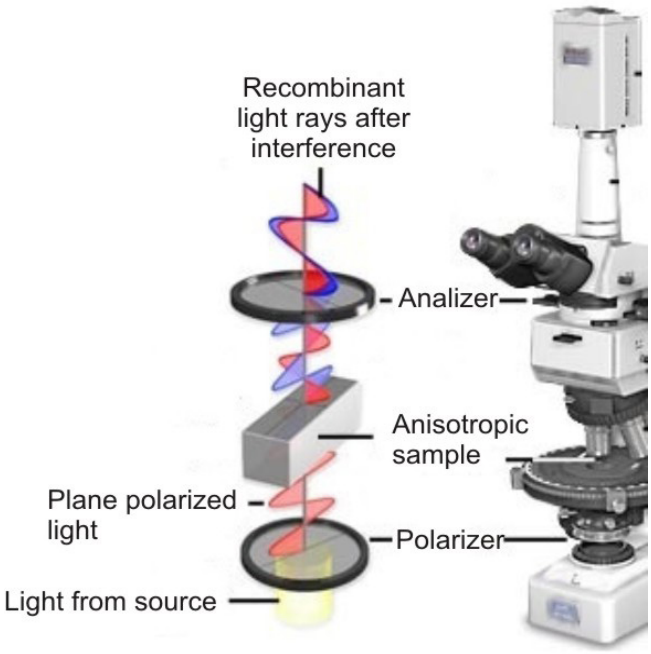

Figure 21. **Polarization Light Microscopy**. Configuration of a polarized light microscope equipped with two polarizers placed in the optical pathway before and after of a hypothetical anisotropic specimen (adapted from the Nikon website).

Polarization experiments were performed with an inverted microscope Zeiss 35 with a Plan-Apochromat 100× NA 1.4 oil objective for the observation of freshly isolated living rat ATII cells and an Eclipse E600POL with a Plan-Apochromat objective 10× for the visualization of reconstituted vesicles of dipalmitoylphosphatidylcholine (DPPC), both fitted with a heating and cooling stage. In both cases, crossed polarizers were placed between the DIC bright field condenser and the rear aperture of the objective. Initial observations were carried out at 30 °C and temperature was subsequently increased to 45 °C and reduced again to the initial values.

Scanning electron microscopy

Undifferentiated DMSCs, differentiated ATII-LCs under SC or ALI culture conditions, A549 cells and human primary ATII cells were grown on Transwell inserts for 4 days, washed with phosphate buffered saline (PBS), and fixed with 1 % paraformaldehyde in 200 mM HEPES pH 7.4 at room temperature for 60 min and then washed again three times with PBS. Afterwards, cells were dehydrated twice on their supporting filters through an ethanol gradient: 30, 40, 50, 60, 70, 80, 90, 96 and 100 % for 10 min at room temperature for each ethanol concentration. Complete drying of the samples was performed by incubation with 3-hexamethyldisilazane (HMDS) (Fluka, Germany) for 10 min. HMDS was removed from the preparations by dissecation. Dried filters

were cut with a scalpel and mounted on aluminium stubs and sputter coated with gold. Samples were observed using an EVO HD15 (Zeiss, Göttingen, Germany) equipped with a field emission gun at 5 kV under high vaccum conditions.

Anionic fluorescent PLGA nanoparticles were also visualized by scanning electron microscopy (SEM), upon direct deposition of the sample onto aluminium stubs. Cationic PLGA NPs could not be properly visualized under SEM because of its oily content.

Transmission Electron Microscopy (TEM)

Pelleted DMSCs and ATII-LCs differentiated under SC conditons, secreted material from ATII-LCs as well as isolated subfractions from NS complexes were firstly concentrated by ultracentrifugation at 13000 rpm for 15 min and then fixed with 2.5 % glutaraldehyde 0.1 M PBS pH 7.4 for 6 h at 4 °C. Carbon grids were used as supports and were previously subjected to depolarization for 30 s at 500 V. For negative staining (only in the case of NS subfractions), a small drop of fixed sample was placed onto the grid and leaved for 1 min in the support. Afterwards, the excess of material was removed with a piece of filter paper and the preparation was allowed to dry for 2 min. Then, for staining a small drop of uranyl acetate (2 % in the same buffer than fixation solution) was deposited onto the grid and was in contact with the sample for 1 min, eliminating the excess of fluid at the end of incubation.

For section observations, after treatment with glutaraldehyde, samples were post-fixed with 1 % osmium tetroxide for 1 h at room temperature and then dehydrated upon incubation with a graded series of acetone (30, 40, 50, 60, 70, 80, 90, 95 and 100 %) for 10 min each. Finally, samples were embedded in Spurr resin (Polysciences, Warrington, PA, USA) by consecutive incubations with mixtures resin/acetone 1:3 (1 h), 1:1 (1 h), 3:1 (2 h) and pure resin (overnight). Resin was polymerized by incubation at 65 °C for 24h. Finally, samples were embedded in Spurr resin (Polysciences, USA) and ultrathin sections of 50 nm were cut on an ultramicrotome.

Both uranyl acetate-stained preparations and osmium tetroxide-stained sections were observed in a JEM-1230 (JEOL, USA) electron microscope.

Cryo-electron microscopy

Cryo-electron microscopy (cryo-EM) is a method in which biological samples can be imaged in a frozen hydrated state. Rapid cooling of aqueous samples at-178 °C prevents generation of ice crystals and as a result the object is preserved in native conditions without any chemical fixation or drying (Frank, Radermacher et al. 1996; Hrabe and Foster 2011; Pereiro and Chichón 2014).

Material secreted by ATII-LCs differentiated under SC conditons was applied to holey-carbon grids (Quantifoil Multi A Cu/Rh 300 mesh) for 1 min, blotted for 1 s and plunged into nitrogen-cooled liquid ethane in a Leica EM-CPC vitrification device as previously described (Dubochet, Adrian et al. 1988; de la Presa, Rueda et al. 2009; Arranz, Coloma et al. 2012). The vitrified grids were stored at liquid nitrogen temperature in a container before data collection. The grids were used for image acquisition under cryogenic conditions with a Gatan side-entry cryo-holder and transferred to a FEI Tecnai G2 F20 electron cryomicroscope operating at 200 kV. Images were recorded with a FEI Eagle 4x4k charge coupled device camera at different nominal magnifications of x39000, x68.000 and x109.000. When appropriate, measurements were taken from the micrographs by means of histograms using the ImageJ software.

Cryo-electron tomography

Aliquots of native surfactant complexes were applied to grids, vitrified and transferred as described above for cryo-EM. In cryo-electron tomography (cryo-ET), images are collected as the sample is tilted in the path of the beam (tilt series) and the data are then computationally reconstructed into a high-resolution volume (tomogram). The tilt-series were acquired with the FEI Xplore 3D software at a nominal defocus of -5 to -8 um using a Saxton scheme (from -65 to +65° with normally a set of 57-67 images). Tilt-series were processed in a Linux Fujitsu-Siemens Celius V810 biopteron with 16 Gb of RAM. Image stacks were preprocessed and aligned using the IMOD software package using gold nanoparticles as fiducials. The aligned tilt-series were reconstructed with TAPIR algorithm implemented in the IVE/Priism software package. For each reconstructed volume, a denoising procedure to discern and interpret the structural features

was applied. Denoised volumes were segmented using AMIRA (TGS Europe, Merignac, France) with semiautomatic masking generation tools. For the visualization of the three-dimensional volumes, both AMIRA and Chimera 24 softwares were used.

Cryo soft X-ray microscopy

Native surfactant complexes and material secreted by ATII-LCs differentiated under SC conditons were loaded on glow discharged bare copper grids for 1 min at room temperature. Fast freezing was performed in the same conditions as described above for cryo-ET.

Full-field transmission X-ray microscopy was performed at the undulator beamline U41 at the BESSY II synchrotron (Berlin, Germany). Briefly, synchrotron radiation is the electromagnetic radiation emitted when charged particles (i.e.: electrons) are radially accelerated in an electron ring through magnetic fields to high speeds in several stages, generating a final energy in the GeV range (Elder, Gurewitsch et al. 1947) (**Figure 22**) . A synchrotron light source typically begins with an electron gun, containing a man-made material, to which an electrical and thermal current is applied (**Fig. 22B**). This results in electrons “lifting off” and beginning their journey by being propelled down a linear accelerator (linac). Then, electrons enter a circular-shaped booster ring, where they are accelerated to relativistic speeds. Finally, they enter into another ring, often called a “storage ring”, where they circulate for hours. The electron travel in a straight line, so at points around the ring, special bending magnets help them maintain their circular path. When electrons are manipulated by bending magnets to change their direction, they emit a fan of radiation (synchrotron light). This radiation branches off the storage ring and enters laboratories or beamlines. Here it is refined with devices such as monochromators and mirrors, before it is shone on the sample. There is a unique spectral region termed the “water window”, bounded by the carbon and oxygen k-absorption edges at 284 and 540 eV, respectively, where soft X-rays are strongly absorbed by carbon-rich structures (protein, lipid, membranes) whereas attenuation by surrounding oxygen-dominated material (ice) is minimal. Thus, biological specimens can be imaged at around 500 eV without the need of additional contrast agents (Carzaniga, Domart et al. 2014).

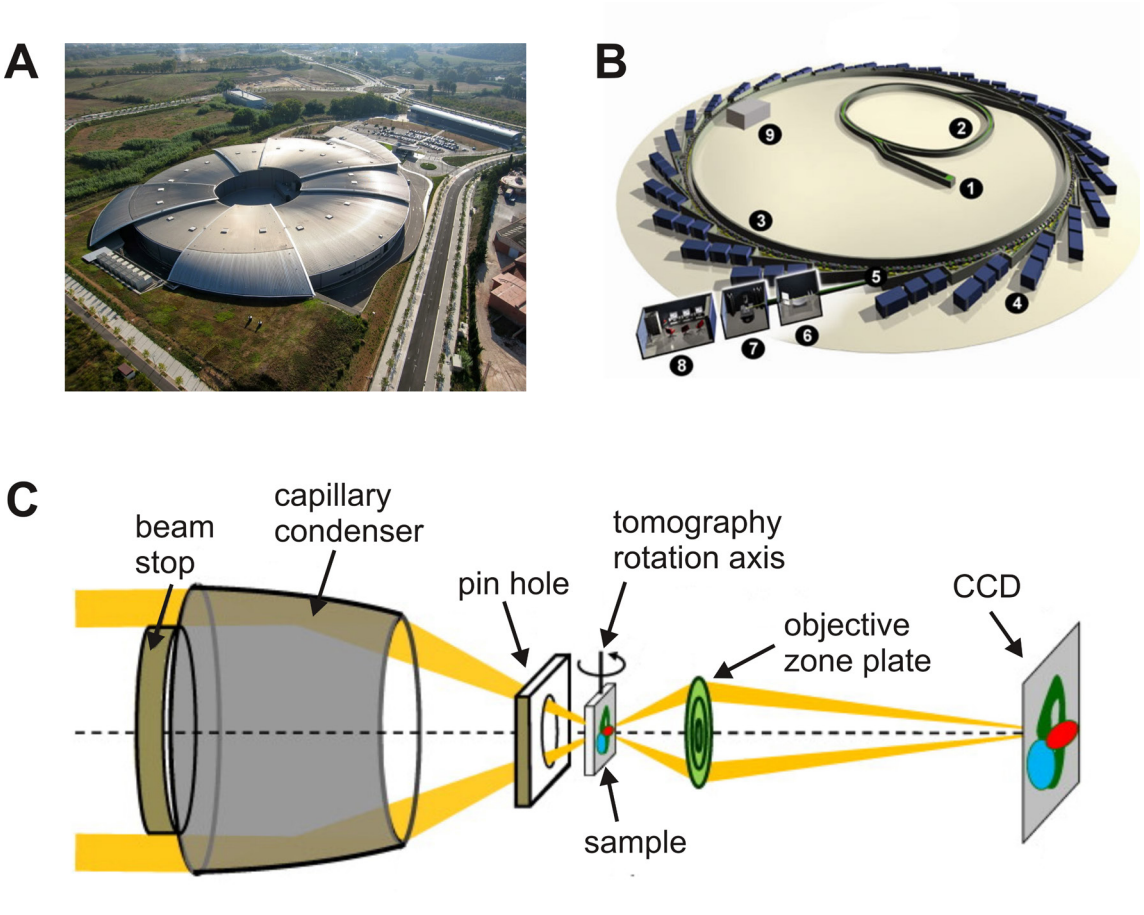

Figure 22. Cryo soft X-ray microscopy. **A**. Bird's eye view of a synchrotron facility (ALBA synchrotron, Barcelona, Spain). Note the considerable size of this kind of facilities. Taken from http://www.cells.es/. **B**. A synchrotron is typically constituted by the following components: injection system (1), booster (2), storage ring (3), beamlines (4), front ends (5), optics hutch (6), experimental hutch (7), control cabin (8), and radiofrequency cavity (9). Adapted from http://www.diamond.ac.uk/. **C**. Basic schematic representation of a transmission X-ray microscope. A condenser glass capillary focus the light onto the sample which is rotated to collect the tilt angle projections. The zone plate forms the image of the sample onto the CCD camera detector. Adapted from https://confluence.aps.anl.gov.

Similarly to other microscopes, the X-ray microscope requires a source and a means of delivering the beam to the sample (condenser), collecting the beam once it has passed through the sample (objective) and detecting the resulting image (**Fig. 22C**). In the experiments presented as part of this Thesis, the source is originated from synchrotron radiation and the desired X-ray energy is selected by a monochromator, which is then focused onto the sample using a capillary condenser. Then, X-rays are collected using a diffractive, focusing optical element termed a zone plate. Zone plates are made from concentric rings of material, in such a way that the smaller the width of the outermost zone the higher governs the maximum resolution achievable.

Finally, X-rays are detected by a CCD detector, whose active chip remains inside the vacuum space of the microscope. Soft X-ray tomography follows a similar protocol to electron tomography as the projection images are collected by rotating the specimen over an angular range that depends on the sample stage set-up and with an angular step that can be varied depending on sample needs, usually 1° step (Pereiro and Chichón 2014).

In our experimental conditions, tilt series of ±65° at 2.43 nm wavelength (photon energy E= 510 eV) were recorded as previously reported (Carrascosa, Chichón et al. 2009). A complete tomographic data set using a constant 1° tilt increment yielded 131 projections in 35 min. The condenser was a single-bounce ellipsoidal glass capillary (XRADIA) with a working distance of about 5 mm and focal spot size of about 1 μm FWHM. The sample stage was constituted by an FEI compustage modified for X-ray synchrotron beam geometry and a Gatan model 630 cryo-holder. Images were formed by Fresnel objective zone plates (Helmholtz Zentrum, Berlin). Two different zone plate objectives were used: one high resolution objective with 900 zones, focal length of 0.925 nm (E = 510 eV) and outermost zone width of drN = 25 nm, and another medium resolution objective for larger depth of field with 560 zones, focal length of 1.5 mm (E = 510 eV) and outermost zone width of drN = 40 nm. The monochromatized photon flux impinging on the sample was on the order of 109 photons/ (μm2s). The enlarged projections formed by the zone plate objective were recorded by a Peltier-cooled, back thinned, direct illuminated 1340x1300 pixel soft X-ray CCD camera (Roper Scientific PI-SX 1300) with a pixel size of 20 μm. Image processing was performed as previously described for cryo-ET.

Atomic force microscopy

Atomic force microscopy (AFM) is a technique that permits the acquisition of high resolution images in real time by measuring different physical properties of a sample at nanometric scale. AFM is particularly valuable since it allows observation of samples in their native environment without fixing and in a non-invasive manner, providing topographical and mechanical information about biological structures (Fotiadis, Scheuring et al. 2002; Gaczynska and Osmulski 2008). An atomic force microscope basically contains the following components: 1) A fine probe consisting

of a cantilevered beam attached to a sharp probe which scans near the surface; 2) A piezoelectric translation system controlling the tip/surface separation and translations in the same plane; 3) A feedback system which holds the tip near the surface adjusting the vertical separation between tip and surface (Cohen and Bitler 2008) (**Figure 23**). To prevent the detachment of the sample from the support, the object has to be strongly immobilized on an atomically flat surface in the range of micrometers. For this purpose, mica moscovita is the most used substrate for electrostatic attachment of bioparticles, since this mineral can be easily peeled off exposing a clean and flat surface.

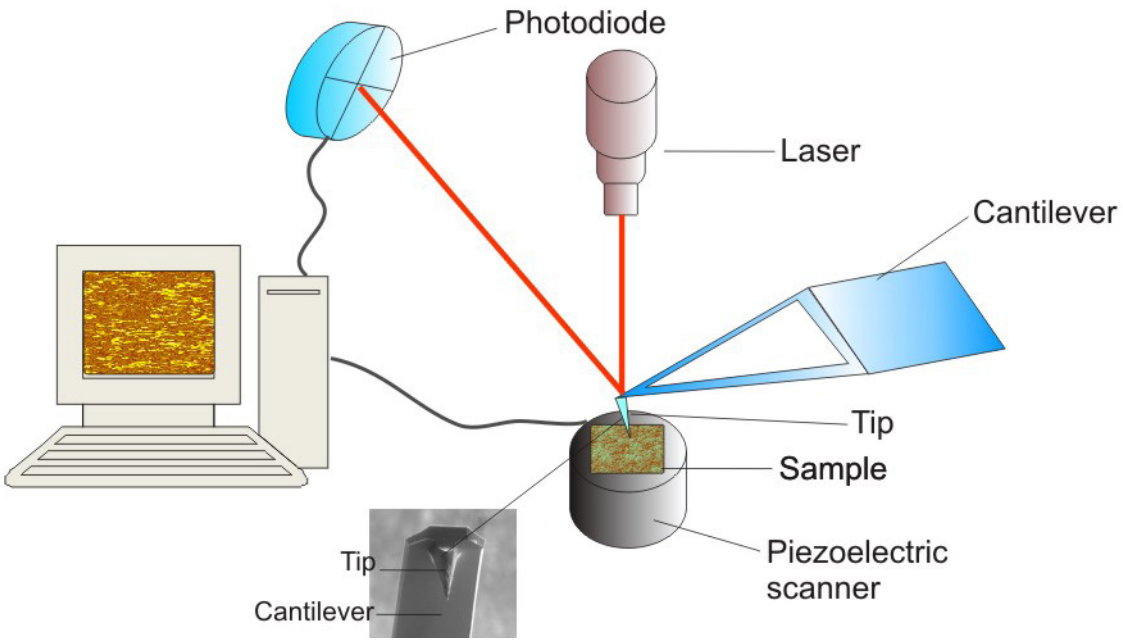

Figure 23. **Atomic Force Microscopy (AFM)**. Schematic representation of the principal components of an atomic force microscope, including piezoelectric scanner, tip, laser, photodiode and an electronic control system. Scale bar in the picture represents 10 µm.

There are three major modes of operation in AFM: contact, oscillating (tapping) and force. In the contact mode, both tip and sample are in direct contact leading to the cantilever deflection whereas in tapping, the tip touches the sample very briefly and with a low force in a more non-invasive conditions. In tapping mode, the probe vibrates vertically while scanning and the proximity of the atoms of the scanned sample provokes variations in the amplitude of oscillations of the probe due to van der Waals and electrostatic forces. Modifications in the

amplitude are translated into a topography image offering a 3D map of the outer surface of the object. When changes in the phase of the vibrating cantilever instead of amplitude are recorded, “phase images” are generated containing height information and offering a 3D-like appearance. Moreover, contact and tapping modes can be fusioned, where the tip oscillates while keeping constant contact with the sample (Tinazli, Piehler et al. 2007). Finally, in the force mode (also called force spectroscopy), cartesian coordinates of the surface sample are not provided but the strength of the interaction between the tip and the sample is determined in the order of picoNewtons (Radmacher, Cleveland et al. 1994), usually modifying the tip with a receptor-specific ligand. Force and tapping modes can be also combined giving rise to the jumping mode or pulsed force microscopy, providing at the same time data about topography and adhesion force (Moreno-Herrero, Colchero et al. 2004).

Suspensions of secreted LBPs were directly deposited on top of a freshly exfoliated mica substrate to be adsorpted, incubating the samples until solvent evaporation. The AFM images were obtained with a Multimode Nanoscope IIIA equipped with a type E scanner (Veeco Instruments, Santa Barbara, CA), operated in tapping mode. Tips used were RTESP phosphorus (n) doped silicon probes with a typical radius of less than 10 nm, nominal spring constant of 40 mN/m and resonance frequency between 266 and 309 KHz. Topography and phase images were recorded from each sample with 256 scan lines and a frame rate of 0.5 Hz.

FUNCTIONAL ASSAYS

Real-time exocytosis monitoring assay

DMSCs and ATII-LCs differentiated for 5 days under SC conditions were grown on 8-well chamber slides (Ibidi, Instrumentación y componentes, Zaragoza, Spain) and incubated with 50 nM LysoTracker Green DND-26 (LTG) (Invitrogen, Fisher Scientific, Madrid, Spain) for 20 min in DMEM and then washed with buffered solution. Cells were next mounted into a heated chamber (37° C) for live imaging. Exocytosis was stimulated with ATP and PMA and secreted surfactant was stained in the continuous presence of 4 µM FM 1-43 (Invitrogen, Fisher Scientific, Madrid, Spain) as previously described (Haller, Ortmayr et al. 1998). Images were collected on a LSM 510

Meta Confocal Microscope (Zeiss, Carl Zeiss AG, Jena, Germany) mounted on a Zeiss Axiovert 200M inverted microscope using 1 to 5 % Argon laser power (488 nm) and a Kalman filter to average both scans. Emitted light was collected by a META detector set to 497-508 and 604-754 nm for LTG and FM 1-43 emissions, respectively. Single plane (4 µm) and z-stack images (4 µm, z-step=2 µm) of multiple focal planes (from 6 to 8) were obtained using a 63x oil-immersion objective. Images were acquired at 1.024 x 1.024 or 2.048 x 2.048 pixel resolution (1 pixel = 140 or 70 nm, respectively). For image handling and z-stack projections we used the public domain software ImageJ v.1.32j (Wayne Rasband, National Institute of Health).

Adsorption kinetics assay

Surfactant adsorption kinetics into air-liquid interfaces were evaluated with a high-throughput screening method based on fluorescence microplate readers. Surfactant materials were stained with a trace of BodipyPC (Invitrogen, Fisher Scientific, Madrid, Spain), upon preincubation with the probe at 45 °C for 1 h (probe/surfactant = 1 mol/mol %). Accumulation of surfactant at the interface was evaluated in 96-well micro-titer plates as described by Ravasio et al. (Ravasio, Cruz et al. 2008) in a FLUORSTAR Optima Microplate Reader (BMG Labtech, Offenburg, Germany). Briefly, wells were filled with a solution containing 5 mg/ml of the strongly light-absorbing agent Brilliant Black (BB) and labeled-surfactant samples (0.5 µg/well) were injected at the bottom of the wells. After orbital shaking, fluorescence coming from surface-adsorbed material (as well as the material accumulated up to 100 nm in the subphase) was measured by the instrument, whereas fluorescence coming from non-adsorbed complexes was quenched by BB (**Figure 24**). To evaluate the inhibitory effect of plasma proteins and cholesterol on the adsorption of the surfactant materials, experiments were also performed in the presence of increasing concentrations of human serum or meconium, respectively. Data in these experiments are presented in relative fluorescence units corrected by subtraction of the measured background (RFU-bg).

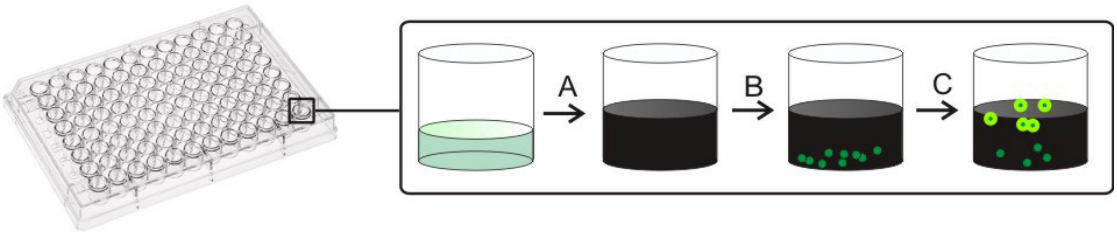

Figure 24. **Interfacial adsorption microplate assay**. The quenching agent Brilliant Black (BB) is added to a well from a microtiter plate previously containing an aqueous solution (1). An aliquot of fluorescently-labelled surfactant is injected at the bottom of the well but its fluorescence is quenched by BB (2). Upon orbital shaking, the sample adsorbs into the air-liquid interface resulting in that the fluorescence is no longer blocked and can be detected from the top of the plate to monitor the adsorption kinetics (3).

Captive Bubble Surfactometer (CBS)

The biophysical behaviour of the different subfractions purified from NS samples was assessed using a fully computer-controlled CBS evolved from the original setup developed by Dr. Samuel Schurch and co-workers in the 80's at Calgary University (Canada) (Schurch, Bachofen et al. 1989). The CBS allows to monitor the surface activity of surfactant samples once adsorpted into the air-liquid interface of an air bubble confined in a chamber under physiologically relevant conditions (see **Figure 25**). Surface tension, area and volume are calculated from bubble height and diameter, using automated video capture hardware and software (Schoel, Schurch et al. 1994).

The chamber basically consists of a glass cylinder with a metallic base perforated by a little hole (2 mm) through which a bubble of approximately 0.035-0.040 cm^3 can be created, permitting the air to enter into the chamber and through which a capillary is inserted for sample injection. Once the bubble is created, it floats against a hydrophilic roof consisting of an agarose cap (1 % w/v), by buoyancy. The cap is adjusted to a piston in such a way that bubble volume can be controlled by varying the hydrostatic pressure in the chamber as a result of the compression or expansion of the space between the cap and the metallic base, which is sealed. As bubble volume is decreased, the surface area is subsequently reduced and surface tension of the surfactant film falls (**Figure 26**). The chamber is filled with a buffered solution containing

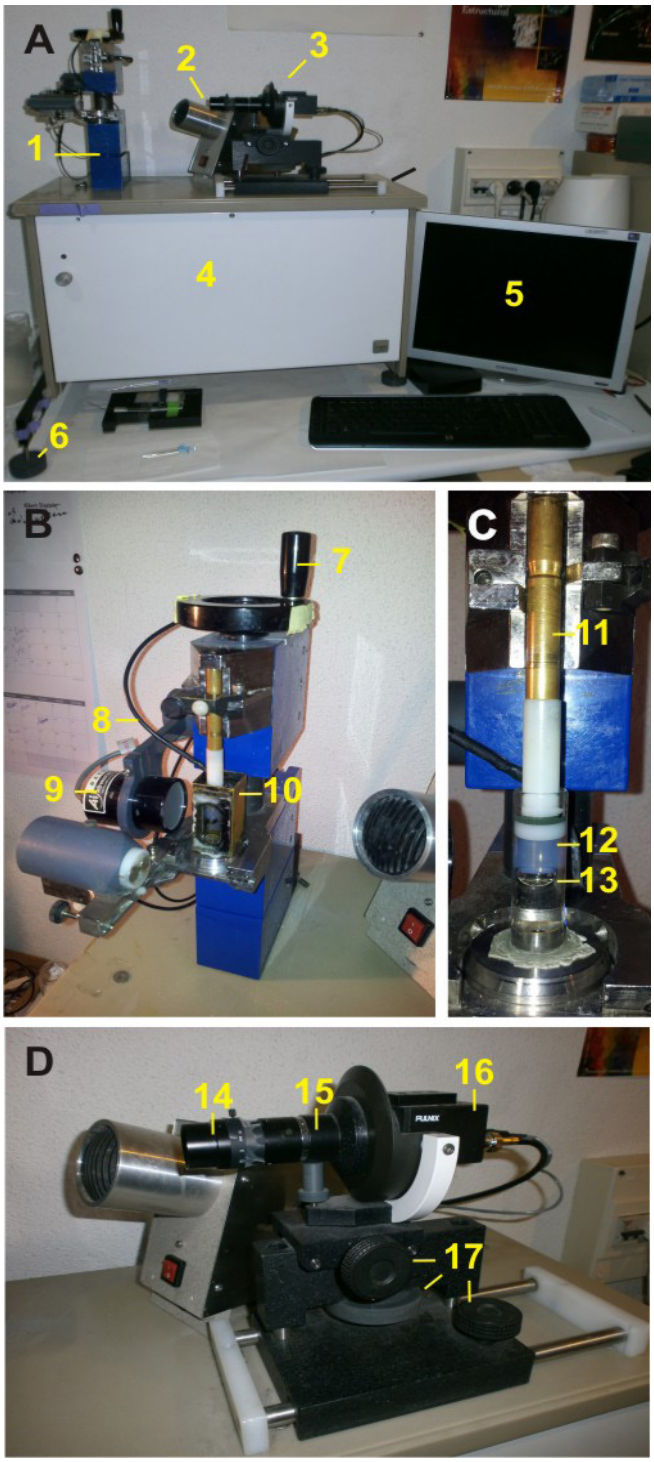

Figure 25. **Captive Bubble Surfactometer (CBS) system**. **A**. Overview of the principal components of the CBS: 1) Captive bubble apparatus, 2) Air Heater, 3) Camera, 4) Electronics, 5) Computer, 6) Tilt adjustment screws. **B**. Detail of the CBS apparatus: 7) Adjustment knob for settling bubble volume, 8) Temperature probe, 9) Infrared illuminator, 10) Water bath container. **C**. Magnification of the bubble chamber: 11) Piston, 12) Agarose plug, 13) Air bubble. **D**. Videocamera with base: 14) Camera lens, 15) Camera lens extension tube, 16) CCD videocamera, 17) Linear adjustments for X, Y and Z.

5 mM Tris, 150 mM NaCl pH 7.4 as well as 10 % sucrose, in order to increase the density of the solution, leading the surfactant material to float directly against the bubble avoiding a dilution effect in the hypophase. The inclusion of sucrose has been previously demonstrated to have no effects in surfactant performance (Gunasekara, Schurch et al. 2005). Temperature is controlled by enclosing the chamber in a metallic jacket containing a water bath which permits a homogeneous distribution of the heat provided by an external source. The chamber is thermostated at 37 °C by a feedback system monitored with a thermocouple in contact with the water and connected to the computer.

Despite the fact that surfactant preparations are routinely assayed at optimal concentrations of 25 mg/mL, we tested samples at concentrations on the limit of activity (12 mg/mL) in order to

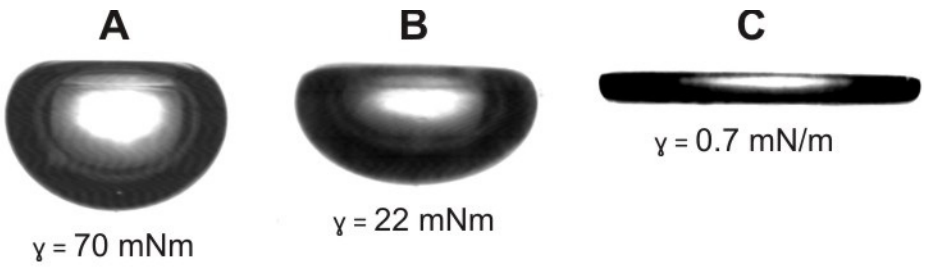

Figure 26. **Changes in bubble shape as a consequence of surface tension variations**. An initial bubble is created (**A**) and this gets flatter as the surface tension is reduced after injection of a surfactant sample down to equilibrium surface tension (**B**). Upon compression, an active surfactant leads to a decrease in surface tension to values close to 0 mN/m (**C**).

detect subtle differences among the different fractions. Experimentally, the evaluation of the surfactant performance of the samples was carried out as follows:

- Degasification: before sample application, the bubble was expanded in the sealed chamber for 10 min, allowing the liberation of the dissolved air in the aqueous subphase as little bubbles that join the expanded one, due to the pressure inside the chamber.

- Measurement of the initial adsorption kinetics: it simulates the accumulation of surfactant complexes at the air-liquid interface present in lung alveoli forming a film that reduces surface tension to equilibrium. In this first stage, around 200 nL of sample are injected into the chamber through a capillary connected to a 10 µL-Hamilton syringe directly touching the bubble surface and so applying the surfactant into the interface. Then, variations in surface tension are registered as changes in bubble shape (from a rounded to a flattened contour) during 5 min after sample application. An active surfactant reduces the normal surface tension of the aqueous subphase (70 mN/m) to the equilibrium surface tension of surfactant (20-23 mN/m) in a few seconds.

- Measurement of post-expansion kinetics: in this stage, the chamber is sealed and the bubble is rapidly expanded to a maximum volume of 0.15 cm^3. Surface tension is then monitored for 5 additional min while the reorganization, transfer and spreading of

the surfactant is taking place.

- Quasi-static compression-expansion cycling: it consists of 4 successive compression-expansion cycles at low speed, taking as initial volume the one the bubble reached during post-expansion. First, the bubble is compressed in a series of compression-relaxation steps, each reducing 20 % its previous volume, until reaching the minimum bubble size just before the interfacial film collapses. Bubble collapse can be detected by the operator when there is a decrease of the width of the bubble whilst there is no more flattening and subsequently no change in surface tension. Once the bubble has reached the minimum volume it is subjected again to expansion-relaxation cycles until acquiring the initial volume. To make data analysis easier, surface tension is plotted against the relative area of the bubble (with respect to the initial area), permitting the calculation of the compression rate. In principle, this quasi-static analysis does not have physiological significance since animal lungs does not perform respiratory cycles at such low speed. However, it is appropriate to describe the intrinsic kinetic properties of the sample since its biophysical behaviour is not hampered by putative kinetic effects imposed by a compression-expansion speed that might be quicker than the reorganization processes of the material.

- Compression-expansion dynamic cycling: finally and after finishing quasi-static cycling, the bubble is subjected to fast compression-expansion cycles at a rate of 20 cycles/min, mimicking the physiological performance. The compression range of the bubble is defined in the previous stage and so avoiding bubble collapse. Typically, only the cycles 1, 10 and 20 are represented against relative area.

- Stability after mechanical perturbations: additionally, after physiological dynamic cycling, the stability of the interfacial film can be assessed in terms of maintenance of a low surface tension during moderately long periods of time under mechanical perturbations (in physiological terms, sudden movements, external impact, coughing, etc.). For this purpose, films are compressed to the minimum surface tension possible without collapsing them, and then perturbed by a pendulum hammer consisting of

a steel rod attached to a rectangular metal block, whose small face acts as the striking surface. This block is released from a position of 90° to the vertical where it strikes the chamber (**Figure 27**). Experimentally, 10 perturbations are carried out in succession and surface tension is measured after each hit.

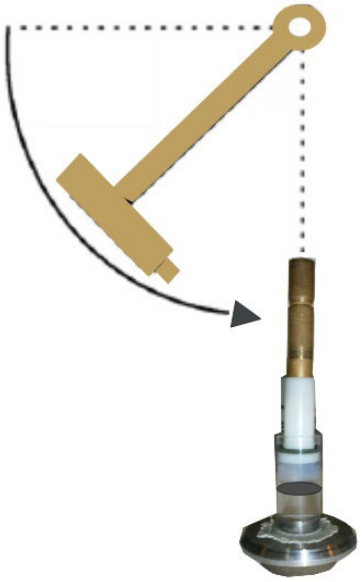

Figure 27. **Experimental setup for the evaluation of mechanical stability of surfactant films**. Once the bubble is led to maximum compression, a pendulum hammer is used to introduce repetitive mechanical perturbations whilst surface tension is monitored.

Bioelectrical measurements

Transepithelial electrical resistance (TEER) is a universally stablished biophysical parameter that provides information about the tightness of a cell monolayer and monitors the growth of epithelial tissue *in vitro.* TEER measures the capacity of the monolayer to oppose the flow of the current passing through it when a voltage is applied. Sharp increases in TEER values are correlated with highly confluent and tight cell monolayers (Benson, Cramer et al. 2013). TEER was measured using an epithelial Volt-Ohm-Meter (EVOM) (World Precision Instruments Inc., Sarasota, FL, USA) connected with planar chopstick electrodes (**Figure 28**). TEER measurements were performed submerging one of the probing electrodes in the apical compartment and the other one in the basolateral part (see **Figure 28B**). The difference of voltage across both electrodes was taken every 24 h from 0 to 6 days of time in culture. For cells differentiated at the ALI, prewarmed medium was added in the apical compartment and cells were then allowed to equilibrate for 15 min before TEER measurement. Values were corrected for the background value contributed by growth support and medium.

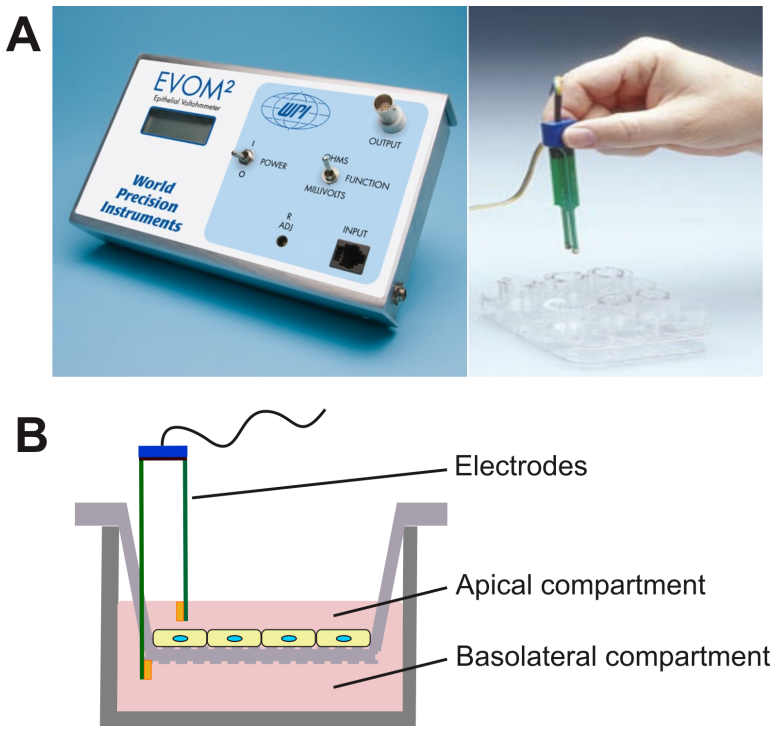

Figure 28. **Measurement of transepithelial resistance (TEER) in cell monolayers**. **A**. Experimental setup to determine TEER consituted by an Epithelial Volt-Ohm-meter (EVOM) (taken from "www.wpiinc.com") (left) and chopstick electrodes (taken from "www.pharmaceutical-int.com") (right). **B**.Schematic drawing representing the measurement of TEER in cells grown in Transwell systems.

Transport studies

Transport experiments with the paracellular fluorescent marker sodium fluorescein were carried out in freshly prepared Krebs-Ringer buffer (KRB) pH 7.4, containing 15 mM HEPES, 116.4 mM NaCl, 5.4 mM KCl, 0.78 mM NaH_2PO_4, 25 mM $NaHCO_3$, 1.8 mM $CaCl_2$, 0.81 mM $MgSO_4$ and 5.55 mM glucose, as adapted from a previous published protocol (Salomon, Muchitsch et al. 2014). DMSCs were differentiated under SC and ALI conditions on Transwell Clear supports. TEER values were determined after 4-5 days of differentiation and prior to the transport experiment in order to control the state of the monolayer. Initially, both compartments of the Transwell system were washed with prewarmed KRB, followed by 30 min of equilibration with KRB at 37°C. Then, the incubation buffer was substituted by a solution of sodium fluorescein 50 µM in KRB in the apical compartment (520 µL) and blank KRB was added to the basolateral compartment (1.5 mL). The initial donor concentration was quantified by taking 20 µL from the apical compartment directly

after the addition of the donor fluids. Differentiated cells were maintained at 37°C throughout the experiment, and 200 µL -samples were collected from the basolateral compartment at 20, 40, 60, 90 and 120 min. The collected volumes were replaced by adding 200 µL of KRB to the receiver compartment to keep a constant volume. At the end of the experiment, 20 µL from the donor compartment was taken to calculate the final concentration. The fluorescence of samples was evaluated in 96-well plates in an automated plate reader (Tecan Deutschland GmbH, Crailsheim, Germany) at excitation and emission wavelengths of 485 and 520 nm, respectively. A calibration curve was prepared in triplicate with sodium fluorescein in KRB with the following concentrations: 10, 8, 6, 4, 2, 1, 0.5 and 0 µg/mL. At the end of the experiment, TEER values were measured again to verify the cell layer integrity.

To assess the estimated membrane permeability (cm/s), the apparent permeability coefficient of the monolayers for sodium fluorescein was determined using the following equation: $P_{app}=(dQ/dt)\times A^{-1}\times c_0^{-1}$, being dQ/dt, flux of the substrate (µg/s); A, area of the membrane (cm^2); and c_0, initial concentration in the donor compartment (µg/ml).

After plotting the transported amount of sodium fluorescein against the time, a regression line was applied for the linear part of the curve. The slope of the regression line corresponded to the flux across the monolayer.

Cell viability assay

The cytotoxic effect of nanoparticles was assessed using the MTT assay, a widespread simple and accurate method to evaluate cell viability based on the activity of living cells via mitochondrial dehydrogenases (Mosmann 1983; Denizot and Lang 1986). MTT (3-(4,5-dimethylthiazol-2-yl)-2,5-diphenyl tetrazolium bromide) displays a yellowish colour and mitochondrial dehydrogenases of viable cells are able to cleave the tetrazolium ring, yielding insoluble purple formazan crystals. Formazan can be solubilized in DMSO resulting in a purple solution spectrophotometrically measurable. Any variation in the number of cells results in a change in the amount of formazan yielded, indicating the degree of cytoxicity caused by the test compound. Differentiated ATII-

LCs under SC conditions grown in 96 well-plates were incubated with anionic or cationic PLGA or silver NPs at concentrations of 1, 2.5, 5, 10, 50 and 100 µg/mL in KRB for 24 h . Cells grown in culture medium alone were considered as a high viability control (100 % viability) and others incubated with Triton X-100 (1 % v/v) were used as a low viability control (0 % viability). A549 cells were also used as a control of robustness and tolerance to the exposure to anionic PLGA and silver NPs. After 24 h of incubation, the medium containing NPs was removed and cells were washed with KRB. Then, fresh buffer containing 10 % (v/v) of MTT reagent (5 mg/mL) was added and cells were incubated for 4 h at 37 °C with shaking and protected from light. At this point, the buffer was removed and DMSO was added to the microwells to dissolve the formazan crystals formed inside the cells. Absorbance at 550 nm was measured in a multiwell plate reader (Tecan Deutschland GmbH, Crailsheim, Germany). Cell viability was calculated by the following equation: % cell viability= $(Abs_{exp} - Abs_{low\ control})/(Abs_{high\ control} - Abs_{low\ control})$.

Aerosolization of non ionic PLGA nanoparticles

Air-Liquid interface cell exposure system (ALICE)

The ALICE is a validated device for dose-controlled delivery of NPs or other substances in liquids or solutions to cells cultured under air-liquid interface conditions (Lenz, Karg et al. 2009) (**Figure 29**). Its operation principle is based on a method of cloud settling combined with single particle sedimentation. The term “cloud settling” refers to the situation in which the droplet concentration is high enough to provide a sufficient flow resistance to provoke the air to go around, instead of through, the cloud of droplets.

The ALICE system consists of the following principal components:

- A nebulizer or droplet generator, in charge of providing the dense cloud of droplets (80-130 g/m^3). The liquid sample to be tested is nebulized by a perforated, piezoelectrically-driven vibrating membrane. When the membrane vibrates (at a frequency of 117 kHz),

it generates acoustic pressure waves, which press small amounts of fluid through the tapered holes.

- The exposure chamber, a polycarbonate 12 liter-box where the droplets are deposited onto the cells placed at the bottom of the chamber, is designed to hold up to twelve transwell inserts. Its transparent nature permits an easy visualization of the bulk motion of the cloud.

- The flow system wich is operated with a closed loop flow system generated by an air pump and a flow meter yielding rates of 5 L/min. The flow rate is standardized to this value to assure that the cloud is transported to the central part of the chamber to provide with a uniform spatial distribution of the aerosolized substance.

Cell exposure to FA-PLGA nanoparticles

Differentiated ATII-LCs under ALI conditions in Transwell systems were exposed to FA-PLGA NPs using the air-liquid interface cell exposure system (ALICE) (Vitrocell® Cloud 12/12, Vitrocell Systems GMbH) as previously described (Lenz, Karg et al. 2009; Brandenberger, Rothen-Rutishauser et al. 2010; Herzog, Clift et al. 2013). The base module was filled with prewarmed culture medium prior to the insertion of the supports covered by cells. 100 µL of FA-PLGA nanoparticles at concentrations of 10 µg/mL and 25 µg/mL in PBS were nebulized forming a cloud which was settled for 5 min. These concentrations were chosen taking into account the results provided by the cytotoxicity experiments to avoid a deleterious effect in the cells as well as the efficiency in the aerosolization procedure (around 70 %). The nebulizer gradually filled the chamber with the droplet cloud and as soon as the nebulizer was empty, the air flow was stopped and the droplets settled to the ground onto the cells. Then, the inserts with cells were taken out and placed back in the incubator maintaining ALI conditions for post-incubation and analytical processing.

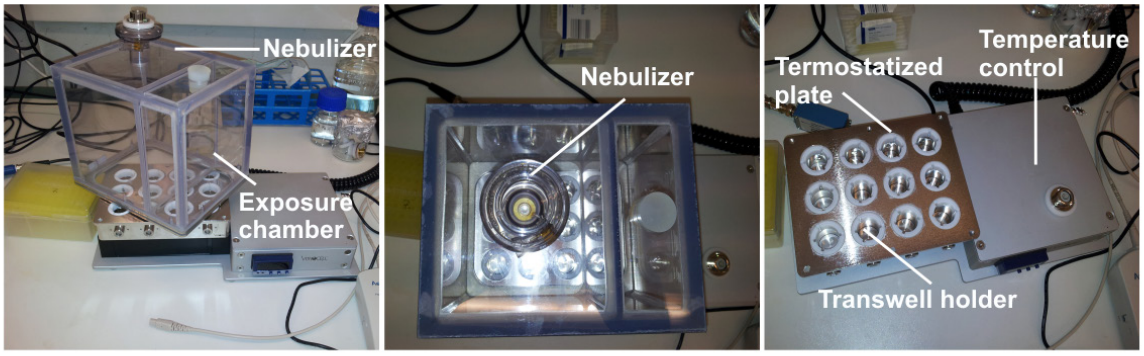

Figure 29. **Air Liquid Cell Exposure (ALICE) system**. Images of the ALICE Vitrocell® Cloud 12/12 device, constituted by a nebulizer for aerosolization of liquid formulations and a exposure chamber with controlled flow allowing deposition of aerosolized liquids onto cells in cultivation.

Cellular uptake of PLGA nanoparticles

Cells were incubated for 3 h and 24 h after the exposure to FA-PLGA NPs with the ALICE system and cells were immunostained at room temperature as follows. Cells were washed with PBS twice and fixed with 3 % paraformaldehyde in PBS for 30 min. After fixation, blocking was carried out by incubation with 50 mM NH_4Cl/PBS for 15 min. Next, cells were permeabilized with 0.05 % saponin/1 % BSA/PBS and incubated for 20 min. Afterwards, actin was stained with AlexaFluor 680-phalloidin (Invitrogen) in a dilution of 1:500 for 30 min. After washing with PBS, nuclear staining was performed by incubation with DAPI (1:5000) for 20 min. Samples were washed and inserts were cut with a scalpel and mounted with a coverslip in a slide with mounting medium (Dako) and stored at 4 °C in darkness. Cells not exposed to NPs were also used as a negative control to exclude any side effects.

Slides were visualized by confocal electron microscopy under a LSM 710, Axio Obsever microscope (Zeiss). Single plane (4 µm) and z-stack images (14 µm, z-step= 0.4 µm) of multiple focal planes were obtained using a LD C-Apochromat 40x/1.1 W Korr M27 objective. Excitation wavelengths for Alexa Fluor 680, DAPI and fluoresceinamine from NPs were 633, 405 and 488 nm, respectively. Image visualization and processing was performed using ZEN software (Zeiss).

DATA REPRODUCIBILITY AND STATISTICS

When possible, figures represent the mean ± standard deviation after averaging data from at least three independent experiments. In other cases, like cycling isotherms, illustrative curves are shown after at least three repetitions. Comparisons among the experimental groups were made using the Student's *t*-test or an analysis of variance (ANOVA) using the Holm-Sidak method, with significance level p= 0.05.

Chapter 1

Part of the experiments included in the present chapter were performed at the Department of Medical Physics (Inssbruck University, Austria), with the assisstance and supervision of Prof. Dr. Thomas Haller and at the Department of Chemistry of Imperial College London (United Kingdom), in collaboration with Dr. Nicholas Brooks.

INTRODUCTION

Phospholipids, neutral lipids and the associated proteins essentially constituting the pulmonary surfactant system (Goerke 1998; Blanco and Pérez-Gil 2007; Pérez-Gil and Weaver 2010), are produced in alveolar type II (ATII) cells located in the distal airways of the lung. The protein components are synthesized in the endoplasmic reticulum, processed in the Golgi apparatus and late endosomes/multivesicular bodies and partly assembled in the intracellular storage organelles known as lamellar bodies (LBs), whereas surfactant lipids may traffic directly from the ER to the LBs (Wright and Clements 1987; Pérez-Gil and Weaver 2010; Vanhecke, Herrmann et al. 2010).

A typical ATII cell can have 100-150 LBs with various sizes but typically of 1 µm in diameter. LBs are lysosome-related vesicles with an acidic pH of about 6 (Chander, Johnson et al. 1986). Proteomic profiling of LBs reveals a highly dynamic organelle containing proteins corresponding to different functional categories, mainly associated with lipid-related functions and involved in the biosynthetic, secretory and endocytic pathways of lung surfactant (Wang, Chintagari et al. 2008; Ridsdale, Na et al. 2011). Interestingly, the lipid importer ABCA3 has been proposed to play a key rol in surfactant biogenesis incorporating phosphatidylcholine (PC) and phosphatidylglycerol (PG) through the limiting membrane and into the LB (Ban, Matsumura et al. 2007; Ridsdale, Na et al. 2011). Deficiencies in this transporter are associated with some respiratory syndromes of variable severity (Fitzgerald, Xavier et al. 2007). By transmission electron microscopy, LBs appear as osmiophilic vesicles with tightly packed, relatively periodic arranged lamellae, surrounded by an outer limiting membrane (Vanhecke, Herrmann et al. 2010). Interestingly, morphological differences in LBs can be discerned among species. Human LBs are constituted by concentric arranged lamellae revealing a dense projection core enriched in SP-B, whereas LBs from rodents do not contain this specific protein accumulation and their lamellae are organized in parallel (Ochs 2010), probably due to a different spatial distribution of the surfactant proteins, particularly SP-B (Brasch, Johnen et al. 2004; Pérez-Gil 2008).

Exocytosis of LBs is a constitutive and regulated process, which can be stimulated by certain chemical or physical factors implicated in the delay between stimulus and fusion of the surfactant

secretory vesicles, the expansion of the fusion pore, the release of vesicle content, and, finally, its extracellular dispersion (Chander and Fisher 1990; Mason and Voelker 1998; Dietl, Haller et al. 2001; Dietl and Haller 2005). Upon secretion, LBs are released as dense particulate entities (lamellar body-like particles, LBPs) which remain in a compact state until reaching the alveolar air-liquid interface (Haller, Dietl et al. 2004). At this point, LBPs disintegrate leading to an instantaneous spreading of material onto the interface and formation of an active surface film. It has been recently reported how the adsorptive capacity of LBPs into an air-liquid interface is affected by some physicochemical parameters, such as pH and temperature (Hobi, Siber et al. 2014). A particular dramatic impact on interfacial adsorption was seen by proteolytic treatment of LBPs, suggesting the importance of surfactant protein for adsorption and surface film formation. It had been previously established that the films formed by adsorbed LBPs exhibit a lateral structural heterogeneity manifested by a lipid phase coexistence displaying segregated ordered and disordered regions (Ravasio, Olmeda et al. 2010). In addition, progressive adsorption of LBPs leads to the appearance of large protruded 3-dimensional (3-D) complex structures as well as a stiffening and solidification of the ensuing surface films. Interestingly, the solid-like character and the 3-D structures are not observed upon adsorption of surfactant purified from bronchoalveolar lavage (BAL). These findings suggested that surfactant derived from BAL, which is typically used as a standard material and a reference for optimal surfactant function, could only partially represent the properties of the film existing in the alveolar spaces, perhaps preventing a proper interpretation of the structure and behavior of surfactant in the native situation.

In the present chapter and to further investigate the genuine structural organization of LBPs, we have assessed the packing and hydration properties of native lung surfactant membranes isolated from porcine bronchoalveolar lavage in comparison with surfactant stored in the form of intracellular LBs as well as in LBPs secreted by primary cultures of rat AT II cells. We have also analyzed the nanostructural features of adsorbed LBPs as well as their response to inhibitory agents in terms of surface activity and stability. Our findings corroborate the existence of significant structural differences between both types of surfactant organizations and their correlation with functional efficiency at the air-liquid interface.

RESULTS

Membrane thermotropic properties

To evaluate the packing and hydration properties of the native surfactant forms we took advantage of the spectroscopic features of the probe Laurdan, which is sensitive to the hydration level of the lipid headgroup region and allows to detect changes in membrane phase properties. We started our investigations in intact rat ATII cells, the source of pulmonary surfactant, where we found that staining of intracellular LBs by Laurdan was extremely time- and T-dependent (**Figure 1.1**). At 37 °C and after 1 h of incubation, most of the probe was accumulated close to the limiting membrane of LBs (**Fig.1.1B**) whereas diffusion of the probe into deeper layers of LBs occurred at prolonged incubation times (3 h). As obvious from this figure, LBs were the main site of Laurdan accumulation and individual LBs showed a consistent spectral emission of Laurdan with only small differences in the distribution between lipid ordered (blue) and lipid disordered (green) states.

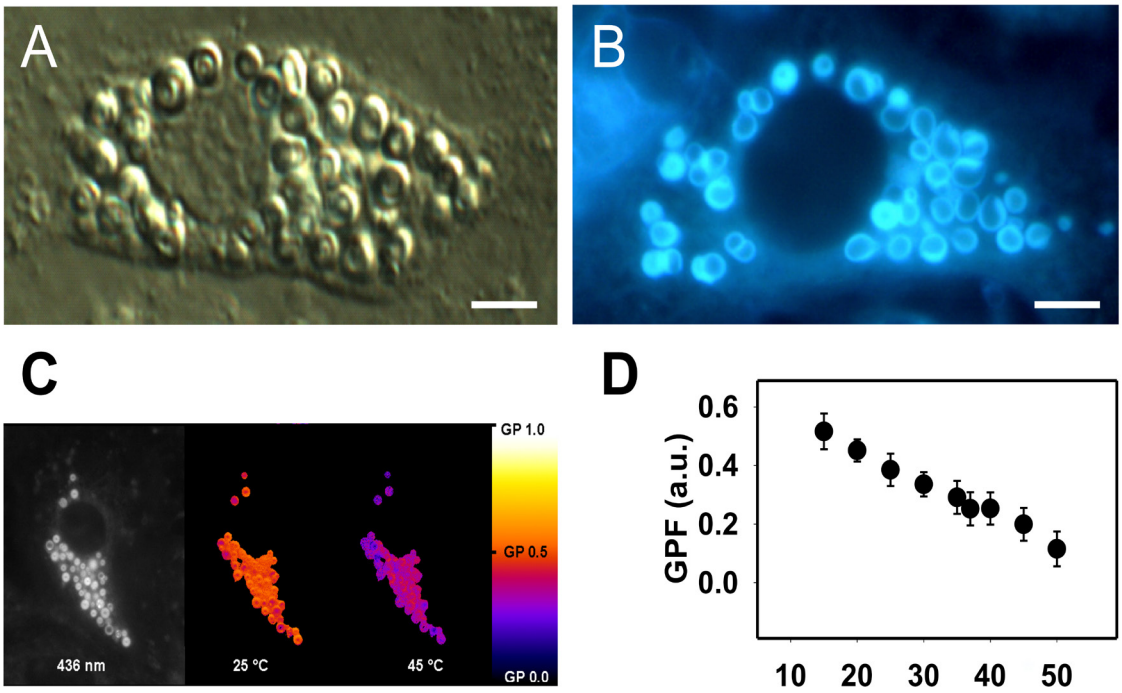

Figure 1.1. Laurdan fluorescence in living rat ATII cell cultures. **A**. One single ATII cell displaying its characteristic cytoplasm full of storing lamellar bodies under brightfield microscopy. **B**. Laurdan fluorescence from labeled lamellar bodies suggesting a progressive labelling of the membranes from outer to inner locations. **C**. GPF representation in one ATII cell evidencing the sensitivity to temperature-dependent structural changes in LB membranes. **D**. Plot of the thermotropic profile of GPF in intracellular LB membranes. Scale bars represent 5 µm.

In some LBs, a sort of opening lacking of fluorescence signal could be discerned (**Fig.1.1B**, arrow). The thermotropic phase behaviour was tested by applying a T-ramp (15 to 50 °C) to the stained cells (**Fig. 1.1C**, **D**), demonstrating a relatively high dehydrated and packed state below and even above physiological temperatures. At 25 °C, LB membranes showed GPF values of around 0.4, similarly to what has been previously reported for condensed pure DPPC monolayers but significantly higher than those obtained from expanded fully hydrated POPC bilayer and monolayer structures, which display values around -0.2 at the same temperature (Picardi, Cruz et al. 2011). However, at 45 °C GPF in intracellular surfactant membranes still remained in positive values of around 0.20 (dehydrated, condensed packing) compared to the fairly expanded and hydrated character of DPPC, POPC or DPPC/PG bilayers, which exhibit values below 0 at equivalent temperatures (Picardi, Cruz et al. 2011).

To gain additional insight into structural features of the lipid assemblies present in LBs, we examined living ATII cells by incident polarized light microscopy (**Figure 1.2**). Birrefringent signal coming from intracellular lamellar bodies (**Fig. 1.2A**) as wells as secreted LBPs (**Fig**. **1.2A** insert) appeared as bright crosses, suggesting the presence of crystal-like highly ordered structures. The relationship between signal intensity and temperature was shown to be inverse, as polarization decreased when temperature was increased (**Fig. 1.2A** right panel and **1.2C**). At high temperature, the signal seemed to disappear but returned again after cooling.

DPPC vesicles were also examined and similarly to LBs, they were found to display optical signs of birrefringence at temperatures below T_m. However, in this case, the intensity of the polarization signal was not significantly declined when temperature was increased (**Fig. 1.2B**). In summary, the thermotropic profiles obtained from polarization microscopy and Laurdan fluorescence were similar, and even showed a linear correlation (**Fig. 1.2D**).

Laurdan fluorescence, but not polarization, could be applied to test for differences between released LBPs, native surfactant membranes and membranes reconstituted from its organic extracts (**Figure 1.3**). Whereas NS and OE exhibited a typical broaden phase transition, from an ordered (blue emission) to a disordered state (green emission), ending slightly above 37 °C (**Fig**. **1.3A** and **1.3C**), released LBPs showed a significantly less pronounced GP change upon the

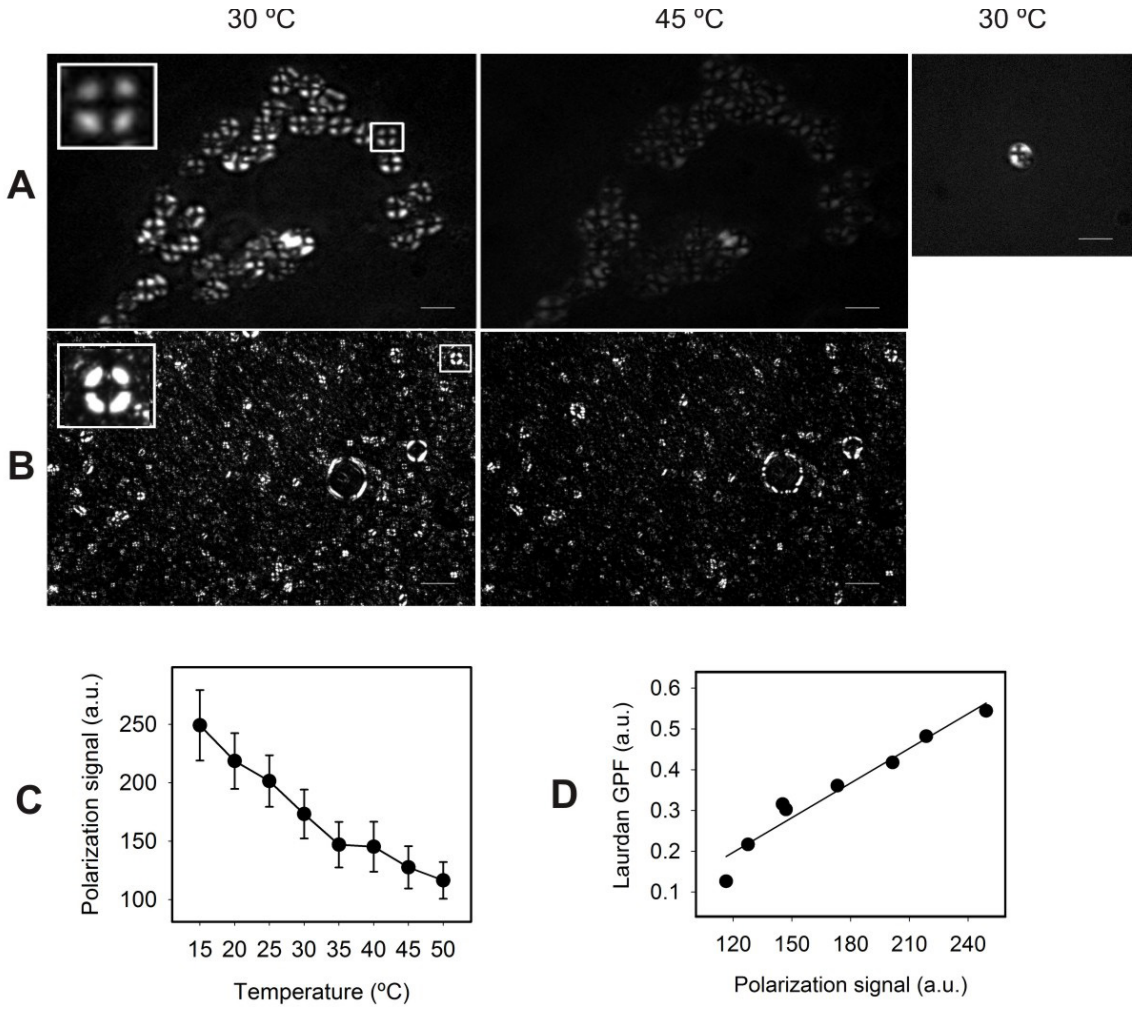

Figure 1.2. **Polarized light microscopy of intracellular and secreted lamellar bodies**. Birrefringent cross polarization signal coming from intracellular LB membranes (**A**) and DPPC vesicles (**B**), at 30 °C (left) and 45 °C (right) and exocyted LBPs (A, insert) at 30 °C. **C**. Plot showing the inverse relation between polarization signal and temperature. **D**. Plot presenting the significative correlation between Laurdan and polarization signals.

same thermal treatment by maintaining a blue emission throughout the entire T-range up to non physiological high temperatures (**Fig. 1.3B** and **1.3C**), similar to that obtained with intracellular LBs. Thus, LBs as well as LBPs exhibited an apparently more limited phase transition, which is different from that of NS or OE. Nevertheless, when compared intracellular and freshly released LBs at high temperatures such as 50 °C, the second ones exhibited even upper GPF values (0.11 vs 0.32, respectively), demonstrating a striking condensed and dehydrated character.

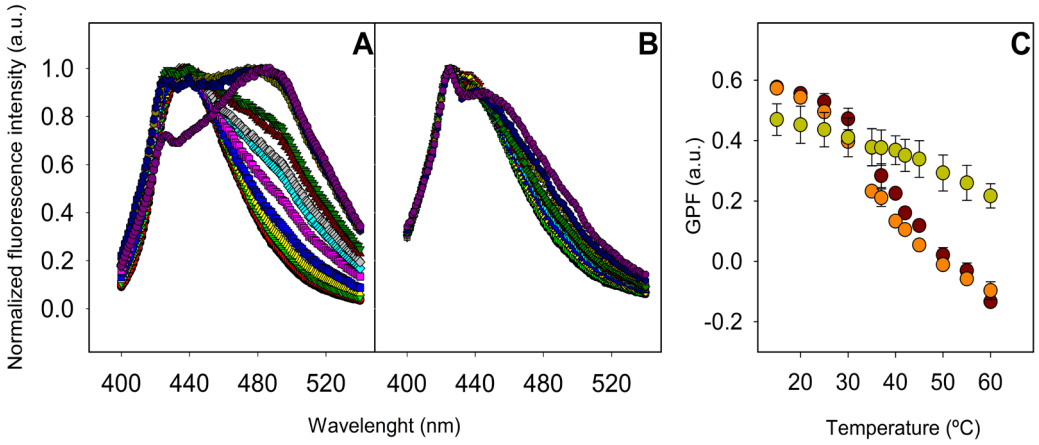

Figure 1.3. **Laurdan fluorescence in surfactant preparations in cuvette experiments**. Fluorescence spectra of Laurdan in suspensions of native surfactant (NS) membranes purified from BAL (**A**) or suspensions of secreted LBPs from rat ATII cells (**B**) recorded at 10 °C (●), 15 °C (●), 20 °C (▼), 25 °C (▲), 30 °C (■), 35 °C (■), 37 °C (◆), 40 °C (◆) , 42 °C (▲), 45 °C (▼), 50 °C(⬢), 55 °C(⬢) and 60 °C(●). Fluorescence spectra of the probe in reconstituted membranes from the organic extract of NS were almost identical to the spectra of NS and they are not shown. **C**. Thermotropic profiles of Generalized Polarization Function of the fluorescence in NS membranes (●), membranes reconstituted from organic extract of NS (●) and LBPs (●).

ATR-FTIR spectra also evidenced differences in the thermotropic behaviour and structural organization of lipid phases in LBPs (**Figure 1.4**). LBPs displayed a particular thermotropic profile shifted to substantially higher wavenumbers, and their T_m was increased in comparison with that of NS or OE membranes (**Fig 1.4A**). The increase of wavenumber in the CH_2 stretching bands upon heating above T_m is attributed to the presence of gauche conformers along the acyl chains. The frequency of the LBPs band was shifted to higher wavenumbers than observed in NS, indicating more intrinsically disordered acyl chains in LBPs (**Fig. 1.4C**). CH_2 bending bands are sensitive to hexagonally packed hydrocarbon chains. LBPs showed displaced bands with relation to NS or its OE, suggesting the potential presence in LBPs of non-lamellar lipid phases (**Fig. 1.4B**).

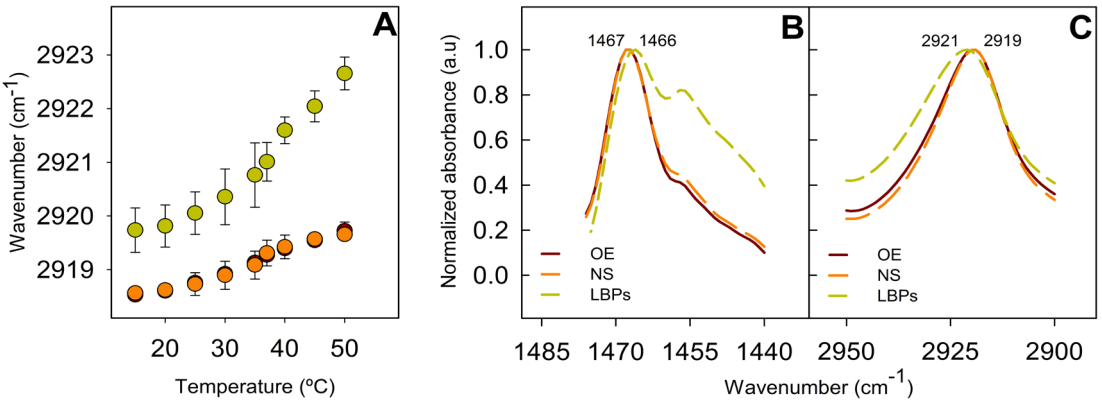

Figure 1.4. **ATR-FTIR spectroscopy of surfactant preparations**. Thermotropic behaviour of native surfactant membranes (●) or membranes reconstituted from its organic extract (●) and secreted LBPs (●) according to the CH_2 stretching bands wavelength (**A**). ATR-FTIR spectra of NS, OE and LBPs corresponding to the CH_2 bending band (**B**) or to the CH_2 stretching band (**C**). Numbers inside the plots indicate the peak values for NS (orange line) and LBPs (yellow dotted line) in the corresponding absorption band.

Lateral organization of membranes derived from LBPs

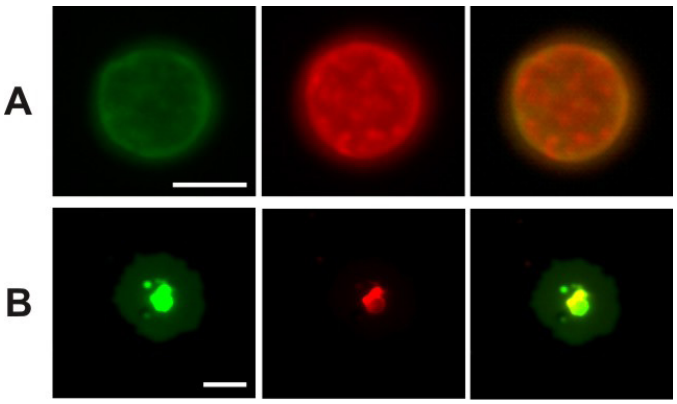

Figure 1.5. **Giant Unilamellar Vesicles (GUVs) prepared from LBPs**. Images prior to adsorption (**A**) and after spontaneous spreading of the sample (**B**). The giant vesicles are labeled with the lipophilic fluorescence probes Bodipy-PC (green, left panel) and DiIC 18 (red, central panel). Merge of the channels is displayed in right panel. Rounded red areas in the images correspond to fluid ordered regions, and the green background corresponds to fluid disordered phase. The scale bars correspond to 5 µm in A and 10 µm in B.

GUVs formed from material of LBPs were generated to determine their lateral phase structure. Images of single GUVs composed of LBPs doped with the fluorescent probes Bodipy-PC and DiIC18 can be observed in **Figure 1.5**. The particular round shape of the domains as well as the partition properties of the different fluorescent probes suggested that the lateral organization of the vesicles corresponded to a fluid ordered/fluid disordered-like phase coexistence (**Fig 1.5A**).

In Fig. **1.5B**, one vesicle adsorbed onto the glass support can be observed. Once the vesicle spread, a different structural organization took place and the previous type of coexistence

seemed to disappear revealing a core region surrounded by an area of more disordered material.

Nanostructure of adsorbed LBPs

To further explore the lateral structure of the membranes constituting LBPs at submicrometer and nanometric scales we examined their organization by AFM. **Figure 1.6** shows AFM images obtained from the structures that LBPs spontaneously form upon adsorption and direct spreading onto the mica support. In **Fig**. **1.6A** homogeneous membranous patches with round protruding boundaries and containing a central core displaying a particular pattern composed of structures of different heights can be discerned. Topological analysis showed that the distribution of heights observed in the central core is more heterogeneous than the height distribution observed in the surrounding area. The central area is magnified in **Fig**. **1.6B**, revealing numerous well-defined sub-micron sized structures with similar diameters (around 0.1 μm) and a height of around 7-8 nm with respect to the general lipid patch and distributed with certain regularity (distanced 0.1 μm with respect to each other). Although with a minor proportion, other structural organizations were observed as seen in **Fig. 1.6C,** which shows a membrane patch with similar morphology but without the presence of a distinguishable central area and displaying various nano-sized areas with at least four different levels of height.

Adsorption properties and resistance to inhibition

To investigate the interfacial adsorption properties of LBPs in the presence of inhibitory agents, we used a method that allows evaluation of the amount of surfactant material accumulating at the interface and the resistance of the formed surface films and associated structures against mechanical agitation. The deleterious effect of serum proteins and meconium has been previously shown to cause a significant impairment of the surface properties of surfactant, associated with severe respiratory disorders such as acute respiratory distress syndrome or meconium aspiration syndrome, respectively (López-Rodríguez, Echaide et al. 2011; López-Rodríguez, Ospina et al. 2012).

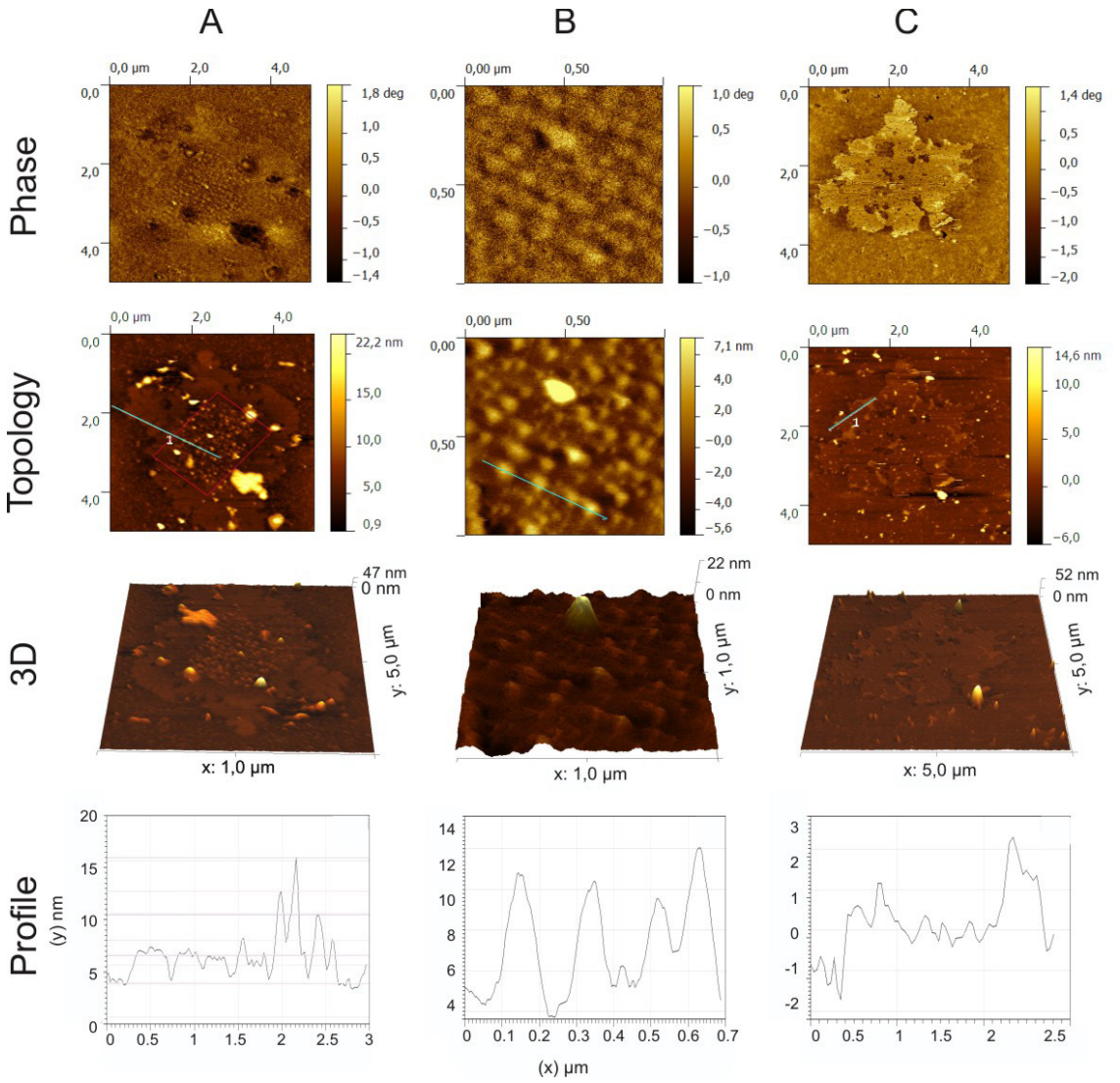

Figure 1.6. **AFM scanning images from adsorbed LBPs**. Images under phase contrast mode, topology images, tridimensional projections and topological profiles (corresponding to the blue lines marked in topology images) of suspensions of LBPs upon adsorption onto mica supports at different magnifications. Image **B** corresponds to a magnification of the area highlighted in **A**. Lateral distances are 5 µm in A and C and 1 µm in B.

In **Figure. 1.7**, adsorption kinetics in the presence of increasing amounts of serum (**Fig. 1.7A**) or meconium (**Fig. 1.7C**) of comparable quantities of suspensions of native surfactant (left panel), its reconstituted organic extract (middle panel) or LBPs (right panel) are displayed. The results show how all the materials were able to reach the interface quickly and stably remain associated with it, while their exposure to increasing concentrations of either of the two inhibitory agents, produced a progressive reduction in the amount of interfacial surfactant. However, LBPs showed a marked resistance to inhibition, displaying significantly better adsorption kinetics than native

surfactant membranes in the presence of equivalent concentrations of inhibitory agents (**Fig. 1.7B,D**).

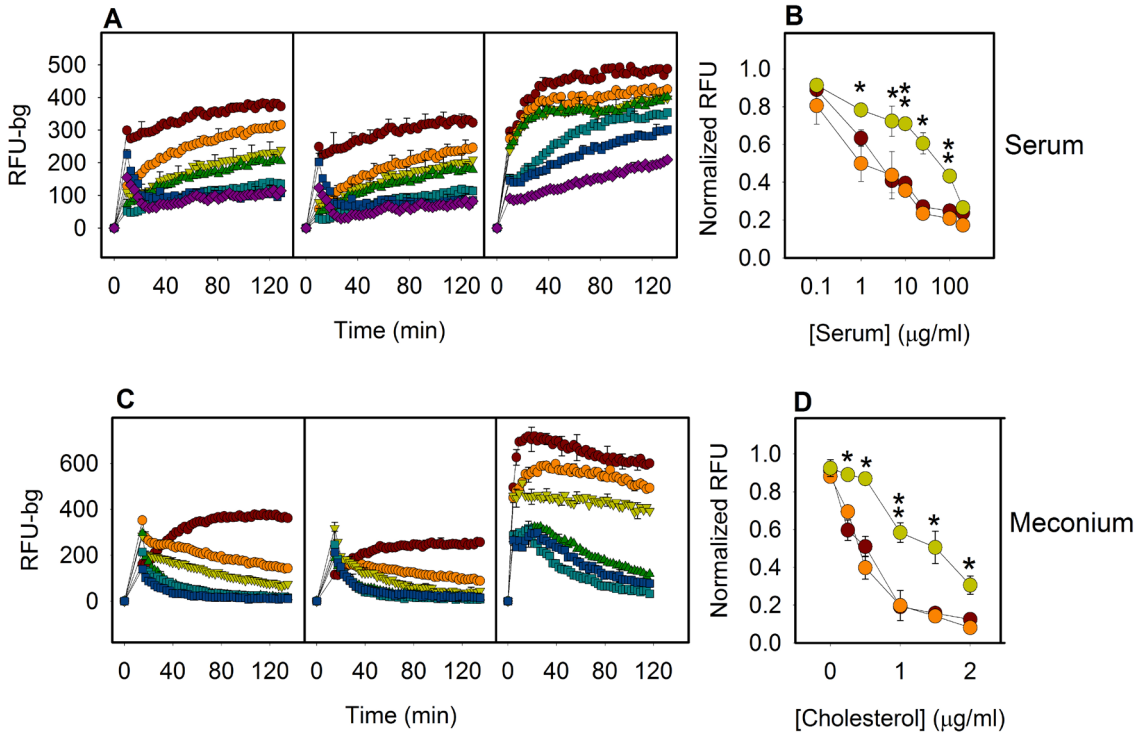

Figure 1.7. **Resistance to inhibition in terms of interfacial adsorption properties of surfactant preparations**. Dose-dependent inhibitory effect of human serum proteins (**A**) or meconium (**C**) on the adsorption kinetics of native surfactant (NS, left panel) membranes reconstituted from its organic extract (OE, central panel) and secreted LBPs from rat ATII cells (right panel) Serum protein concentrations were 0 (●), 1 (●), 5 (▼) 10 (▲), 25 (■) 100 (■) and 200 (◆) μg/ml and cholesterol concentrations in meconium were 0 (●), 0.25(●), 0.5 (▼), 1 (▲), 1.5 (■) and 2(■)μg/ml. Fluorescence values taken after 60 min of adsorption of NS (●), OE (●) and LBPs (●) as a function of serum protein concentration (**B**) or meconium (**D**). Adsorption efficacy in terms of amount of adsorbed material into the surface was significantly (*p<0.05 and ** p<0.01) higher in the case of LBPs than in NS and its OE at elevated concentrations of inhibitory agents. (RFU – bg = Relative fluorescence units – background).

DISCUSSION

The assembly of lung surfactant membranes in the lamellar bodies (LBs) of alveolar type II cells requires ABCA3 transporters as well as the energy provided by ATP hydrolysis. Considering these requirements, an hypothesis can be raised that the energy expenditure during LB biogenesis confers to surfactant complexes an "energy-loaded state", which later might sustain the remarkable efficiency by which released LBPs avidly transform into an interfacial film (Ravasio, Olmeda et al. 2010). In contrast, native surfactant (NS) complexes purified from bronchoalveolar lavages have been usually considered as the most representative surfactant material, a sort of "gold standard", for defining structure-function determinants and optimal surfactant functions. However, taking into account that the isolation procedure consists of collecting material from very different regions of the respiratory tract and that this material may contain the product of different states of metabolic and physical conversions (i.e. already exposed to an air-liquid interface or even recycled), the resultant samples may consist only partially the functional active fraction secreted to the lung alveoli. In fact, previous studies provided evidence that interfacial films formed by freshly secreted LBPs have significantly different structures and properties than films formed by whole natural surfactant purified from animal lungs (Ravasio, Olmeda et al. 2010), which could also contain already "spent" or partly inactivated surfactant.

To gain more insight into the real behaviour of freshly assembled and secreted surfactant within the alveolar spaces we investigated the specific organization of lipids and proteins in surfactant membranes directly obtained from alveolar type II cells and compared these data with surfactant purified from animal lungs. On the one hand, we assessed the thermotropic behaviour of surfactant membranes in terms of packing and hydration by monitoring the fluorescent probe Laurdan. This probe is sensitive to the polarity of the environment and is also known to partition into both ordered and disordered regions providing a general overview of lipid organization. The results show that membranes constituting freshly secreted LBPs posses a highly dehydrated and packed state in comparison with NS and membranes reconstituted from its organic extract (OE). This is astonishing because in NS, a highly dehydrated and packed state can only be seen by applying a lateral compression. This observation is also consistent with previous morphological

descriptions in which released LBPs appear as dense particulate entities which retain a highly packed character until contacting the air-liquid interface (Haller, Dietl et al. 2004). In addition, it also reflects consistence with the observation that the efficiency in surfactant performance at the interface is related to the propensity of surfactant layers to reach highly dehydrated states (Picardi, Cruz et al. 2011).

On the other hand, we also took advantage of the spectral properties of Laurdan to obtain qualitative and quantitative information of the packing state of surfactant stored within the cells. Labeling of primary cultures of ATII cells with the probe resulted in its preferred accumulation in LBs. However, accumulation was not uniform as fluorescence intensity was maximal in regions close to the vesicle's periphery. This could reflect the time-dependent diffusion of the probe into deeper surfactant layers or the existence of more compact layers constituting a diffusion barrier near the central core. Also, labeling differs among individual LBs within the same cell, which could reflect the coexistence of different stages in biogenesis and maturation of these organelles. Interestingly, a defined site of the packed structure exhibits a sort of opening in many of the LBs, lacking fluorescence signal. It is tempting to speculate with the possibility that the "opening" could be the location of a putative protein-based "machinery" in charge of controlling the opening and spreading of pre-packed membranes once contacted with the air-liquid interface, although further investigation will be needed to confirm this hypothesis. Importantly, Laurdan reveals a highly dehydrated state of the surfactant lipids in LBs and a thermotropic profile that is similar to that of LBPs.

The thermotropic profile as revealed by Laurdan spectroscopy reveals a striking similarity to the changes obtained by polarization microscopy. Although the former method is most likely reporting about changes in lipid packing and hydration and the latter most likely about periodical molecular organization, it can be assumed that both inform essentially about the same phenomenon connected with the transition from ordered into disordered states. Polarization, however, is non-invasive and thus serves as an acceptable positive control for the use of Laurdan as an invasive lipophilic probe. It is known that anisotropic lipids forming crystal-like structures are able to produce birrefringence patterns under polarized light (Butovich, Lu et al. 2014). Considering this, we interpret that the optical anisotropy of LBs is probably the result of the

radial-symmetric orientation of the phospholipid acyl chains and that the strong birrefringent signal suggests that LBs exist in a liquid-crystal arrangement at physiological temperatures. We further speculate that the polarization intensity may be determined by either the amount of bilayers per unit of volume and/or the degree of molecular alignment of the acyl chains with respect to the orientation of the polarized light wave front. As a matter of fact, the preponderance of anisotropy reflected in these cross-signals has been observed in other lipid preparations being also associated to smectic liquid-crystalline states (Katz, Shipley et al. 1976). The fact that the polarization signal diminished at heating towards an optically isotropic state but increased again after cooling could be consistent with a reversible kind of structural reorganization such a phase transition. Indeed, the observation of isotropic phases in other lipid samples at high temperature has been related to organizations in such a way that one of the three-dimensional crystallographic cubic space groups is satisfied (Shipley, Avecilla et al. 1974) resulting in a cubic symmetry with finite-length rods of lipids linked and interwoven (Luzzati, Gulik-Krzywicki et al. 1968). Interestingly, preparations containing exclusively DPPC molecules, which are known to be arranged in pure lamellar phases, did not seem to experiment this type of transition maintaining a birrefingent signal after heating.

By Attenuated Total Reflectance-Fourier Transformed Infrared Spectroscopy (ATR-FTIR) we also acquired thermotropic profiles that revealed temperature-dependent changes in packing and lipid order, without the necessity of introducing extrinsic probes. The results again demonstrate that the IR thermotropic profile of LBPs is significantly different from those of NS membranes or membranes reconstituted from its OE. The intensity of the CH_2 asymmetric stretching IR absorption band, which is sensitive to conformation, increases upon heating above T_m, which is attributed to the presence of gauche conformers along the acyl chains (Casal and Mantsch 1984; Lotta, Virtanen et al. 1988; Lewis and McElhaney 2013). In LBPs, the frequency of the band is shifted to significantly higher wavenumbers than observed in NS, indicating more intrinsically disordered acyl chains. This higher disordered state of the acyl chains in LBPs as determined by ATR-FTIR is apparently in conflict with the results obtained by the Laurdan measurements, which demonstrated a higher packing and lower hydration. However, these inconsistencies could be conciliated considering the possible presence of non-lamellar phases (Lewis and

McElhaney 2013). We examined the IR spectra at the CH_2 bending absorption band, which is dependent on acyl chain packing and conformation and so sensitive to the presence of non-lamellar phases (Wallach, Verma et al. 1979; Casal and Mantsch 1984). This band also reflects important differences between LBP membranes and both NS and its OE, which are known to be organized constituting two lamellar phases with different thicknesses, as observed by Small Angle X-ray Scattering (SAXS) analysis (Bernardino de la Serna, Vargas et al. 2013). Recently, it has been proposed that non-lamellar phases might indeed exist in surfactant lipid complexes and that these phases could be involved in the interconnection of the active surface film with multilayered structures acting as a surfactant reservoir at the aqueous subphase (Chavarha, Khoojinian et al. 2010). By using lipid model systems, it has also been shown that surfactant proteins SP-B and SP-C promote the formation of cubic phases (Chavarha, Khoojinian et al. 2010; Chavarha, Loney et al. 2012). Furthermore, surface-active lipids have been shown to facilitate the formation of hexagonal H_{II} phases (Perkins, Dause et al. 1996), highlighting the importance of lipid polymorphism in surfactant function. Unfortunately though, ATR-FTIR does not provide sufficient structural information to definitely prove or disprove the presence of particular lipid phases as could be the case for a number of other methods. These methods, however, in particular X-ray diffraction or P^{31} NMR, could not be applied to study LBP samples due to the extremely limited amount of LBPs that can be collected from isolated cells.

Considering the complex composition of lipids and proteins in lung surfactant, the role of phase coexistence has already been suggested as a key feature in functional terms (Bernardino de la Serna, Pérez-Gil et al. 2004; Casals and Cañadas 2012). Our results obtained upon examination of the lateral phase structure of intact GUVs prepared from LBP membranes are consistent with previous reports from Ravasio and collaborators (Ravasio, Olmeda et al. 2010) who demonstrated that the films formed by adsorbed LBPs spontaneously segregate into both ordered and disordered phases. We have also observed that adsorption of LBP-derived GUVs on solid supports results in the formation of structures with a particular organization, dominated by disordered regions, which could be interpreted as an intermediary stage in the adsorption process.

Examination by AFM revealed that once adsorbed onto the mica support, LBPs generate structures with two different areas including a central core exhibiting well-defined domains distanced with certain regularity surrounded by flat patches of membranes. The prominent domains could be interpreted as the result of the formation of large protruded 3-dimensional structures typically observed from LBPs adsorbed on air-liquid interfaces (Ravasio, Olmeda et al. 2010). The periodical distribution of the domains present in the core resemble a lattice-like structure and could suggest the presence of membrane-associated scaffolds of proteins, imposing these distances. Moreover, the complexity observed in the nanostructure of adsorbed LBPs displays marked differences with respect to the organization of NS membranes visualized under AFM (Blanco, Cruz et al. 2012).

Finally, we evaluated the adsorptive properties of LBPs in the presence of two pathophysiologically relevant inhibitors, serum proteins and meconium. Both agents are well known to significantly disturb and impair surfactant function (Taeusch, Bernardino de la Serna et al. 2005; Gunasekara, Schoel et al. 2008; López-Rodríguez, Echaide et al. 2011; López-Rodríguez and Pérez-Gil 2014). The higher adsorptive capacity of LBPs in comparison with whole NS membranes has already been demonstrated (Ravasio, Cruz et al. 2008). Consistent with previous biophysical studies (López-Rodríguez, Ospina et al. 2012; Hobi, Siber et al. 2014), we also observed that these inhibitors lead to a dramatic reduction in the accumulation of surfactant material into the air-liquid interface and so reduce its adsorptive capability. Here, we have shown that freshly secreted LBPs display a significantly higher resistance to both serum proteins and cholesterol than whole NS and complexes reconstituted from its OE. These findings suggest that LBPs are endowed with adsorptive mechanisms that are clearly different from those of NS or its OE. Although the nature and molecular identity of these mechanisms is still enigmatic, the present study is putting forward the idea that either a peculiar phase organization in the membranes of LBPs, or the presence of a protein scaffold on the outermost LBP membrane constitutes a mechanism by which an efficient adsorption can occur, even in the presence of strong inhibitory substances. The elucidation of these mechanisms would be of high relevance for the design of novel therapeutic materials with less susceptibility to inhibition and a higher efficiency for the treatment of respiratory pathologies such as ARDS or interstitial lung diseases.

In summary, our results show that the surfactant membranes as they are assembled and freshly released by the ATII cells display very distinctive features. They are in a highly packed and dehydrated state with an optimized adsorptive performance towards an air-liquid interface, and with a high resistance to inactivation. These features are very different from those of natural surfactant typically isolated from animal lungs and classically used in surfactant research, and could arise from the fact that LBPs are a primordial form in which surfactant is released, still containing the whole complement of lipids and proteins in a possibly unaltered structural configuration. Future investigations will be necessary to unveil this configuration at a molecular level and to apply this knowledge to the design and production of new optimized therapeutic surfactants.

Chapter 2

INTRODUCTION

Pulmonary surfactant is a membrane-based non-homogeneous material and it has been shown to exist in a variety of discrete subtypes with different features, which are generated during normal lung function (Guthmann, Haupt et al. 1995; Putman, Creuwels et al. 1996), namely a lamellar body-like form, a tubular myelin form and a small vesicular form (Wright and Clements 1987; Gross, Kellam et al. 2000). The widely accepted model of alveolar surfactant metabolism implies that freshly secreted lamellar bodies convert to tubular myelin, which is thought to represent the reservoir of material for the surface film at the alveolar interface. Then, the processes of compression/expansion cycling of the interface occurring during breathing result in the generation of small and low sedimentable forms with poor activity and are probably assigned for their removal from the airspaces (Magoon, Wright et al. 1983; Gross and Narine 1989; Guthmann, Haupt et al. 1995). The proportions of these subtypes change in the perinatal period (Spain, Silbajoris et al. 1987), as a result of physiological events (i.e. deep breathing or exercise) (Nicholas, Power et al. 1982) or in response to certain drugs (Miles, Bowman et al. 1986). The existence of different surfactant-related structures in the same or different pulmonary compartments and their connection with processes involved in secretion, reorganization, recycling or adaptation of the surfactant system to different physiopathological contexts, is still a fully open question.

Although a number of methods have been described in the literature to separate surfactant subtypes, these have not been standardized and have varied among studies, preventing a proper interpretation of the results and leading to discrepancies among investigators. It was in 1979 when the group of Thet described the heterogeneity of pulmonary surfactant with respect to its sedimentation properties (Thet, Clerch et al. 1979). Over the last three decades, researchers have utilized different centrifugation schemes to obtain purified fractions of pulmonary surfactant. In general, two alternative types of separation methods from bronchoalveolar lavage fluid (BAL) have been established: differential centrifugation and equilibrium buoyant density gradient centrifugation (Gross, Kellam et al. 2000).

Differential centrifugation has been traditionally used to fractionate BAL from animal lungs into large aggregates (LA), large membrane-based structures with relatively high density and surface active, and small aggregates (SA), of light density and worse surface activity (Pérez-Gil 2008). LA have been associated to the maintenance of alveolar stability through the reduction of surface tension at the alveoli (Brackenbury, Malloy et al. 2002). *In vivo*, during respiration, LA are converted into SA, which are either recycled back into the pneumocyte or cleared from the air-spaces (Gross and Narine 1989). Interestingly, the conversion of large into small surfactant aggregates *in vivo* can be reproduced and studied *in vitro* by a technique known as "surface-area cycling" (Gross and Narine 1989; Veldhuizen, Hearn et al. 1994). Moreover, alterations in the ratio of SA to LA are associated to some pathological situations, being abnormally increased, for instance, in N-nitroso-N-methylurethane-induced lung injury in rabbits (Higuchi, Lewis et al. 1992) or decreased in BAL obtained upon radiation pneumonitis (Gross 1991). From an experimental point of view, the protocol to separate the two fractions is easy to perform and it is based on a single step ultracentrifugation at 40000 x g for 15 min, resulting in a pelleted fraction (LA, around 25 %) and a supernatant (SA, around 75 %) (Veldhuizen, Inchley et al. 1993; Veldhuizen, Hearn et al. 1994). Additionally, surfactant subfractions can be also separated by sequential centrifugation, obtaining the different forms as pelleted fractions; i.e.: centrifugation at 1000 x g for 20 min, 60000 x g for 60 min and 100000 x g for 16 h (Magoon, Wright et al. 1983).

On the other hand, by using density gradient centrifugation, pulmonary surfactant can be separated into three peaks termed light, heavy and ultraheavy fractions (Gross and Narine 1989). The "light" subtype has little surface activity and it is mainly comprised by small unilamellar vesicles. The "heavy" fraction consists of small amounts of tubular myelin and empty vesicles whereas the "ultraheavy" portion contains aggregates of tubular myelin as well as lamellar body-like structures. In terms of metabolic correspondence and similarly to the case of LA and SA, the ultraheavy form is thought to be generated upon secretion into the alveolar compartments, giving rise to the heavy and light forms and this conversion can be also mimicked in vitro by "area cycling" (Gross and Narine 1989). This approach to obtain the different surfactant fractions is more laborious than the first method and it is normally based on continuous or discontinuous sucrose gradients and longer centrifugations, i.e.: 196000 x g at 8 °C for 16 h. In this case, yields

are normally around 45 % (ultraheavy and heavy forms) and 55 % (light form) (Gross, Kellam et al. 2000).

In Chapter 1, we gained insight into some distinctive structural features of freshly secreted surfactant in the form of lamellar body-like particles (LBPs) released from primary cultures of rat alveolar type II cells. However, the limited yield of material achieved at a "cell culture scale" (few micrograms) prevents the utilization of a number of techniques extremely useful to elucidate some features of LBPs which still remain unclear. In the search of additional sources of this relevant material, but also to identify other defined surfactant structures playing specific roles in the airways, we have subjected the whole native pulmonary surfactant, to further purification by using an adapted method originally conceived for the isolation of lamellar bodies from lung tissue. By discontinuous sucrose density gradient, we have fractioned these native surfactant complexes from porcine BAL as described in the previous chapter, into five additional discrete subforms. In chapter 2, we have aimed to analyze the different native surfactant subfractions correlating surface activity with morphology and biochemical composition. Our results suggest that the "gold standard" of an efficient surfactant, which has been traditionally considered as a simple compartment of homogeneous material, is constituted by multiple types of structures, some of them probably not directly related with surface-active properties but with surfactant homeostasis.

RESULTS

Ultrastructural analysis of surfactant subfractions

Morphological differences could be identified in the various subfractions isolated from NS complexes, as revealed by transmission electron microscopy (**Figures 2.1 and 2.2**). N2 contained large aggregates of spherical corpuscles with a fairly uniform size distribution of about 1-2 µm, composed by a high number of parallel membranes consistent with the morphology of typical lamellar body-like particles (LBPs) as illustrated in **Fig**. **2.1A,B** and **2.2A-G**. Although the multillamelated character was characteristic in this subfraction, a variable density of packaging of

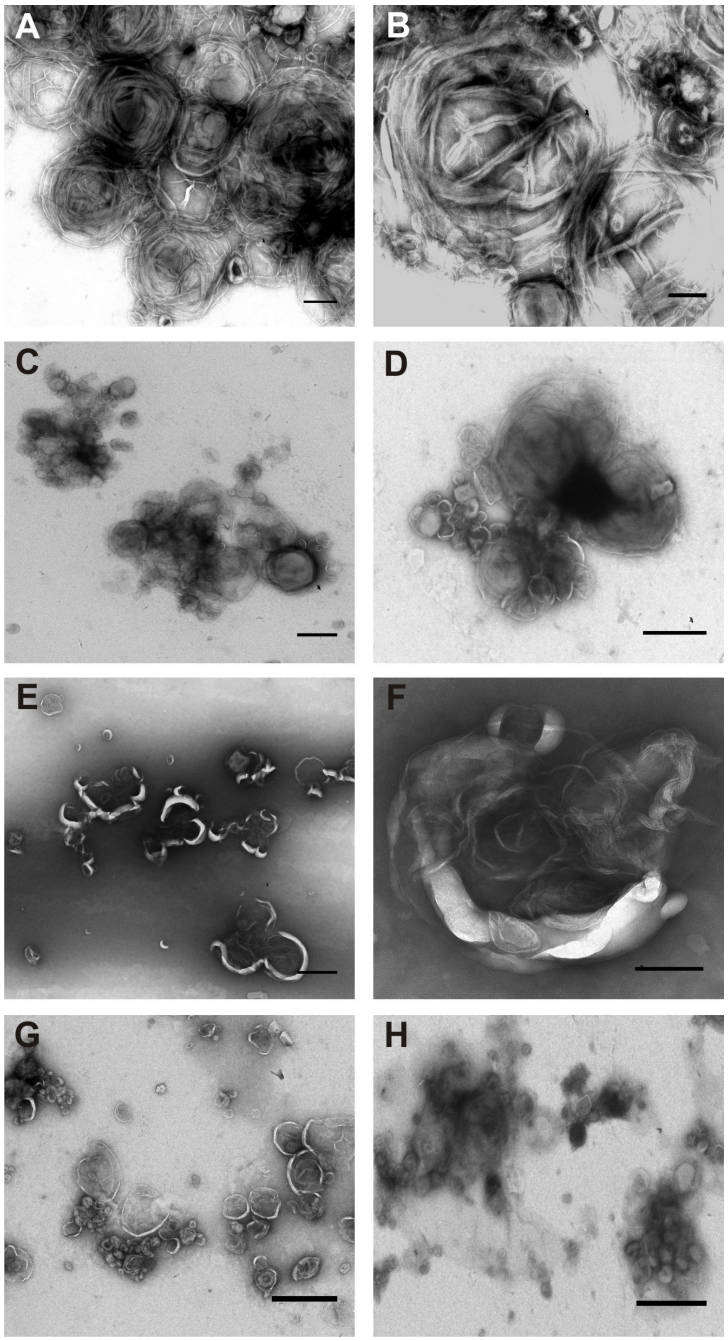

Figure 2.1. **Morphological analysis of surfactant subtypes by negative staining**. Micrographs corresponding to different subfractions purified from native surfactant stained with uranyl acetate and visualized under transmission electron microscopy. **A**, **B**. N2, scale bar = 0.5 µm. **C**, **D**. N3, scale bar = 1 µm. **E**, **F**. N4, scale bars = 1 µm and 0.2 µm, respectively. **G**, **H**. N5, scale bars = 0.5 and 2 µm, respectively.

lamellae could be discerned, observing intact LBPs (**Fig**. **2.1A,B**) but also partially dilated corpuscles (**Fig**. **2.2A-G**), with broken limiting membranes in some places probably due to lipid extraction as a consequence of the chemical fixation performed for the inclusions into resin. Occasionally, areas with multiple paralel membranes of ~ 8 nm in thickness reflecting a noticeable periodicity with apparently imposed repetitive distances (around 20 nm between neighbouring membranes) were visualized (**Fig**. **2.2D**), partially resembling incipient features of the organization of tubular myelin figures. Interestingly, tubules forming tubular myelin have been described to be also of 8 nm in thickness (Williams 1977), although the canonical lattice-like appearance of this structure was not detected. Nevertheless, one should not be discard the possibility that these images represent longitudinal sections of tubes instead of cross sections (squares). On the other hand,

the spacing between the layers (~ 20 nm) does not correspond with that reported for tubular myelin (~ 50 nm) but it coincides with descriptions of transitions from regular square lattice structures to parallel systems of smaller repeat period (less than 23 nm) previously observed in isolated surfactant fractions (Gil and Reiss 1973).

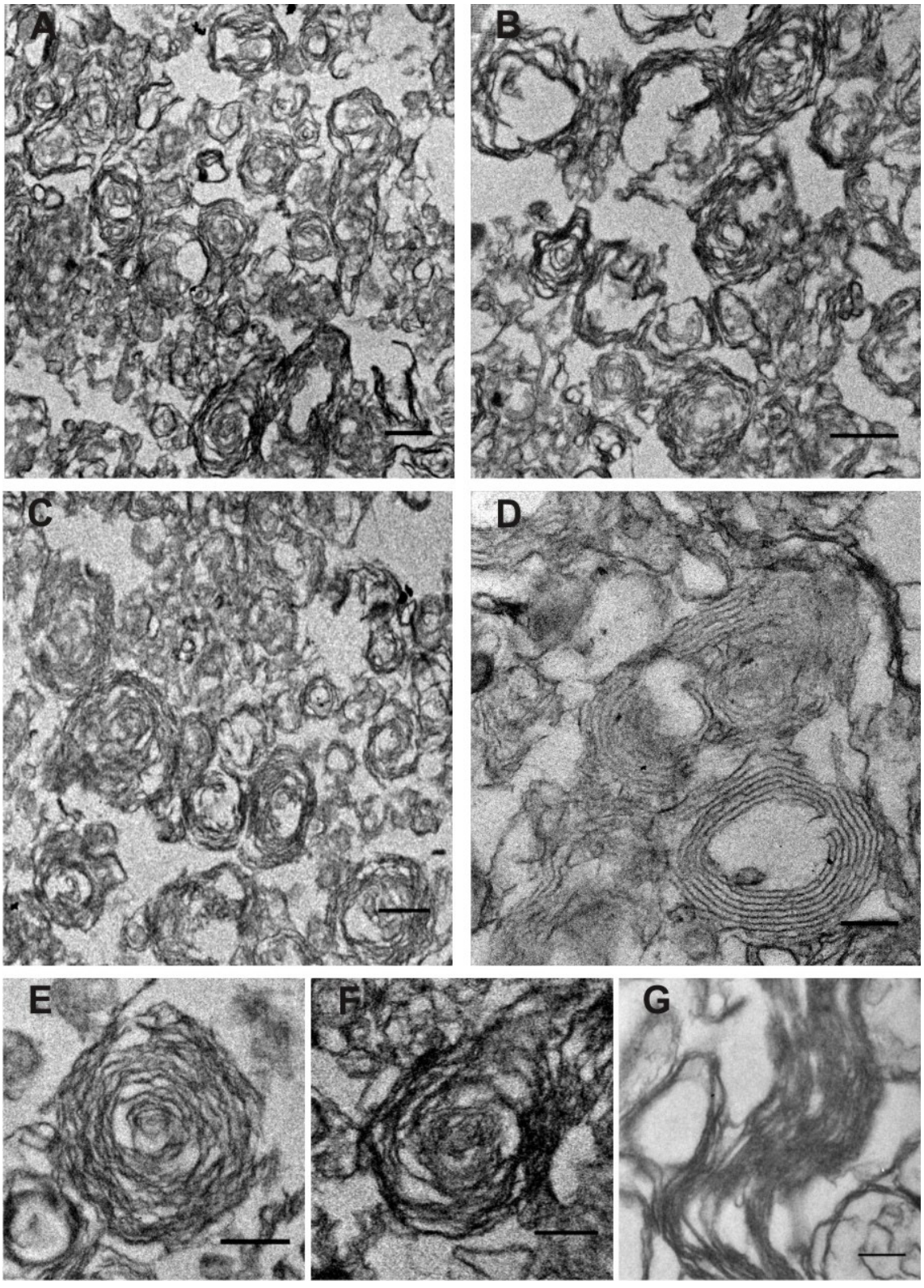

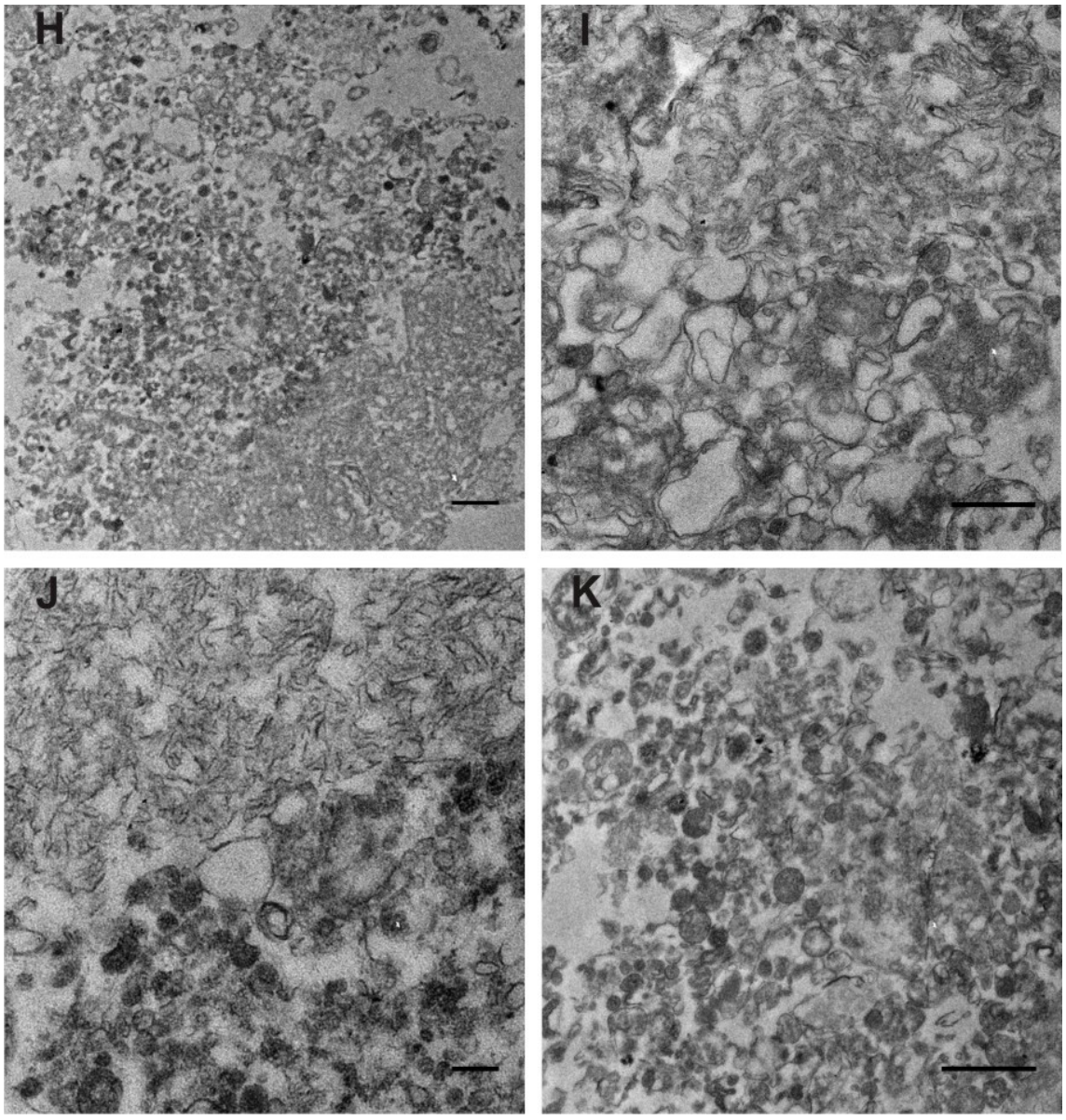

Figure 2.2. **Ultrastructural features of subfractions N2 and N5**. Micrographs of resin-embedded sections of material from the isolated subfractions N2 (**A**-**G**) and N5 (**H**-**K**) stained with osmium tetroxide and visualized under transmission electron microscopy. Scale bars = 1 µm in A, B, H and K; 0.5 µm in D, E and I; 0.2 µm in F, G and J.

N3 (**Fig**. **2.1C,D**) comprised a more heterogeneous material in terms of size, with less compact lamellar body-like structures as well as small vesicles of less than 500 nm of diameter. N4 (**Fig**. **2.1E,F**) included disorganized and seemingly less complex material in the form of vesicles and membranous sheets. The pellet, N5 (**Fig**. **2.1G,H** and **2.2H-K**) mainly contained clusters of nano-sized oligomellar and unilamellar vesicles as well as completely unfolded membrane patches and amorphous material. Most vesicles appeared as highly osmiophylic and they seemed to have an internal relatively formless content.

Biochemical composition of surfactant subfractions

Content in phospholipids, proteins and cholesterol was measured in the different NS fractions, determining the total amounts as well as their relative proportions with respect to the whole NS complexes (**Figure 2.3A**). A marked tendency of decreasing in the content of phospholipid was observed from the lightest to the heaviest subfractions. Indeed, more than 50 % of phospholipid was located in N2, whereas N5 accounted only for around 3 % with respect to the total. However, the total amount of protein presented an opposite trend and light fractions appeared to contain relatively less protein than heavy fractions. 18 % of protein was found in N2, considerably less than in N4 (30 %) although the pellet contained a lower proportion (22 %) compared to N4. As a consequence of these results, lipid/protein ratios (**Fig. 2.3B**) exhibited a overall decline from the less dense fraction N2 (36, lipid/protein, w/w) to the denser fractions N4 and N5 (less than 3).

A

	Subfraction				
	N2	**N3**	**N4**	**N5**	**Whole NS**
Phospholipid (mg)	39.37 ± 2.1	27.11 ± 3.9	4.89 ± 1	1.92 ± 0.2	73.77 ± 1
% of total	53	37	7	3	100
Protein (mg)	1.09 ± 0.1	1.84 ± 0.2	1.85 ± 0.41	1.36 ± 0.3	6.24 ± 0.8
% of total	18	30	30	22	100
Cholesterol (mg)	376	384	393	551	1715
% of total	21	22	24	33	100

B

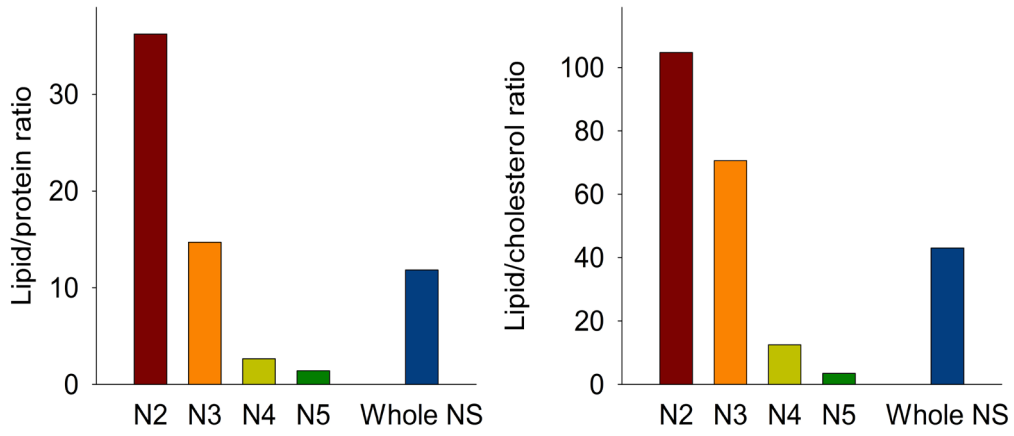

Figure 2.3. **Lipid and protein content of surfactant subfractions**. **A**. Table showing the mean amount (mg) of total phospholipid, protein and cholesterol present in each band (N2-N5) upon subfractionation of 500 µL of whole NS. Also shown is the proportion (%) of each fraction with respect to the total NS. **B**. Plots indicating the ratios lipid/protein (left) and lipid/cholesterol (right) among the isolated subfractions and complete native surfactant complexes.

On the other hand, the amount of cholesterol was found to increase from the lightest fraction (21 % in N2), to the heaviest subtype (around 33 % in the pelleted fraction N5). Similarly to the lipid/protein ratio, the proportion between phospholipid and cholesterol (**Fig. 2.3B**) drastically diminished from the less dense fraction (more than 100) to the densest fractions (around 3.5 in N5).

In addition, the distribution of individual lipid species among the individual subfractions in comparison with the pattern present in whole NS was also determined (**Figure 2.4**). From a qualitative point of view, the composition of lipid species in the surfactant subtypes showed little difference if any, containing mainly PC, PG and PE (**Fig. 2.4A**). Another lipid band below the one corresponding to PC can be observed in all the samples, although its identification is hampered due to an insufficient resolution. In the lane corresponding to whole NS (NS) an additonal diffuse band with a low chromatographic mobility can be visualized. Although it seems to be apparently absent into the different isolated subfractions, a weak signal can be discerned, particularly in the case of N5. The band corresponded to cholesterol can be also hardly distinguished, due to the fact that the development with iodine vapors is not optimimal for its visualization.

Finally, in order to analyze from a quantitative point of view the apparent differences of content in the most significant surfactant species of the different subfractions, the corresponding bands of PC and PG were scratched and subjected to quantitation by phosphorus mineralization and molar percentages with respect to total phospholipids were calculated (**Fig**. **2.4B**). With respect to the content in PC species and in accordance with the results observed by TLC, the lighter subfractions N2 (55 % molar) and particularly N3 (around 75 % molar) were the ones with higher enrichment, being the major recipients of PC from whole NS (aproximately 70 % molar, the average between N2 and N3). In the case of the denser subtypes, the proportion was markedly reduced to 20-30 % molar in both N4 and N5. In reference to the content in PG, N2, N3 and N4 displayed a similar molar percentage (around 3-4 % molar), while was slightly reduced in the pellet N5 (around 2.5 % molar). Unlike PC, the total amount of PG species seemed to be equally distributed among all the NS subtypes.

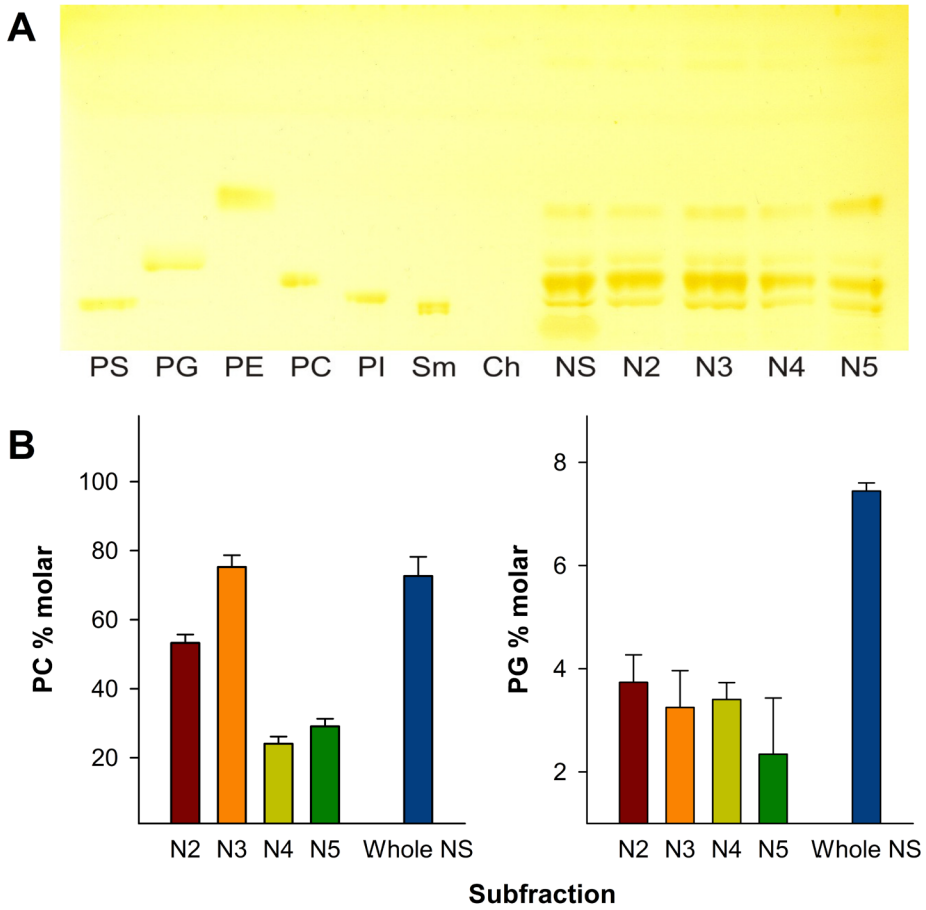

Figure 2.4. **Compositional analysis of the lipid fraction of surfactant subtypes**. Lipid composition of the isolated subfractions and complete native surfactant as analyzed by thin-layer-chromatography (**A**). Quantitative compositional profile of PC and PG classes as determined by phosphorus quantitation of each of the TLC bands in the regions defined in the chromatogram (**B**).

Surfactant proteins in subfractions

The determination of content in surfactant proteins A, B and C revealed a distinctive compositional pattern among the different surfactant subfractions, as illustrated in **Figure 2.5**.

A gradual increment in the amount of SP-A from the light to the heavy subfractions was found. In the **top panel**, a weak band in N2 with mobility corresponding to 38 kDa (likely SP-A monomer) could be discerned whereas the more dense fraction N5 seemed to be most enriched in SP-A, with several bands of different molecular weight. Of note, a band above the one corresponding to the monomeric form could be perceived in all individual fractions except in N2. This could be explained as result of a partial reduction of disulfide bonds (which affected particularly to whole NS, where the monomer expression seems negligible) and it could be attributed to a dimeric

state. On the other hand, at least 3 bands of low molecular weight were detected predominantly in N5, possibly representing non glycosilated forms or a partial proteolytic degradation of SP-A.

The distribution of both hidrophobic proteins SP-B and SP-C in the different subfractions differed considerably compared to SP-A . As seen in the **middle panel,** the monomeric form of SP-B (around 8.7 kDa) was found to be more abundant in the less dense subfractions N2 and N3 whilst it was patently reduced in the heaviest subtypes N4 and particularly in N5.

In the case of SP-C (**bottom panel**), although it was present in all the subfractions, a different profile of forms with a clearly diverse oligomerization degree was observed. This can be attributed to an inefficient action of β-mercaptoethanol or due to the original state of the samples. Furthermore, distorsion of bands as a result of the high lipid concentration in the samples has to be taken into account as possible explanation for the different sizes observed in the blot, difficulting an accurate interpretation. The monomer (around 3.7 kDa) could be only clearly distinguished in whole NS and N3, whereas polimeric forms, between 10-15

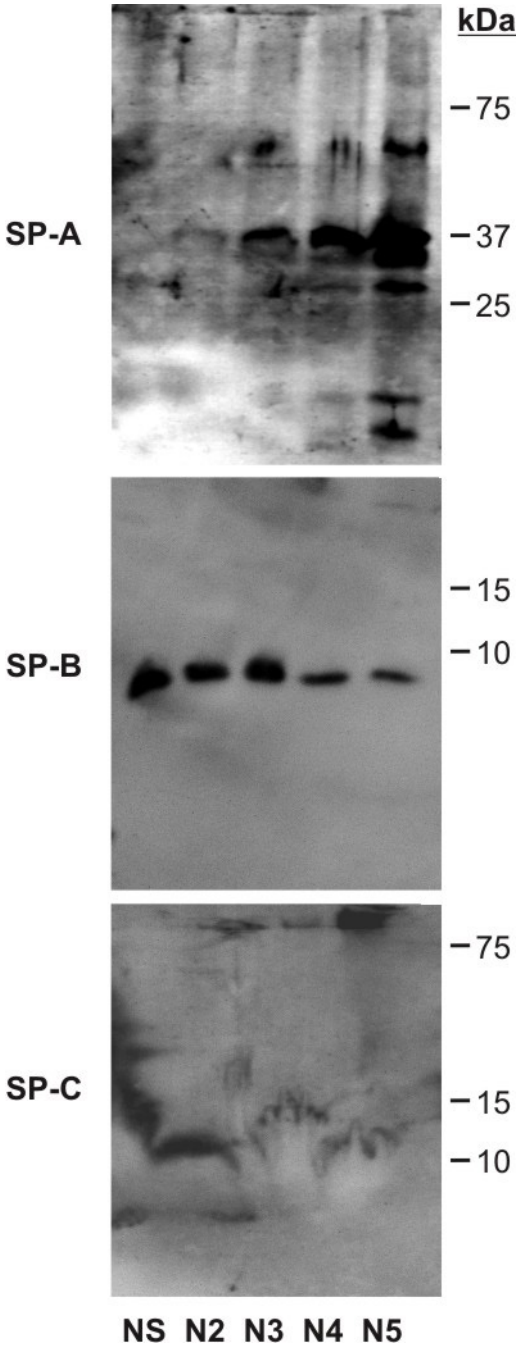

Figure 2.5. **Content of surfactant associated proteins of surfactant subfractions**. Representative western blots of surfactant proteins A, B and C in isolated subfractions and complete native surfactant complexes. For comparison, total protein corresponding to 100 µg of lipid, was loaded into each lane of a 10 % (SP-A) and 16 % (SP-B, SP-C) acrylamide gel. Gels were run in reducing conditons upond incubation of the samples with β-mercaptoethanol.

kDa, were present in all the samples. The most conspicuous SP-C signal was observed in N2, which was found to be the most enriched in SP-C. Noticeably, a high amount of aggregates of high molecular weight appeared "trapped" in the concentrating part of the gel, predominantly in the lane corresponding to N5.

Surface activity evaluation of surfactant subfractions

Functional assessment of the different surfactant fractions was performed by captive bubble surfactometry revealing a different activity among the isolated subfractions isolated from whole NS complexes (**Figures 2.6**, **2.7** and **Table 2.1**). Firstly, after sample injection, adsorption of surfactant material and subsequent drop in surface tension to equilibrium values (around 20-25 mN/m) was found to take place in all samples at some point (**Figure 2.6**, left panels). However, N2 was shown to be the most active fraction in film formation, provoking an almost instanteneous (5 s) decline to values near to 20 mN/m. N3 displayed a similar rate compared to N2 reaching the equilibrium after 5 s being slightly more efficient than complete NS. The heaviest fractions were much less competent and the equilibrium was further delayed, being reached later, after 20 s (N4) or 60 s (N5).

Five minutes after the initial surface film formation, bubbles were rapidly expanded, measuring the tension reduction corresponding to the incorporation of remaining material present in the aqueous hypohase (**Figure 2.6**, right panels). The evaluation of this stage is particularly adventageous in comparison with the initial adsorption since this is not subjected to possible experimental artifacts (i.e. proximity of the capillary to the bubble) and it is closer to the real situation in which surfactant adsorpts to an expanding surface already occupied by surfactant (Schurch, Green et al. 1998; Schurch, Ospina et al. 2010). All films, except that formed by N5, were similarly active as evidenced by the drops in surface tension after expansion to equilibrium values close to 22 mN/m. In correspondence with the initial adsoprtion, N2 and N3 were the most efficient fractions to re-stablish surface films during interfacial expansion, reaching the equilibrium very quickly (5 s), even faster than whole NS (20 s). N4 was comparable in activity to the complete NS attaining equilibrium values within 20 s. In contrast, N5 showed a slower kinetics, reaching a surface tension of ~ 24 mN/m after 300 s.

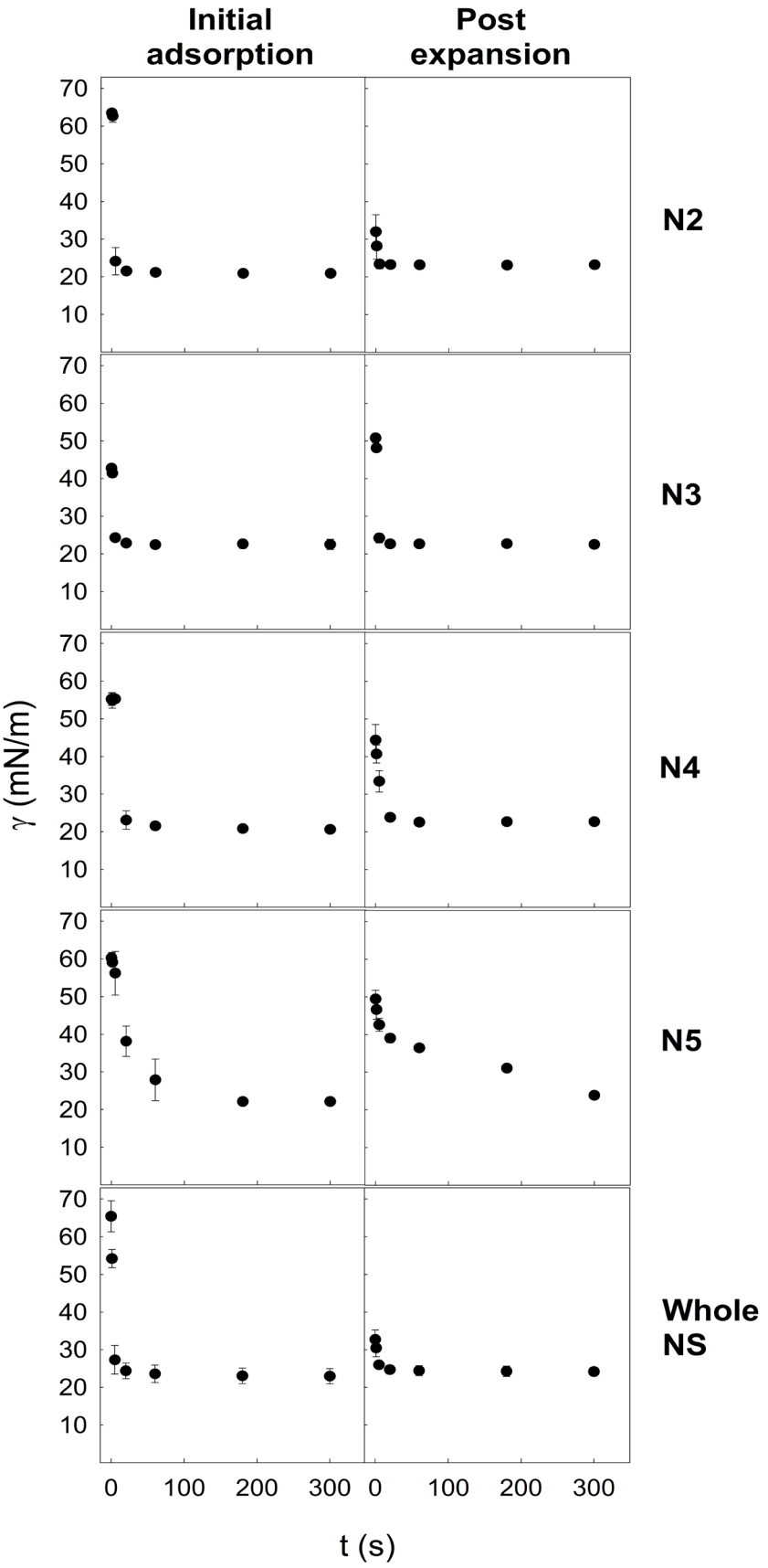

Figure 2.6. **Interfacial adsorption of isolated surfactant subfractions.** Initial (left panels) and post-expansion (right panels) adsorption kinetics of purified surfactant subtypes and complete native surfactant assemblies.

Afterwards, the surface behaviour of the different films was evaluated under slow quasistatic compression/expansion cycling, permiting the films to relax for several seconds between compression steps. **Figure 2.7** (left panels) summarizes compression-expansion isotherms reveling important differences between samples. The first quasi-static cycle (brown circles) showed clearly greater hysteresis than the subsequent cycles in the case of N3 and N4 in a similar way to the cycles exhibited by complete NS complexes. Of note, this well characterized behaviour was not detected in the subfraction N2 and particularly in N5, where all the isotherms seemed to exhibit a comparable range of hysteresis. Indeed, films formed by N2 showed behaviour distinct from those of other samples, with relative area changes lower than 40 % in contrast to N3, N4 and N5 (~ 60 %) or to whole NS (~ 50 %). Maximum surface tensions did not exceed 30 mN/m in any of the samples. Minimum values close to 0 mN/m were reached in all samples except for N5, which did not attain values lower than 20 mN/m, revealing a poor surface activity. Finally, at the fourth quasi-static cycle (green circles) smaller area changes and less hysteresis indicative of a changed film configuration and/or structure (Schurch, Ospina et al. 2010) were observed in all samples with the exception of N5 which displayed a long plateau in all cycles.

Figure 2.7 (right panels) illustrates the dynamic compression/expansion isotherms centered on the 1st, 10th and 20th cycles of films formed by the different fractions. Again, patent differences among the samples could be discerned. Films formed by N2, N3 or whole NS were completely functional and behaved similarly, exhibiting dynamic cycles almost identical with pratically no hysteresis and slightly higher maximum tensions than that at the end of the fourth quasi-static cycle. A slightly less inclined slope could be noticed in N2 isotherms, which needed less than 15 % of area reduction to reach the lowest surface tension, in comparison to N3 (~ 20 %) and particularly to complete NS (> 20%). N4 worked similarly to N3, except for the first dynamic cycle that exhibited some hysteresis. Films formed by N5 were again poorly active, exhibiting very high maximal tension values (close to 50 mN/m), whereas the minimal values were not lower than 7 mN/m. In addition, films formed from N5 required much larger area reductions (> 40 % to reach the lowest tensions) and more hysteresis than films formed by the other fractions.

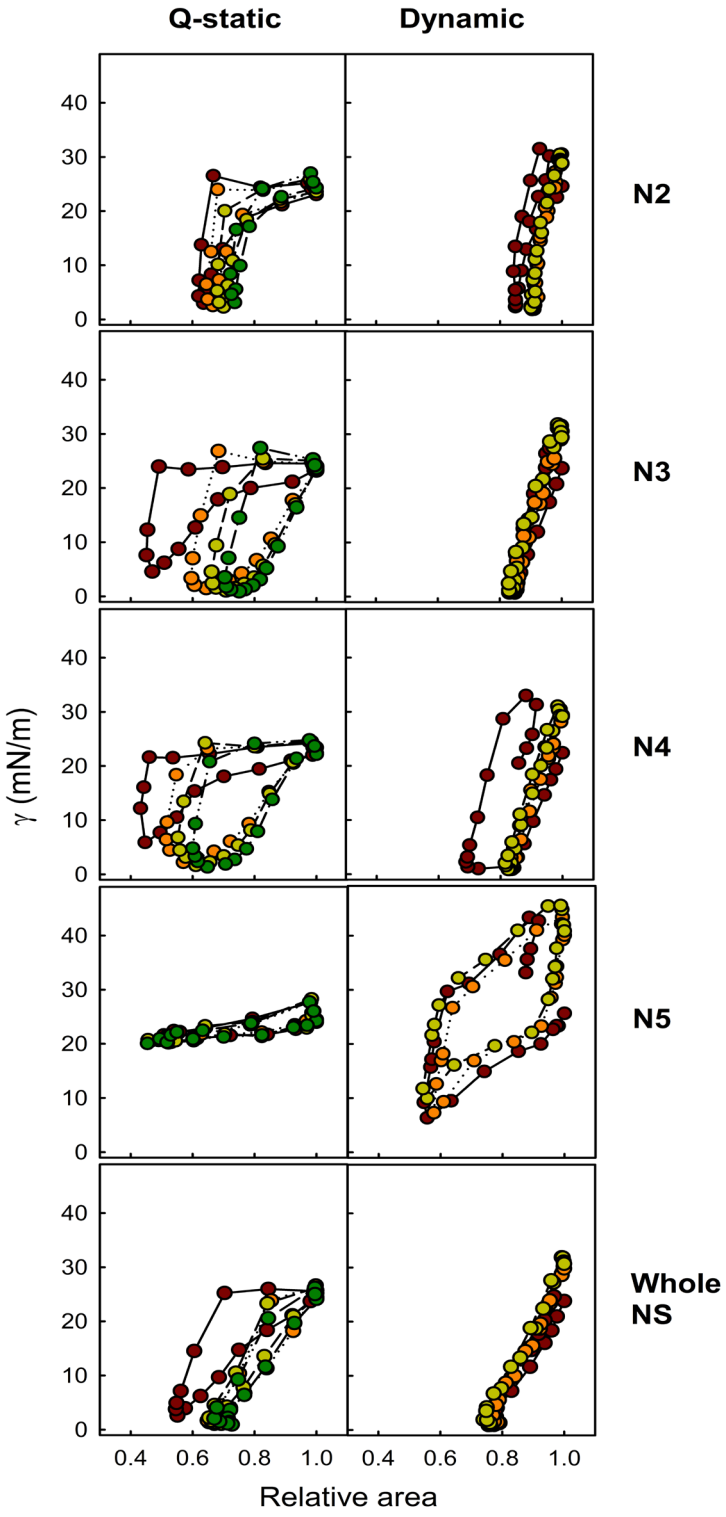

Figure 2.7. **Compression-expansion isotherms of surfactant subfraction films**. Quasi-static (left panels) and dynamic (right panels) compression/ expansion isotherms from films formed from surfactant subfractions and complete native surfactant. A representative experiment is shown here after repeating three independent experiments with each sample.

	IA	PE	4th Quasi-static cycle			20th Dynamic cycle		
	γ_{min} (mN/m)	γ_{min} (mN/m)	γ_{min} (mN/m)	γ_{max} (mN/m)	Relative A_{min}	γ_{min} (mN/m)	γ_{max} (mN/m)	Relative A_{min}
N2	23.03 ± 1.65	22.86 ± 0.96	0.86 ± 0.38	24.72 ± 0.89	0.55 ± 0.09	0.53 ± 0.13	35.04 ± 6.34	0.85 ± 0.03
N3	21.95 ± 0.95	22.61 ± 0.19	1.04 ± 0.11	25.95 ± 1.25	0.72 ± 0.03	0.81 ± 0.15	31.48 ± 16.80	0.79 ± 0.07
N4	20.60 ± 0.36	22.56 ± 0.50	2.27 ± 0.81	25.77 ± 1.37	0.50 ± 0.00	1.05 ± 0.19	32.00 ± 1.58	0.79 ± 0.04
N5	21.95 ± 0.46	23.85 ± 0.13	20.07 ± 0.01	28.87 ± 1.63	0.44 ± 0.02	7.76 ± 3.08	47.73 ± 3.09	0.57 ± 0.03
Whole NS	22.94 ± 2.03	24.08 ± 1.23	1.23 ± 0.40	26.09 ± 1.55	0.61 ± 0.18	1.06 ± 0.44	30.31 ± 1.49	0.79 ± 0.05

Table 2.1.Surface activity of films constituted from surfactant subfractions as evaluated in a Captive Bubble Surfactometer. Resume of the parameters obtained at the different experimental stages: IA (initial adsorption), PE (post-expansion adsorption), quasi-static cycles (fourth cycle) and dynamic cycles (twentieth cycle).

Finally, after the full experimental protocol, the stability of the different films was investigated by monitoring changes in surface tension after mechanical perturbations introduced into compressed stages. In **Figure 2.8**, surface tension is plotted as a function of the number of perturbations introduced into the CBS chamber by the pendulum hammer. Complete NS was shown to form the most stable films, following a trend that finished in a plateau of around 4 mN/m to get a stable surface tension after more than 15 perturbations. Films of subfractions N2, N3 and N4 showed an analogous behaviour and plateaued at around 5-6 mN/m, generating stable collapsed structures after a higher number of perturbations. Since the heaviest fraction N5 was unable to reach comparable minimum values under dynamic cycling, it was not included in the evaluation of stability.

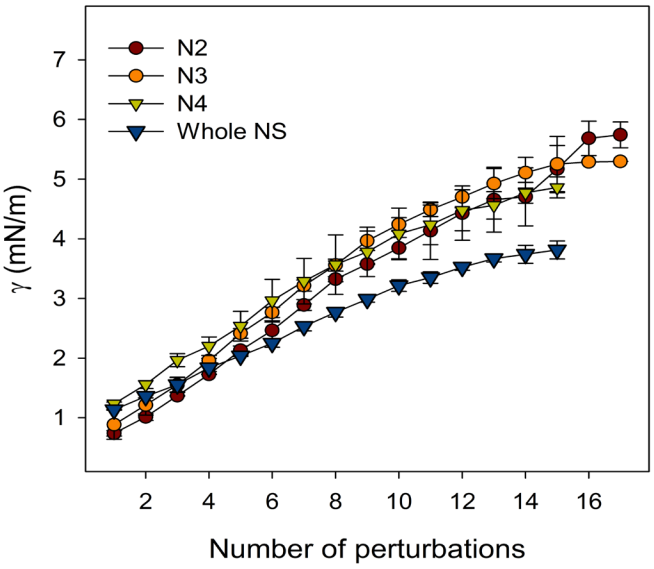

Figure 2.8. **Film stability against mechanical perturbations.** Plot representing surface tension as a function of the number of perturbations introduced in the compressed bubble by the pendulum hammer.

DISCUSSION

The extracellular surfactant structures have various levels of complexity and densities depending on the stage of surfactant metabolism and these can be separated into subtypes with distinctive morphologies and characteristics but likely maintaining certain metabolic relation with each other (Putman, Creuwels et al. 1996). In Chapter 2, we have fractioned the lipid protein assemblies purified as porcine NS complexes into several subforms differing in ultrastructural appearance, composition and ability to reduce surface tension at air-liquid interfaces during

simulated breathing cycling. To accomplish this task we have taken advantage of a separation protocol based on a density gradient centrifugation similar to that originally designed by Gross and Narine to achieve the separation of surfactant in light, heavy and ultraheavy subforms (Gross and Narine 1989; Gross and Narine 1989). However, the composition and activity of the fractions have been only marginally characterized. The modifications we have implemented in our experimental 4 step-purification method have resulted in a different subfractioning of NS. Indeed, whereas traditional techniques directly layer alveolar lavage fluid onto a continuous sucrose gradient without any preliminary "cleaning up" procedure, we have subjected BAL to a previous low-speed centrifugation to sediment cells and then to an ultracentrifugation step at 100000 x g for 1 h in where we think the pelleted part is mainly constituted by the fraction corresponded to the heavy/ultraheavy forms (or large agreggates) with a negligible contribution of light forms (or small agreggates). This conclusion is supported by the fact that for efficiently precipitating the small vesicular forms of surfactant, other investigators subject BAL to longer ultracentrifugations, around 16 h at 100000 x g (Magoon, Wright et al. 1983; Oulton, MacDonald et al. 1993; Guthmann, Haupt et al. 1995; Knells, Ahmed et al. 1995). On the other hand, after applying the product of the first isolation onto the NaBr gradient and later onto the sucrose gradient , the lightest assessable layer (N2) contains material consistent with the lamellar body fraction. Thus, we think that our method results in a further division of different populations included into the ultraheavy fraction (or large aggregates). In this line, the possibility of the existence of additional complexity levels beyond small/large or light/heavy subfractioning has been previously proposed, suggesting that these portions might be intrinsically heterogeneous containing more than one type of structures (Pérez-Gil 2008).

Of note, we have not observed clear evidences of tubular myelin, which presence has been previously shown in both heavy and ultraheavy forms (Gross and Narine 1989). However, it has been reported that the morphology of the heaviest fractions is particularly susceptible to resuspension and manipulation, resulting in the disintegration of lamellar bodies into membrane sheets to configure tubular myelin figures (Putman, Creuwels et al. 1996). Furthermore, the formation of tubular myelin has been described to be seriously affected by temperature, pH or the ionic environment (Gil and Reiss 1973; Williams 1977). Thus, these discrepances could

be attributed to a differential handling of the samples, among other subtle methodological variations.

The electron microscopic observation of the NS subfractions suggests that our isolation method results in the separation of presumably two populations of lamellar bodies with different density (fractions N2 and N3) in concordance with previous findings reported by Magoon and collaborators (Magoon, Wright et al. 1983), which also described two fractions enriched in lamellar bodies (called light and dense lamellar bodies) upon surfactant subfractioning with sucrose gradients. Although the phospholipid composition and the proportion of PC and PG in the two lamellar body fractions were equiparable, the phospholipid to protein ratio, however, was higher in the light lamellar bodies, also consistent with Magoon's results. In general, the lipid composition of the individual subfractions showed only minor differences, althouh N4 and N5 contained much less proportion of PC species than N2 and N3, with concomitant functional consequences.

Unlike the lighter fractions, the assignation of N4 and N5 to specific metabolic stages of the life cycle of surfactant results more complicated due to the absence of representative structural features. We suggest that they might be part of the heterogenity that other authors have observed in the densest fractions, describing them as large vesicles and membranous material (Magoon, Wright et al. 1983; Gross and Narine 1989; Putman, Creuwels et al. 1996).

In the light of the results, we consider that differences in parameters, such as the lipid to cholesterol ratio or in the distribution of surfactant associated proteins, are of particular importance given the clear effect of these components in modulating the surface activity and dynamic behaviour of surfactant. Indeed, the influence of cholesterol in both surfactant structure and function has been previously outlined and it has been proposed that its proportion in the composition of surfactant membranes is strictly regulated (Orgeig and Daniels 2001; Orgeig, Daniels et al. 2003; Bernardino de la Serna, Pérez-Gil et al. 2004). In fact, the modulation of cholesterol levels has been shown to be key in the adaptation to diverse specific situations (i.e.: strenuous exercise, changing body temperature) (Langman, Orgeig et al. 1996; Orgeig, Bernhard et al. 2007). In addition, alterations and particularly exacerbated cholesterol levels in surfactant

have been associated to pathological states such as acute respiratory distress syndrome (Markart, Ruppert et al. 2007) or idiopathic pulmonary fibrosis (Fireman, Spitzer et al. 1996), among others.

Our data show that N4 and specially N5 contain the highest proportion of cholesterol with respect to the total phospholipid content and this seem to be reflected in their poor perfomance at the captive bubble surfactometer, demonstrating an impaired function during compression-expansion cycling. Abnormally increased levels of cholesterol have been proved to generate excessively fluid membranes and subsequently an early collapse of the interfacial films due to a disproportionate liquefying of the L_{β} ordered phases of the lipid membranes (Bernardino de la Serna, Oradd et al. 2009). Thus, the compromised phase segregation of membrane domains, which is essential for the surfactant dynamic properties would explain the dysfunctional mechanical plasticity exhibited by N5.

However and as we stated before, the decreased surfactant activity displayed by the densest fractions could be attributed, not only to an excess of cholesterol and a reduced content in PC (the most important lipid for surfactant adsorption) but also to the alteration in the pattern of surfactant proteins. By immunoblot, we have observed that N4 and predominantly N5 contain significantly less amount of functional forms of SP-B and SP-C, compared to the other fractions. The consequences of insufficient amount of both hydropobic proteins would explain the slower lipid transfer from the subphase to the interfacial film and thus, the possible lack of refinement during film compression resulting in an apparent inefficient re-extension of material from the reservoir during expansion, and the subsequent increase in the hysteresis of the dynamic cycles (Taneva and Keough 1994; Creuwels, Boer et al. 1995; Kramer, Wintergalen et al. 2000; Krol, Ross et al. 2000; Baoukina and Tieleman 2011; Olmeda, García-Álvarez et al. 2013). Strikingly, the subfraction N5 was shown to comprise a considerable amount of oligomerizated SP-C forming aggregates of high molecular weight what could be also related to the high cholesterol content. Indeed, a specific interaction between cholesterol and SP-C through the palmitoylated segment of the protein has been previously proposed altough this feature has not been verified so far (Baumgart, Ospina et al. 2010; López-Rodríguez and Pérez-Gil 2014). On the other hand, SP-C has been described to strongly destabilize bilayers, promoting their disintegration and dispersion

(Parra, Moleiro et al. 2011). This could lead us to postulate that fractions N4 and particularly N5, might be responsible of sustaining the presence of cholesterol reservoirs in the airways. The mobilization of cholesterol, in and out of the most active surfactant structures, as it has been described in certain physiological conditions, may include transfer of cholesterol between the lighter and the heavier fractions revealed here. Thus, we speculate that N5 exerts an alternative function at modulating surfactant homeostasis, governing the transit of cholesterol from the membranes present in the active surfactant films to the subphase and/or vice versa, rather than participating in surfactant performance at the air-liquid interface. An alternative function for the densest fractions is also plausible taking into consideration the high accumulation of SP-A. However, the interpretation is complex considering that this protein has additional roles (defensive) beyond its potential contribution to optimize the intrinsic biophysical properties of pulmonary surfactant (Wright 2003).

As expected, N2 and N3, as representative of lamellar body-enriched fractions, displayed a superior performance at the captive bubble surfactometer in terms of a rapid interfacial adsoprtion and efficient compression/expansion dynamics with virtually no hysteresis, in virtue of their optimized lipid and protein composition and probably due to their singular structural organization (Ravasio, Olmeda et al. 2010; Hobi, Siber et al. 2014). Moreover, taking into consideration the considerable resistance to inhibition displayed by freshly secreted LBPs from type II cells (see chapter 1), the assessment of the surface activity at the CBS of these fractions in the presence of serum or meconium would be particularly relevant to see the potential effect of deleterious components in close to physiological conditions.

Considering our initial attempt of finding alternative sources of lamellar body-like particles, we could conclude that the present isolation technique based on the subfractioning of pre-purified NS complexes from porcine BAL, allow us to obtain signficant amount of material with characteristic features highly consistent with LBPs. This method does not require extensive animal sacrifice and it is thus, economical and ethical-friendly, since we take advantage of pigs already slaughtered. We think that, in conjuction with the perceptible improved yield, it will allow

us to get access to new experimental methodologies that will shed light on the structural and functional aspects of freshly secreted surfactant which remain still obscure. However, we should bear in mind the possible differences between recently collected complexes released from cell cultures and the material that has been already exposed to the lung environment and has been in contact with other molecules with a potential unknown effect. Thus, further experiments will be needed to assess to what extent LBPs from NS are analogous to those freshly exocyted from type II cells in culture.

Chapter 2
appendix

The experiments presented in this section were carried out at the National Center of Biotechnology (Madrid, Spain) in collaboration with Dr. José María Valpuesta, Dr. Javier Chichón, Dr. Rocío Arranz and Javier Conesa. Soft X-ray cryo-electron microscopy studies were accomplished at the facilities of the BESSY II synchrotron (Berlin, Germany).

INTRODUCTION

The results revealed in Chapter 2 indicate that native surfactant purified from animal lungs, which has been considered so far as the best surfactant material in terms of physiological-like surface behaviour, is not a homogenous material and contains a variety of distinct structures with presumably different functions. We have analyzed the morphological features of the different constituents of native surfactant complexes using traditional TEM, a widely used technique suitable to examine ultrastructural fine details of specimens. Nevertheless, sample preparation for TEM is time consuming and requires laborious protocols, including fixation, staining, dehydration, resin embedding and sectioning of the samples. Most importantly, the samples might suffer structural or chemical alterations as a consequence of their processing (i.e.: lipid extraction result of the dehydration process), giving rise to potential artifacts.

Around 40 years ago, the group of Glaeser pioneered cryo-electron microscopy, the imaging of frozen hydrated samples at low temperature, in their natural aqueous habitat (Glaeser and Hobbs 1975; Glaeser and Taylor 1978). Although the first images were obscured by ice crystal damage, the subsequent introduction of plunge freezing and cryo-transfer methods permitted the vitrification of the samples avoiding the generation of ice crystals (Dubochet, Adrian et al. 1988). Indeed, cryo-fixation avoids dehydration, staining and physical sectioning allowing sample visualization in a closer to native state. In the present work we have visualized native surfactant assemblies upon cryo-electron tomography (cryo-ET), a method to image macromolecular complexes three-dimensionally in their native settings with the best possible structural preservation (Lucic, Forster et al. 2005). Furthermore, the tomographic combination of electron microscope images allows the reconstruction of three-dimensional structures at resolutions of a few nanometers (Fung, Liu et al. 1996). However, an important limitation of the cryo-ET methodology is derived from the poor penetration due to the multiple scattering of electrons in soft materials and as a result, electron tomographic reconstruction is limited to around 0.5 µm thick samples (Carrascosa, Chichon et al. 2009). Bearing this in mind, we also took advantage of cryo soft X-ray tomography (cryo-SXT), whose penetration power permits to obtain high contrast images from several microns thick samples (up to 10 µm thickness) (Schneider, Guttmann et al. 2010). Therefore, the combination of X-ray imaging with the preservation of the samples at

cryogenic temperatures minimize the effect of radiation damage in biological samples (Schneider 1998).

In this appendix of Chapter 2 we have implemented the microscopic techniques stated above to analyze the different morphological entities present in native surfactant in a close to native state and with further structural detail. This approach has let us to get additional insight into the particular arrangements that pulmonary surfactant display in its multiple biological forms.

RESULTS AND DISCUSSION

We have explored the ultrastructure of cryo-fixed whole pulmonary native surfactant (NS) complexes under fully hydrated conditions close to the native situation and avoiding intensive sample processing and so precluding the generation of potential artifacts.

First, cryo-EM allowed us to visualize the relatively simpler material present in NS assemblies due to the thickness limitation of this technique. Even then, NS membranes displayed a high complexity level, adopting a variety of morphological arrangements (**Figures AP1 and AP2**). In general terms, the structural diversity consisted of unilamellar vesicles (**Fig. AP1A**), interspersed with oligolamellar and multillamelar structures (**Fig. AP1B, C**), patches with piled membranes (**Fig. AP1E**, **F**) and apparent fragmented membranes or filaments (**Fig. AP1A, D**). The unilamellar vesicles had variable dimensions (250-400 nm in diameter) and appeared to enclose a dense material. Oligolamellar and multillamelar liposomes, occasionally exhibiting aggregation signs, were generally larger (350-800 nm in diameter) and similarly to unilamellar vesicles, they also seemed to contain an amorphous material in the inner compartments.

Additionally, areas with regularly spaced stacked membranes of around 8 nm in thickness were also observed (**Fig. AP1F**). Interestingly, separation distances from one layer to its adjacent were of around 30 nm, close with those previously reported for natural surfactant structures (Weibel, Kistler et al. 1966; Gil and Reiss 1973) and also to those described in DPPC/PG and DPPC/PI + SP-A mixtures (Poulain, Akiyama et al. 1999). These data slightly differ with our previous results shown in Chapter 2 (Figure 2.2D, page 135), where we described similar structures, although we used a different microscopic technique in that case.

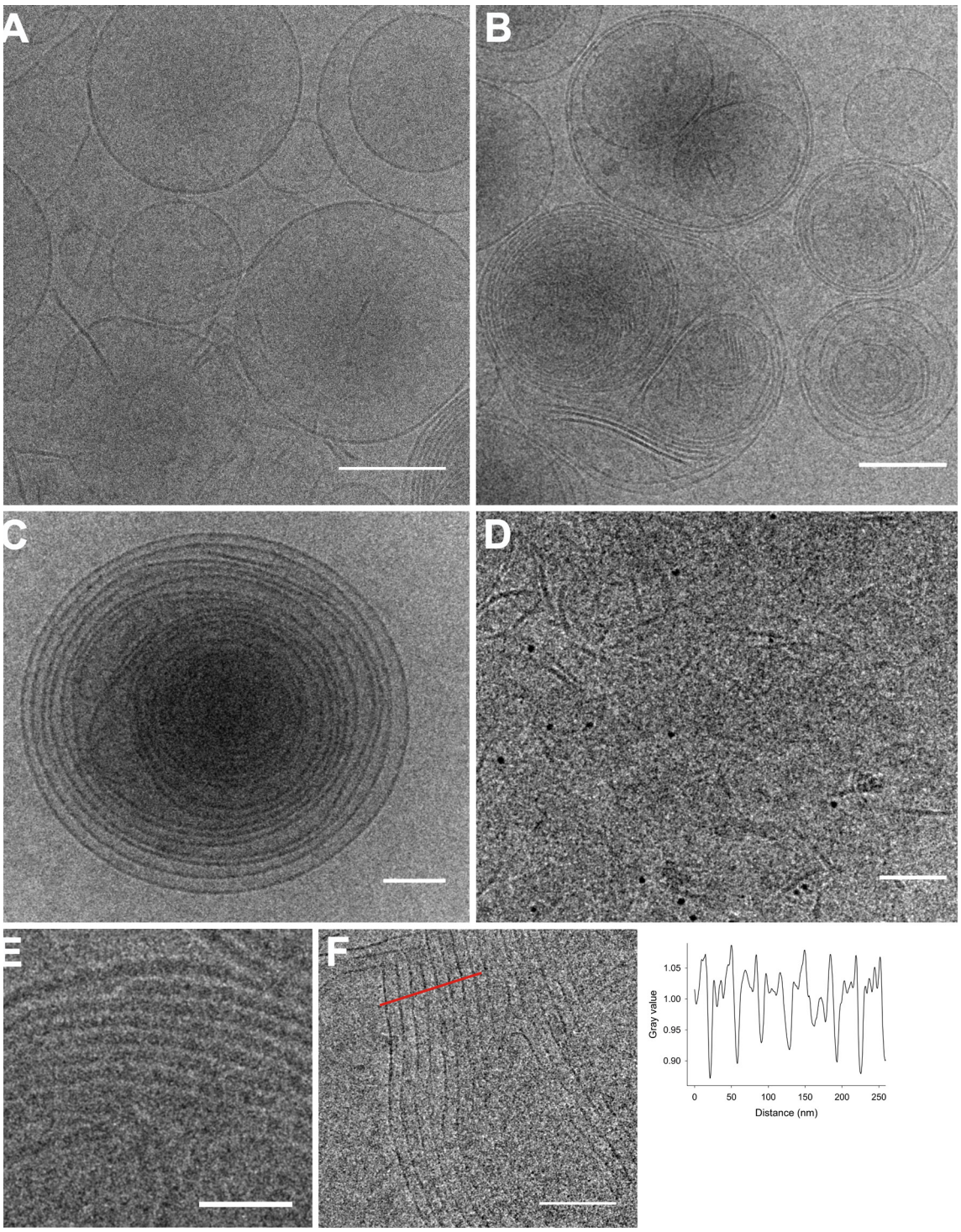

Figure AP1. **Ultrastructure of native pulmonary surfactant membranes as studied by cryo-electron microscopy**.Representative projections of the morphological variability found in native surfactant complexes as examined with cryo-electron microscopy in close-to-native conditions. Distances among membrane sheets (red line) in panel F are calculated by means of a histogram. Scale bars represent 200 nm (**A**, **B**, **F**), 100 nm (**E**) and 50 nm (**C**, **D**).

On the other hand, the formation of tightly apposed multilamellated structures like those observed in **Fig. AP1E** has been also experimentally reproduced by combining SP-A, SP-B, and DPPC/PG liposomes (Poulain, Allen et al. 1992), suggesting the probable involvement of these proteins in the generation of these particular arrangements. In fact, previous results evidence that SP-B promotes the creation of highly cohesive multillamelar structures, which might be related to the high resistance that pulmonary surfactant exhibits under mechanical perturbations (Bernardino de la Serna, Vargas et al. 2013). **Figure AP2A** shows large membranous sheets with interllamelar swapping, probably due to the SP-B action to establish membrane-membrane contacts.

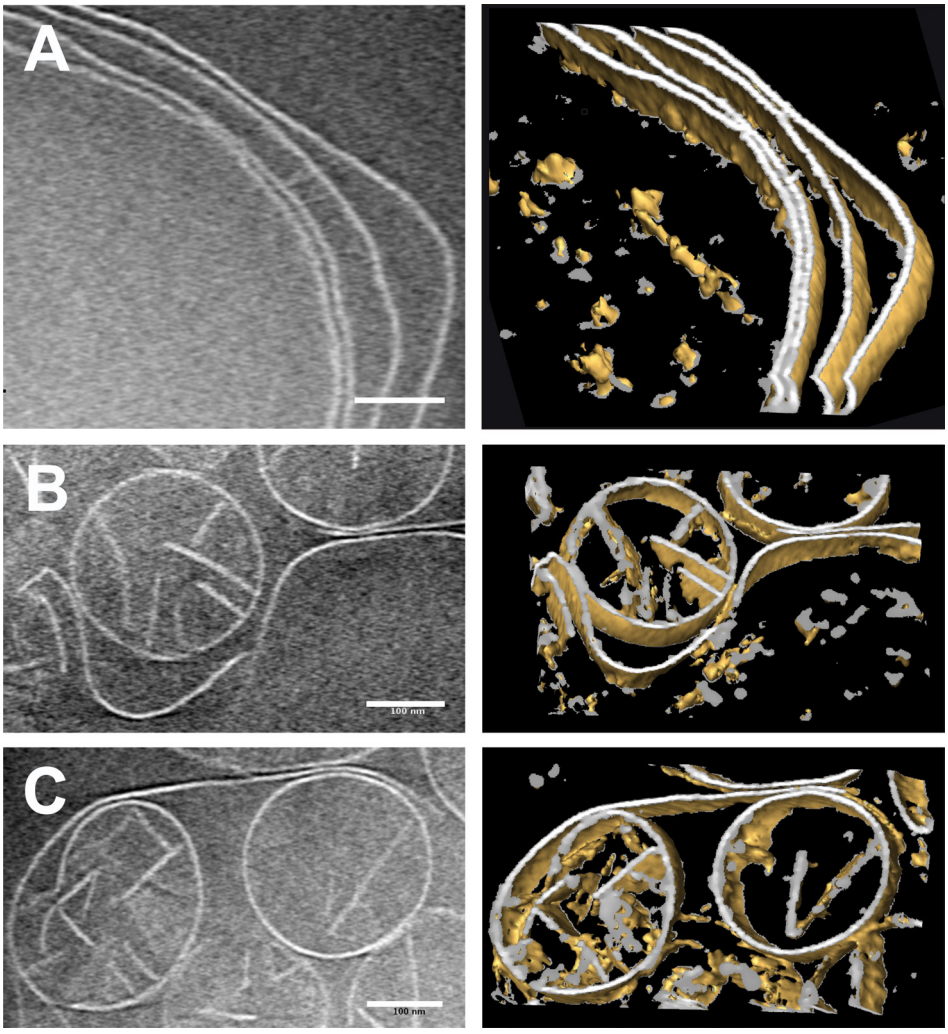

Figure AP2. **Cryo-electron tomography of native surfactant complexes**. Tomographic slices (left) and volumetric reconstructions (right) from different tomograms (**A**-**C**) providing with a 3-D view of the structural features characteristic of native surfactant assemblies. Scale bars in all images represent 100 nm.

Moreover, the tomographic reconstructions provide an exceptional insight on additional structural features hardly noticeable at the 2-D projections. **Figures AP2B** and **AP2C** unveil the existence of disk-shaped structures with apparent folded membranes or invaginations, occasionally interconnected at some points between them. In this regard, SP-B has been previously shown to promote formation of small membrane disks of 50-70 nm from disrupted liposomes (Poulain, Allen et al. 1992). The dimensions reported by Poulain and collaborators do not coincide with those observed in our samples, although this could be explained considering that the lipid composition that they used in their experiments was a simplified version of the complex compositional heterogeneity present in native surfactant. Of note, the inner membranes present in the disks display marked kinks as well as discernible boundaries, strongly suggesting the presence of protein imposing these particular arrangements or the occurrence of lipids with capabilities to generate highly curved geometrical constraints.

As stated before, some structures of higher complexity and size present in the native surfactant samples were beyond of the power resolution of cryo-EM. To overcome this restriction, we implemented the technique of cryo-soft X-ray tomography at the BESSY synchrotron radiation source (Berlin, Germany). To our knowledge, this is the first time that native surfactant complexes have been examined by means of this approach. Importantly, we were able to directly image structures consistent with lamellar body-like particles (LBPs) in a fully hydrated environment (**Figure AP3**),

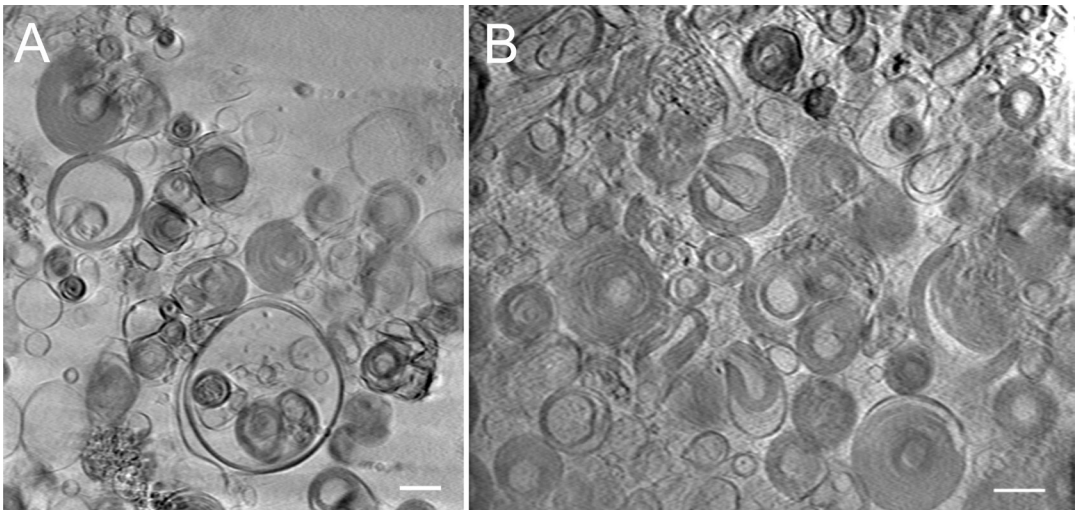

Figure AP3. **Cryo soft X-ray tomography of native surfactant complexes**. Representative tomographic slices (**A**, **B**) of the morphological heterogeneity present in native surfactant complexes as documented by cryo soft X-rays microscopy at a synchrotron radiation source. Scale bars represent 1 μm.

which maintains the original shape and structure of these membrane assemblies, among other membranous organizations including large (around 2 µm) and small (100-700 nm) unilamellar vesicles. A small fraction of intact LBPs of 1-2 µm diameter was detected, whereas most of these structures appeared partially disrupted or already unravelled. In fact, LBPs were found exhibiting a variety of morphological arrangements and packing states, allowing us to sketch the different steps of their gradual unravelling process (**Figure AP4**). Of note, a sort of pore was clearly discerned close to the outer layers of LBPs (**Fig. AP4AB, C, D**), in consistence with our previous results shown in Chapter 1 with Laurdan-stained intracellular lamellar-bodies (see page 115). We have already postulated the presence of a protein-based gate-like machinery present in these areas, in charge of controlling the opening and spreading of the surfactant membranes. We speculate that this "protein complex" would act as a pressure-sensitive valve, which after contacting with the air-water interface, could undergo a conformational change, which could permit the opening of the structure (**Fig. AP4 B**) leading to the ejection of the internal membranes at a first moment, as insinuated in **Fig. AP4 C** and **D**. In view of this, we presume that membrane propelling takes place "from inside to outside" in the LBPs, since the inner layers seem to be first expelled, whereas the outer layers appear intact.

The next steps in the unravelling process would consist on a progressive rupture and unpacking of the LBP (**Fig. AP4 E**), giving rise to lace-shaped forms (**Fig. AP4 F**) and finally to interconnected membrane sheets with lower organization levels (**Fig. AP4 G**). In the native environment, this would derivate either into the formation of the surface film and/or other interrelated structures like tubular myelin or the surface-associated multilayered reservoirs.

On the other hand, the possibility of cryo-soft X ray tomography to build tridimensional reconstructions allowed us to get further insight into the LBP structure (**Figure AP5)**. **Fig. AP5B**, **C** and **D** show the volumetric representation of the diverse packing areas of a partially unravelled LBP, from different perspectives. Indeed, part of the examined LBP was shown to be still compact and dense at some areas, whereas in others it seemed to be unpacked generating long membranous projections as well as small loops (**Fig. AP5E**). Interestingly, those

internal membranes in contact with the “opening area” of the LBP adopted a remarkable curled morphology (**Fig. AP5E,** red colored in inset) with multiple membrane-membrane contacts, which might be promoted by SP-B (Bernardino de la Serna, Vargas et al. 2013). We conjecture that this could be effect of a modified state of mechanical tension, once the internal pressure is relaxed after the opening of the structure.

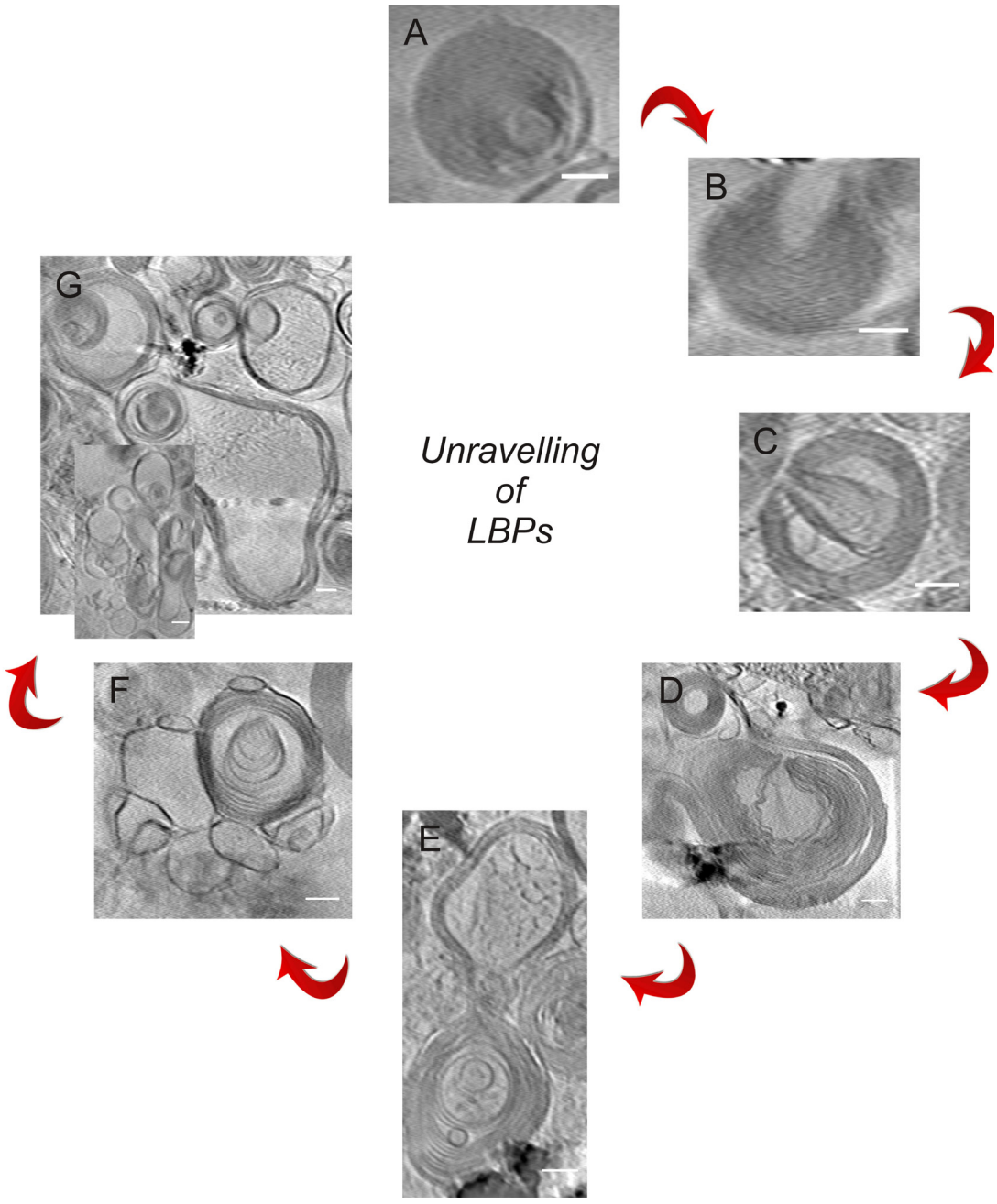

Figure AP4. **Unpacking of lamellar body-like particles**. Tomographic slices showing different lamellar body-like particles throughout their gradual process of unravelling, from a highly packed state to a network of disorganized membranes, as examined under cryo soft X-ray microscopy. Scale bars

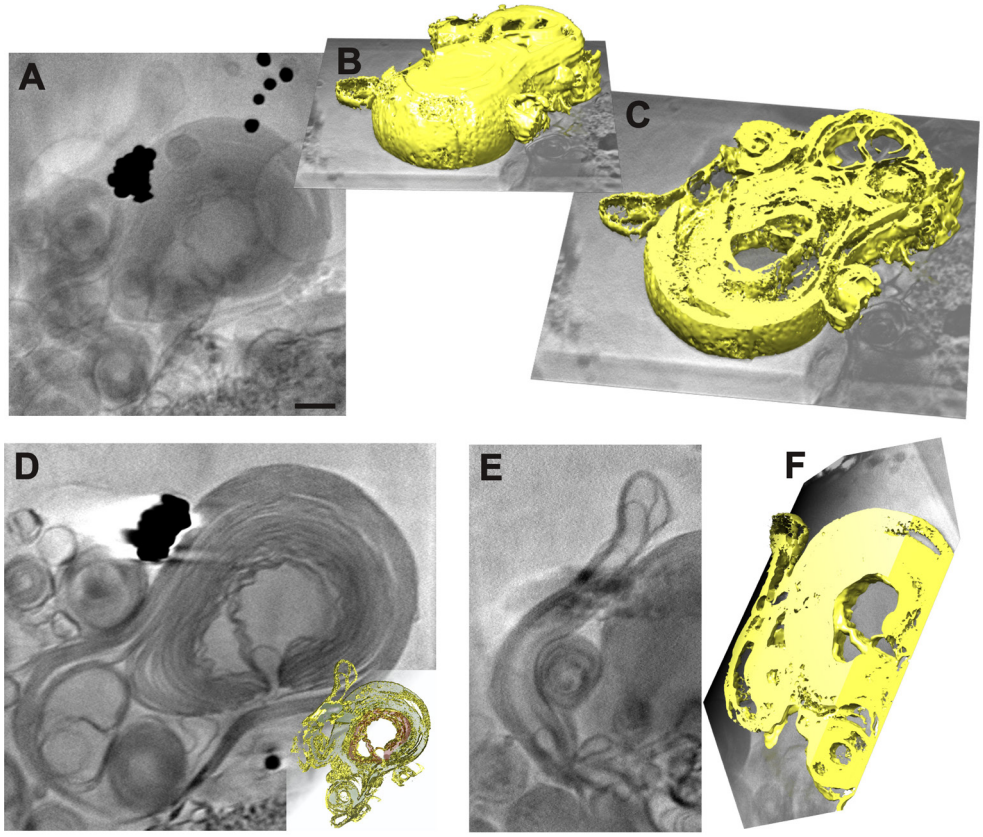

Figure AP5. Tridimensional modeling of a partially unravelled lamellar body-like particle. **A**. 2D soft X-ray cryo projection of a LBP in the process of unravelling. Scale bar represents 500 nm. **B**, **C**. 3D volumetric representation of the tomogram from different spatial orientations. **D**. Tomographic slice and segmentation (inset). Note that the membranes display a distinct curled shape (red) in the area close to the opening, by which internal membranes might be ejected through. **E**, **F**. Tomographic slice (E) and reconstructed volume (F) showing an area where the membranous sheets from the LBP exhibit an unpacked and disorganized state.

In conclusion, we have examined the morphology of NS complexes as purified from BAL under close to native conditions, maximizing their physical preservation and so circumventing potential artifacts, by means of cryo-fixation. In spite of the fact that electron tomography has been already implemented by other authors to observe A549 cells and to generate 3D visualizations of lung multivesicular bodies (Mayhew, Muhlfeld et al. 2009), the higher power penetration of soft X-rays is crucial to resolve complex structural organizations, such as those displayed by LBPs. Despite being a high-end approach, which requires sophisticated instrumentation and a high level of expertise, the potential of this technique has been proven to be enormous, allowing us to obtain unprecedented images and 3D renderizations and subsequently qualitative and quantitative information useful for the interpretation of the various biological forms in which lung surfactant occurs.

Chapter 3

Part of the experiments presented in this chapter were performed at the Research Institute of 12 de Octubre Hospital and at Medical Innsbrück University (Austria) in collaboration with Prof. Dr. Thomas Haller, and published in the following article:

Cerrada A, de la Torre P, Grande J, Haller T, Flores AI, et al. (2014) Human Decidua-Derived Mesenchymal Stem Cells Differentiate into Functional Alveolar Type II-Like Cells that Synthesize and Secrete Pulmonary Surfactant Complexes. PLoS ONE 9(10): e110195.

INTRODUCTION

Preceding chapters have discussed the singular features presented by lung surfactant when is intracellularly stored and subsequently exocyted in the form of lamellar bodies by cultures of primary alveolar type II (ATII) cells, as well as the relevance of this process. Indeed, much research has been carried out to study pulmonary surfactant biogenesis and secretion in primary cultures of isolated ATII cells purified mainly from mammalian lungs. However, this methodology is laborious, expensive, animal demanding and the yield of cells is low (Jennings, Bertocchi et al. 2005). Therefore, it does not necessarily conform with the 3-R principle of refining, reducing and replacing animal testing as defined by the Basler declaration (http://www.basel-declaration.org/). In addition, isolated primary ATII cells in culture rapidly lose their original phenotypical features differentiating into type I-like cells and failing to proliferate, precluding their use for long term studies (Dobbs, Williams et al. 1985; Mason, Lewis et al. 2002). On the other hand, commercially available cell lines such as the adult rat pulmonary epithelial cell line L2 or the adenocarcinomic human alveolar basal epithelial cells A549 are inherently problematic. Their origin and state of differentiation are poorly defined, and no study exists to unambiguously demonstrate that these cell lines release functionally active surfactant components after physiological stimulations. Alternatively, immortal cells isolated from transgenic mouse models (H-2K^{b}-tsA58) circumvent the problem of short-term culture to a certain extent, but are still depending on the use of laboratory animals. In consequence, surfactant-producing pneumocyte-like cell lines are not well established yet, preventing a proper and exhaustive characterization of biosynthetic and trafficking pathways involved in surfactant biogenesis. In this context, it is mandatory the search of new strategies to obtain *in vitro* ATII cells.

In recent years, stem cells have been extensively investigated as a potential source of alveolar epithelial cells (Wong and Rossant 2013). Murine (Siti-Ismail, Samadikuchaksaraei et al. 2012; Ali, Edgar et al. 2002; Rippon, Polak et al. 2006; Samadikuchaksaraei and Bishop 2006; Van Vranken, Rippon et al. 2007; Winkler, Mauritz et al. 2008; Roszell, Mondrinos et al. 2009; Schmeckebier, Mauritz et al. 2013) and human (Samadikuchaksaraei, Cohen et al. 2006; Van Vranken, Rippon et al. 2007; Wang, Haviland et al. 2007) embryonic stem cells, adult bone marrow-derived

mesenchymal stem cells (MSCs) from rat (Knoll, Brockmeyer et al. 2013) and human (Wang, Bunnell et al. 2005; Ma, Gai et al. 2011), as well as MSCs obtained from amniotic fluid (Carraro, Perin et al. 2008), amnion (Moodley, Ilancheran et al. 2010) or umbilical cord blood (Berger, Adams et al. 2006) have been differentiated into cells with phenotypical features consistent with ATII cells.

A population of MSCs isolated from human extraembryonic membranes by the group of Flores (Macías, Grande et al. 2010) and termed Decidua-derived Mesenchymal Stem Cells (DMSCs) have the capacity to differentiate into cells that have remarkable similarities with alveolar type II cells. In fact, human placenta, besides playing a fundamental role during fetal development, feto-maternal tolerance and nutrition, it is also an important reservoir of stem cells (Matikainen and Laine 2005; Parolini, Alviano et al. 2008). Placental tissue exhibits certain advantages as a source of stem cells including MSCs, such as easy isolation of cells without any invasive procedures, absence of viral infection and nonexistence of ethical problems (Hemberger, Yang et al. 2008; Marcus and Woodbury 2008). The extraembryonic membranes of human placenta are composed of fetal (amniotic and chorionic structures) and maternal tissues (decidua) (Pipino, Shangaris et al. 2013). DMSCs belong to the maternal part of the placental membranes, i.e., the decidua, and display high plasticity and high differentiation capacity into derivatives of all germ layers (Hemberger, Yang et al. 2008; Macías, Grande et al. 2010; Bornstein, Macías et al. 2012). Mesodermal (chondrogenic, osteogenic, myogenic and cardiogenic), ectodermal (neurogenic) and endodermal (lung epithelial cells) differentiation of DMSCs was demonstrated by evaluation of specific markers for each cell lineage. Indeed, this multipotent behaviour is explained by the fact that DMSCs express OCT-4 and REX-1, two transcription factors associated to pluripotency of embryonic stem cells. In addition, DMSCs express GATA-4, a transcription factor involved in organogenesis and in mesodermal and endodermal differentiation during embryogenesis. Interestingly, DMSCs have a limited life span and their expansion capacity decrease with time and at around a median of 20 passages cells stop dividing, precluding an aptitude for spontaneous transformation. This feature has been also confirmed by studying telomerase activity, which levels were low compared to a positive control and were undetected beyond passage 10. The limited proliferation capacity of DMSCs, the genomic stability after proliferation in culture and

the low and limited telomerase activity suggest that DMSCs are safe cells and will not produce tumors after transplantation. Additionally, DMSCs can be cryopreserved in liquid nitrogen for long periods of time while maintaining their original phenotype, exponential growth and differentiation characteristics suggesting that DMSCs could be stored in cell banks as an "off-the-shelf" treatment based on expanded DMSCs and ready to be used for cell therapies.

In the present chapter, the differentiation of DMSCs into Alveolar Type II-Like Cells (ATII-LCs) has characterized in depth. We evaluated the capability of ATII-LCs to express genes encoding lung specific markers and whether those genes are translated into proteins. In addition we assessed the ability of ATII-LCs to generate surfactant-like assemblies, to accumulate them in specialized storage organelles and to secrete them upon a proper stimulation. Finally, we analyzed the biophysical properties of the secreted material and whether this secreted material has functional properties as a surface active agent. Our results suggest that the ATII-LCs could be a novel and very promising cell model to study intrinsic ATII characteristics and functions.

RESULTS

Morphological features of ATII-LCs

DMSCs are a homogeneous population of fibroblast-like cells with spindle-like shape and similar morphological characteristics to bone marrow MSCs (**Figure 3.1A**). After 1-2 days of culture in pulmonary differentiation medium, few differences could be observed although some areas started to undergo slight morphological modifications (**Fig. 3.1B-C**). However, after 3-4 days in differentiation media, the morphological changes were apparent such as a more epithelioid shape (**Fig. 3.1D-F**) and the presence of light-dense cytoplasmic granules (**Fig. 3.1F, arrows**). The morphology of these dense particles in the cytoplasm of ATII-LCs was examined by transmission electron microscopy, revealing ellipsoid and circular membranous structures with multiple, variably densely packed concentric lamellae (**Figure 3.2**). These structures resemble the complex internal organization of the phospholipid-rich surfactant stores (lamellar bodies)

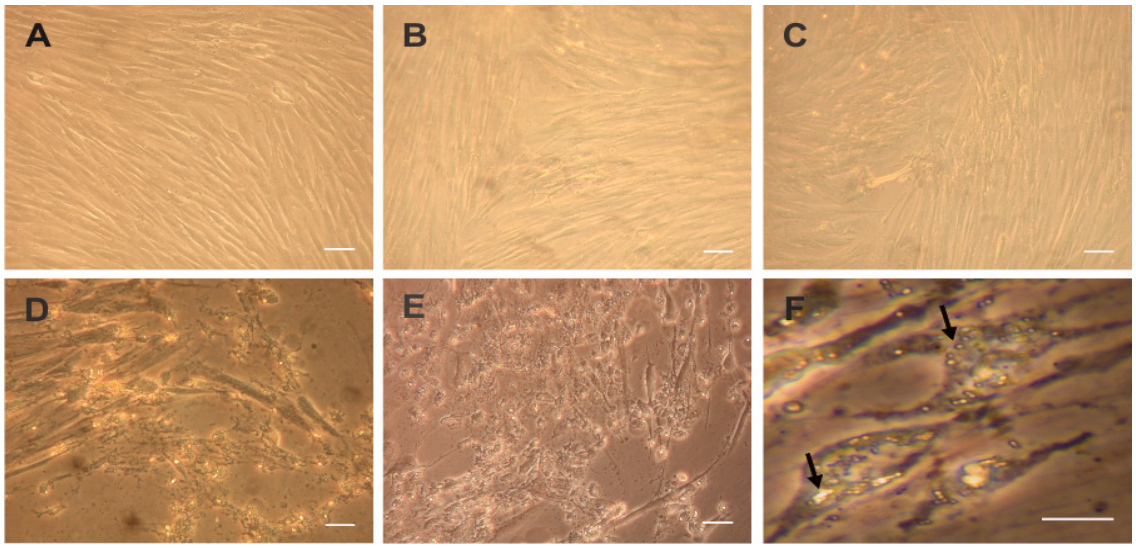

Figure 3.1. **Morphology of DMSCs and ATII-LCs**. Phase contrast images visualizing morphological changes of DMSCs during differentiation into ATII-LCs. **A**. Undifferentiated DMSCs showing a smooth and fibroblast-like morphology. **B**-**C**. Differentiated ATII-LCs after 1 (B) or 2 (C) days of incubation in differentiation medium, exhibiting scarce morphological changes with respect to the undifferentiated state. **D**-**F**. Images corresponding to ATII-LCs after 3 (D) or 4 (E, F) differentiation days displaying a more flattened shape and a highly granulated cytoplasm. **F**. Magnified view of 4 days differentiated-ATII-LCs containing groups of highly-refractive cytoplasmic particles (arrows). Scale bars in A-E correspond to 100 µm and in F to 50 µm.

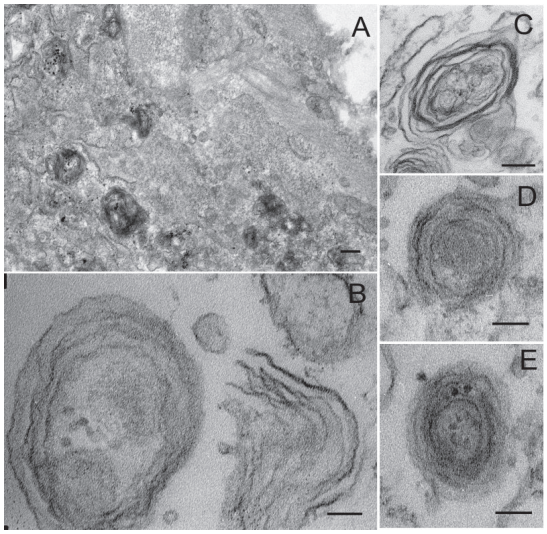

Figure 3.2. **Ultrastructure of ATII-LCsTransmission electron micrographs of differentiated ATII-LCs**. **A**. Presence of numerous electron-dense cytoplasmic organelles and cell surface associated structures, probably microvilli. (x20,000; scale bar = 200 nm). **B**. Membranous structures containing multiple concentric lamellae (left) and one partially unraveled fragmented lamellar body-like complex (right), displaying numerous unpacked membranes (x 120,000; scale bar = 50 nm) **C**-**E**. Individual membranous structures with ellipsoid (C) or circular (D, E) shapes and a multilamellar ultrastructure (x 40000, scale bar = 200 nm).

in ATII cells, and are similar in morphology to the lamellar body-like granules obtained from bronchoalveolar lavage and observed under the same conditions (Ravasio, Olmeda et al. 2010). In addition, ATII-LCs exhibited at the culture-exposed cell side the presence of structures with the appearance of incipient microvilli (**Fig. 3.2A**), suggesting that the cells might be initiating a polarized morphological differentiation.

The differentiation of DMSCs to ATII-LCs showed high reproducibility. Several different placentas have been used and all of them differentiated into ATII-

LCs. Examination under the microscope revealed that in all cases near 100 % of cells in the tissue culture plate developed the intracellular dense particles associated with lamellar body biogenesis, indicating a very high differentiation yield.

Synthesis of surfactant lipids

We then explored whether the morphological differentiation of DMSCs into ATII-LCs, with the assembly of apparently lamellar body-like structures, could be associated with activation of the synthesis of genuine surfactant phospholipid species, i.e. with the accumulation of disaturated phospholipids, and particularly of dipalmitoylphosphatidylcholine (DPPC). **Table 3.1.A** summarizes the data of the lipidomic analysis obtained by mass spectrometry, of the whole PC (phosphatidylcholine) fraction from full membranes obtained from the different pelleted cells. For the complet set of data regarding the content in single PC molecular species, see **Table 3.1.B**. Membranes from non-differentiated DMSCs contained 17.6 % of PC disaturated species, and only around 10 % of PC was DPPC. However, upon differentiation, ATII-LCs apparently doubled their content up to 35 % of disaturated PC species, with more than 25 % being DPPC. Although the small number of samples analyzed precludes a proper statistical analysis of differences, these results showed that the content in total disaturated PCs and DPPC of differentiated ATII-LCs was similar to that determined for a cell population enriched in true type II pneumocytes, as purified from lung tissue.

Gene expression of alveolar epithelial markers

We investigated by end-point PCR in ATII-LCs whether the effect of the pulmonary differentiation media led to the expression of specific genes indicative of lung development and related to pulmonary surfactant (**Figure 3.3**). The data shows that ATII-LCs express FOXA1, FOXA2 and TTF1 mRNAs, which are known to be involved in specification of endoderm. GPR116, which plays an essential role in the regulation of lung surfactant homeostasis was also expressed in ATII-LCs, as well as CTFR, a gene implicated in epithelial fluid transport in the lung. Aspartyl proteases Napsin

Table 3.1. A. Fraction of saturated phosphatidylcholines in undifferentiated (DMSCs) and differentiated (ATII-LCs) decidua-derived mesenchimal cells in comparison with primary ATII pneumocytes

	Cell types		
	DMSCs (n=2)	**ATII-LCs** (n=3)	**ATII**
% DPPC	10,2 ± 2,8	25,4 ± 9,3	26,4
% PC disat.	17,6 ± 3,6	35,5 ± 12,3	40,3

mean values ± s.d. have been calculated with respect to total PC

B. Total fraction of phosphatidylcholine molecular species in undifferentiated (DMSCs) and differentiated (ATII-LCs) decidua-derived mesenchimal cells in comparison with primary ATII pneumocytes

	Cell types		
PC* molecular species	**DMSCs (n=2)**	**ATII-LCs (n=3)**	**ATII (n=1)**
28:0-PC	0.5 ± 0.01	0.2 ± 0.1	0.5
30:0-PC	5.0 ± 0.4	6.8 ± 2.7	10.5
30:1-PC	1.6 ± 0.2	0.5 ± 0.1	1.1
32:0-PC	10.2 ± 2.8	25.4 ± 9.3	26.4
32:1-PC	13.7 ± 0.5	10.0 ± 0.9	16.3
32:2-PC	2.7 ± 0.3	0.8 ± 0.2	2.2
34:0-PC	1.8 ± 0.4	3.1 ± 0.3	2.8
34:1-PC	21.8 ± 0.3	23.0 ± 3.1	9.9
34:2-PC	11.1 ± 1.3	5.6 ± 1.2	8.8
34:3-PC	1.1 ± 0.1	0.4 ± 0.1	1.5
34:4-PC	0.1 ± 0.01	-	0.4
36:0-PC	-	-	0.1
36:1-PC	5.8 ± 0.1	7.0 ± 2.5	0.5
36:2-PC	16.0 ± 0.4	9.6 ± 3.9	2.3
36:3-PC	-	1.4 ± 0.4	2.0
36:4-PC	1.1 ± 0.1	0.9 ± 0.2	7.4
36:5-PC	0.3 ± 0.02	0.2 ± 0.1	0.8
38:2-PC	1.2 ± 0.1	0.6 ± 0.4	0.1
38:3-PC	1.8 ± 0.1	1.1 ± 0.8	0.6
38:4-PC	1.0 ± 0.1	1.0 ± 0.4	2.6
38:5-PC	1.3 ± 0.1	1.1 ± 0.5	1.0
38:6-PC	0.6 ± 0.1	0.5 ± 0.1	1.2
40:5-PC	0.6 ± 0.1	0.4 ± 0.3	0.3
40:6-PC	0.4 ± 0.1	0.2 ± 0.2	0.1
40:6-PC	0.2 ± 0.01	0.2 ± 0.1	0.3

*The different molecular species are identified as **n:m-PC**, where **n** is the total number of carbons of the *sn-1* and *sn-2* acyl chains, and **m**, the total number of double bonds mean values ± s.d. have been calculated as percent fraction with respect to total PC

A and Cathepsin H, which participate in the proteolytic processing of surfactant proteins were expressed in differentiated cells as well. The expression of genes encoding surfactant proteins A, B, C and D and ABCA3 was distinctively found in ATII-LCs, at different time points. Surprisingly, all these genes were also detected in undifferentiated DMSCs, although the differentiation treatment resulted in an up-regulation of these genes according to the band densities.

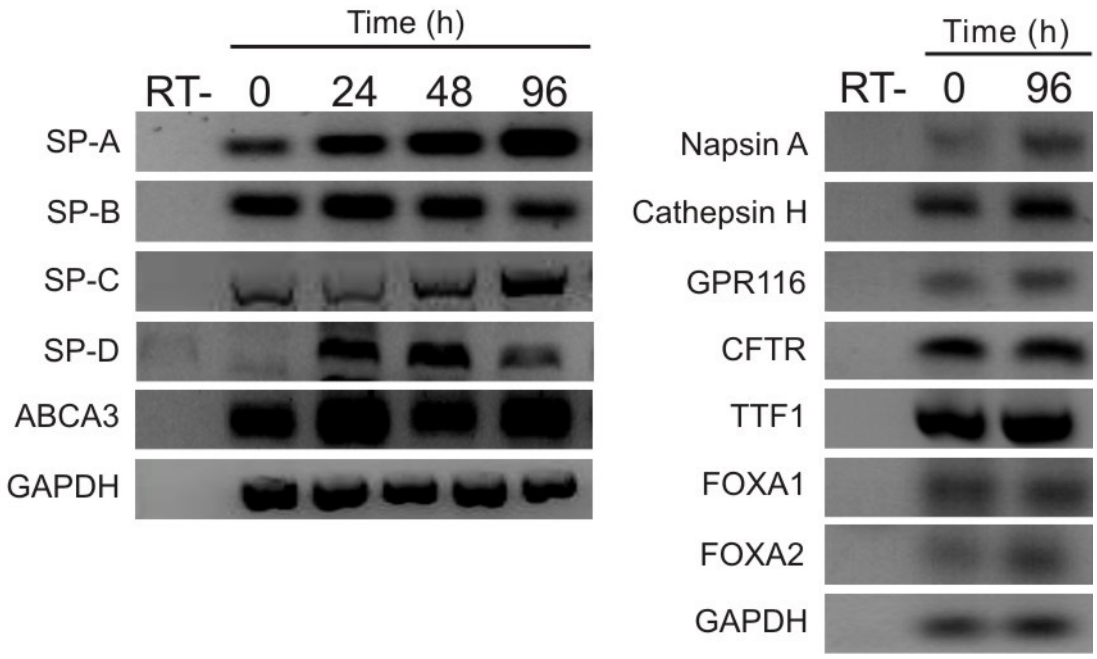

Figure 3.3. Gene expression of surfactant and lung development markers in ATII-LCs. Specific markers of pulmonary surfactant function and maturation examined by endpoint reverse transcription PCR (RT-PCR). Expression of genes encoding surfactant proteins A, B, C and D as well as ABCA3 was analyzed in DMSCs and ATII-LCs after 24, 48 or 96 h of differentiation. mRNAs codifying Thyroid transcription factor 1 (TTF1), Forkhead box protein A1 and A2 (FOXA1 and FOXA2, respectively), Cathepsin H, Napsin A, G-protein coupled receptor 116 (GPR116) and Cystic fibrosis transmembrane conductance regulator (CFTR) were evaluated at maximum point of differentiation (96 h). Glyceraldehyde-3-phosphate dehydrogenase (GAPDH) expression was used as loading control of complementary DNA. Left lane represents the RT control (RT-).

Quantitative time-course of surfactant-related gene expression

To evaluate whether the expression of surfactant-related genes is regulated throughout differentiation, we assessed the presence of specific mRNAs in DMSCs and in ATII-LCs after various incubation times in the differentiation medium (24, 48 and 96 h) by real-time PCR (**Figure 3.4**). SP-A mRNA levels were found to be 4-fold significantly increased ($p<0.001$) with respect to the gene expression level of DMSCs, at 96 h of differentiation. Similarly, SP-C mRNA

expression showed a marked increase during differentiation, reaching levels of 7-fold induction at 96 h ($p<0.001$). However, the maximum increase in the level of gene expression for the proteins SP-B ($p<0.05$) and SP-D ($p<0.001$) took place at the beginning of differentiation, reaching values around 3-fold of induction at 24 h. The expression of these two genes decreased at 48 h and this level was maintained until 96 h.

We also examined the gene expression pattern of the surfactant lipid importer ABCA3, which plays a critical role in the biogenesis of surfactant complexes in ATII cells. ABCA3 gene expression level was 3-fold ($p<0.001$) increased from 24h to 96 h of PLC differentiation.

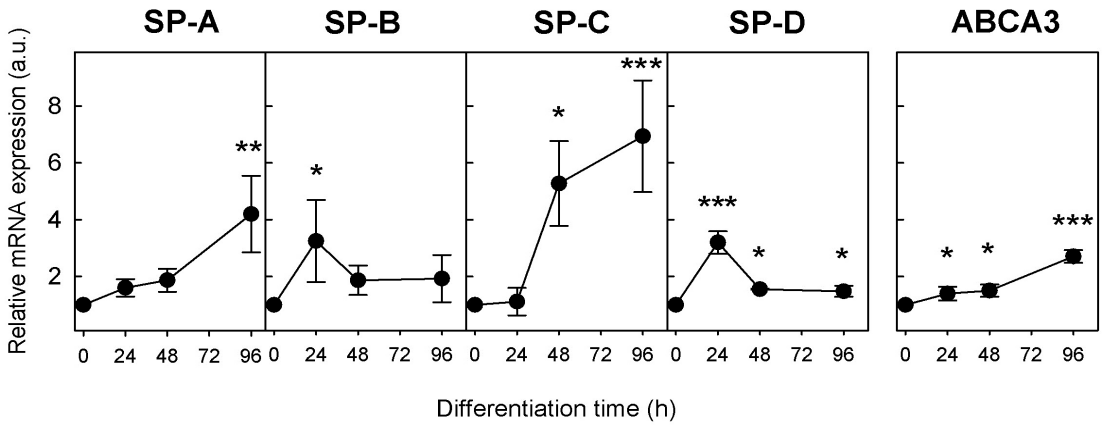

Figure 3.4. **Time-course expression of pulmonary surfactant-related genes during ATII-LC differentiation**. Gene expression of surfactant proteins SP-A to SP-D and the lipid transporter ABCA3 during differentiation of DMSCs as determined by quantitative real-time PCR. Values are expressed as means (N=5) of fold induction with respect to mRNA levels in DMSCs. Human adult lung was used as a calibration control. The results were normalized to TBP values used as a housekeeping gene and represented as mean ± standard deviation. * $p<0.05$), ** $p<0.01$, *** $p<0.001$.

Expression of surfactant proteins

To determine whether ATII-LCs also synthesize, process and secrete surfactant proteins into the extracellular medium, the expression of these proteins was evaluated by western blot in both, DMSCs and ATII-LCs after 4-days in differentiation media, as well as in their respective incubation media (**Figure 3.5**). Enhanced levels of surfactant proteins SP-A, SP-B and SP-C were observed in ATII-LCs compared to DMSCs. Increased expression of dimeric (≈72 kDa), and particularly multimeric forms of SP-A (>150 kDa) can be discerned in ATII-LCs, likely as a consequence of only

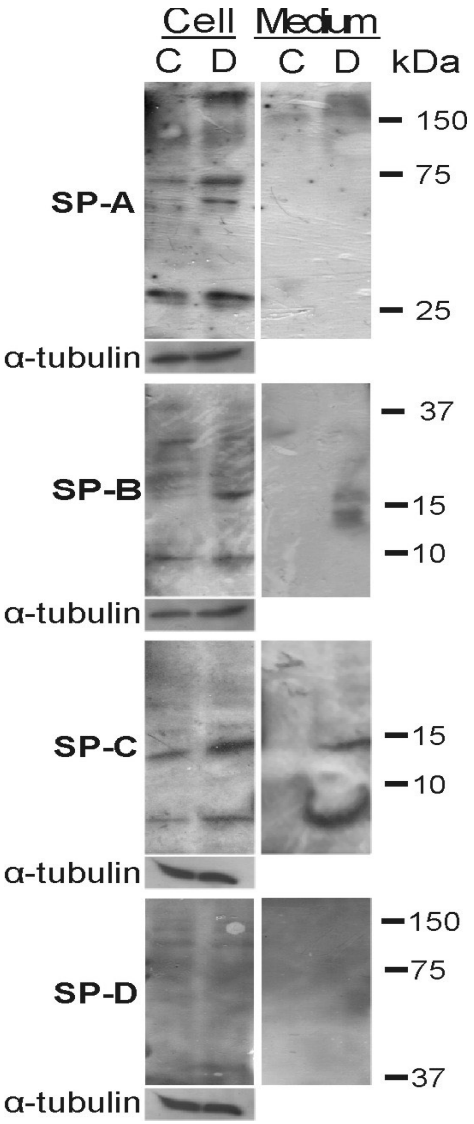

Figure 3.5. **Pulmonary surfactant proteins in ATII-LC cultures**. Western blots of pulmonary surfactant proteins (SP-A to SP-D) in DMSCs and ATII-LCs as well as the secreted proteins in the respective cell culture supernatants. The figure compares representative western blots (N=3) after loading equivalent amounts of total protein, using α-tubulin expression as a loading control. (C = control DMSCs; D = differentiated ATII-LCs).

partial reduction of disulfides in the proteins embedded into the large secreted lipid-protein complexes. Presence of monomeric (≈ 8.7 kDa) and dimeric (≈ 17.4 kDa) forms of SP-B as well as monomeric (≈ 3.7 kDa) forms of SP-C are also more noticeable in the case of differentiated cells. Protein bands corresponding to molecular weights compatible with the presence of precursors of SP-B (proSP-B, ≈ 43 kDa) and SP-C (proSP-C, ≈21 kDa) as well as other intermediaries can be also distinguishable. Expression of SP-D was barely detectable. Presence of the mature forms of these proteins was also evident in the culture medium of ATII-LCs compared to DMSCs, suggesting that ATII-LCs were metabolically active and secreted these proteins. Basal expression of all the surfactant proteins was noticed in DMSCs, particularly in the case of SP-A and SP-C.

Surfactant exocytosis

Since regulated secretion of lung surfactant is considered to be the most important functional characteristic of ATII cells, we aimed to explore the ability of ATII-LCs to exocytose their surfactant-like stores after stimulation. For this purpose, we used a method previously described to monitor the exocytotic activity of primary cultures of ATII cells, taking advantage of the special properties of the fluorescent probes LTG and FM 1-43. LTG permeates through the plasma membrane and accumulates into acidic compartments such

as surfactant-accumulating lamellar bodies and lysosomes. Thus, LTG was visualized as bright green fluorescence not only in ATII-LCs but also in DMSCs (**Figure 3.6**). We stained cells with LTG to firstly demonstrate the presence of acidic compartments, secondly to visualize the cells and to get the LBs in the focal plane, and lastly to make sure that always approximately the same amount of LTG-positive vesicles and cells are in the respective field of measurement. The cells were then stimulated with ATP (100 µM) and PMA (100 nM) which are secretagogues in native ATII cells. At this point, FM 1-43, a membrane-impermeable dye that has no fluorescence in

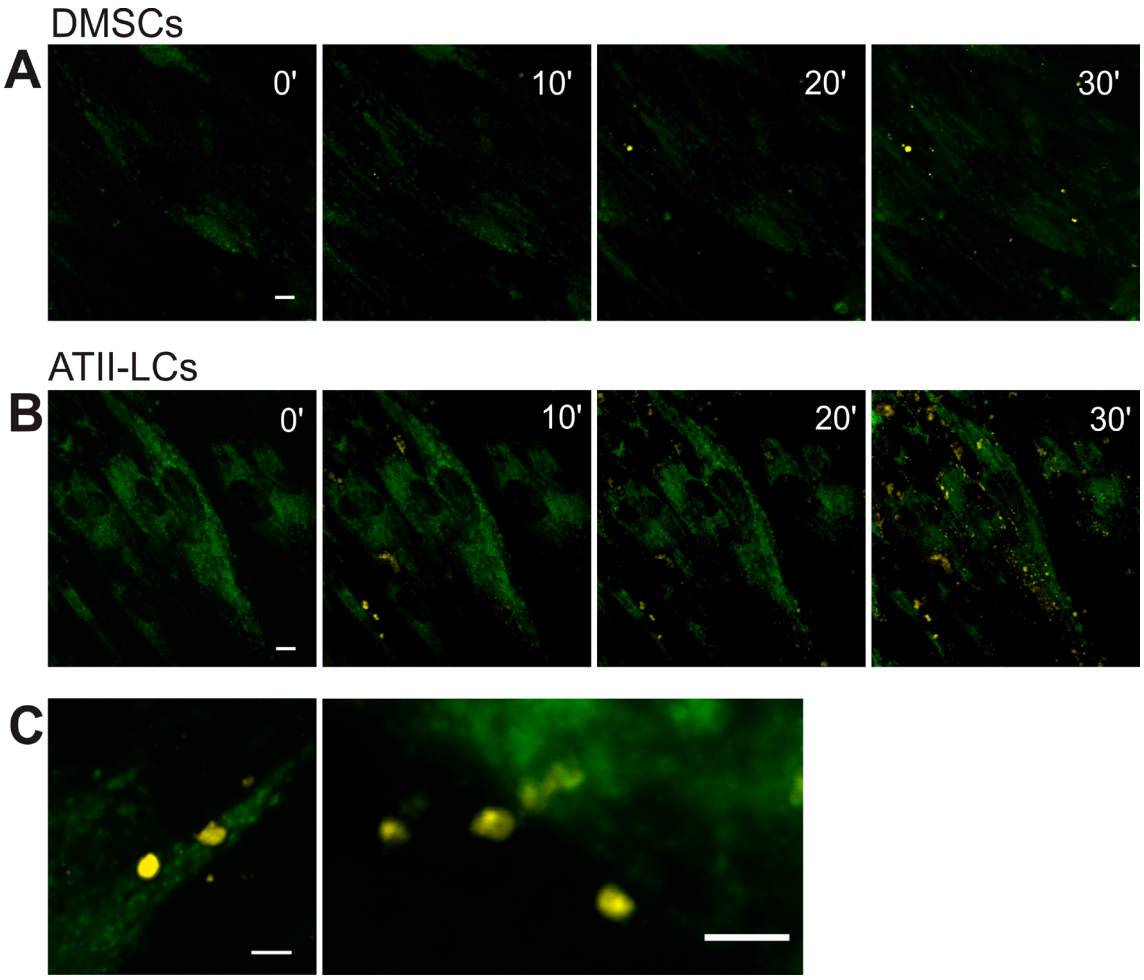

Figure 3.6. Secretion of pulmonary surfactant-like complexes by ATII-LCs. Confocal microscopy of DMSCs (**A**) and ATII-LCs (**B**, **C**) during stimulated exocytosis. Images are z-stack projections of multiple focal planes. Non stimulated DMSCs or ATII-LCs were preincubated with LTG, showing green fluorescence originating from acidic compartments (e.g. lysosomes, late endosomes and Lamellar Bodies). Yellow fluorescence denotes FM 1-43 fluorescence, a lipid sensing probe. FM 1-43 was added to the cultures together with the secretagoges ATP and PMA immediately after time 0. Upon fusion of lipid-charged vesicles with the plasma membrane, bright yellow fluorescence resulted from FM1-43 incorporation into secreted surfactant-like complexes. (**C**) Representative images of single confocal sections evidencing a high amount of secreted lipid assemblies associated to some ATII-LCs. Images were slightly corrected for a small loss in LTG fluorescence due to photobleaching. (Scale bar= 10 µm).

aqueous solution but exhibits fluorescence once intercalated into lipid membranes, was added to the cells. FM 1-43 enters through the fusion pore of the exocytosed vesicles, staining their lipid content and thus emitting a conspicuous yellow fluorescence. Stimulation of ATII-LCs cultures resulted in a progressive appearance of secreted lipid material visualized as bright yellow spots forming clusters at the periphery of the cells. In contrast, DMSCs were practically unresponsive to secretagogues. As a negative control, non-stimulated cells incubated in the presence of FM1-43 but in the absence of secretagogues showed no fluorescent response.

To further investigate the ultrastructural features of the lipid complexes secreted by the ATII-LCs, exocytosed material harvested from the extracellular medium was examined by transmission electron microscopy (TEM) (**Figure 3.7**). We discerned the presence of partially disorganized lamellar particles (**Fig. 3.7B and C**), as well as apparently unraveled lipid membranes. These membranes frequently showed the presence of defined structures, with marked kinks at some areas, suggesting the presence of membrane-associated proteins imposing significant perturbations (**Fig. 3.7A, D and E**). In the case of DMSCs, the scarce amount of secreted material harvested upon stimulation made impossible its structural examination.

Additionally, secreted material by ATII-LCs was studied in a close-to-native state taking advantage of cryo-electron microscopy (**Figure 3.8**). The polymorphic appearance of this material was also confirmed with this technique, with a variety of winding membranous structures with manifest twists (**Fig. 3.8A, B**), multillamelar vesicles with piled membranes (**Fig.3. 8C**) as well as intact and disrupted liposomes with a dense material inside (**Fig. 3.8F-H**). Interestingly, the external part of some vesicles seemed to be covered by proteins stablishing contacts between adyacent membranes (**Fig. 3.8D, E**). Occasionally, rounded liposomes could be discerned containing protein-like filaments (**Fig.3. 8H**), although is most cases, the content of these vesicles remained undefined.

Finally, ultrastructural analysis of the secreted material from ATII-LCs by using cryo-x-ray tomography (**Figure 3.9**) allowed us to visualize diverse unilamellar and multilamellar vesicles as well as multivesicular bodies of varied sizes, from one to several microns, enclosing in some cases a dense material (**Fig. 3.9 A,B,D**). Occasionally, the vesicles appeared partially disrupted

and the content seemed to be already released (**Fig. 3.9B, white arrow**). Worth mentioning is the fact that a type of sharp opening could be discerned in some liposomes (**Fig. 3.9A, B; black arrows**).

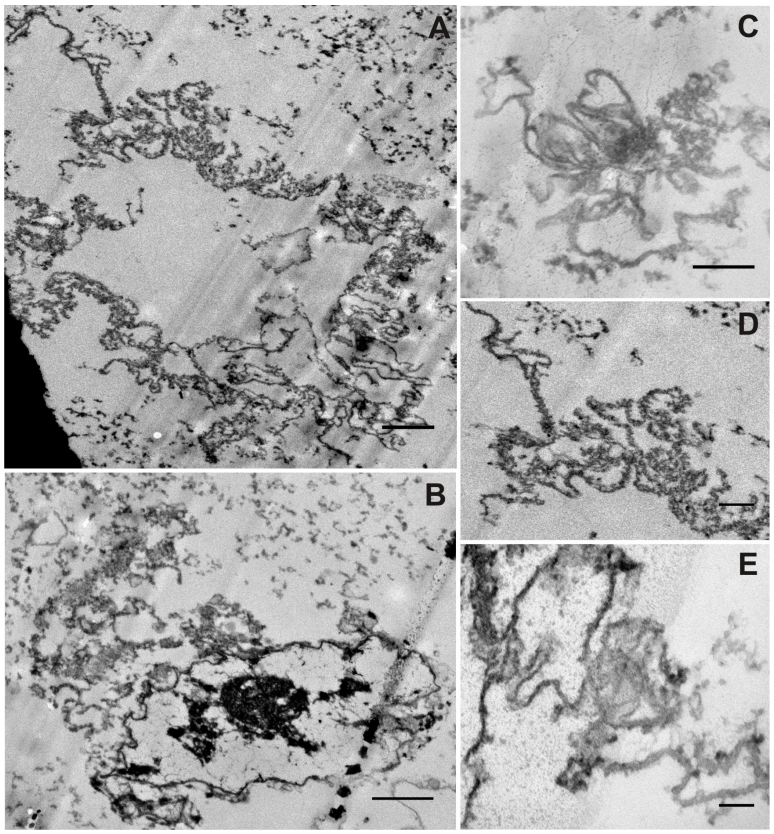

Figure 3.7. **Ultrastructure of membrane complexes secreted by ATII-LCs**. Transmission electron micrographs show harvested membranous complexes exocytosed by ATII-LCs upon stimulation with secretagoges for 6 h at 37°C. **A**, **D**. Multiple lipid membranes with numerous kinks constituting intricate structures possibly due to the presence of membrane-associated proteins. **B**, **C**, **E**. Membranous assemblies with some highly electron-dense areas, resembling the appearance of secreted and partially unraveled lamellar body-like particles. (Scale bars correspond to 1.000 nm in A and B, to 500 nm in C and D and 200 nm in E).

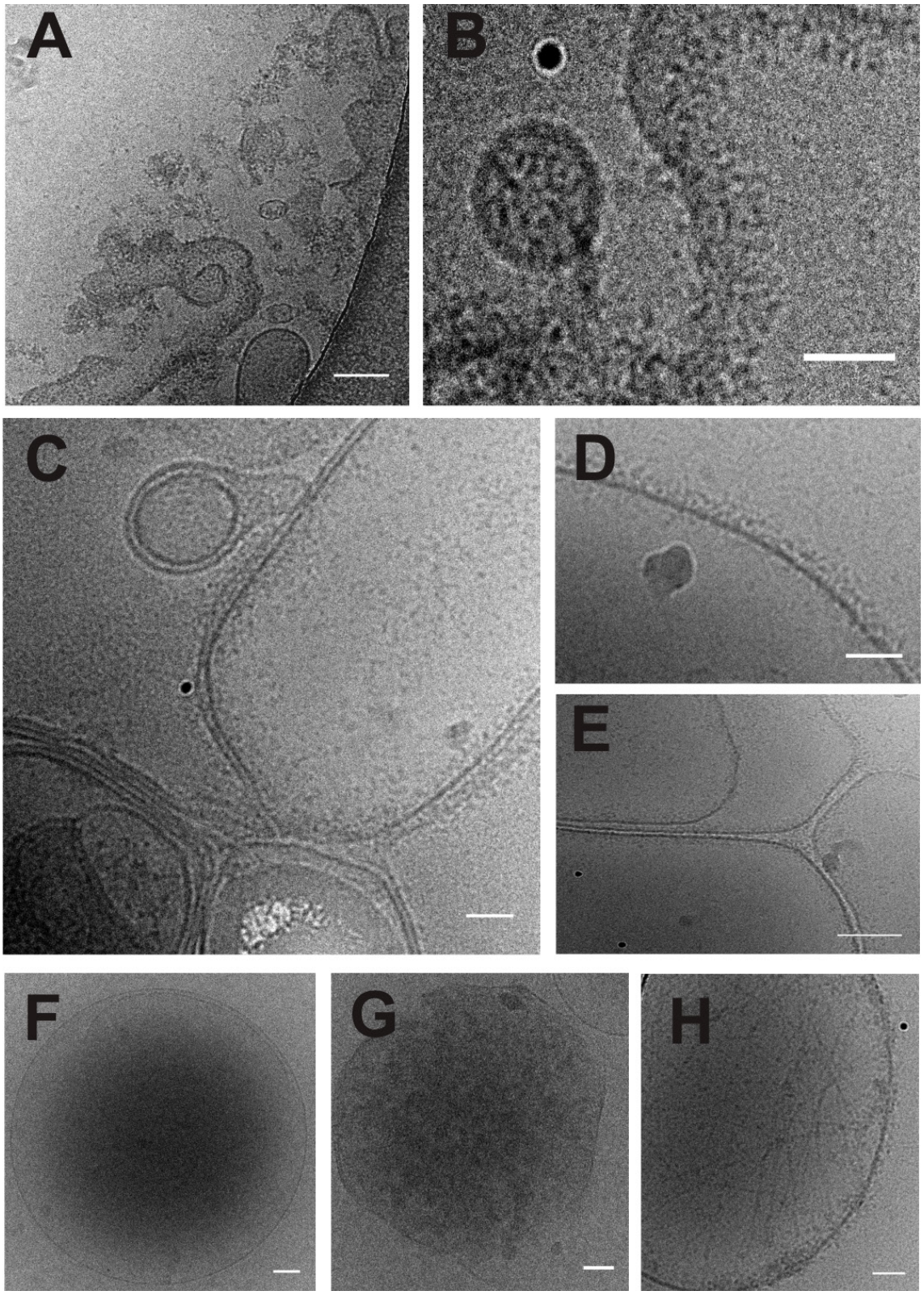

Figure 3.8. **Ultrastructural analysis of secreted material from ATII-LCs in a hydrated state.** Cryo-electron micrographs of the membranous assemblies exocyted by differentiated ATII-LCs processed without any chemical fixation. **A**, **B**. Heterogeneous lipid membranes adopting twisted morphologies probably modulated by protein components. **C**-**E**. Multillamelar lipid complexes exhibiting particulate structures in the outer layer contacting adjacent membranes. **F**-**H**. Intact (F) or partially disrupted (G) liposomes with a diffuse electrondense core or enclosing numerous filaments (H). (Scale bars correspond to 100 nm in A, E-G and to 50 nm in B-D and H).

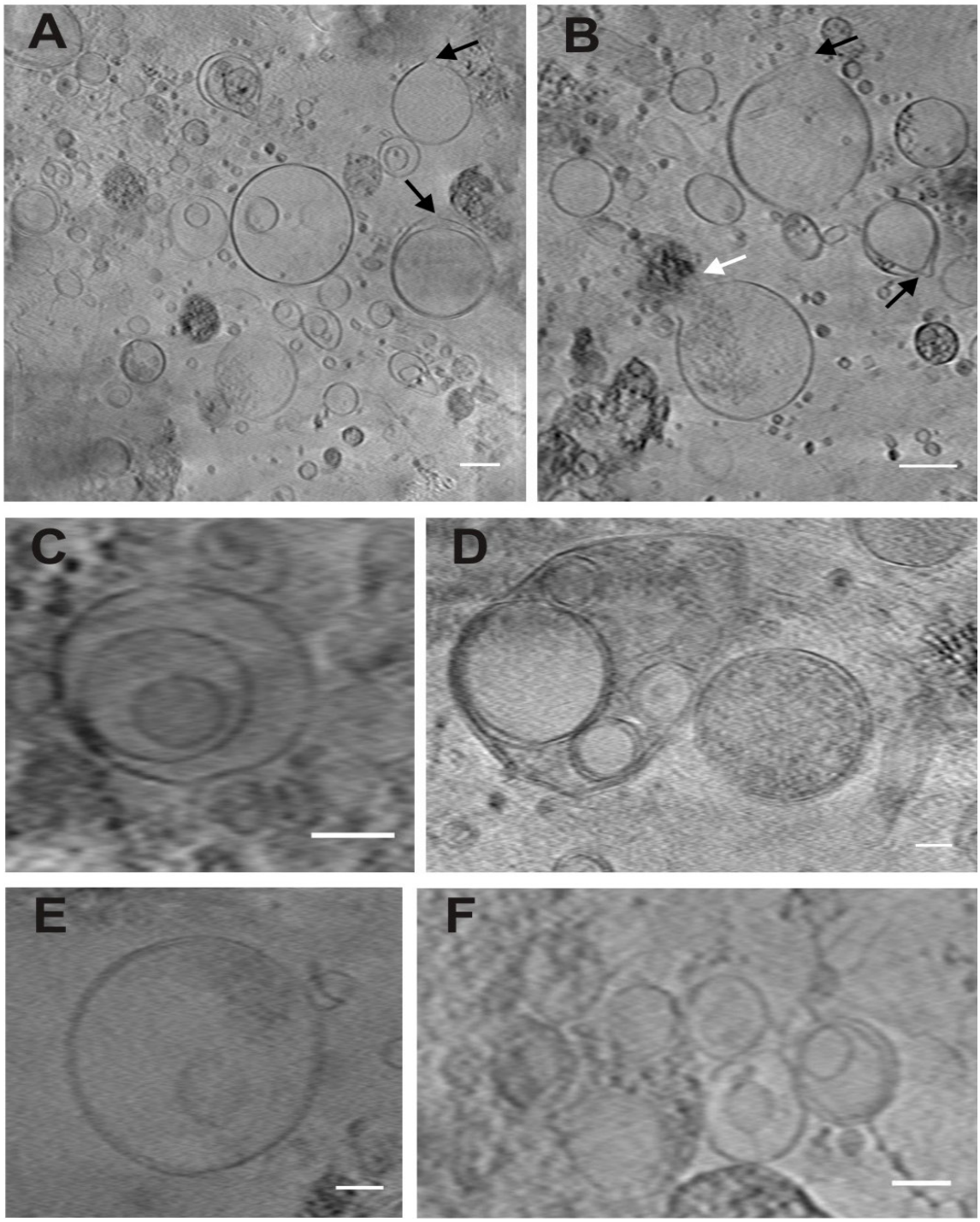

Figure 3.9. **Lipid complexes exocyted by ATII-LCs examined under cryo-x-ray tomography**. Cryo-x-ray tomographic sections of secreted material by differentiated cells state obtained taking advantage of an energy synchrotron source. Polymorphic unilamellar and multilamellar vesicles of various sizes without apparent internal content as well as containing a dense material inside or already released (white arrow in **B**) can be distinguished. A spiky opening can be noticed in some liposomes (black arrows in A and B), indicative of areas of evagination or disrupture. Occasionally, micron sized-multivesicular bodies (4-5 µm) containing internal vesicles were observed (**D**). (Scale bars represent 1000 nm in A and B and 500 nm in **C**-**F**).

Biophysical activity of secreted surfactant-like material

One of the most important properties of a functional surfactant is its capability to adsorb and accumulate rapidly and efficiently at the air-liquid interface, in order to form surface active films. To evaluate the interfacial adsorption properties of the material secreted by ATII-LCs, we have used a method developed in our laboratory that measures the kinetics of accumulation of surfactant at the interface and the resistance of the formed surface films and associated structures against mechanical agitation (Ravasio, Cruz et al. 2008). Surfactant-like complexes exocytosed by ATII-LCs displayed a rapid adsorption into the air-water interface. This adsorption was even faster than that of natural surfactant purified from bronchoalveolar lavages (BAL), which is typically used as standard material and a reference for optimal surfactant function. The scarce secreted material from stimulated DMSCs showed almost no adsorption properties, displaying a negligible accumulation at the interface (**Figure 3.10A**).

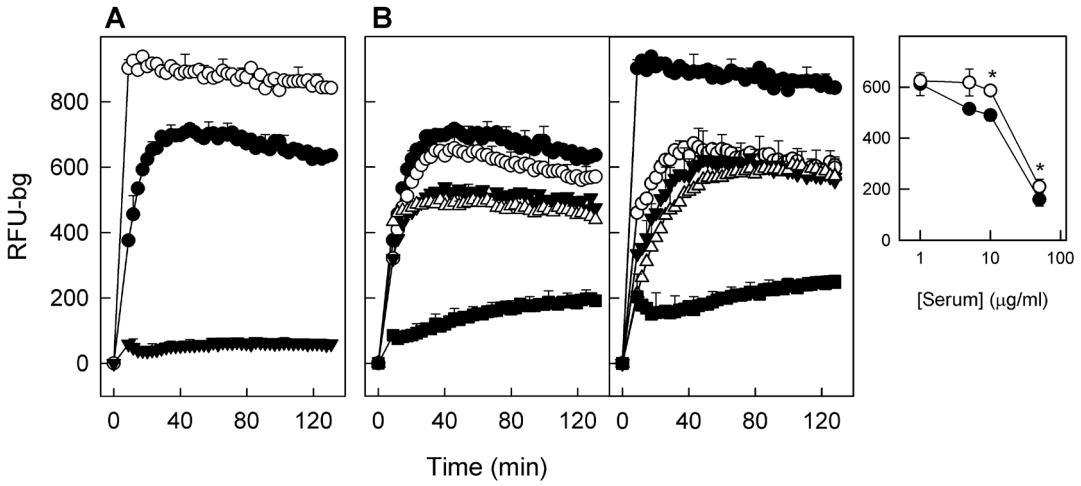

Figure 3.10. Interfacial adsorption properties of pulmonary surfactant-like complexes secreted by ATII-LCs. **A**. Comparison of surface adsorption properties of surfactant-like assemblies secreted by stimulated ATII-LCs (open circles) or secreted material by DMSCs (closed triangles) with respect to native surfactant purified from BAL (closed circles). Formation of a stably surface-associated lipid film is monitored by collecting BODIPY-fluorescence from the top of 96-wells during constant orbital shaking as described in detail in (38). Values of fluorescence were corrected for background (basal fluorescence prior to injection of labeled samples) and plotted as the mean of 5 experiments (N=5) ± standard deviation. **B**. Dose-dependent inhibitory effect of human serum proteins on the adsorption kinetics of Native Surfactant (NS, left panel) or material secreted from ATII-LCs (SM, right panel) Serum protein concentrations were 0 (●), 1 (○), 5 (▼) 10 (△) and 50 (■) μg/ml. **Insert**. Fluorescence values taken after 60 min of adsorption of SM from ATII-LCs (open circles) or of NS (closed circles) as a function of serum protein concentration. Adsorption efficacy in terms of amount of adsorbed material into the surface was significantly ($p<0.05$) higher in the case of SM than in NS at elevated serum concentrations (*). (RFU – bg = Background-substracted relative fluorescent units).

Lung surfactant is, under some circumstances, susceptible to inhibition by substances such us serum proteins, for example, leaking from the blood into the airspaces in cases of a breakdown of the alveolar-capillary barrier function during e.g. high altitude pulmonary edema formation. We have compared the inhibitory effect of serum on the adsorption rate of both natural surfactant purified from BAL and material secreted by ATII-LCs (**Fig. 3.10B**). Surfactant-like material secreted by ATII-LCs showed a noticeable resistance to serum inhibition, displaying significantly better adsorption kinetics than native surfactant membranes, which was particularly evident in the presence of the highest concentrations of serum ($p<0.05$) (**Fig. 3.10B**).

DISCUSSION

The present lack of suitable *in vitro* models to provide an easier and simplified way to understand key biological mechanisms in lung alveolar cells necessarily claims for the development of new strategies. In this context, we have taken advantage of a population of adult mesenchymal stem cells isolated from the maternal portion of human extraembryonic membranes (Decidua-derived Mesenchymal Stem Cells, DMSCs) capable to differentiate into derivatives of all germ layers, including ATII-like cells (Macías, Grande et al. 2010). The present work demonstrates that placenta-derived Alveolar Type II-Like Cells (ATII-LCs) not only differentiate towards an ATII cell-like phenotype but develop into truly functional units with the potential of expressing lung and surfactant-related genes and proteins, and with the capability of producing, storing and secreting highly surface-active, lipid-based assemblies into the extracellular fluid, thereby mimicking the exocytotic behavior of native ATII cells (Pérez-Gil and Weaver 2010).

Examination of ATII-LCs by light and transmission electron microscopy reveals that the cell morphology is consistent with the ATII cell phenotype, including characteristic lamellar body-like structures analogous to those observed in material obtained from bronchoalveolar lavage (Ravasio, Olmeda et al. 2010), and a cell shape suggesting incipient formation of microvilli in contact with the aqueous phase.

On the other hand, ATII-LCs overexpress mRNAs encoding surfactant proteins A-D and ABCA3 in response to the differentiation signals. Noticeably, mRNA levels of SP-B and SP-D, were upregulated at the onset of the differentiation process, (early expression genes) whereas mRNA levels of the late expression genes SP-A and SP-C were increased later (late expression genes). The biological relevance of this distinct expression pattern is unclear but will be explored in future studies. Previous studies reported an earlier expression in human fetuses of the SP-B and SP-C genes preceding the expression of SP-A, suggesting that during lung development, hydrophobic surfactant proteins SP-B and SP-C are independently regulated of the hydrophilic protein SP-A (Mendelson and Boggaram 1990; Mendelson and Boggaram 1991; Pryhuber, Hull et al. 1991).

It has been reported that the expression of mRNAs encoding surfactant proteins and ABCA3 is collectively regulated by a number of transcription factors like the thyroid transcription factor-1 (TTF-1) and the Forkhead ortholog a1 and a2 (FOXA1 and FOXA2) (Bohinski, Di Lauro et al. 1994; Wan, Xu et al. 2004). Importantly, we found expression of the genes encoding these characteristic markers for endodermal development, the germ layer which gives rise to alveolar epithelium. TTF-1 has been described to be expressed in the respiratory epithelium of the rat, appearing not only in fetal lung buds of the embryonic rat lung being essential for lung development and differentiation (Ikeda, Clark et al. 1995; Boggaram 2009), but also in adult ATII cells (Hosgor, Ijzendoorn et al. 2002). Interestingly, TTF-1 has been previously reported as an ATII cell marker in other lung differentiations from mesenchymal stem cells (Gu, Yan et al. 2014). In combination with TTF-1, FOX A factors, detected during the stem cell differentiation into endoderm (Levinson-Dushnik and Benvenisty 1997), have been reported to regulate the expression of SP-B (Zhou, Lim et al. 1996). Therefore, surfactant protein gene expression in the lung is regulated by complex mechanisms and combinatorial actions of multiple transcription factors (Boggaram 2003, Kalin, Wang et al. 2008). The particular signaling pathways involved in the differentiation of DMSCs into the lung phenotype under our culture conditions remains as an open question that will need further investigation but that was not the purpose of the present work.

As stated before, we also found expression of these genes in non-differentiated DMSCs. Without excluding the possibility that they might have a specific function in the placental

environment, the semi-quantitative nature of end-point PCR prevents an accurate determination hampering the visualization of subtle differences in the expression of these genes.

Our results indicate an initial differentiation towards a surfactant producing ATII-LC phenotype. However, we should not discard the fact that patterns of protein expression at longer times under differentiation conditions could be related with further differentiation into other phenotypes such as those of type I pneumocytes. Differentiation of ATII cells of pulmonary origin into ATI cells is widely documented both in vitro and in vivo (Fuchs, Hollins et al. 2003; Steimer, Laue et al. 2006).

Our findings showed that the onset for enhanced expression of all these mRNAs correlated with the appearance of lamellar body-like intracellular particles suggesting an evident signal of lung maturation (Stahlman, Gray et al. 1992; Zhou, Lim et al. 1996; Stahlman, Besnard et al. 2007). Surprisingly, DMSCs were shown to already express basal levels of surfactant proteins. This could be related to their placental origin. Presence of SP-A and SP-D has been previously reported in human amniotic epithelium and chorio-decidual layers (Miyamura, Malhotra et al. 1994; Sun, Brockman et al. 2006). As a matter of fact, SP-A has been proposed to participate as an inductor of parturition (Sun, Brockman et al. 2006). In addition, SP-A and SP-D lectin domains have been described to display an active role in the recognition and clearance of pathogens from amniotic fluid (Miyamura, Malhotra et al. 1994). Presence of SP-B and SP-C has also been demonstrated in placenta and other fetal environments (Newman, Phizackerley et al. 1991; Sati, Seval-Celik et al. 2007). Although their role is still under debate, it has been suggested that SP-C might participate in modulating inflammatory responses in the extraembryonic environment (Newman, Phizackerley et al. 1991). Our results demonstrate that differentiated ATII-LCs have the capability to properly process surfactant proteins from their precursors into the mature forms, a process that has been specifically linked with the ATII phenotype, but that should likely be extended to other epithelia layers related with the fetal/environment interface. This complete processing is consistent with the enhanced expression in ATII-LCs of the genes encoding the aspartyl proteases Napsin A and Cathepsin H, which are known to be expressed in fetal lung and adult ATII cells and being involved in the maturation of SP-B and SP-C (Ueno, Linder et al. 2004).

Interestingly, the amount of surfactant proteins found in the extracellular fluid of ATII-LC cultures was also higher than that in the medium of DMSCs, which is suggestive of a functional and metabolically active state of ATII-LCs. This statement would be additionally supported by the increased expression of the gene encoding the G-protein couple receptor GPR116. Indeed, this receptor plays a critical role in lung surfactant homeostasis, controlling surfactant composition as well as its accumulation in the alveolar spaces and uptake by ATII cells, sustaining normal surfactant levels (Bridges, Ludwig et al. 2013; Yang, Hilton et al. 2013). With respect to the maintenance of the proper lung volumes, ATII-LCs were also able to express mRNA codifying the cystic fibrosis transmembrane conductance receptor (CFTR), which has been also described in the developing lung as well as in freshly isolated ATII cells (Brochiero, Dagenais et al. 2004). CTFR is an important regulator of Cl^- and liquid transport in the lung alveolus and mutations in its gene are known to cause cystic fibrosis (Fang, Song et al. 2006).

The major function of ATII cells is the production and secretion of surfactant. The fact that ATII-LCs are able to synthetize and accumulate disaturated phospholipid species and to secrete functional membranous lipid complexes upon stimulation with secretagogues further supports the differentiated state of ATII-LCs and their pneumocyte-like functionality. We have implemented a method in ATII-LCs to real-time visualizing single events of surfactant release, previously described and validated for native ATII cell primary cultures (Miklavc, Mair et al. 2011; Haller, Ortmayr et al. 1998; Frick, Eschertzhuber et al. 2001; Frick, Bertocchi et al. 2004; Haller, Dietl et al. 2004). Despite the fact that LTG staining was not specifically limited to LBs due to the great amount of lysosome-related small vesicles also present in DMSCs, ATII-LCs displayed much more acidic compartments (probably LBs) than DMSCs and only ATII-LCs were clearly responsive to the addition of secretagogues. Upon incubating with ATP and PMA, ATII-LCs exocytosed an appreciable number of lipid vesicles stained with FM1-43 as discrete spherical fluorescent spots. These observations indicate that the secreted material remains in an aggregated state and does not readily disperse into the buffer solution as it has been also described for material secreted by ATII cell primary cultures (Haller, Ortmayr et al. 1998). Interestingly, the time course of exocytosis

in ATII-LCs displayed a slow rate mimicking the secretory behavior well documented in rat ATII cell primary cultures (Haller, Ortmayr et al. 1998; Frick, Bertocchi et al. 2004).

As revealed by ultrastructural analysis, surfactant-like material secreted from ATII-LCs contained a mixture of different structures, mainly partially unpacked osmiophilic entities and multiple lipid membrane patches with particular morphologies, probably residual features from a previous more complex organization as well as relatively simpler unillamelar and multillamelar vesicles loaded in some cases with a dense material inside. In general terms, the structures observed resemble the lipoprotein complexes exocytosed upon stimulation by native ATII cells (Ravasio, Olmeda et al. 2010), and had similar efficient interfacial adsorption capabilities. Previous work had demonstrated that surfactant complexes freshly secreted by primary cultures of type II pneumocytes adsorb to the interface at higher rates than surfactant complexes isolated from bronchoalveolar lavage (Ravasio, Cruz et al. 2008). These results have been interpreted considering that material obtained from airspaces could actually contain not only freshly secreted surfactant but also surfactant complexes that may have been already consumed, partly inactivated due to oxidation, or to insertion of spurious components. The fact that material secreted by ATII-LCs shows superior interfacial adsorption than surfactant purified from lungs argues in favour of their true functional pneumocyte-like phenotype. Pulmonary surfactant-like assemblies secreted by ATII-LCs even displayed a higher resistance to inhibition by serum than whole native surfactant purified from BAL. The limited amounts of material available up to now has prevented us to assess whether the interfacial films formed by the material produced by ATII-LCs are also competent to reach and sustain very low tensions under compression-expansion dynamics. Future optimization and scaling-up of conditions for cell culture, differentiation and secreted surfactant harvesting will allow to evaluate not only the full performance of this surfactant but the potential of this strategy to approach the biotechnological production, at large scale, of humanized clinical surfactants for therapeutic applications.

Under the differentiation conditions used in this work, the cultures appear as highly enriched in ATII-LCs, exhibiting remarkable yields of differentiation as previously assessed in immunocytochemical stainings for proSP-C (Macías, Grande et al. 2010). ATII-LCs display a

dynamic phenotype throughout the differentiation process from initial immature phases to mature functional stages, and once differentiated, ATII-LCs cannot be expanded further in culture. In contrast to other placenta-derived MSCs from fetal membranes (amnion and chorion) and chorionic villi (Portmann-Lanz, Schoeberlein et al. 2006; Okamoto, Miyoshi et al. 2007; Soncini, Vertua et al. 2007), DMSCs exhibit a notably high life span and subsequently, large amount of cells can be obtained as an important source to generate great amounts of ATII-LCs. Our differentiation procedure has shown to be highly effective, simple and quick, but we presume that ATII-LCs are still in a less differentiated state than true ATII cells as compared to cells in the lung epithelium *in situ* or in freshly isolated primary cultures of ATII cells. We speculate that the pneumocyte-like phenotype of ATII-LCs could progress further to full differentiation upon immersion into a context more similar to the native lung environment, either by transplantation into the tissue *in vivo* or by the use of cell culture models that incorporate features like the presence of an air-liquid interface. In this sense, Transwell devices have been reported as successful for lung differentiation by other groups (Wang, Bunnell et al. 2005; Knoll, Brockmeyer et al. 2013), and it could provide additional signaling and cell-to-cell contacts that would improve full differentiation of ATII-LCs.

The multipotent adult DMSCs used here display important advantages over other sources of adult stem cells, such as a high accessibility, since placental tissue is an unrestricted material that is discarded after the birth, its use does not evoke any ethical concerns, and the cells are easily isolated with a high yield. DMSCs can be cultured and expanded for long periods of time, and this could be a novel source to harvest freshly secreted surfactant complexes for further investigations.

Clinically, administration of MSCs from different origins into animal models of lung injury has been demonstrated by a number of authors to be a valuable therapeutic tool (Spitalieri, Quitadamo et al. 2012; Duchesneau, Wong et al. 2010; Wang, Bunnell et al. 2005; Wong, Dutly et al. 2007; Cargnoni, Gibelli et al. 2009; Wong, Keating et al. 2009; Knoll, Brockmeyer et al. 2013; Wang, Li et al. 2013). It has been recently reported that DMSCs could be useful for future clinical applications (Bornstein, Macías et al. 2012; Vegh, Grau et al. 2013). DMSCs subjected to

hepatic differentiation conditions have shown remarkable functional capabilities, suitable to be used as models for studying liver physiology as well as liver diseases with a potential application in hepatic regeneration (Bornstein, Macías et al. 2012). On the other hand, the migration and engraftment of DMSCs into mammary tumors and the inhibitory effect of the cells on the growth of primary tumors and in the development of new tumors has been demonstrated (Vegh, Grau et al. 2013). DMSCs do not express the major histocompatibility complex class II and the T cell costimulatory molecules, conferring them an intrinsically hypoimmunogenic and immunomodulating properties (Macías, Grande et al. 2010). DMSCs or ATII-LCs could therefore open new strategies as a potential therapeutic agent for the treatment of lung injury.

In conclusion, the results reported in this work support the idea that ATII-LCs could be considered as appropriate cell models mimicking *ex vivo* ATII. This model could be used to introduce genetic modifications to study surfactant biogenesis, in particular, protein and lipid synthesis, maturation, and trafficking, as well as the packing and storage of surfactant lipid-protein complexes into LBs.

Chapter 4

The experiments presented in this chapter were carried out at the Helmholtz Institute for Pharmaceutical Research/ Saarland University (Saarbrucken, Germany) under the supervision of Prof. Dr. Claus-Michael Lehr and Dr. Cristiane Carvahlo.

INTRODUCTION

In the previous chapter we have described a new cell model based on derived placental stem cells, with phenotypical features consistent with alveolar type II (ATII) cells able to synthesize, store and secrete active lipid protein complexes with conspicuous surface properties. The culture method we have described to obtain alveolar type II-like cells (ATII-LCs) was shown to be simple, reliable and highly reproducible. However, as previously stated, we postulate that the differentiated alveolar-like cells are not fully mature as compared to native pneumocytes. It is well known that the physiological microenvironment directly impacts the ATII cell morphology, proliferation, differentiation, secretion, movement, signal transduction, and gene expression pathways (Dobbs, Pian et al. 1997; Grek, Newton et al. 2009). Therefore, we speculate that our experimental differentiation method, based on conventional submerged cultures in plastic plates, might not properly mimic the *in vivo* alveolar situation, likely crucial for the normal gene expression and cellular function of ATII cells. For this reason, our research in this chapter has been focused on the optimization of cultures trying to further approach the native conditions.

Classically, primary ATII cells have been grown in submerged cultures and not exposed to air (Dobbs 1990; Kalina, Riklis et al. 1993; Sugihara, Toda et al. 1993). To closely resemble the *in vivo* situation, air-liquid interface (ALI) cultures have been implemented. In ALI cultures the medium is added only into the basolateral surface of cells and the apical part is exposed to the air-phase. Early versions of modern ALI cell culture techniques were introduced in the 1970s, where alveolar macrophages were seeding on porous membrane filters attached to surfaces of reservoirs filled with nutritive medium and maintained alive in direct contact with the atmosphere (Voisin, Aerts et al. 1975; Voisin, Aerts et al. 1977; Paur, Cassee et al. 2011). The distinctive effect of the ALI cell culture system has been reported to be important for the morphological differentiation and development of cilia in tracheal and bronchial epithelial cells (Whitcutt, Adler et al. 1988; Yamaya, Finkbeiner et al. 1992; Kaartinen, Nettesheim et al. 1993; Grainger, Greenwell et al. 2006; Sakagami 2006; Berube, Prytherch et al. 2010), as well as for the promotion

of the expression and maintenance of a differentiated type II phenotype of isolated ATII cells in contrast to submerged cultivation (Kohsa, Yamada et al. 1996; Alcorn, Smith et al. 1997; Dobbs, Pian et al. 1997; Ito, Ahmad et al. 2011). Interestingly, the usefulness of interfaced cultures has been also described to be crucial for the differentiation of stem cells into lung cell derivatives (Wang, Bunnell et al. 2005; Van Haute, De Block et al. 2009; Knoll, Brockmeyer et al. 2013; Ghaedi, Méndez et al. 2014). The distinctive effect on the differentiation of bone marrow-isolated human mesenchymal stem cells cultured into the ALI has been well characterized and compared to submerged cultures (Wang, Bunnell et al. 2005). In fact, the differentiation of human embryonic stem cells under interfaced conditions has demonstrated the capacity of these cells to derive into the main cells of the lung epithelial tissue (Van Haute, De Block et al. 2009). Recently, the initial differentiation of human induced pluripotent stem cells into ATII cells and subsequently into alveolar type I cells has been also demonstrated, generating an air-liquid condition in a rolling bioreactor (Ghaedi, Méndez et al. 2014).

In spite that the significance of ALI cultures has been now well-accepted, an interest in discerning the mechanisms involved in the improvement in cell differentiation has increased in the last few years. Indeed, some investigators have evidenced the importance of the oxygen tension in culture medium. In fact, isolated primary rat ATII cells seem to generate oxygen gradients in the air-liquid cultivation due to the high number of active mitochondria (Mamchaoui and Saumon 2000). On the other hand, it has been described that hypoxia plays an important role on the expression of surfactant proteins and induces the down-regulation of SP-B and SP-C in murine lung epithelial cells (Grek, Newton et al. 2009). In addition, levels of hypoxia inducible factor (HIF) have been investigated in cultures of rat ATII cells under submerged and air-liquid conditions. These studies have revealed that the presence of HIF increased in liquid covered cultures with respect to ALI conditions and this rise is correlated with a decline in the expression of surfactant proteins, which can be restored upon supplementation with oxygen (Ito, Ahmad et al. 2011). Thus, HIF signaling and oxygen tension at the surface of cells appears to be important factors that influence the phenotype of ATII cells.

Additionally, the extracellular matrix (ECM) is also well known to be a critical element in the cellular microenvironment. In physiological conditions, alveolar cells are supported by a unique fibrillar ECM that contains principally collagen, fibronectin, and laminin (Rannels and Rannels 1989; Dunsmore 2008; Cortiella, Niles et al. 2010). Other constituents, such as proteoglycans and in particular, perlecan (heparan sulfate proteoglycan 2) and nidogen, were also found connecting the networks formed by other components of the ECM and participating in cell-extracellular matrix interactions (Koval, Ward et al. 2010; Eisenberg, Safi et al. 2011). ECM is secreted and constantly modified by cells as they grow and develop *in vivo* and it is one of the main factors influencing cell mammary specific metabolism and cell behaviour *in vitro* (Emerman, Burwen et al. 1979; Delabarre, Claudon et al. 1997; Hopkinson, DeBiase et al. 2008). In fact, cell-ECM interactions play crucial roles in maintaining a proper adhesion, cell motility and differentiation (Eisenberg, Safi et al. 2011).

The effect of the different components of the ECM in the maintenance and development of the differentiated phenotypes of primary lung alveolar cells in culture has been examined by several groups (Lwebuga-Mukasa, Thulin et al. 1984; Adamson, King et al. 1989; Sannes 1991, Elbert, Schafer et al. 1999; Fuchs, Hollins et al. 2003). Moreover, approaches including ECM as a part of the culture systems have been also effectively implemented for the derivation into lung epithelial cells of murine embryonic stem cells (Cortiella, Niles et al. 2010), as well as human induced pluripotent stem cells (Ghaedi, Mendez et al. 2014; Huang, Islam et al. 2014).

On the other hand, it is well known that the lung distal airways offer advantageous features such as their large absorptive area, extensive vasculature and relatively low extracellular and intracellular enzymatic activity, making them a privileged route for drug delivery (Liu, Shao et al. 1993; Foster, Oster et al. 1998). In addition, interest in pulmonary administration of therapeutic drugs is currently increasing due to many other factors, i.e., the increasing number of new therapeutic peptide and protein pharmaceuticals with associated difficulties in their delivery by other routes or the continued interest

in direct targeting of therapeutic agents for respiratory disorders or in the systemic delivery of drugs by inhalation (Forbes and Ehrhardt 2005; Patton and Byron 2007; Sung, Pulliam et al. 2007). As a result, different methods to assess and predict the biological effects of new compounds in an early stage of their development are currently highly demanded. Taking into consideration the principle of the 3R (Replacement, Reduction and Replacement, already discussed in the prior chapter), the increasing efforts to reduce the number of animals used routinely for toxicological tests, make necessary the design of new *in vitro* methods to accomplish that task. Compared to *in vivo* approaches, *in vitro* systems offer the simplicity, robustness and a better control of the experiments and their data interpretation, besides the benefits of reducing operational costs and the use of animals (Sakagami 2006). In the alveolar field there are not suitable cell lines available and the isolation and culture of primary ATII cells is the preferred election in most cases (Elbert, Schafer et al. 1999; Forbes and Ehrhardt 2005). However, despite the fact that primary cultures may represent a closer option for simulating the *in vivo* situation, they present several disadvantages, such a high heterogeneity and low reproducibility, besides the difficulties in terms of resources and time to obtain them (de Souza Carvalho, Daum et al. 2014).

Taking into consideration all the facts previously mentioned, we were interested in validating our novel cell model of ATII-LCs as a suitable tool for toxicological studies, competent to assess the biocompatibility and safety of new nanoscale materials of utility for lung biopharmaceutics.

The relevance of nanotechnology has increased considerably in the development of new drug delivery systems. Nanoparticles (NPs) are defined by the European Commission as particles smaller than 100 nm in at least one dimension (Commission 2011). A high number of methods and raw materials for the preparation of polymeric nanocarriers is currently available and these must be chosen according to the final application. In particular, polylactic-co-glycolic acid (PLGA) polymers have been reported as a convenient material for NP preparations, due to its favorable properties such as

biodegradability, biocompatibility and low or absent cytotoxicity (Kitchell and Wise 1985; Johansen, Men et al. 2000; Grayson, Voskerician et al. 2004; Wu 2004). *In vivo,* the degradation of PLGA NPs takes place by simple hydrolysis that generates carbon dioxide and water, which are easily eliminated from the body. However, their degradation yields acidic monomers leading to a lower pH inside the NP, which can result with the undesirable degradation of the cargo molecule (Fu, Pack et al. 2000). To overcome this inconvenience, supplementary excipients such as poly-vinyl alcohol (PVA) or poly-ethylene-glycol (PEG) have been incorporated into the NP matrix and are currently widely employed as coadjutants improving colloidal stability (Owens and Peppas 2006; Santander-Ortega, Bastos-González et al. 2007). Additionally, PLGA NPs can be modified during their synthesis to modify their properties of degradation, offering an excellent pharmacokinetic control of drug delivery. Moreover, PLGA NPs are appropriate for the encapsulation and delivery of a variety of therapeutic agents, including, but not limited to, low molecular weight compounds (Panyam and Labhasetwar 2004; Faraji and Wipf 2009). Importantly, NPs based on PLGA have been approved by the US Food and Drug Administration (FDA) for human use.

In the last years, extensive research has been carried out in the use of inorganic materials, i.e., the development of metallic nanoparticles with multiple applications. In particular, silver NPs (AgNPs) are the most commonly used engineered NPs in commercialized products due to their antimicrobial properties (Greulich, Kittler et al. 2009; Hackenberg, Scherzed et al. 2011; Herzog, Clift et al. 2013; Gliga, Skoglund et al. 2014; Kim, Shin da et al. 2014). However, the use of silver as an antimicrobial agent is not a novel concept, as it has been used since the 17th century as a medicinal product (Klasen 2000; Herzog, Clift et al. 2013). Nowadays, AgNPs are used in a variety of products such as cosmetics, clothing, electric home appliances, room sprays and even in the food industry (Greulich, Kittler et al. 2009). Considering their well-known antiseptic activities, distinct silver compounds are clinically used to reduce skin infections in the treatment of burns, and as coatings of various surfaces, such as catheters and implants in order to reduce infections (Roe, Karandikar et al. 2008). Additionally, AgNPs have gained attention for

medical imaging and biosensing purposes. Despite the widespread application of AgNPs, there is a serious lack of information concerning their biological effects on human cells, and therefore, their potential cytotoxicity need to be assessed. In particular, an exposure route *via* inhalation is of primary concern for humans in an occupational setting as the respiratory system is one of the major entrance sites for nanomaterials. In this context, much research has been performed using *in vitro* cultures of lung cells to examine the possible deleterious effect of AgNPs on the human lung (Herzog, Clift et al. 2013; Suliman, Ali et al. 2013; Gliga, Skoglund et al. 2014; Kim, Shin da et al. 2014).

In this chapter, we have explored the influence of different factors in the differentiation of mesenchymal stem cells into ATII-LCs under conditions mimicking the alveolar microenvironment. For this purpose, we have differentiated the cells exposing them to air-liquid interfaces. We have then assessed the potential effect of this particular environment in terms of morphology, barrier properties and expression of surfactant and transporter proteins, in comparison with conventional submerged cultures. Moreover, we have also evaluated the result of differentiating the cells seeded over components present in the lung extracellular matrix.

On the other hand, we have investigated the potential adverse effects of PLGA and silver NPs in terms of cell viability of alveolar epithelial cells, taking advantage of the novel *in* vitro cell model of ATII-LCs. Additionally, we have exposed ATII-LCs differentiated in ALI cultures to aerosolized fluorescent PLGA NPs and examined their subsequent cellular uptake using a specific air-liquid cell exposure system.

RESULTS

Morphological features of ATII-LCs grown at the air-liquid interface

The effects of ALI culture conditions on cell morphology were examined by optical light microscopy and compared to SC conditions. After 4-5 days of differentiation in Transwell systems, ATII-LCs could be discerned as shortened cells with respect to the undifferentiated state, undergoing a more rounded shape and showing no substantial differences in comparison to differentiated cells under SC conditions **(Figure. 4.1)**. In general, the longevity of the culture (around 7 days) in terms of maintenance of cell atachment did not reveal any significant variations due to the influence of the air-liquid interface when compared to SC conditions either. However, more gaps without cells covering the porous membranes were observed in air-interfaced cultures probably due to cellular stress because of consecutive washing.

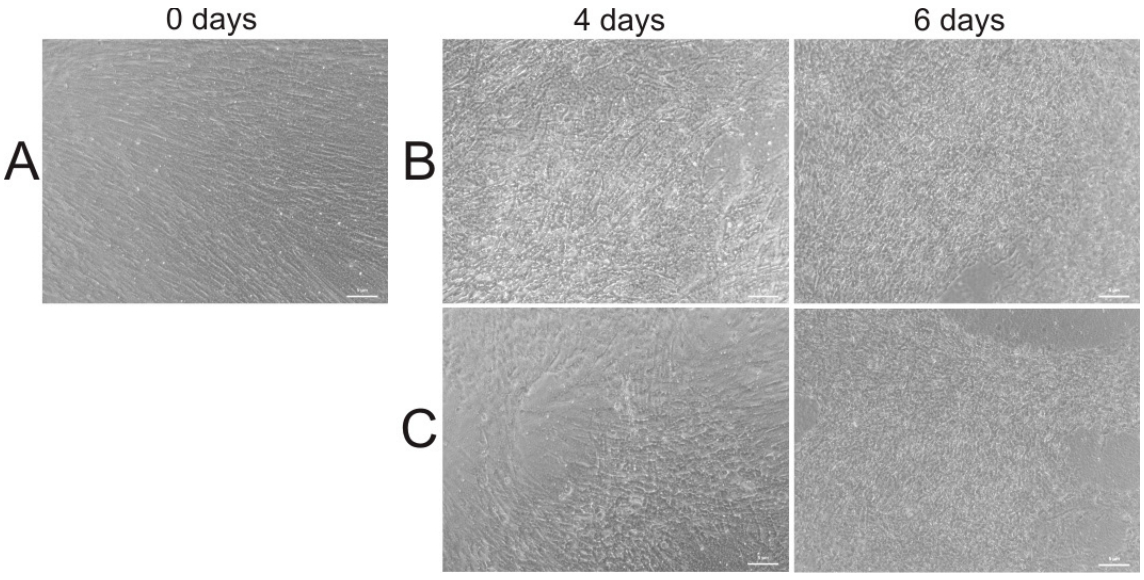

Figure 4.1. **Morphological assessment by optical microscopy of ATII-LCS differentiated in transwell inserts under submerged culture (SC) and air-liquid interface (ALI) culture conditions**. **A**. Decidua-derived mesenchymal stem cells (DMSCs) visually confluent prior to differentiation. **B**. ATII-LCs after 4 and 6 days of differentiation under SC conditions. **C**. ATII-LCs after 4 and 6 days of differentiation under ALI culture conditions. Note: Sample imaging is hampered due to a partial defocus imposed by the excessive distance between sample and objective. Scale bars = 5 µm.

The influence of the cell culture substrate on the cell differentiation was also tested after covering the permeable inserts with a mixture of collagen and fibronectin **(Figure. 4.2)**. Differences in cell morphology could not be detected in any of the culture conditions. However, differentiated ATII-LCs cultured in both, SC and ALI conditions, were able to maintain their attachment to the substrate for longer times, about 2 more days, when compared to cells cultured in membrane inserts without any coating.

The morphology of the differentiated ATII-LCs was further investigated by scanning electron microscopy and compared to primary human ATII cells and A549 cells, both type of cells also seeded on filter membranes (**Figure 4.3**). Primary ATII cells were observed as cuboidal in shape, being its cytosolic area limited to a zone near to the nucleus. The apical surface of the cells was seen to be covered by multiple protrusions and structures consistent with microvilli. Furthermore, numerous filopodia were visualized extended from lateral borders contacting and attaching the cells to the surface of the filter (**Fig 4.3A left panel**). In addition, some ATI cells could be also discerned, with a larger size, typical flattened morphology and absence of distinctive structures on the surface (**Fig 4.3A right panel**). Undifferentiated DMSCs appeared with an elongated and flat spindle-like morphology typical of a fibroblast and with a relatively smooth external surface (**Fig 4.3C**). After 5 days of differentiation under ALI conditions, ATII-LCs suffered remarkable morfological changes exhibiting a cuboidal epitheliod form with abundant invaginations and protuberations on the cell surface that resemble microvilli (**Fig. 4.3D**). The cells displayed a cellular surface that presents notable similarities with the primary human ATII cells. The resemblance of ATII-LCs differentiated under ALI conditions was not so evident when compared to the A549 line (**Fig 4.3B**). ATII-LCs differentiated under SC conditions (**Fig. 4.3E**), did not exhibit significant morphological differences in terms of shape and surface topography, with respect to the differentiated cells at the ALI in terms of shape and surface topography.

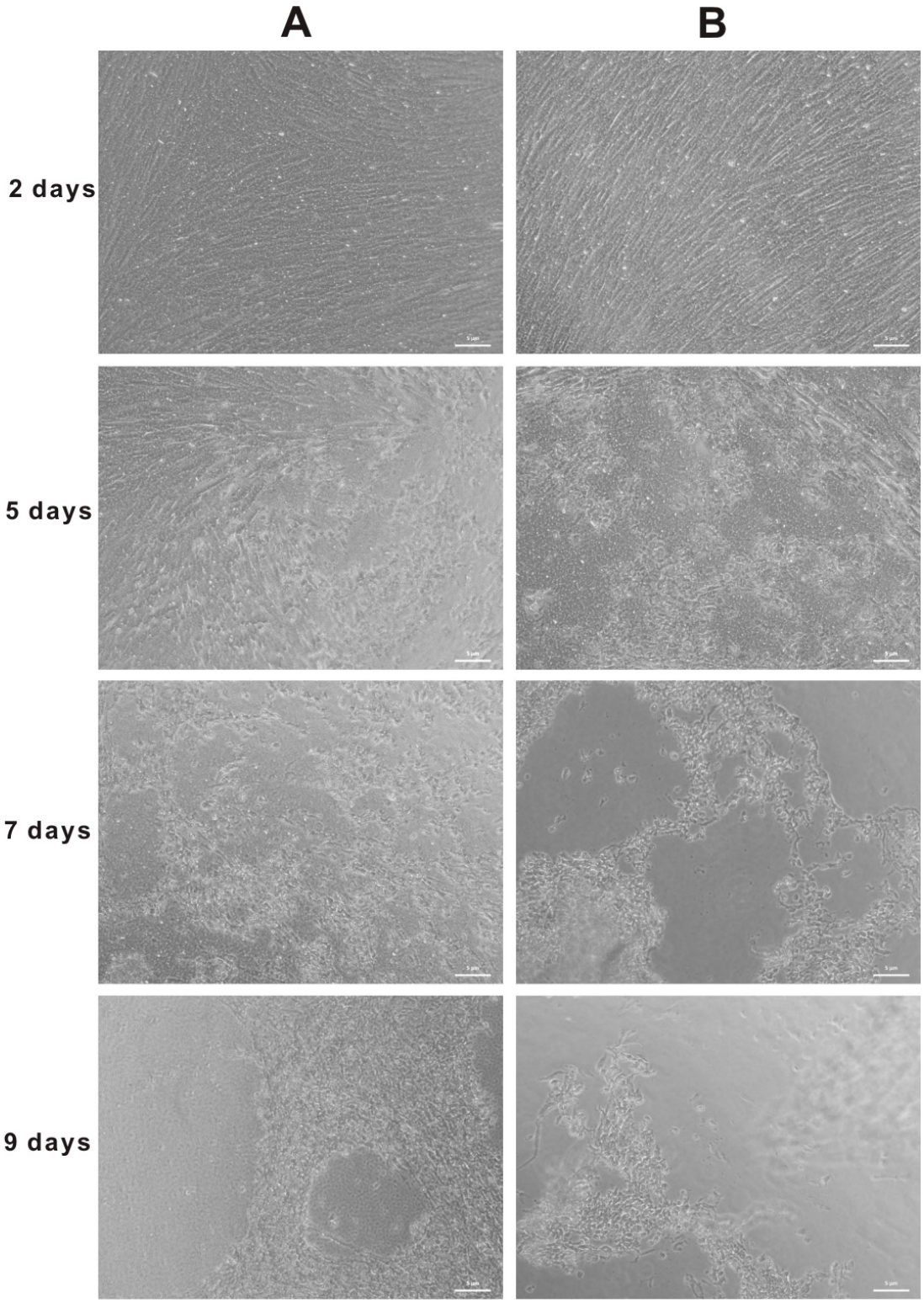

Figure 4.2. **Morphological examination of ATII-LCs seeded on transwell inserts coated with fibronectin and collagen throughout the differentiation process**. **A**. Differentiated ATII-LCs under SC conditions. **B**. Differentiated ATII-LCs under ALI culture conditions.

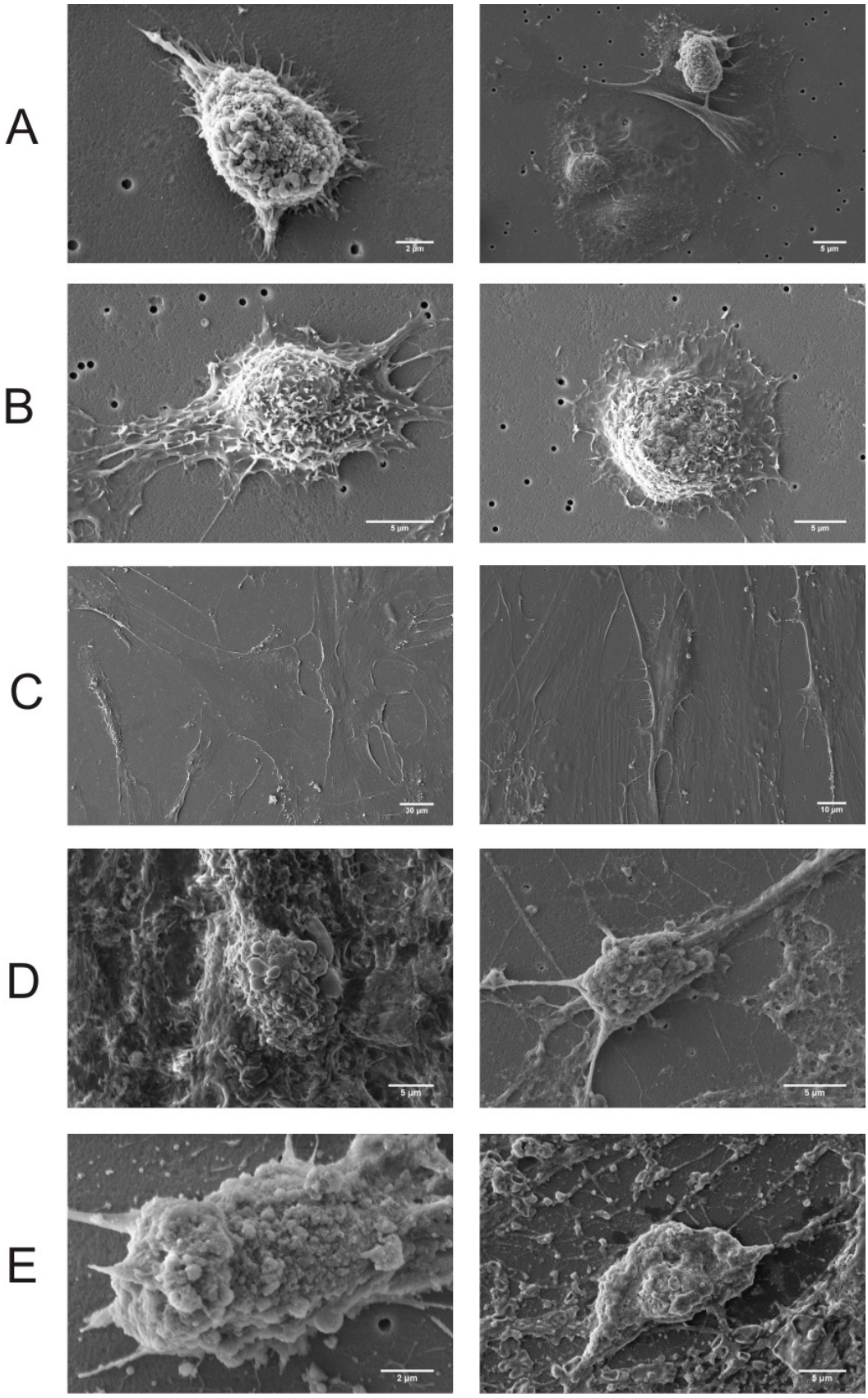

Figure 4.3. **Morphological analysis by scanning electron microscopy**. **A**. Freshly isolated alveolar epithelial cells (scale bars = 2 and 5 µm) **B**. A549 cells (scale bars = 5 µm). **C**. Undifferentiated DMSCs (scale bars = 30 and 10 µm) . **D**. Differentiated ATII-LCS under ALI culture conditions (scale bars = 5 µm). **E**. Differentiated ATII-LC under SC condtions (scale bars = 2 and 5 µm).

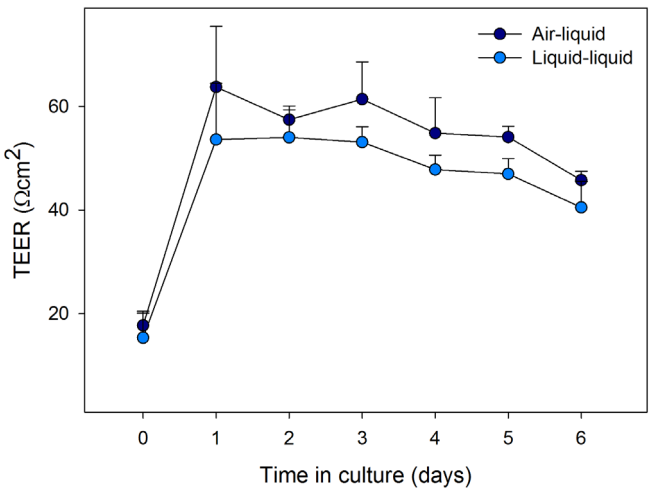

Figure 4.4. **Measurement of transepithelial electrical resistance (TEER) in ATII-LC cultures**. TEER values of ATII-LCs differentiated under SC conditions (light blue) and under ALI culture conditions (dark blue) throughout the differentiation process.

Barrier properties

Transepithelial electrical resistance (TEER) values of ATII-LCs differentiated at the ALI were slightly higher compared to cells treated under SC conditions throughout the days of culture, although this variation was not found to be statistically significant (**Figure. 4.4**). In both differentiation conditions, TEER values were increased at the beginning of the treatment, reaching peak values of 75 Ωcm^2 and then remained unchanged during the whole treatment, displaying a relative plateau with values ranging from 50 to 60 Ωcm^2. A decline in TEER was recorded at the end of the lifetime of the culture that coincides with the general loss of cell attachment. According to these TEER values, ATII-LCs cannot be considered to form a electrically confluent monolayer, since their TEER levels are lower than the standards levels reported for conventional cell monolayers of other epithelial cell types (> 300 Ωcm^2).

The capacity to configure a tight monolayer was also investigated when the cells were differentiated under SC and ALI conditions in the Transwell systems coated with collagen and fibronectin (**Figure 4.5**). Consistently with the previous result, cells showed a gradual increase in TEER values at the beginning of the differentiation and a decline in the last days of the process. Differentiated cells exposed to the ALI displayed higher TEER values than cells treated under SC conditions, but the difference was not statistically significant. In both cases, the conditions did not lead to the formation of a tight monolayer and the TEER values remained low throughout the differentiation and similar to those found

with the uncoated Transwells.

On the other hand, passive fluxes and cumulative transport of the paracellular marker sodium fluorescein across monolayers of differentiated cells was also assessed (**Fig. 4.6)**. Apparent permeabiliy coefficients (P_{app}) were calculated to be 0.29 ± 2.85 x 10^{-5} cm/s and 0.31 ± 2.01 x 10^{-5} cm/s in cells exposed to ALI and SC conditions, respectively (Fig. 4.6A). According to the preceding findings, these data reveal no differences in the tightness of cell monolayers. The differences in the restriction of passive fluxes of sodium fluorescein across monolayers were not statistically different when comparing both culture conditions.

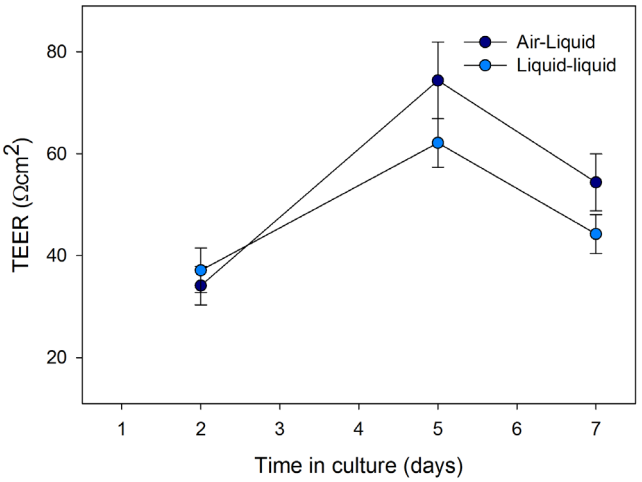

Figure 4.5. Measurement of transepithelial electrical resistance (TEER) in ATII-LCs differentiated in transwell inserts coated with fibronecting and collagen. TEER values of ATII-LCs differentiated under SC conditions (light blue) and under ALI culture conditions (dark blue) throughout the differentiation process.

A

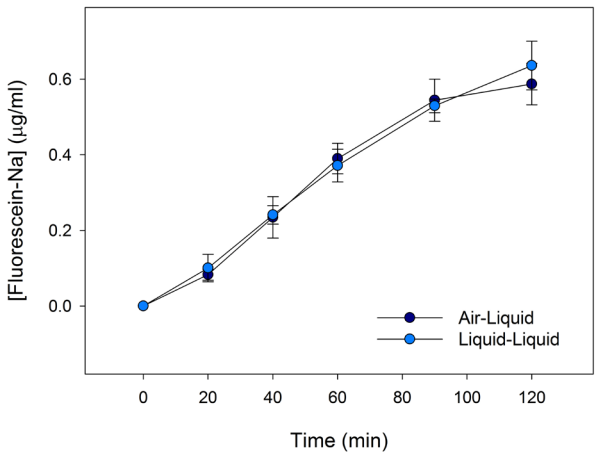

B

Culture condition	Apparent permeability coeficient (cm/s)
ATII-LCs Air-Liquid	0.289 ± 2.85x10^{-5}
ATII-LCs Liquid-Liquid	0.312 ± 2.01x10^{-5}

Figure 4.6. Transport of sodium fluorescein across ATII-LC monolayers.
A. Time-course of the paracellular marker sodium fluorescein in the apical-to-basolateral direction across monolayers of ATII-LCs differentiated under SC conditions (light blue) and ALI culture conditions (dark blue).
B. Apparent permeability coefficients calculated for sodium fluorescein in both culture conditions.

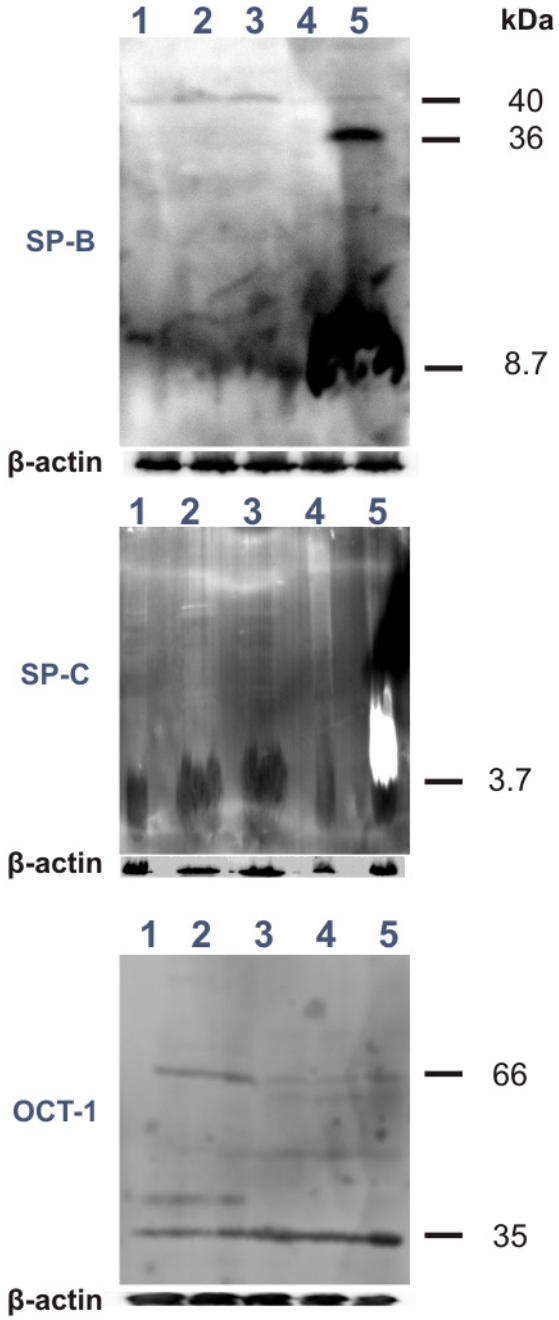

Figure 4.7. **Protein expression by western blot**. Content in surfactant proteins B (SP-B) and C (SP-C) and organic cation transporter 1 (OCT-1) was evaluated in undifferentiated DMSCs (lane 1), differentiated ATII-LCs under SC conditions and ALI culture conditions (lanes 2 and 3, respectively), A549 cells (lane 4) and human primary ATII cells (lane 5). Bars indicate molecular weights of the corresponding bands. ß-actin was used as a loading control.

Protein expression

The impact of the differentiation of DMSCs under the ALI in the expression of the surfactant proteins SP-B and SP-C, as well as in the organic cation transport 1 (OCT-1) was investigated by immunoblotting (**Figure 4.7**). Consistently with our previous results, incubation in the differentiation media SAGM revealed an increase in the expression of SP-B, not only of its precursor form (~ 40 kDa) but also of its mature form (~ 8.7 kDa). However, no clear differences between cells differentiated in SC and ALI conditions could be noticed. Interestingly, SP-B content in ATII-LCs was found to be higher than in A549 cells, both the precursors and the mature forms. In the case of primary human ATII cells, the amount of SP-B was observed to be notably higher than in ATII-LCs differentiated under both culture conditions. However, the distortions found in the protein bands due to the presence of high amount of lipids associated to the proteins prevent a proper quantitative analysis of the data.

In relation with SP-C, the band corresponding with the mature form in ATII-LCs (~3.7 kDa) showed similar intensity independently of the differentiation conditions, but the intensity was higher when compared to undifferentiated DMSCs or to the A549 cell line. In contrast and similarly to the results found for SP-B, human primary ATII cells contained higher amounts of SP-C, as intepreted by the negative staining due to a saturation effect observed in the blot. However, due to the uncertain information provided by the protein loading control (β-actin), differences in expression of SP-C might not be definitively stated, and these results should be currently considered as preliminary results.

On the other hand, cell differentiation in SAGM provoked an increase of the expression of OCT-1 close to the levels of human primary cells. However, the ALI conditions produced a slightly increase on OCT-1 expression when compared to SC conditions, equivalent to the expression in A549 cells. The bands of around 65 kDa corresponded to the dimeric form of the protein could be attributed to an incomplete disulfide reduction with β-mercaptoethanol.

Characterization of nanoparticles

As detailed in the materials and methods section, two different kinds of PLGA nanoparticles were prepared according to emulsion-diffusion-evaporation and self-assembly techniques, using various stabilizers that allow to modify the surface charge. Anionic and cationic chitosan- coated PLGA NPs exhibited mean diameters of 140.6 nm and 120.6 nm, respectively. Both formulations had a narrow size distribution with a poly-dispersity index in the 0.01-0.2 range. Zeta-potential measurements defined the influence of stabilizers on surface charge: PVA-PLGA NPs displayed a negative zeta-potential (ζ=-21.5 mV), whereas chitosan-coated PLGA CS-PLGA were positively charged (ζ=16.5 mV) (**Fig. 4.8**) Commercially available silver nanoparticles (AgNPs) consisted of particles of about 15 nm size with a narrow size distribution with > 99 % number of particles with a size below 20 nm according to manufacturer.

A

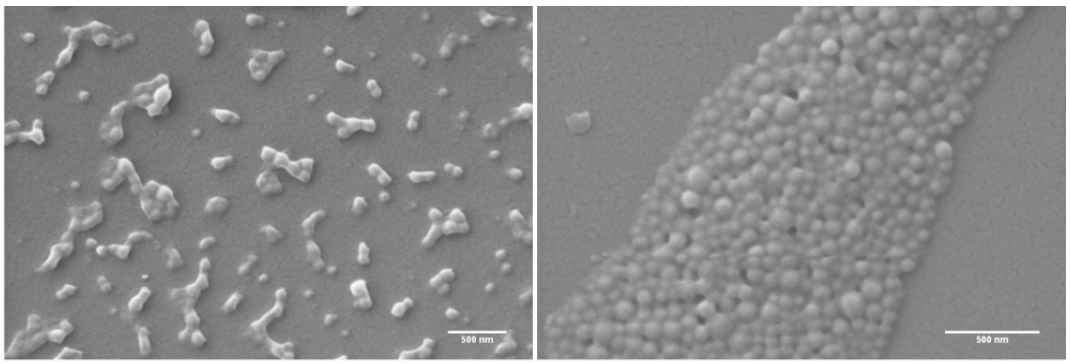

B

	FA-PLGA	CS-PLGA
Particle size (nm)	140.6	120.6
PdI	0.013	0.15
Zeta potential (mV)	-21.5	16.5

Figure 4.8. Nanoparticle characterization by scanning electron microscopy (SEM) and dinamic light scattering. **A**. SEM pictures documenting morphology of fluoreseinamine (FA) PLGA NPs. Scale bars = 500 nm. **B**. Particle size, polidispersity index (PdI) and zeta potential of FA-PLGA and chitosan-PLGA (CS-PLGA) nanoparticles by analysis with ZetaSizer Nano ZS.

Effect of nanoparticles on cell viability

In order to explore the toxic effect of the different types of NPs on cultures of ATII-LCs differentiated under SC conditions as well as on A549 cells, cellular damage after exposure to NPs was evaluated in terms of mitochondrial function by the MTT assay. Treatments with exposure for 24 h to anionic PLGA NPs revealed certain cytotoxic effect in ATII-LCs at relative low concentrations (**Figure 4.9A**). Although concentrations of NPs of 1 and 2.5 µg/mL were shown to be tolerable for cells, exhibiting viability percentages around 95-90 %, higher concentrations, (i.e: 50 and 100 µg/mL) triggered a decrease in viability to levels lower than 60 %. A549 cells exhibited a somewhat higher sensitivity than ATII-LCS in the range of low concentrations, but the difference was not statistically significant. The toxicity of high concentrations of PLGA NPs was similar in both, A549 cells and ATII-LCs.

On the other hand, the cationic CS-PLGA NPs produced minor cytotoxic effects on ATII-LCs at elevated concentrations of particles, reaching values of viabilitity around

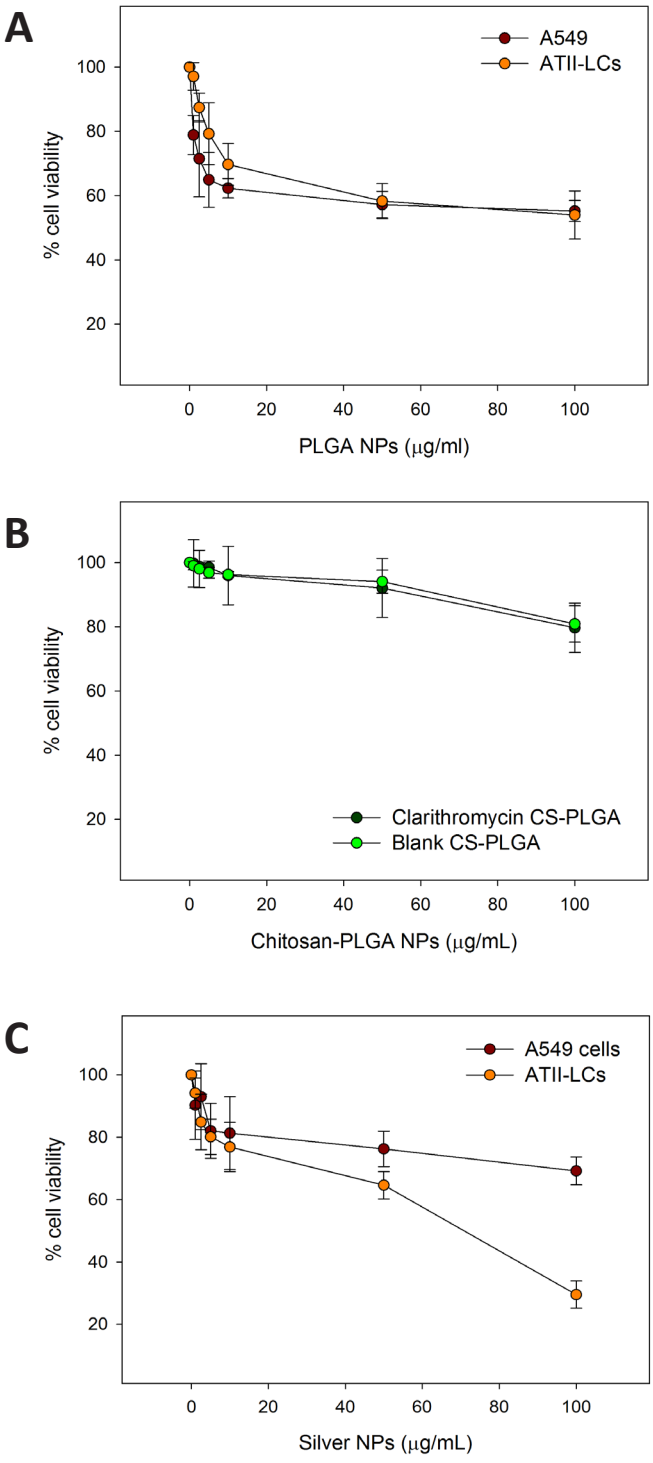

Figure 4.9. **Evaluation of citotoxicity by MTT assay after incubation with the different types of nanoparticles**. Cell viability after 24 h of exposure to different concentrations of anionic PLGA NPs (**A**), cationic chitosan modified PLGA NPs (**B**) and silver NPs (**C**) of differentiated ATII-LCs and A549 cells (in **A**, **C**).

90 % at 50 µg/mL and 80 % at 100 µg/mL (**Figure. 4.9B**). Interestingly, CS-NPs charged with clarythromycin did not shown any particular harmful influence in cell survival since mitochondrial function displayed a similar behaviour when compared to unloaded CS-NPs. Compared to anionic PLGA NPs, cationic NPs were more tolerable by the ATII-LCs, particularly when used at elevated concentrations, i.e.; 80 % vs 60 % of cell viability at 100 µg/ml.

AgNPs seem to have a similar effect in cell citotoxicity than anionic PLGA NPs with a rapid decay at low concentrations. Again, when compared to cationic PLGA NPs, AgNPs had a more citotoxic effect at all the dillutions tested. It is remarkable that AgNPs triggered a significant dose-response toxicity in ATII-LC cultures, reaching the significantly low rates of 30 % of cell viability at the highest

concentrations evaluated of 100 μg/ml (**Fig. 4.9C**). On the other hand, A549 cells seem to be more resistant at higher concentrations of AgNPs than ATII-LCs, with a cell viability of around 70 % at both, 50 and 100 μg/ml.

Cellular uptake of fluorescent PLGA nanoparticles

Internalization of fluorescent-labeled FA-PLGA NPs by ATII-LCs grown on Transwell supports and differentiated under ALI conditions was assessed by confocal electron microscopy after deposition using the ALICE system. Relatively low amounts of NPs could be discerned in the citoplasm of the ATII-LCs 3 h after the exposure (**Figure 4.10A**). However, a remarkable increase in the number of NPs visualized as individual or agreggated green fluorescent spots were observed in the citoplasm of the cells at 24 h of incubation. Additionally, the uptake of NPs was confirmed by z-stacks represented in an orthogonal view, revealing particles penetrating into the cells in a dose-response dependent manner or already internalized and located at the same planes than nuclei and/or actin filaments of the citoplasm (**Figure 4.10.B**). ATII-LCs not exposed to NPs were shown to have a general morphology and nuclear aspect similar to untreated cells suggesting that neither the deposition technique nor the exposure to particles had any particular adverse effect in the differentiated cells under ALI conditions.

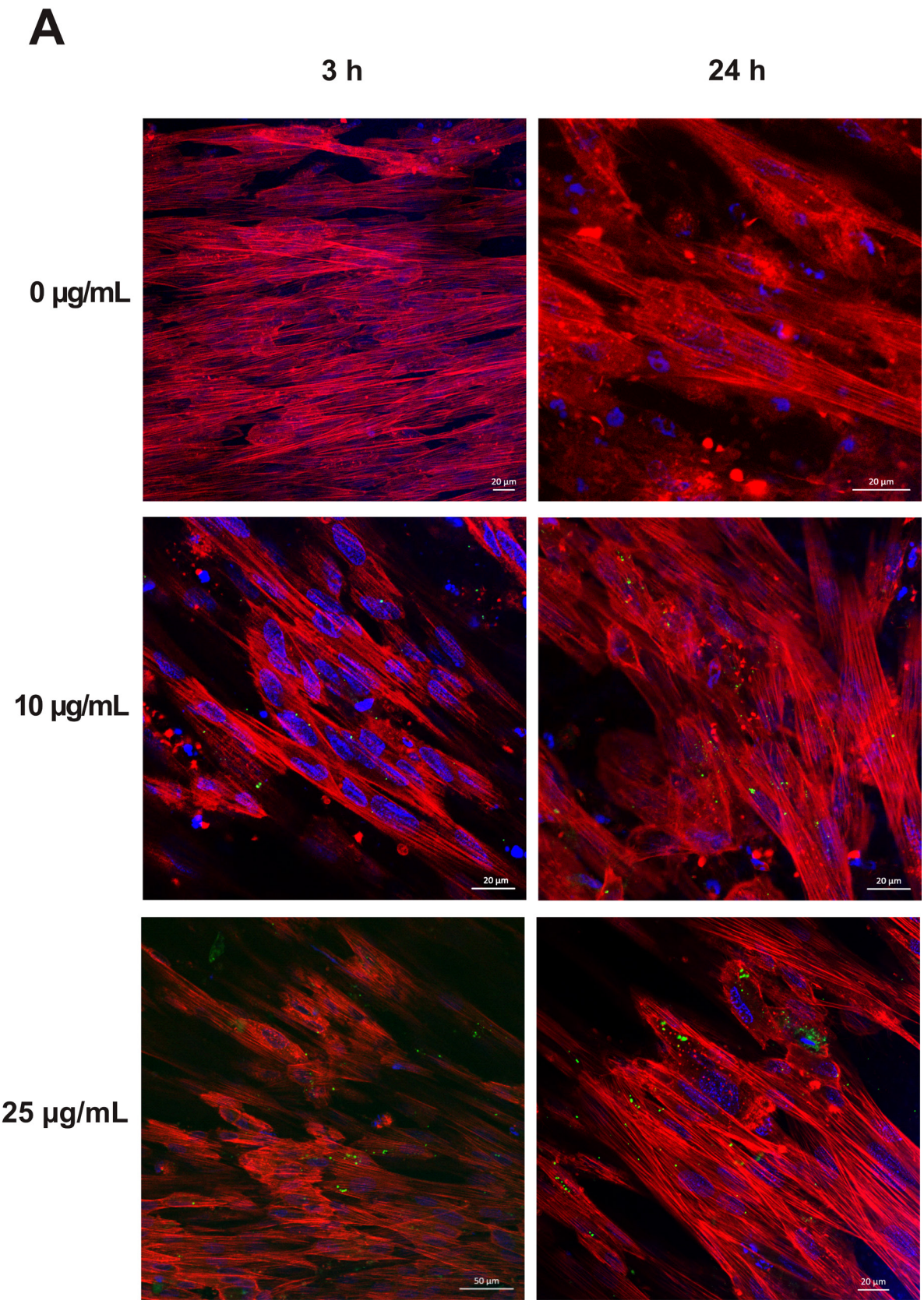
A
3 h
24 h
0 µg/mL
10 µg/mL
25 µg/mL
20 µm
20 µm
20 µm
20 µm
50 µm
20 µm

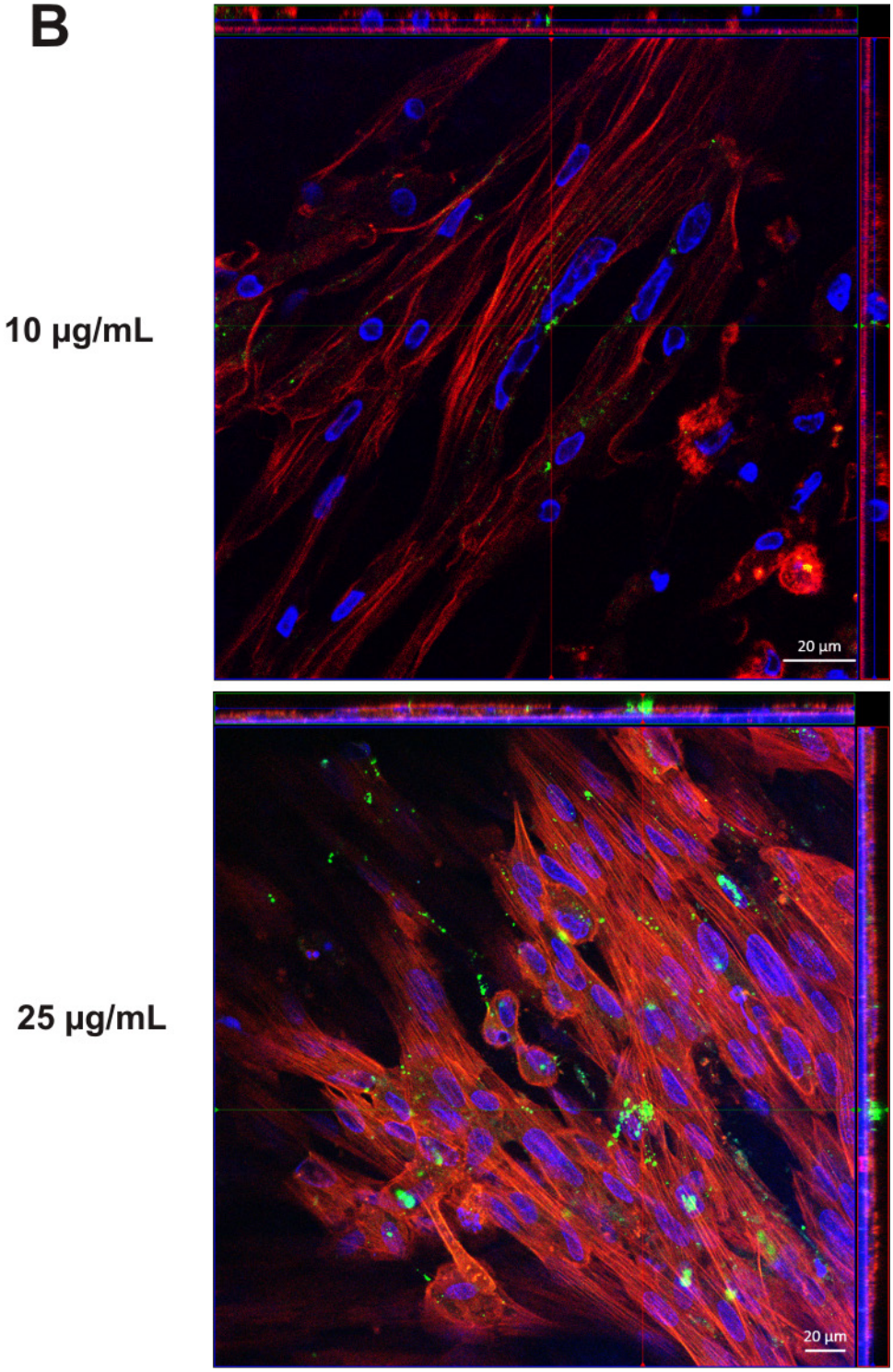

Figure 4.10. **Cellular uptake of fluorescent PLGA nanoparticles**. **A**. Images showing two different concentrations of fluoresceinamine PLGA NPs (green fluorescence) deposited using ALICE device onto ATII-LCs incubated for 3 and 24 h. Negative control without NPs is shown. **B**. Images corresponding to fluorescent PLGA NPs after 24 h of incubation incorporating an orthogonal view (x,y plane) created from confocal microscopy sections allowing observation of the sample in depth. Nuclei and actin filaments are stained in blue and red, respectively. Scale bars = 20 µm.

DISCUSSION

The integrity of the alveolar epithelium of the distal lung is crucial for an efficient gas exchange and, at the same time, to define an effective pulmonary delivery of drugs. Although ATII cells represent only approximately 5 % of its surface (Crapo, Barry et al. 1982), they become essential due to their important physiological functions including surfactant production and renewal of ATI cells (Daum, Kuehn et al. 2012). Considering its key role in the lung functions, useful *in vitro* models of ATII cells are strongly needed to evaluate the safety of novel inhaled terapeutic drugs in the first stages of their development. In the previous chapter, we have reported a new model based on the differentiation of human mesenchymal stem cells into lung derived-cells (ATII-LCs) with the ability to accumulate, sinthesize and secrete functionally active surfactant-like assemblies. Despite ATII-LCs reach a considerable functional state, we hipothesized that the differentiation could be extended to a fully mature stage modifying the *in vitro* culture conditions.

For this purpose, we subjected DMSCs to differentiation under air-liquid interface (ALI) conditions mimicking the native situation. For this, DMSCs were seeded on top of permeable supports and exposed their apical part to the air. We observed that ATII-LCs derivated under ALI conditions underwent notorious morphological modifications. Differentiated cells changed from a flat and elongated fibroblast-like aspect to a more cuboidal shape displaying a complex external surface with abundant microstructures resembling microvilli, as seen by scanning electron microscopy. In spite of the fact that this finding could also be indicative of cell polarization, this feature could not be definitely confirmed at this point since cell polarity is not only based on morphological evidences, but also in vectorial processes such as fluid transport or exocytosis, among others. Significantly, the structural features of ATII-LCs showed high similarity with those of native primary ATII cells isolated from human lung. Furthermore, the images acquired by optical microscopy to verify the reorganization of the cell monolayers of differentiated cells under ALI conditions are also quite similar to those of primary alveolar

cells as reported by other authors (Kohsa, Yamada et al. 1996; Delabarre, Claudon et al. 1997). However, we hardly discerned significant differences in air-exposed ATII-LCs with respect to ATII-LCs differentiated in subermerged cultures. The absence of substantial differences in terms of cytoarchitecture when comparing both culture conditions has been also previously observed for native ATII cells (Kohsa, Yamada et al. 1996).

Afterwards, we proceed to quantify the barrier integrity of the cell monolayers by measuring transepithelial electrical resistance (TEER), an independent and non invasive technique (Benson, Cramer et al. 2013). In both, air-liquid and submerged conditions, we determined that after an initial peek at the beginning of the differentiation, TEER levels remained constant throughout the whole differentiation process, coinciding with the stationary growth phase. This tendency has been also reported in other studies with epithelial cells (Rothen-Rutishauser, Kramer et al. 1998; Braun, Hammerle et al. 2000). On the other hand, TEER levels never reached the 300 Ωcm^2, the normal TEER values commonly reported for tightly packed monolayers (Cheek, Evans et al. 1989; Elbert, Schafer et al. 1999; Salomon, Muchitsch et al. 2014). Indeed, other respiratoy cells known to have strong barrier properties, show elevated resistance values. For example, TEER values obatained for Calu-3 (cell model for the bronchial epithelium) monolayers have been shown to plateau with values reaching around 470 Ωcm^2 when grown under the ALI condition (Haghi, Young et al. 2010), although these values can be significantly increased when cultured in submerged conditions (Stentebjerg-Andersen, Notlevsen et al. 2011). Another bronchial cell line, the 16HBE14o- cells reach TEER values of aproximately 330 Ωcm^2 (Wan, Winton et al. 2000). NCI-H441 cells, which are presumably of Clara-cell origin, are able to reach peak values of 1010 Ωcm^2 under submerged culture conditions, although under air-liquid conditions TEER values are lower than 300 Ωcm^2 (Salomon, Muchitsch et al. 2014). Surprisingly, as seen in various studies, submerged cultures lead to better barrier properties in lung cells but the mechanisms involved still remain unclear. In general, electrically packed monolayers are strongly correlated with the presence of tight junctions, which are located at cell-cell contact sites. The tight junctions consist of several different classes of transmembrane and peripheral proteins,

such as zonula occludens protein 1, E-cadherin and claudin (de Souza Carvalho, Daum et al. 2014).

Interestingly, freshly isolated primary ATII cells, which still mantain their original phenotype in culture also display low TEER levels (Elbert, Schafer et al. 1999; Geys, Nemery et al. 2007). Indeed, the low TEER values of pure populations of ATII cells suggest the absence of epithelial barrier formation mediated by thight junctions (Mason and Williams 1980; Germann, Ueberschar et al. 1993). Nevertheless, when primary ATII cells dedifferentiate into ATI-like phenotype they generate tight monolayers, reaching significant high TEER values over 2000 Ωcm^2 (Elbert, Schafer et al. 1999). This finding could support the hypothesis that our differentiated cultures contain a pure population of ATII-LCs and excluding the potential of differentiation into ATI cells. However, the presence of a minor subpopulation of ATI-like differentiated cells cannot be discarded, although it would be insufficient to stablish a measurable electrically tigh monolayer. This hypothesis should be confirmed by analyzing the presence of characteristic markers of ATI cells such as caveolin-1, aquoporin or RAGE, for instance.

To corroborate the results obtained about barrier properties of ATII-LC cultures, transport studies with a fluorescent paracellular marker were performed. Passive fluxes of sodium fluorescein across monolayers of ATII-LCs were barely restricted, according to the calculated apparent permeability coefficients. The levels were around $0.3x10^{-5}$ cm/s in both culture conditions, and these values are significantly higher than those reported for tight cell monolayers, such those formed by NCI-H441 with levels of $0.5x10^{-8}$ cm/s for the same molecule (Salomon, Muchitsch et al. 2014). Thus, TEER values were closely related to trans-monolayer permeability of sodium fluorescein suggesting the absence of formation of high-resistance cell monolayers by ATII-LCs in either of the differentiation conditions analyzed.

On the other hand, the potential impact of components of the extracellular matrix (ECM) in the differentiation process towards ATII-LCs has been assessed. For this purpose, undifferentiated DMSCs were seeded and differentiated in cell inserts coated with fibronectin and collagen. Both compositional and physical signals provided by ECM have been previously reported as crucial for differentiation of stem cells into various cell lineages (Levenberg, Huang et al. 2003; Yim and Leong 2005), with lung cells being no exception (Cortiella, Niles et al. 2010). Our results suggest that although coatings did not have an appreciable influence in terms of cytoarchitecture or barrier properties, ATII-LCs could be maintained for longer periods of time in culture without detachment, until 9 days compared to the 6-7 days in uncoated filters. We hypothesize that this "retention effect" might be due to an improved adherence of cells to the substrate. In fact, it is well known that integrins and other receptors present on the cell surface actively interact with ECM components (Hopkinson, DeBiase et al. 2008). For example, fibronectin contains domains for specific binding to integrins which are essential for the activation of fibronectin and subsequently assembled into a network of fibrils at the cell surface. Intracellularly, integrins also link fibrils to the actin cytoeskeleton iniciating a series of signalling pathways that are involved in a variety of physiological procesess including cell adhesion (Wierzbicka-Patynowski and Schwarzbauer 2003). Though, discerning whether the improvement in cell adherence is the result of activation of downstream signalling cascades, an effect of a reinforced mechanical attachment, or both mechanims acting simultaneously will require further investigation and it is beyond the focus of the present work.

Despite the fact that the inserts were coated with a mixture of collagen and fibronectin already validated for other authors for succesfully growing ATII cells (Elbert, Schafer et al. 1999; Daum, Kuehn et al. 2012), it is probably that other important components of the ECM should be also taken into account. In this sense, laminin-311 (fomerly known as laminin 6) is specifically abundant in the alveolar basement membrane within the lung and it has been described to have an important role participating in mechanosignaling pathways induced by stretch (Budinger, Urich et al. 2008). Besides the effect of specific

compounds, general susbtrate stiffness is known to influence cell adhesion by means of organization of focal adhesion structures and the actin cytoeskeleton (Eisenberg, Safi et al. 2011). Moreover, recent attempts have been focused on developing advanced engineered culture systems, using whole acellular lung as a matrix to support the generation of lung tissue, allowing differentiation of human stem cells into epithelial and endothelial cell lineages (Cortiella, Niles et al. 2010).

In general, considering the inherent notorious complexity of the alveolar ECM, additional elements would have to be taken into account for future improvements in the culture substrate.

Lastly, we also assessed the intracellular content of surfactant proteins SP-B and SP-C, as well as the organic cation transporter 1 (OCT-1) in ATII-LCs under both SC and ALI differentiation conditions, making a comparison with the A459 cell line and freshly isolated human primary ATII cells.

The results showed that the expression levels of SP-B and SP-C in ATII-LCs did not seem to be affected by the influence of the ALI interface when compared to SC conditions. Interestingly, ATII-LCs showed to produce higher amounts of surfactant proteins than the established A549 cell line, although these levels were lower when compared to those found in primary ATII cells. However, unlike the previous results reported in chapter 3, we did not check the amount of protein secreted to the culture medium. Bearing in mind that SP-B, and particularly SP-C are significantly secreted into the extracellular medium by ATII-LCs, potential variances in this secretory behaviour should be also analyzed in differentiated cells exposed to air.

The presence of OCT-1 protein was also evaluated in ATII-LCs, since its expression has been recently described in the primary culture of freshly isolated ATII cells (Salomon, Muchitsch et al. 2014), as well as in A549 cells and bronchial cell lines (Salomon, Endter et al. 2012). OCT-1 is a member of the human polyspecific organic cation transporter

(OCT/N) family, and it is critical for the clearance of many endogenous small organic cations, in addition to a variety of drugs and environmental toxins. In fact, OCT-1 has been proposed to have therapeutic significance in alveolar epithelial cells because many drugs administrated via inhalation are organic cations and thus potential substrates for this protein (Salomon and Ehrhardt 2012). We confirmed the capability of ATII-LCs to express OCT-1 at similar levels of expression independently of the differentiation conditions. Its expression is comparable to that of A549 cells and slightly lower than detected in primary cells.

Previous findings reported an association between low levels of hypoxia inducible factors present at the interfaced cultures of ATII cells and the promotion of the expression of surfactant proteins (Ito, Ahmad et al. 2011). According to this findings, an increment of these factors was also expected in our differentiated cells. However, we observed that in our ALI conditions, a considerable amount of fluid in the apical compartment was always present and continually generated even when it was removed daily. This fluid in the apical compartment could be a contribution of both, the apical liquid that cells normally produce at the ALI (Gueven, Glatthaar et al. 1996), and liquid coming from the basolateral compartment due to the absence of a "sealed" monolayer. The fact that ATII-LCs do not form a tigh monolayer would indicate that the cells are not differentiated in true ALI conditions. Then, the attenuated effects observed in our experiments, at least in terms of protein expression, might be attributed to this effect.

In summary, we could partially conclude that the differentiation of DMSCs under the influence of an interfaced condition does not have a major impact neither in terms of cytoarchitecture or barrier formation nor in the expression of ATII cell markers. However, these data do not necessarily discard that the ALI could affect other relevant parameters that were not analyzed in this work, such as the lipid biosynthesis or the surfactant storing and exocytosis. To our knowledge, in spite that other authors have used the ALI for lung differentiation, the potential effect of ALI as an isolated factor with respect to

submerged cultures has not been specifically addressed. We have also analyzed the effect of two components of the ECM as a culture support under the same culture conditions. The results suggest that even the addition of these two coating factors to the ALI and SC culture conditions might be still insufficient for the cells to reach a much closer state of maturation to that of primary ATII cells, including their capability to generate ATI cells. We hypothesize that additional paracrine cell-derived soluble factors could be necessary to definitely enhance the complete differentiation towards ATII cells. For instance, it has been described that in the developing lung, fibroblasts promote the synthesis of surfactant by ATII cells through paracrine activity mediated by neuroregulin-1 (Dammann, Nielsen et al. 2003). Taking this into account, the incorporation of co-culture systems could be a next step to further optimize our cell model. Indeed, more complex cell models for the alveolar epithelium have been previously stablished combining pure cultures of ATII cells with microvascular endothelial cells to closer mimic the blood-air barrier (Gueven, Glatthaar et al. 1996). Later, more sophisticated co-cultures constituted by monocyte-derived macrophages and dendritic cells, together with epithelial cells using either A549 cells (Rothen-Rutishauser, Kiama et al. 2005) or isolated primary human ATII cells (Lehmann, Daum et al. 2011) have been documented. Other systems of higher complexity have been also reported, like tridimensional cultures incorporating four cell types, such as A549 cells, macrophages, mast cells and endothelial cells (Alfaro-Moreno, Nawrot et al. 2008).

Interestingly, cocultures have also been shown to be valuable for differentiation of stem cells into lung cell types. For example, human mesenchymal stem cells from bone marrow have been differentiated in the presence of primary alveolar epithelial cells grown on transwell filters at the ALI generating a pseudostratified airway epithelia (Wang, Bunnell et al. 2005).

However, when purity in cultures is strictly required or to simplify the model system, co-cultivation with other cell types might be substituted by the addition of the conditioned media obtained from fibroblast or the addition of different isolated factors. In this line,

the positive effects of glucocorticoid application in lung maturation during embryonic development have been associated to an increase in disaturated phosphatidylcholine species or in the expression of surfactant protein mRNAs (Oshika, Liu et al. 1998), possibly mediated by keratinocyte growth factor (KGF) (Chelly, Henrion et al. 2001). Despite the fact that our differentiation medium already contain hydrocortisone, other glucocorticoids could be additionally tested. For instance, dexamethasone and betamethasone have been shown to increase SP-B levels in NCI-H441 cells (Ladenburger, Seehase et al. 2010). Moreover, specific growth factors prompting surfactant expression like the previously mentioned neuroregulins, KGF or leptin, could be also considered to be incorporated in our differentiation cultures.

Although the exposure of DMSCs to the ALI does not appear to reach a definitive ATII phenotype, the results suggest that ATII-LCs, differentiated either under SC or ALI culture conditions are still a valuable *in vitro* model of ATII cells. Because of these results, we aimed to explore the usefulness of ATII-LCs for pulmonary toxicological studies. We assessed the potential harmful effects of nanoparticles that may traverse the lung barrier and presumably interact with local ATII cells.

The results of this Thesis showed that ATII-LCs presented different sensitivities as a function of the kind of nanoparticle tested. Silver nanoparticles (AgNPs) have been shown to produce strong adverse effects over various cultured cell types (AshaRani, Low Kah Mun et al. 2009; Greulich, Kittler et al. 2009; Eom and Choi 2010; Hackenberg, Scherzed et al. 2011; Pascarelli, Moretti et al. 2013). Human lung cells are also very sensitive to AgNPs (Herzog, Clift et al. 2013; Suliman, Ali et al. 2013; Gliga, Skoglund et al. 2014; Kim, Shin da et al. 2014). Indeed, we also confirmed that AgNPs are cytotoxic in a concentration dependent manner for ATII-LCs, even at relatively low concentrations (10 µg/mL). Interestingly, in other studies performed with stem cells, toxic effects of AgNPs are also appreciable at concentrations of 5-10 µg/mL, such as in human mesenchymal stem cells (Greulich, Kittler et al. 2009; Hackenberg, Scherzed et al. 2011) and murine

embryonic stem cells (Ahamed, Karns et al. 2008). Although A459 cells also resulted to be damaged by AgNPs, they were less sensitive than ATII-LCs at the same nanoparticle concentrations. The citotoxic effect of AgNPs observed here against A459 is in agreement with previous studies, where the authors reported cell viabilities of around 70 % after 24 h of contact with AgNPs and at a concentrations of 100 µg/mL (Lankoff, Sandberg et al. 2012). The relative resistance of A549 cells could be attributed to their inherent robustness as reported for fast growing tumor-derived cell lines, and argues against their usefulness as cell model to evaluate potential pulmonary cytotoxicity on a routine basis.

In general, the generation of reactive oxygen species and oxidative stress seem to play a crucial role in the toxicity induced by AgNPs (Park, Yi et al. 2010), but the analysis of the mechanisms behind their cytotoxicity is beyond the present study. Moreover, although the range of concentrations used in our experiments was commonly employed in previous reports, some researchers recommend to use lower concentrations of NPs on in vitro experiments, in order to mimic a more realistic exposure scenario (Gangwal, Brown et al. 2011). This would be particularly relevant when the *in vitro* results have to be extrapolated to real-world situations, i.e.: lung deposition after occupational exposure to nanomaterials.

PLGA is the most investigated polymer for the preparation of microspheres for pulmonary drug administration because of its beneficial properties of biocompatibility and biodegradability (Loira-Pastoriza, Todoroff et al. 2014). We were then interested in checking the safety of nanoparticles composed by PLGA against ATII-LCs. We tested three types of self-made PLGA NPs prepared with two different methodologies. Anionic PLGA NPs made by a emulsion-evaporation technique were shown to be unexpectedly cytotoxic for ATII-LCs, reducing cell viabilitiy rates to around 60-70 % at concentrations of 10 µg/mL. This rapid decay of viability affecting 40 % of the cell population was also observed in A549 cells. However, cationic PLGA-NPs prepared by a self-assembly method and surface-modified with chitosan exerted much lower impairment in ATII-LCs. The cell viabilities were near 100 % after treatment with these cationic NPs at concentrations

of 10 µg/mL and around 80 % at the highest concentrations analyzed. These results are in concordance with previous studies using chitosan-coated PLGA NPs in lung cells (Nafee, Schneider et al. 2009). Indeed, chitosan is particularly benign compared to other cationic polymers and also present some other advantages such as improving the binding of negatively charged plasmids and enhancing their cellular uptake (Richardson, Kolbe et al. 1999; Nafee, Schneider et al. 2009). On the other hand, cationic NPs loaded with clarithromycin did not reveal remarkable deleterious effects over the mitochondrial activity of ATII-LCs either. Although our experiments did not provide information about the release of the drug, this has been previously described as significantly rapid, taking place within a few hours after the exposure of the cells to the NPs (Loira-Pastoriza, Todoroff et al. 2014). In this sense, it is probably that after 24 h of contact with the cells, most of the drug is already released and our results would be indicative of the safety of the clarithromycin formulation into cationic chitosan NPs. In contrast, AgNPs, as an inherently toxic system, provoked a clear citotoxic dose-response in ATII-LCs and in A549 cells. These results are an important proof of concept that our ATII-LCs model could be a relevant in vitro model to evaluate the potential harmful or side effects in the initial steps of the development of pulmonary drugs.

The citotoxicity observed in both cells types, ATII-LCs and A549, when the cells are in contact with our home-made anionic NPs suggests that it is not dependent on the cell type used. The cytotoxic effect of anionic NPs maybe rather related to the specific preparation method used, to the coadyuvants employed or even to the particular preparation itself. The emulsion-diffusion-evaporation technique is widely used for NP preparations, and PVA is known to be rather biocompatible (Feng, Chen et al. 2013). However, the citotoxicity effects of different NPS and its comparison are difficult to interpret due to the variety of parameters that are known to be involved in the toxicity of NPs, such as size, shape, bulk material, surface charge, surface area or the composition of the exposure medium (Greulich, Kittler et al. 2009; Brandenberger, Rothen-Rutishauser et al. 2010). The examination of anionic PLGA NPs under SEM showed that they were aggregated forming much larger particles. The distinctive biological effect of anionic PLGA NPs could

be attributed to a diminished acuracy in the dose-response relationship. However, we cannot rule out that this microscopic observation could be a mere artefact of the drying preparation process. In order to further corroborate these controversial results, new NPs should be prepared and checked, and stock components (PVA, polimer) should be also analyzed independently.

Moreover, although the MTT assay is widely recognised as a reliable method to assess cell viability, other approaches might be also explored in order to obtain complementary information on the nature of the cytotoxic effects. For example, ATP quantitation could be also useful to evaluate the functional integrity of living cells due to the fact that ATP levels normally decrease as a result of any type of cell injury (Nafee, Schneider et al. 2009). The Alamar BLue assay is also used to assess cell viability, based on the reduction potential of metabolically active cells (Gliga, Skoglund et al. 2014). On the other hand, LDH assays are based on the quantification of lactate dehydrogenase (LDH) activity released from the cytosol of dead or plasma membrane-damaged cells into the culture supernatant. Apart from cell viability, other related factors are also usually analysed in toxicity experiments. Genotoxicity of nanomaterials can be investigated with the called “comet assay”, which is based on the microscopic detection of damaged DNA fragments of single cells and visualized with a “comet” morphology after cell lysis, DNA denaturation and electrophoresis (Gliga, Skoglund et al. 2014). Determination of reactive oxygen species in relation to potential damaging oxidative stress processes (Eom and Choi 2010) or evaluation of released proinflammatory cytokines (Greulich, Kittler et al. 2009) can be also a valuable choice for a complete assessment of NP toxicology.

On the other hand, all the *in vitro* citotoxicity experiments performed in this work were carried out under SC culture conditions. Although this type of methods are simple and convenient for soluble molecular toxins, other alternatives have to be taken into account when analyzing airborn particles. Indeed, SC constitute just a partially realistic way of exposure for aerosols, since *in vivo* exposure to airborn particles takes place at the ALI and not under complete SC conditions (Paur, Cassee et al. 2011).

Moreover, adsorption of other molecules present in the culture medium or particle agglomeration generating larger assemblies should be considered to possibly alter the biological effect of NPs (Limbach, Li et al. 2005).

Several systems have been developed to facilitate modelling of NP exposure of cells cultured under the ALI conditions. In this context, we took advantage of a sophisticated device called Air Liquid Interface Cell Exposure (ALICE) system to directly deposit fluorescent PLGA-NPS on ATII-LCs differentiated in interfaced cultures in order to mimic a more realistic situation. Indeed, the ALICE system displays ideal characteristics to study particle-cell interactions. In addition, this system also mimics particle deposition in the respiratory tract following inhalation, as opposed to submerged exposure conditions where the particles have to penetrate a thick layer of cell culture media. After exposing ATII-LCs to PLGA-NPs for 3 or 24 h, we could not detect any change in cell morphology after examination by confocal microscopy. We also obtained optical sections to generate an orthogonal view that allow observation of the translocation of NPs inside of the cells and thus confirming internalization. Different mechanisms of cellular internalization of NPs have been proposed (i.e.: actin-based phagocytosis, clathrin-mediated endocytosis, etc.), being critical the influence of NP surface properties in all processes (Paur, Cassee et al. 2011). However, the experiments presented here do not provide information about the specific uptake mechanism and subsequent intracellular route. Additionally, although these preliminary results suggest that ATII-LCs are able to sucessfully uptake NPs, this approach does not completely exclude that, in some particular cases, the particles could be located between the lateral part of adyacent cells and not truly internalized. In this sense, the examination of the cells after NPs exposure by transmision electron microscopy could aid to confirm the actual uptake of NPs by ATII-LCs, and also to reveal the intracellular location and cellular fate of the NPs. Interestingly, the ability of ATII-LCs to intenalize NPs is atractive not only from the point of view of toxicology studies, but also to optimize potential gene delivery strategies. In fact, PLGA NPs have been formulated as DNA carriers achieving high cellular association and making gene editing possible (Ravi Kumar, Bakowsky et al. 2004; Fields, Quijano et al. 2014).

In summary, in this Chapter 4 we have shown some preliminary experiments focused on the optimization of the ATII-LC culture model by introducing advanced elements in order to mimic the *in vivo* conditions. We conclude that, despite the fact that air interfaced cultures and modified substrates are likely to be key aspects to develop a relevant model of alveolar epithelial cells, considering the complexity of the native microenvironment, further supporting signalling have to be taken into account to optimize the differentiation process. Still, the current ATII-LC model is a promising sensor to assess the safety and cytoxicity of nanoscaled materials permiting a rapid assessment of the safety of new compounds, drug candidates or formulations. The exposure of ATII-LCs to nanomaterials in a more realistic air interfaced situations will also permit to gain reliable insights in the elucidation of cellular uptake mechanisms and the metabolism of xenobiotics delivered to the lung.

General discussion

It was not until 1929 when the Swiss physician Kurt von Neegaard questioned the prevailing hypothesis that breathing consisted exclusively of an alternative balance between the force of the respiratory muscles and the elastic coil of the chest wall and lung tissue (von Neegaard 1929). Indeed, he concluded that the alveoli may have a wet lining and that besides their elastic recoil, the force of surface tension should be also taken into account. Firstly, it was suggested that the airspaces were lined by an insoluble protein layer with the capacity of reducing the tension of the alveolar surface (Pattle 1955). Years later, this partial misconception was subsequently corrected, unveiling pulmonary surfactant (PS) as a membrane-like, lipid-protein complex (Klaus, Clements et al. 1961; Pattle and Thomas 1961), whose lack was potentially correlated with lung pathology (Avery and Mead 1959). From its origins, the expansion of the surfactant field has been the result of the convergence of multiple disciplines including biochemistry, molecular biology, physics, or therapeutics, among others.

The present PhD Thesis has also taken advantage of multidisciplinary approaches, from membrane biophysics to alveolar and stem cell biology, contributing with innovative looks at surfactant research.

During the last years and so far, PS complexes, as isolated from animal bronchoalveolar lavage (BAL), have been considered the standard material for the investigation of structure-function determinants and a reference of optimal function in surfactant research. This has been possible since the source of material permits to obtain virtually unlimited amounts of surfactant, what allows the fulfillment of a variety of experiments. On the other hand, this material is particularly useful because a major part of the lipid-protein complexes present in these preparation are the most active structures of surfactant, as we confirmed in **Chapter 2**. However, we have observed that there is a considerable morphological and functional heterogeneity in NS. Whereas the most active structures are consistent with LBPs, the less functional material might be already spent, or deactivated, or participating in not surface-related roles (i.e.: surfactant homeostasis and/or refinement). Additionally, some surfactant structures could be originally located in conductive locations or in upper airways, being involved in other processes, such as innate defense actions or in the clearance of pathogens via the mucociliary escalator (Haagsman, Herias et al. 2003; Wright 2005). Taking this into account, we propose that the study of the structure and functional

properties of freshly secreted surfactant illustrates in a more reliable way the real behaviour of surfactant at the alveolar spaces. This approach has supposed a technological challenge due to the necessity to optimize analytical methods to study and evaluate the structure and surface behaviour of very small samples, such as those available from cell cultures.

Firstly, we have demonstrated that PS is intracellularly assembled in lamellar bodies (LBs) as highly packed/dehydrated states, which are considerably resistant to temperature-driven structural changes. Interestingly, when surfactant is secreted in the form of lamellar body-like particles (LBPs), it maintains this particular structural arrangement, in the absence of external compression and even at high temperatures. Indeed, the efficiency of PS to show appropriated functional properties and to stabilize the respiratory surface depends critically on the capacity of PS to form highly packed films at the air-liquid interface at the very demanding physiological conditions (Picardi, Cruz et al. 2011).

Additionally, LBPs demonstrate a superior interfacial activity and a remarkable resistance to inhibition, compared to films formed by whole NS. Thus, the elaborated architecture in LBPs may have been evolutionarily optimized for this purpose and highly packed LBPs could be less susceptible to inactivation by binding deleterious components than the more exposed membranes of NS or those of clinical surfactants (Taeusch, Bernardino de la Serna et al. 2005; Pérez-Gil 2008). In fact, previous results suggest that LBPs conserve this stable packed state until the precise moment when the interface requires to be replenished, being the transfer of material from LBPs into the interface prompted by surface tension (Bertocchi, Ravasio et al. 2005). Thus, surface tension would be the force that drives LBPs disintegration. In this regard, the present PhD thesis provides strong evidences that point to the existence of a protein-based mechanism at the limiting membrane of LBs/LBPs, that might be controlling the cooperative opening of the whole corpuscle (**Chapter 1** and **Chapter 2: appendix**). Interestingly, the presence of a projection core enriched in SP-B has been previously shown in micrographs of LBPs (Ochs 2010). This fact leads us to speculate that the protein machinery at the openings could be SP-B based, which would be acting as a pressure-sensitive “staple” holding all the interconnected LBP membranes. After reaching the air-liquid interface, surface tension would trigger a conformational change in the presumed SP-B complexes, potentially leading to the opening of the structure and the

release of the inner pressure generated during LB biogenesis and the subsequent rapid ejection of the internal membranes. In addition to the fraction of LBPs that adsorbs immediately, another fraction remains packed and surface-associated or it is reorganized into other functional units, although the intriguing mechanisms underlying these transformations are still obscure.

On the other hand and paradoxically, we found that the high packing/dehydration of the LBP membranes at the head group level was not accompanied with an ordered state of the acyl chains, but with acyl chains undergoing a high number of trans-gauche isomerizations. In addition to other evidences and as we have stated in **Chapter 1**, our results point to the potential occurrence of non-lamellar phases in PS, a possibility that has been also suggested by other researchers (Perkins, Dause et al. 1996; Chavarha, Khoojinian et al. 2010; Chavarha, Loney et al. 2012). Indeed, current models propose that the lipid multilayers present in the alveolar subphase are interconnected with interfacial phospholipids through surfactant proteins, by means of porous structures (Keating, Zuo et al. 2012) or non-lamellar phases (Chavarha, Khoojinian et al. 2010). In this line, it has been proposed that the existence of interconnected poring structures organized as bicontinuous assemblies might play an important role favoring the transport of molecules and oxygen diffusion (Pérez-Gil 2008; Olmeda, Villén et al. 2010).

Moreover, lipid-protein structures reminiscent of nonbilayer lipids, such as tubular myelin, have been shown to be crucial in the rapid transfer of lipids from LBPs to the air-water interface (Perkins, Dause et al. 1996). In this regard, it is tempting to think that the structure of tubular myelin could be somehow “pre-loaded” inside LBPs and it would be responsible for the non-lamellar signals, although this hypothesis remains to be fully explored. In fact, although it is generally accepted that lipid polymorphic phase behaviour may be key in the effective functioning of PS, direct evidences of the existence of stable non-bilayer lipid structures in natural materials, beyond transient intermediates in membrane fusion mainly deduced from the analysis of artificial model systems, are still lacking. In the current research, the extremely limited amount of material available from primary cell cultures of rat alveolar type II (ATII) cells (in the order of micrograms and sub micrograms of phospholipid) prevented a deeper structural analysis to confirm the existence of non-lamellar phases. Our attempts to circumvent this limitation led us to explore alternative sources to obtain freshly secreted surfactant.

On the one hand, we found that surfactant material purified from BAL was shown to contain to some extent structures consistent with LBPs, which permitted us to gain additional insight into the peculiar organization of these structures. By means of cutting-edge techniques such as cryo-electron tomography and soft x-ray tomography (**Chapter 2: appendix**), we could discern how the membranes are assembled into these structure as well as to postulate the manner in which they are progressively unraveled, as discussed above. Indeed, this material could be considered as a potential candidate for examination under X-ray diffraction or P^{31} NMR in order to address the question of the lipid polymorphism in PS. However, we have to take into account that in the LBP-rich fractions isolated from NS, intact structures coexist with others with a variable extent of unpacking, which could interfere with the presumably non-lamellar signal coming from the intact ones.

On the other hand, bearing in mind the handicaps of primary ATII cells, i.e. the intensive use of animals to collect small amounts of secreted surfactant, we considered the possibility of implementing immortal cell lines. Despite the fact that cell lines are often used as models for primary cells since they are easier to culture and have a high proliferation rate, the phenotype they express may not be consistent with the true phenotype of their primary counterparts. In view of the lack of reliable established surfactant-producing alveolar cell lines, we explored the possibility of deriving stem cells into cells with phenotypic features of type II cells. We characterized the pulmonary-primed differentiation of a population of mesenchymal stem cells isolated from human placenta into alveolar type II-like cells (ATII-LCs) (**Chapter 3**). ATII-LCs synthesize and properly process surfactant proteins, accumulate phospholipids in membranous forms in organelles that remind LBs and secrete this membranous material upon exposure to secretagoges. Strikingly, the material exocyted by ATII-LCs display remarkable interfacial activity and it is also less prone to inactivation, mimicking the properties of that secreted by “true” ATII cells isolated from lung tissue. Since mesenchymal stem cells can be cultured and multiplied at some scale, their differentiation and eventual use as biofactories could be a promising way to access to freshly secreted surfactant. The scaling-up of the cultures could promote their utilization as surfactant-producers for restorative therapies with exogenous clinical materials. Furthermore, crucial questions about surfactant biosynthesis and trafficking pathways that are

still not answered could be addressed thanks to this new cell model. In this regard, either the introduction of modified genes or the silencing of genes encoding surfactant proteins might be a powerful approach to shed light on the structure-function determinants in PS by analyzing the isolated or combined influence of proteins in surfactant biogenesis.

Besides the utilization of ATII-LCs for the investigation of cell processes, we also show in this Thesis that they are valuable as a drug screening tool. Nowadays, drug administration via the lung is considered as a favorable non-invasive route for local and systemic delivery, considering the large area of the respiratory surface, among other factors (Hidalgo, Cruz et al. 2015). As reported in **Chapter 4**, ATII-LCs display an interesting capacity to distinctively sense the cytotoxicity of different nanoscaled materials of biopharmaceutical interest. The success of innovative strategies for pulmonary drug delivery will much depend on the choice of appropriated *in vitro* models to deeper understand how the therapeutic molecules interact with alveolar cells and the subsequent metabolic responses. In this context, ATII-LCs could be promising candidates to achieve the *in vitro-in vivo* correlation required to reliably predict the clinical performance of novel formulations precluding preclinical animal tests.

However, we are aware that the phenotype expressed by ATII-LCs may not completely represent that of the primary system and that ATII-LCs would be still in a partially immature state. In this regard, we aimed to optimize our culture methodology in order to provide cells with further stimulation, trying to mimic the native environment. For this purpose, advanced cell culture techniques, such as differentiating the cells at air-liquid interfaces and over substrates simulating the alveolar extracellular matrix, were implemented. The preliminary results shown in **Chapter 4**, suggest that whole cell differentiation may require of a complex synergetic signaling, integrating not only physical and chemical factors, but also the active interaction with other cell types originally present in the alveolar epithelium.

In spite of the fact that PS has been intensively investigated during the last 40 years, central aspects such as structure-activity correlations or the critical steps in surfactant adsorption and spreading are not completely understood. In this PhD Thesis, we have shed some light on the

structural determinants that the evolution may have promoted in PS to sustain its indispensable functions for the respiratory dynamics. The implementation of both primary ATII cells and modeled ATII-LCs could permit to gain further insight into the molecular mechanisms defining PS and subsequently the development and production of better clinical surfactant preparations with higher resistance to inactivation.

Conclusions

The experimental work presented in this PhD thesis has shed further light on the structural and functional nature of the diverse biological forms of pulmonary surfactant (PS) complexes and particularly of its intracellular and freshly secreted states, taking advantage of previously established as well as newly developed cellular models of alveolar type II (ATII) cells. In general terms, we may conclude that:

1. The structural and functional properties of the PS system varies during the course of its biological cycle. Intracellular surfactant stored as lamellar bodies (LBs) in alveolar type II cells displays a highly packed and dehydrated state at the phospholipid head group region as well as a crystalline-like order. Once exocyted by primary cell cultures into the extracellular medium in the form of lamellar body-like particles (LBPs), PS remains in a highly packed/dehydrated state, even at supraphysiological temperatures. However, the acyl chains of the phospholipid components of LBPs seem to be intrinsically disordered, pointing to the potential existence in freshly secreted PS of geometrical configurations different from those of lamellar phases.

2. Surfactant freshly secreted in the form of LBPs exhibits a remarkable adsorptive activity to generate interfacial films and a higher intrinsic resistance to inactivating agents such as serum proteins or meconium.

3. The outer membrane of LBPs likely contains a protein-based machinery configuring a gating mechanism, which might participate in the initial steps of the adsorption and unravelling of the LBPs once reached an air-liquid interface, prompting at first instance the ejection of the inner membranes.

4. Native surfactant (NS) material as purified from animal bronchoalveolar lavages (BAL) lacks the original structural configuration demonstrated by either LBs/LBPs as well as the boosted biophysical surface capabilities of freshly secreted surfactant. In this sense, NS fails to closely represent PS at the physiological alveolar environment, compared to freshly secreted PS obtained from cell cultures.

5. The diminished structural and functional features of NS compared to freshly secreted LBPs are likely the result of the morphological and functional variety of structures that the material isolated from BAL encloses. NS contains a mixture of highly active forms coexisting with less

active structures, which may possess other potential functions different from surface tension reduction.

6. Decidua-derived mesenchymal stem cells (DMSCs) isolated from human placenta can be efficiently differentiated into cells with phenotypical features similar to ATII cells. ATII-like cells (ATII-LCs) express genes involved in lung development, alveolar homeostasis as well as those encoding for surfactant proteins and their processing enzymes. Surfactant proteins A, B and C are efficiently translated into their mature forms and surfactant-related lipids, such as disaturated phospholipids, are incremented in ATII-LCs.

7. Surfactant lipids and proteins are assembled into cytoplasmic organelles of ATII-LCs resembling LBs. Upon physiological stimulation and mimicking primary cells, ATII-LCs exocyte a lipid-rich material, which exhibits faster interfacial adsorption kinetics than standard NS, even in the presence of inhibitory agents.

8. The properties exhibited by ATII-LCs could make them a useful *in vitro* model for the study of the biosynthesis of PS, including protein processing, lipid trafficking as well as the packing and storage of surfactant assemblies.

9. ATII-LCs demonstrate sensitivity to the cytotoxic effect of nanostructured pharmaceutical preparations and ability to internalize nanoparticles upon exposure by aerosolization, constituting a useful tool for the high-throughput screening of novel pulmonary-delivered drugs.

10. Differentiation of DMSCs into ATII-LCs is not significantly enhanced under the influence of an air-liquid interface or components of the alveolar extracellular matrix, in terms of morphology, expression of surfactant proteins or barrier properties. Further cell differentiation may require of a more complex synergetic signaling, integrating not only physical and chemical factors, but also the active interaction with other cell types naturally present in the alveolar environment.

References

Abe, A., M. Hiraoka, S. Wild, S. E. Wilcoxen, R. Paine, 3rd and J. A. Shayman (2004). “Lysosomal phospholipase A2 is selectively expressed in alveolar macrophages.” J Biol Chem **279**(41): 42605-42611.

Adamson, I. Y., G. M. King and L. Young (1989). “Influence of extracellular matrix and collagen components on alveolar type 2 cell morphology and function.” In Vitro Cell Dev Biol **25**(6): 494-502.

Agassandian, M. and R. K. Mallampalli (2013). “Surfactant phospholipid metabolism.” Biochim Biophys Acta **1831**(3): 612-625.

Ahamed, M., M. Karns, M. Goodson, J. Rowe, S. M. Hussain, J. J. Schlager and Y. Hong (2008). “DNA damage response to different surface chemistry of silver nanoparticles in mammalian cells.” Toxicol Appl Pharmacol **233**(3): 404-410.

Akiyama, J., A. Hoffman, C. Brown, L. Allen, J. Edmondson, F. Poulain and S. Hawgood (2002). “Tissue distribution of surfactant proteins A and D in the mouse.” J Histochem Cytochem **50**(7): 993-996.

Alcorn, J. L., M. E. Smith, J. F. Smith, L. R. Margraf and C. R. Mendelson (1997). “Primary cell culture of human type II pneumonocytes: maintenance of a differentiated phenotype and transfection with recombinant adenoviruses.” Am J Respir Cell Mol Biol **17**(6): 672-682.

Alegre-Cebollada, J., A. Martínez del Pozo, J. G. Gavilanes and E. Goormaghtigh (2007). “Infrared spectroscopy study on the conformational changes leading to pore formation of the toxin sticholysin II.” Biophys J **93**(9): 3191-3201.

Alfaro-Moreno, E., T. S. Nawrot, B. M. Vanaudenaerde, M. F. Hoylaerts, J. A. Vanoirbeek, B. Nemery and P. H. Hoet (2008). “Co-cultures of multiple cell types mimic pulmonary cell communication in response to urban PM10.” Eur Respir J **32**(5): 1184-1194.

Ali, N. N., A. J. Edgar, A. Samadikuchaksaraei, C. M. Timson, H. M. Romanska, J. M. Polak and A. E. Bishop (2002). “Derivation of type II alveolar epithelial cells from murine embryonic stem cells.” Tissue Eng **8**(4): 541-550.

Andreeva, A. V., M. A. Kutuzov and T. A. Voyno-Yasenetskaya (2007). “Regulation of surfactant secretion in alveolar type II cells.” Am J Physiol Lung Cell Mol Physiol **293**(2): L259-271.

Arranz, R., R. Coloma, F. J. Chichón, J. J. Conesa, J. L. Carrascosa, J. M. Valpuesta, J. Ortin and J. Martin-Benito (2012). “The structure of native influenza virion ribonucleoproteins.” Science **338**(6114): 1634-1637.

AshaRani, P. V., G. Low Kah Mun, M. P. Hande and S. Valiyaveettil (2009). “Cytotoxicity and genotoxicity of silver nanoparticles in human cells.” ACS Nano **3**(2): 279-290.

Avery, M. E. and J. Mead (1959). “Surface properties in relation to atelectasis and hyaline membrane disease.” AMA J Dis Child **97**(5, Part 1): 517-523.

Balis, J. U., S. D. Bumgarner, J. E. Paciga, J. F. Paterson and S. A. Shelley (1984). “Synthesis of lung surfactant-associated glycoproteins by A549 cells: description of an in vitro model for human type II cell dysfunction.” Exp Lung Res **6**(3-4): 197-213.

Ban, N., Y. Matsumura, H. Sakai, Y. Takanezawa, M. Sasaki, H. Arai and N. Inagaki (2007). “ABCA3 as a lipid transporter in pulmonary surfactant biogenesis.” J Biol Chem **282**(13): 9628-9634.

Baoukina, S. and D. P. Tieleman (2011). “Lung surfactant protein SP-B promotes formation of bilayer reservoirs from monolayer and lipid transfer between the interface and subphase.” Biophys J **100**(7): 1678-1687.

Batenburg, J. J. (1992). “Surfactant phospholipids: synthesis and storage.” Am J Physiol **262**(4 Pt 1): L367-385.

Baumgart, F., O. L. Ospina, I. Mingarro, I. Rodríguez-Crespo and J. Pérez-Gil (2010). "Palmitoylation of pulmonary surfactant protein SP-C is critical for its functional cooperation with SP-B to sustain compression/expansion dynamics in cholesterol-containing surfactant films." Biophys J **99**(10): 3234-3243.

Beers, M. F. and S. Mulugeta (2005). "Surfactant protein C biosynthesis and its emerging role in conformational lung disease." Annu Rev Physiol **67**: 663-696.

Benson, K., S. Cramer and H.-J. Galla (2013). "Impedance-based cell monitoring: barrier properties and beyond." Fluids and Barriers of the CNS **10**(1): 5.

Berger, M. J., S. D. Adams, B. M. Tigges, S. L. Sprague, X. J. Wang, D. P. Collins and D. H. McKenna (2006). "Differentiation of umbilical cord blood-derived multilineage progenitor cells into respiratory epithelial cells." Cytotherapy **8**(5): 480-487.

Bernardino de la Serna, J., G. Oradd, L. A. Bagatolli, A. C. Simonsen, D. Marsh, G. Lindblom and J. Pérez-Gil (2009). "Segregated phases in pulmonary surfactant membranes do not show coexistence of lipid populations with differentiated dynamic properties." Biophys J **97**(5): 1381-1389.

Bernardino de la Serna, J., J. Pérez-Gil, A. C. Simonsen and L. A. Bagatolli (2004). "Cholesterol rules: direct observation of the coexistence of two fluid phases in native pulmonary surfactant membranes at physiological temperatures." J Biol Chem **279**(39): 40715-40722.

Bernardino de la Serna, J., R. Vargas, V. Picardi, A. Cruz, R. Arranz, J. M. Valpuesta, L. Mateu and J. Pérez-Gil (2013). "Segregated ordered lipid phases and protein-promoted membrane cohesivity are required for pulmonary surfactant films to stabilize and protect the respiratory surface." Faraday Discuss **161**: 535-548; discussion 563-589.

Bertocchi, C., A. Ravasio, S. Bernet, G. Putz, P. Dietl and T. Haller (2005). "Optical measurement of surface tension in a miniaturized air-liquid interface and its application in lung physiology." Biophysical journal **89**(2): 1353-1361.

Berube, K., Z. Prytherch, C. Job and T. Hughes (2010). "Human primary bronchial lung cell constructs: the new respiratory models." Toxicology **278**(3): 311-318.

Bi, X., C. R. Flach, J. Pérez-Gil, I. Plasencia, D. Andreu, E. Oliveira and R. Mendelsohn (2002). "Secondary structure and lipid interactions of the N-terminal segment of pulmonary surfactant SP-C in Langmuir films: IR reflection-absorption spectroscopy and surface pressure studies." Biochemistry **41**(26): 8385-8395.

Blanco, O., A. Cruz, O. L. Ospina, E. López-Rodríguez, L. Vazquez and J. Pérez-Gil (2012). "Interfacial behavior and structural properties of a clinical lung surfactant from porcine source." Biochim Biophys Acta **1818**(11): 2756-2766.

Blanco, O. and J. Pérez-Gil (2007). "Biochemical and pharmacological differences between preparations of exogenous natural surfactant used to treat Respiratory Distress Syndrome: role of the different components in an efficient pulmonary surfactant." Eur J Pharmacol **568**(1-3): 1-15.

Bligh, E. G. and W. J. Dyer (1959). "A rapid method of total lipid extraction and purification." Can J Biochem Physiol **37**(8): 911-917.

Boggaram, V. (2003). "Regulation of lung surfactant protein gene expression." Front Biosci **8**: d751-764.

Boggaram, V. (2009). "Thyroid transcription factor-1 (TTF-1/Nkx2.1/TITF1) gene regulation in the lung." Clin Sci (Lond) **116**(1): 27-35.

Bohinski, R. J., R. Di Lauro and J. A. Whitsett (1994). "The lung-specific surfactant protein B gene promoter is a target for thyroid transcription factor 1 and hepatocyte nuclear factor 3, indicating common factors for organ-specific gene expression along the foregut axis." Mol Cell Biol **14**(9): 5671-5681.

Bornstein, R., M. I. Macias, P. de la Torre, J. Grande and A. I. Flores (2012). “Human decidua-derived mesenchymal stromal cells differentiate into hepatic-like cells and form functional three-dimensional structures.” Cytotherapy **14**(10): 1182-1192.

Brackenbury, A. M., J. L. Malloy, L. A. McCaig, L. J. Yao, R. A. Veldhuizen and J. F. Lewis (2002). “Evaluation of alveolar surfactant aggregates in vitro and in vivo.” Eur Respir J **19**(1): 41-46.

Brandenberger, C., B. Rothen-Rutishauser, C. Muhlfeld, O. Schmid, G. A. Ferron, K. L. Maier, P. Gehr and A. G. Lenz (2010). “Effects and uptake of gold nanoparticles deposited at the air-liquid interface of a human epithelial airway model.” Toxicol Appl Pharmacol **242**(1): 56-65.

Brasch, F., M. Griese, M. Tredano, G. Johnen, M. Ochs, C. Rieger, S. Mulugeta, K. M. Muller, M. Bahuau and M. F. Beers (2004). “Interstitial lung disease in a baby with a de novo mutation in the SFTPC gene.” Eur Respir J **24**(1): 30-39.

Brasch, F., G. Johnen, A. Winn-Brasch, S. H. Guttentag, A. Schmiedl, N. Kapp, Y. Suzuki, K. M. Muller, J. Richter, S. Hawgood and M. Ochs (2004). “Surfactant protein B in type II pneumocytes and intra-alveolar surfactant forms of human lungs.” Am J Respir Cell Mol Biol **30**(4): 449-458.

Braun, A., S. Hammerle, K. Suda, B. Rothen-Rutishauser, M. Gunthert, S. D. Kramer and H. Wunderli-Allenspach (2000). “Cell cultures as tools in biopharmacy.” Eur J Pharm Sci **11 Suppl 2**: S51-60.

Bridges, J. P., M. Ikegami, L. L. Brilli, X. Chen, R. J. Mason and J. M. Shannon (2010). “LPCAT1 regulates surfactant phospholipid synthesis and is required for transitioning to air breathing in mice.” J Clin Invest **120**(5): 1736-1748.

Bridges, J. P., M. G. Ludwig, M. Mueller, B. Kinzel, A. Sato, Y. Xu, J. A. Whitsett and M. Ikegami (2013). “Orphan G protein-coupled receptor GPR116 regulates pulmonary surfactant pool size.” Am J Respir Cell Mol Biol **49**(3): 348-357.

Brochiero, E., A. Dagenais, A. Prive, Y. Berthiaume and R. Grygorczyk (2004). “Evidence of a functional CFTR Cl(-) channel in adult alveolar epithelial cells.” Am J Physiol Lung Cell Mol Physiol **287**(2): L382-392.

Budinger, G. R., D. Urich, P. J. DeBiase, S. E. Chiarella, Z. O. Burgess, C. M. Baker, S. Soberanes, G. M. Mutlu and J. C. Jones (2008). “Stretch-induced activation of AMP kinase in the lung requires dystroglycan.” Am J Respir Cell Mol Biol **39**(6): 666-672.

Butovich, I. A., H. Lu, A. McMahon, H. Ketelson, M. Senchyna, D. Meadows, E. Campbell, M. Molai and E. Linsenbardt (2014). “Biophysical and morphological evaluation of human normal and dry eye meibum using hot stage polarized light microscopy.” Invest Ophthalmol Vis Sci **55**(1): 87-101.

Canals, D., D. Mormeneo, G. Fabrias, A. Llebaria, J. Casas and A. Delgado (2009). “Synthesis and biological properties of Pachastrissamine (jaspine B) and diastereoisomeric jaspines.” Bioorg Med Chem **17**(1): 235-241.

Cargnoni, A., L. Gibelli, A. Tosini, P. B. Signoroni, C. Nassuato, D. Arienti, G. Lombardi, A. Albertini, G. S. Wengler and O. Parolini (2009). “Transplantation of allogeneic and xenogeneic placenta-derived cells reduces bleomycin-induced lung fibrosis.” Cell Transplant **18**(4): 405-422.

Carraro, G., L. Perin, S. Sedrakyan, S. Giuliani, C. Tiozzo, J. Lee, G. Turcatel, S. P. De Langhe, B. Driscoll, S. Bellusci, P. Minoo, A. Atala, R. E. De Filippo and D. Warburton (2008). “Human amniotic fluid stem cells can integrate and differentiate into epithelial lung lineages.” Stem Cells **26**(11): 2902-2911.

Carrascosa, J. L., F. J. Chichón, E. Pereiro, M. J. Rodríguez, J. J. Fernandez, M. Esteban, S. Heim, P. Guttmann and G. Schneider (2009). “Cryo-X-ray tomography of vaccinia virus membranes and inner compartments.” J Struct Biol **168**(2): 234-239.

Carzaniga, R., M. C. Domart, L. M. Collinson and E. Duke (2014). “Cryo-soft X-ray tomography: a journey into the world of the native-state cell.” Protoplasma **251**(2): 449-458.

Casal, H. L. and H. H. Mantsch (1984). “Polymorphic phase behaviour of phospholipid membranes studied by infrared spectroscopy.” Biochim Biophys Acta **779**(4): 381-401.

Casals, C. (2001). “Role of surfactant protein A (SP-A)/lipid interactions for SP-A functions in the lung.” Pediatr Pathol Mol Med **20**(4): 249-268.

Casals, C. and O. Cañadas (2012). “Role of lipid ordered/disordered phase coexistence in pulmonary surfactant function.” Biochim Biophys Acta **1818**(11): 2550-2562.

Cohen, S. R. and A. Bitler (2008). “Use of AFM in bio-related systems.” Current Opinion in Colloid & Interface Science **13**(5): 316-325.

Commission, T. E. (2011). “Commission Recommendation of 18 October 2011 on the definition of nanomaterial (2011/696/EU).” Brussels, Official Journal of the European Union **L 275/38**.

Cortiella, J., J. Niles, A. Cantu, A. Brettler, A. Pham, G. Vargas, S. Winston, J. Wang, S. Walls and J. E. Nichols (2010). “Influence of acellular natural lung matrix on murine embryonic stem cell differentiation and tissue formation.” Tissue Eng Part A **16**(8): 2565-2580.

Coxson, H. O. and J. C. Hogg (2001). “Erratum: a quantification of the lung surface area in emphysema using computed tomography.” Am J Respir Crit Care Med **163**(6): 1500-1501.

Crapo, J. D., B. E. Barry, P. Gehr, M. Bachofen and E. R. Weibel (1982). “Cell number and cell characteristics of the normal human lung.” Am Rev Respir Dis **126**(2): 332-337.

Creuwels, L. A., E. H. Boer, R. A. Demel, L. M. van Golde and H. P. Haagsman (1995). “Neutralization of the positive charges of surfactant protein C. Effects on structure and function.” J Biol Chem **270**(27): 16225-16229.

Crouch, E. and J. R. Wright (2001). “Surfactant proteins a and d and pulmonary host defense.” Annu Rev Physiol **63**: 521-554.

Crouch, E. C. (2000). “Surfactant protein-D and pulmonary host defense.” Respir Res **1**(2): 93-108.

Cruz, A., C. Casals, K. M. Keough and J. Pérez-Gil (1997). “Different modes of interaction of pulmonary surfactant protein SP-B in phosphatidylcholine bilayers.” Biochem J **327 (Pt 1)**: 133-138.

Cruz, A., L. A. Worthman, A. G. Serrano, C. Casals, K. M. Keough and J. Pérez-Gil (2000). “Microstructure and dynamic surface properties of surfactant protein SP-B/dipalmitoylphosphatidylcholine interfacial films spread from lipid-protein bilayers.” Eur Biophys J **29**(3): 204-213.

Cullis, P. R. and B. de Kruijff (1979). “Lipid polymorphism and the functional roles of lipids in biological membranes.” Biochim Biophys Acta **559**(4): 399-420.

Chander, A. and A. B. Fisher (1990). “Regulation of lung surfactant secretion.” Am J Physiol **258**(6 Pt 1): L241-253.

Chander, A., R. G. Johnson, J. Reicherter and A. B. Fisher (1986). “Lung lamellar bodies maintain an acidic internal pH.” J Biol Chem **261**(13): 6126-6131.

Chavarha, M., H. Khoojinian, L. E. Schulwitz, Jr., S. C. Biswas, S. B. Rananavare and S. B. Hall (2010). “Hydrophobic surfactant proteins induce a phosphatidylethanolamine to form cubic phases.” Biophys J **98**(8): 1549-1557.

Chavarha, M., R. W. Loney, K. Kumar, S. B. Rananavare and S. B. Hall (2012). “Differential effects of the hydrophobic surfactant proteins on the formation of inverse bicontinuous cubic phases.” Langmuir **28**(48): 16596-16604.

Cheek, J. M., M. J. Evans and E. D. Crandall (1989). “Type I cell-like morphology in tight alveolar epithelial monolayers.” Exp Cell Res **184**(2): 375-387.

Chelly, N., A. Henrion, C. Pinteur, B. Chailley-Heu and J. R. Bourbon (2001). “Role of keratinocyte growth factor in the control of surfactant synthesis by fetal lung mesenchyme.” Endocrinology **142**(5): 1814-1819.

Dammann, C. E., H. C. Nielsen and K. L. Carraway, 3rd (2003). “Role of neuregulin-1 beta in the developing lung.” Am J Respir Crit Care Med **167**(12): 1711-1716.

Daniels, C. B. and S. Orgeig (2001). “The comparative biology of pulmonary surfactant: past, present and future.” Comp Biochem Physiol A Mol Integr Physiol **129**(1): 9-36.

Daniels, C. B. and S. Orgeig (2003). “Pulmonary surfactant: the key to the evolution of air breathing.” News Physiol Sci **18**: 151-157.

Daum, N., A. Kuehn, S. Hein, U. F. Schaefer, H. Huwer and C. M. Lehr (2012). “Isolation, cultivation, and application of human alveolar epithelial cells.” Methods Mol Biol **806**: 31-42.

de la Presa, P., T. Rueda, M. del Puerto Morales, F. Javier Chichón, R. Arranz, J. M. Valpuesta and A. Hernando (2009). “Gold nanoparticles generated in ethosome bilayers, as revealed by cryo-electron-tomography.” J Phys Chem B **113**(10): 3051-3057.

de Souza Carvalho, C., N. Daum and C. M. Lehr (2014). “Carrier interactions with the biological barriers of the lung: Advanced in vitro models and challenges for pulmonary drug delivery.” Adv Drug Deliv Rev **75c**: 129-140.

De Vequi-Suplicy, C. C., C. R. Benatti and M. T. Lamy (2006). “Laurdan in fluid bilayers: position and structural sensitivity.” J Fluoresc **16**(3): 431-439.

Delabarre, S., C. Claudon and F. Laurent (1997). “Influence of several extracellular matrix components in primary cultures of bovine mammary epithelial cells.” Tissue Cell **29**(1): 99-106.

Denizot, F. and R. Lang (1986). “Rapid colorimetric assay for cell growth and survival. Modifications to the tetrazolium dye procedure giving improved sensitivity and reliability.” J Immunol Methods **89**(2): 271-277.

Dietl, P. and T. Haller (2005). “Exocytosis of lung surfactant: from the secretory vesicle to the air-liquid interface.” Annu Rev Physiol **67**: 595-621.

Dietl, P., T. Haller and M. Frick (2012). “Spatio-temporal aspects, pathways and actions of Ca(2+) in surfactant secreting pulmonary alveolar type II pneumocytes.” Cell Calcium **52**(3-4): 296-302.

Dietl, P., T. Haller, N. Mair and M. Frick (2001). “Mechanisms of surfactant exocytosis in alveolar type II cells in vitro and in vivo.” News Physiol Sci **16**: 239-243.

Dietl, P., B. Liss, E. Felder, P. Miklavc and H. Wirtz (2010). “Lamellar body exocytosis by cell stretch or purinergic stimulation: possible physiological roles, messengers and mechanisms.” Cell Physiol Biochem **25**(1): 1-12.

Dimer, F. A., A. R. Pohlmann and S. S. Guterres (2013). “Characterization of rheology and release profiles of olanzapine-loaded lipid-core nanocapsules in thermosensitive hydrogel.” J Nanosci Nanotechnol **13**(12): 8144-8153.

Discher, B. M., K. M. Maloney, W. R. Schief, Jr., D. W. Grainger, V. Vogel and S. B. Hall (1996). “Lateral phase separation in interfacial films of pulmonary surfactant.” Biophys J **71**(5): 2583-2590.

Dobbs, L. G. (1990). “Isolation and culture of alveolar type II cells.” Am J Physiol **258**(4 Pt 1): L134-147.

Dobbs, L. G., R. González and M. C. Williams (1986). “An improved method for isolating type II cells in high yield and purity.” Am Rev Respir Dis **134**(1): 141-145.

Dobbs, L. G. and R. J. Mason (1979). “Pulmonary alveolar type II cells isolated from rats. Release of phosphatidylcholine in response to beta-adrenergic stimulation.” J Clin Invest **63**(3): 378-387.

Dobbs, L. G., M. S. Pian, M. Maglio, S. Dumars and L. Allen (1997). “Maintenance of the differentiated type II cell phenotype by culture with an apical air surface.” Am J Physiol **273**(2 Pt 1): L347-354.

Dobbs, L. G., M. C. Williams and A. E. Brandt (1985). “Changes in biochemical characteristics and pattern of lectin binding of alveolar type II cells with time in culture.” Biochim Biophys Acta **846**(1): 155-166.

Douglas, W. H. and M. E. Kaighn (1974). “Clonal isolation of differentiated rat lung cells.” In Vitro **10**(3-4): 230-237.

Dubochet, J., M. Adrian, J. J. Chang, J. C. Homo, J. Lepault, A. W. McDowall and P. Schultz (1988). “Cryo-electron microscopy of vitrified specimens.” Q Rev Biophys **21**(2): 129-228.

Duchesneau, P., A. P. Wong and T. K. Waddell (2010). “Optimization of targeted cell replacement therapy: a new approach for lung disease.” Mol Ther **18**(10): 1830-1836.

Dunsmore, S. E. (2008). “Treatment of COPD: a matrix perspective.” Int J Chron Obstruct Pulmon Dis **3**(1): 113-122.

Dushianthan, A., M. P. Grocott, A. D. Postle and R. Cusack (2011). “Acute respiratory distress syndrome and acute lung injury.” Postgrad Med J **87**(1031): 612-622.

Dutton, J. M., K. Goss, K. R. Khubchandani, C. D. Shah, R. J. Smith and J. M. Snyder (1999). “Surfactant protein A in rabbit sinus and middle ear mucosa.” Ann Otol Rhinol Laryngol **108**(10): 915-924.

Eckenhoff, R. G. and A. P. Somlyo (1988). Rat lung type II cell and lamellar body: elemental composition in situ.

Ehrhardt, C., K. J. Kim and C. M. Lehr (2005). “Isolation and culture of human alveolar epithelial cells.” Methods Mol Med **107**: 207-216.

Eisenberg, J. L., A. Safi, X. Wei, H. D. Espinosa, G. S. Budinger, D. Takawira, S. B. Hopkinson and J. C. Jones (2011). “Substrate stiffness regulates extracellular matrix deposition by alveolar epithelial cells.” Res Rep Biol **2011**(2): 1-12.

Elbert, K. J., U. F. Schafer, H. J. Schafers, K. J. Kim, V. H. Lee and C. M. Lehr (1999). “Monolayers of human alveolar epithelial cells in primary culture for pulmonary absorption and transport studies.” Pharm Res **16**(5): 601-608.

Elder, F. R., A. M. Gurewitsch, R. V. Langmuir and H. C. Pollock (1947). “Radiation from Electrons in a Synchrotron.” Physical Review **71**(11): 829-830.

Emerman, J. T., S. J. Burwen and D. R. Pitelka (1979). “Substrate properties influencing ultrastructural differentiation of mammary epithelial cells in culture.” Tissue Cell **11**(1): 109-119.

Eom, H. J. and J. Choi (2010). “p38 MAPK activation, DNA damage, cell cycle arrest and apoptosis as mechanisms of toxicity of silver nanoparticles in Jurkat T cells.” Environ Sci Technol **44**(21): 8337-8342.

Epand, R. M. (1998). “Lipid polymorphism and protein-lipid interactions.” Biochim Biophys Acta **1376**(3): 353-368.

Fang, X., Y. Song, J. Hirsch, L. J. Galietta, N. Pedemonte, R. L. Zemans, G. Dolganov, A. S. Verkman and M. A. Matthay (2006). “Contribution of CFTR to apical-basolateral fluid transport in cultured human alveolar epithelial type II cells.” Am J Physiol Lung Cell Mol Physiol **290**(2): L242-249.

Faraji, A. H. and P. Wipf (2009). “Nanoparticles in cellular drug delivery.” Bioorg Med Chem **17**(8): 2950-2962.

Feng, S., H. Chen, Y. Liu, Z. Huang, X. Sun, L. Zhou, X. Lu and Q. Gao (2013). “A Novel Vitreous Substitute of Using a Foldable Capsular Vitreous Body Injected with Polyvinylalcohol Hydrogel.” Sci. Rep. **3**.

Fernsler, J. G. and J. A. Zasadzinski (2009). “Competitive Adsorption: A Physical Model for Lung Surfactant Inactivation.” Langmuir : the ACS journal of surfaces and colloids **25**(14): 8131-8143.

Fields, R. J., E. Quijano, N. A. McNeer, C. Caputo, R. Bahal, K. Anandalingam, M. E. Egan, P. M. Glazer and W. M. Saltzman (2014). “Modified Poly(lactic-co-glycolic Acid) Nanoparticles for Enhanced Cellular Uptake and Gene Editing in the Lung.” Adv Healthc Mater.

Fireman, E., S. Spitzer, J. Grief, S. Kivity and M. Topilsky (1996). “Cholesterol crystals in BAL fluid from patients with idiopathic pulmonary fibrosis.” Respir Med **90**(6): 361-363.

Fisher, A. B., C. Dodia, P. Ruckert, J.-Q. Tao and S. R. Bates (2010). “Pathway to lamellar bodies for surfactant protein A.” American Journal of Physiology - Lung Cellular and Molecular Physiology **299**(1): L51-L58.

Fitzgerald, M. L., R. Xavier, K. J. Haley, R. Welti, J. L. Goss, C. E. Brown, D. Z. Zhuang, S. A. Bell, N. Lu, M. McKee, B. Seed and M. W. Freeman (2007). “ABCA3 inactivation in mice causes respiratory failure, loss of pulmonary surfactant, and depletion of lung phosphatidylglycerol.” J Lipid Res **48**(3): 621-632.

Forbes, B. and C. Ehrhardt (2005). “Human respiratory epithelial cell culture for drug delivery applications.” European Journal of Pharmaceutics and Biopharmaceutics **60**(2): 193-205.

Foster, K. A., C. G. Oster, M. M. Mayer, M. L. Avery and K. L. Audus (1998). “Characterization of the A549 cell line as a type II pulmonary epithelial cell model for drug metabolism.” Exp Cell Res **243**(2): 359-366.

Fotiadis, D., S. Scheuring, S. A. Muller, A. Engel and D. J. Muller (2002). “Imaging and manipulation of biological structures with the AFM.” Micron **33**(4): 385-397.

Frank, J., M. Radermacher, P. Penczek, J. Zhu, Y. Li, M. Ladjadj and A. Leith (1996). “SPIDER and WEB: processing and visualization of images in 3D electron microscopy and related fields.” J Struct Biol **116**(1): 190-199.

Frick, M., C. Bertocchi, P. Jennings, T. Haller, N. Mair, W. Singer, W. Pfaller, M. Ritsch-Marte and P. Dietl (2004). “Ca2+ entry is essential for cell strain-induced lamellar body fusion in isolated rat type II pneumocytes.” Am J Physiol Lung Cell Mol Physiol **286**(1): 22.

Frick, M., S. Eschertzhuber, T. Haller, N. Mair and P. Dietl (2001). “Secretion in alveolar type II cells at the interface of constitutive and regulated exocytosis.” Am J Respir Cell Mol Biol **25**(3): 306-315.

Fu, K., D. W. Pack, A. M. Klibanov and R. Langer (2000). “Visual evidence of acidic environment within degrading poly(lactic-co-glycolic acid) (PLGA) microspheres.” Pharm Res **17**(1): 100-106.

Fuchs, S., A. J. Hollins, M. Laue, U. F. Schaefer, K. Roemer, M. Gumbleton and C. M. Lehr (2003). “Differentiation of human alveolar epithelial cells in primary culture: morphological characterization and synthesis of caveolin-1 and surfactant protein-C.” Cell Tissue Res **311**(1): 31-45.

Fung, J. C., W. Liu, W. J. de Ruijter, H. Chen, C. K. Abbey, J. W. Sedat and D. A. Agard (1996). “Toward fully automated high-resolution electron tomography.” J Struct Biol **116**(1): 181-189.

Gaczynska, M. and P. A. Osmulski (2008). “AFM of biological complexes: What can we learn?” Current Opinion in Colloid & Interface Science **13**(5): 351-367.

Gangwal, S., J. S. Brown, A. Wang, K. A. Houck, D. J. Dix, R. J. Kavlock and E. A. Hubal (2011). “Informing selection of nanomaterial concentrations for ToxCast in vitro testing based on occupational exposure potential.” Environ Health Perspect **119**(11): 1539-1546.

García-Verdugo, I., A. Ravasio, E. G. de Paco, M. Synguelakis, N. Ivanova, J. Kanellopoulos and T. Haller (2008). “Long-term exposure to LPS enhances the rate of stimulated exocytosis and surfactant secretion in alveolar type II cells and upregulates P2Y2 receptor expression.” Am J Physiol Lung Cell Mol Physiol **295**(4): L708-717.

Germann, P. G., S. Ueberschar, A. Gerull and M. Emura (1993). “In vitro induction of type II pneumocyte-related differentiation in a clonal fetal bronchiolo-alveolar epithelial cell line (M3E3/C3).” Exp Toxicol Pathol **45**(5-6): 315-324.

Geys, J., B. Nemery and P. H. Hoet (2007). “Optimisation of culture conditions to develop an in vitro pulmonary permeability model.” Toxicol In Vitro **21**(7): 1215-1219.

Ghaedi, M., J. J. Mendez, P. F. Bove, A. Sivarapatna, M. S. Raredon and L. E. Niklason (2014). “Alveolar epithelial differentiation of human induced pluripotent stem cells in a rotating bioreactor.” Biomaterials **35**(2): 699-710.

Giard, D. J., S. A. Aaronson, G. J. Todaro, P. Arnstein, J. H. Kersey, H. Dosik and W. P. Parks (1973). “In vitro cultivation of human tumors: establishment of cell lines derived from a series of solid tumors.” J Natl Cancer Inst **51**(5): 1417-1423.

Giavedoni, L. D. and T. Yilma (1996). “Construction and characterization of replication-competent simian immunodeficiency virus vectors that express gamma interferon.” J Virol **70**(4): 2247-2251.

Gil, J. and O. K. Reiss (1973). “Isolation and characterization of lamellar bodies and tubular myelin from rat lung homogenates.” J Cell Biol **58**(1): 152-171.

Gilfillan, A. M. and S. A. Rooney (1987). “Purinoceptor agonists stimulate phosphatidylcholine secretion in primary cultures of adult rat type II pneumocytes.” Biochim Biophys Acta **917**(1): 18-23.

Glaeser, R. M. and L. W. Hobbs (1975). “Radiation damage in stained catalase at low temperature.” J Microsc **103**(2): 209-214.

Glaeser, R. M. and K. A. Taylor (1978). “Radiation damage relative to transmission electron microscopy of biological specimens at low temperature: a review.” J Microsc **112**(1): 127-138.

Gliga, A. R., S. Skoglund, I. O. Wallinder, B. Fadeel and H. L. Karlsson (2014). “Size-dependent cytotoxicity of silver nanoparticles in human lung cells: the role of cellular uptake, agglomeration and Ag release.” Part Fibre Toxicol **11**: 11.

Gobran, L. I., Z. X. Xu, Z. Lu and S. A. Rooney (1994). “P2u purinoceptor stimulation of surfactant secretion coupled to phosphatidylcholine hydrolysis in type II cells.” Am J Physiol **267**(5 Pt 1): L625-633.

Goerke, J. (1998). “Pulmonary surfactant: functions and molecular composition.” Biochim Biophys Acta **1408**(2-3): 79-89.

Gómez-Gil, L., D. Schürch, E. Goormaghtigh and J. Pérez-Gil (2009). “Pulmonary Surfactant Protein SP-C Counteracts the Deleterious Effects of Cholesterol on the Activity of Surfactant Films under Physiologically Relevant Compression-Expansion Dynamics.” Biophys J **97**(10): 2736-2745.

González, R., Y. H. Yang, C. Griffin, L. Allen, Z. Tigue and L. Dobbs (2005). “Freshly isolated rat alveolar type I cells, type II cells, and cultured type II cells have distinct molecular phenotypes.” Am J Physiol Lung Cell Mol Physiol **288**(1): L179-189.

González, R. F. and L. G. Dobbs (2013). “Isolation and culture of alveolar epithelial Type I and Type II cells from rat lungs.” Methods Mol Biol **945**: 145-159.

Goormaghtigh, E., V. Raussens and J. M. Ruysschaert (1999). “Attenuated total reflection infrared spectroscopy of proteins and lipids in biological membranes.” Biochim Biophys Acta **1422**(2): 105-185.

Goss, V., A. N. Hunt and A. D. Postle (2013). “Regulation of lung surfactant phospholipid synthesis and metabolism.” Biochimica et Biophysica Acta (BBA) - Molecular and Cell Biology of Lipids **1831**(2): 448-458.

Grainger, C. I., L. L. Greenwell, D. J. Lockley, G. P. Martin and B. Forbes (2006). “Culture of Calu-3 cells at the air interface provides a representative model of the airway epithelial barrier.” Pharm Res **23**(7): 1482-1490.

Grayson, A. C., G. Voskerician, A. Lynn, J. M. Anderson, M. J. Cima and R. Langer (2004). "Differential degradation rates in vivo and in vitro of biocompatible poly(lactic acid) and poly(glycolic acid) homo- and co-polymers for a polymeric drug-delivery microchip." J Biomater Sci Polym Ed **15**(10): 1281-1304.

Grek, C. L., D. A. Newton, Y. Qiu, X. Wen, D. D. Spyropoulos and J. E. Baatz (2009). "Characterization of alveolar epithelial cells cultured in semipermeable hollow fibers." Exp Lung Res **35**(2): 155-174.

Greulich, C., S. Kittler, M. Epple, G. Muhr and M. Koller (2009). "Studies on the biocompatibility and the interaction of silver nanoparticles with human mesenchymal stem cells (hMSCs)." Langenbecks Arch Surg **394**(3): 495-502.

Gross, N. J. (1991). "Surfactant subtypes in experimental lung damage: radiation pneumonitis." Am J Physiol **260**(4 Pt 1): L302-310.

Gross, N. J., M. Kellam, J. Young, S. Krishnasamy and R. Dhand (2000). "Separation of alveolar surfactant into subtypes. A comparison of methods." Am J Respir Crit Care Med **162**(2 Pt 1): 617-622.

Gross, N. J. and K. R. Narine (1989). "Surfactant subtypes in mice: characterization and quantitation." J Appl Physiol (1985) **66**(1): 342-349.

Gross, N. J. and K. R. Narine (1989). "Surfactant subtypes of mice: metabolic relationships and conversion in vitro." J Appl Physiol (1985) **67**(1): 414-421.

Gu, C., J. Yan, W. Xu, Y. Li, Y. Xia and C. Chen (2014). "[In vitro differentiation of rat amniotic fluid-derived mesenchymal stem cells into type II alveolar epithelial cells]." Zhonghua Yi Xue Za Zhi **94**(26): 2050-2054.

Gueven, N., B. Glatthaar, H. G. Manke and H. Haemmerle (1996). "Co-cultivation of rat pneumocytes and bovine endothelial cells on a liquid-air interface." Eur Respir J **9**(5): 968-975.

Gunasekara, L., W. M. Schoel, S. Schurch and M. W. Amrein (2008). "A comparative study of mechanisms of surfactant inhibition." Biochim Biophys Acta **1778**(2): 433-444.

Gunasekara, L., S. Schurch, W. M. Schoel, K. Nag, Z. Leonenko, M. Haufs and M. Amrein (2005). "Pulmonary surfactant function is abolished by an elevated proportion of cholesterol." Biochim Biophys Acta **1737**(1): 27-35.

Gunther, A., R. Schmidt, F. Nix, M. Yabut-Perez, C. Guth, S. Rosseau, C. Siebert, F. Grimminger, H. Morr, H. G. Velcovsky and W. Seeger (1999). "Surfactant abnormalities in idiopathic pulmonary fibrosis, hypersensitivity pneumonitis and sarcoidosis." Eur Respir J **14**(3): 565-573.

Guo, X., H. M. Lin, Z. Lin, M. Montano, R. Sansores, G. Wang, S. DiAngelo, A. Pardo, M. Selman and J. Floros (2001). "Surfactant protein gene A, B, and D marker alleles in chronic obstructive pulmonary disease of a Mexican population." Eur Respir J **18**(3): 482-490.

Guthmann, F., B. Harrach-Ruprecht, A. C. Looman, P. A. Stevens, H. Robenek and B. Rustow (1997). "Interaction of lipoproteins with type II pneumocytes in vitro: morphological studies, uptake kinetics and secretion rate of cholesterol." Eur J Cell Biol **74**(2): 197-207.

Guthmann, F., R. Haupt, M. Schlame, P. A. Stevens and B. Rustow (1995). "Alveolar surfactant subfractions differ in their lipid composition." Int J Biochem Cell Biol **27**(10): 1021-1026.

Haagsman, H. P., V. Herias and M. van Eijk (2003). "Surfactant phospholipids and proteins in lung defence." Acta Pharmacol Sin **24**(12): 1301-1303.

Hackenberg, S., A. Scherzed, M. Kessler, S. Hummel, A. Technau, K. Froelich, C. Ginzkey, C. Koehler, R. Hagen and N. Kleinsasser (2011). "Silver nanoparticles: evaluation of DNA damage, toxicity and functional impairment in human mesenchymal stem cells." Toxicol Lett **201**(1): 27-33.

Haghi, M., P. M. Young, D. Traini, R. Jaiswal, J. Gong and M. Bebawy (2010). "Time- and passage-dependent characteristics of a Calu-3 respiratory epithelial cell model." Drug Dev Ind Pharm **36**(10): 1207-1214.

Haller, T., P. Dietl, K. Pfaller, M. Frick, N. Mair, M. Paulmichl, M. W. Hess, J. Furst and K. Maly (2001). "Fusion pore expansion is a slow, discontinuous, and Ca2+-dependent process regulating secretion from alveolar type II cells." J Cell Biol **155**(2): 279-289.

Haller, T., P. Dietl, H. Stockner, M. Frick, N. Mair, I. Tinhofer, A. Ritsch, G. Enhorning and G. Putz (2004). "Tracing surfactant transformation from cellular release to insertion into an air-liquid interface." Am J Physiol Lung Cell Mol Physiol **286**(5): L1009-1015.

Haller, T., J. Ortmayr, F. Friedrich, H. Volkl and P. Dietl (1998). "Dynamics of surfactant release in alveolar type II cells." Proc Natl Acad Sci U S A **95**(4): 1579-1584.

Hawco, M. W., P. J. Davis and K. M. Keough (1981). "Lipid fluidity in lung surfactant: monolayers of saturated and unsaturated lecithins." J Appl Physiol Respir Environ Exerc Physiol **51**(2): 509-515.

Hawgood, S. and K. Shiffer (1991). "Structures and properties of the surfactant-associated proteins." Annu Rev Physiol **53**: 375-394.

Hemberger, M., W. Yang, D. Natale, T. L. Brown, C. Dunk, C. E. Gargett and S. Tanaka (2008). "Stem cells from fetal membranes - a workshop report." Placenta **29**(9): 21.

Herzog, F., M. J. Clift, F. Piccapietra, R. Behra, O. Schmid, A. Petri-Fink and B. Rothen-Rutishauser (2013). "Exposure of silver-nanoparticles and silver-ions to lung cells in vitro at the air-liquid interface." Part Fibre Toxicol **10**: 11.

Hidalgo, A., A. Cruz and J. Pérez-Gil (2015). "Barrier or carrier? Pulmonary surfactant and drug delivery." European Journal of Pharmaceutics and Biopharmaceutics(0).

Higuchi, R., J. Lewis and M. Ikegami (1992). "In vitro conversion of surfactant subtypes is altered in alveolar surfactant isolated from injured lungs." Am Rev Respir Dis **145**(6): 1416-1420.

Hobi, N., G. Siber, V. Bouzas, A. Ravasio, J. Pérez-Gil and T. Haller (2014). "Physiological variables affecting surface film formation by native lamellar body-like pulmonary surfactant particles." Biochim Biophys Acta.

Hobi, N., G. Siber, V. Bouzas, A. Ravasio, J. Pérez-Gil and T. Haller (2014). "Physiological variables affecting surface film formation by native lamellar body-like pulmonary surfactant particles." Biochim Biophys Acta **1838**(7): 1842-1850.

Hoffmann, G., J. Grote, F. Friedrich, N. Mutz and W. Schobersberger (1995). "The pulmonary epithelial cell line L 2 as a new model for an inducible nitric oxide synthase expressing distal airway epithelial cell." Biochem Biophys Res Commun **217**(2): 575-583.

Hopkinson, S. B., P. J. DeBiase, K. Kligys, K. Hamill and J. C. Jones (2008). "Fluorescently tagged laminin subunits facilitate analyses of the properties, assembly and processing of laminins in live and fixed lung epithelial cells and keratinocytes." Matrix Biol **27**(7): 640-647.

Horisawa, E., K. Kubota, I. Tuboi, K. Sato, H. Yamamoto, H. Takeuchi and Y. Kawashima (2002). "Size-dependency of DL-lactide/glycolide copolymer particulates for intra-articular delivery system on phagocytosis in rat synovium." Pharm Res **19**(2): 132-139.

Hosgor, M., Y. Ijzendoorn, W. J. Mooi, D. Tibboel and R. R. De Krijger (2002). "Thyroid transcription factor-1 expression during normal human lung development and in patients with congenital diaphragmatic hernia." J Pediatr Surg **37**(9): 1258-1262.

Hrabe, T. and F. Foster (2011). "Structure Determination by Single Particle Cryo-electron Tomography. In: Encyclopedia of Life Sciences (ELS). John Wiley & Sons, Ltd: Chichester.".

Huang, S. X., M. N. Islam, J. O'Neill, Z. Hu, Y. G. Yang, Y. W. Chen, M. Mumau, M. D. Green, G. Vunjak-Novakovic, J. Bhattacharya and H. W. Snoeck (2014). "Efficient generation of lung and airway epithelial cells from human pluripotent stem cells." Nat Biotechnol **32**(1): 84-91.

Ikeda, K., J. C. Clark, J. R. Shaw-White, M. T. Stahlman, C. J. Boutell and J. A. Whitsett (1995). "Gene structure and expression of human thyroid transcription factor-1 in respiratory epithelial cells." J Biol Chem **270**(14): 8108-8114.

Ikegami, M., S. Grant, T. Korfhagen, R. K. Scheule and J. A. Whitsett (2009). "Surfactant protein-D regulates the postnatal maturation of pulmonary surfactant lipid pool sizes." J Appl Physiol (1985) **106**(5): 1545-1552.

Ito, Y., A. Ahmad, E. Kewley and R. J. Mason (2011). "Hypoxia-inducible factor regulates expression of surfactant protein in alveolar type II cells in vitro." Am J Respir Cell Mol Biol **45**(5): 938-945.

Jennings, P., C. Bertocchi, M. Frick, T. Haller, W. Pfaller and P. Dietl (2005). "Ca2+ induced surfactant secretion in alveolar type II cultures isolated from the H-2Kb-tsA58 transgenic mouse." Cell Physiol Biochem **15**(1-4): 159-166.

Johansen, P., Y. Men, H. P. Merkle and B. Gander (2000). "Revisiting PLA/PLGA microspheres: an analysis of their potential in parenteral vaccination." Eur J Pharm Biopharm **50**(1): 129-146.

Johansson, J. (1998). "Structure and properties of surfactant protein C." Biochim Biophys Acta **1408**(2-3): 161-172.

Johansson, J. and T. Curstedt (1997). "Molecular structures and interactions of pulmonary surfactant components." Eur J Biochem **244**(3): 675-693.

Johansson, J., T. Curstedt and H. Jornvall (1991). "Surfactant protein B: disulfide bridges, structural properties, and kringle similarities." Biochemistry **30**(28): 6917-6921.

Johansson, J., T. Szyperski, T. Curstedt and K. Wuthrich (1994). "The NMR structure of the pulmonary surfactant-associated polypeptide SP-C in an apolar solvent contains a valyl-rich alpha-helix." Biochemistry **33**(19): 6015-6023.

Jornada, D. S. F., L.A; Bueno, K; Gerent, J.F; Petzhold, C.L; and R. C. R. G. Beck, S.S and Pohlmann, A.R. (2012). "Lipid-core nanocapsules: Mechanism of self-assembly, control of size and loading capacity." Soft Matter **8**(6646).

Kaartinen, L., P. Nettesheim, K. B. Adler and S. H. Randell (1993). "Rat tracheal epithelial cell differentiation in vitro." In Vitro Cell Dev Biol Anim **29a**(6): 481-492.

Kalin, T. V., I. C. Wang, L. Meliton, Y. Zhang, S. E. Wert, X. Ren, J. Snyder, S. M. Bell, L. Graf, Jr., J. A. Whitsett and V. V. Kalinichenko (2008). "Forkhead Box m1 transcription factor is required for perinatal lung function." Proc Natl Acad Sci U S A **105**(49): 19330-19335.

Kalina, M., S. Riklis and H. Blau (1993). "Pulmonary epithelial cell proliferation in primary culture of alveolar type II cells." Exp Lung Res **19**(2): 153-175.

Katz, S. S., G. G. Shipley and D. M. Small (1976). "Physical chemistry of the lipids of human atherosclerotic lesions. Demonstration of a lesion intermediate between fatty streaks and advanced plaques." The Journal of Clinical Investigation **58**(1): 200-211.

Keating, E., Y. Y. Zuo, S. M. Tadayyon, N. O. Petersen, F. Possmayer and R. A. W. Veldhuizen (2012). "A modified squeeze-out mechanism for generating high surface pressures with pulmonary surfactant." Biochimica et Biophysica Acta (BBA) - Biomembranes **1818**(5): 1225-1234.

Kemp, S. J., A. J. Thorley, J. Gorelik, M. J. Seckl, M. J. O'Hare, A. Arcaro, Y. Korchev, P. Goldstraw and T. D. Tetley (2008). "Immortalization of human alveolar epithelial cells to investigate nanoparticle uptake." Am J Respir Cell Mol Biol **39**(5): 591-597.

Kikkawa, Y. and K. Yoneda (1974). "The type II epithelial cell of the lung. I. Method of isolation." Lab Invest **30**(1): 76-84.

Kim, H. R., Y. Shin da, Y. J. Park, C. W. Park, S. M. Oh and K. H. Chung (2014). "Silver nanoparticles induce p53-mediated apoptosis in human bronchial epithelial (BEAS-2B) cells." J Toxicol Sci **39**(3): 401-412.

Kingma, P. S. and J. A. Whitsett (2006). "In defense of the lung: surfactant protein A and surfactant protein D." Current Opinion in Pharmacology **6**(3): 277-283.

Kitchell, J. P. and D. L. Wise (1985). "Poly(lactic/glycolic acid) biodegradable drug-polymer matrix systems." Methods Enzymol **112**: 436-448.

Klasen, H. J. (2000). "Historical review of the use of silver in the treatment of burns. I. Early uses." Burns **26**(2): 117-130.

Klaus, M. H., J. A. Clements and R. J. Havel (1961). "Composition of surface-active material isolated from beef lung." Proc Natl Acad Sci U S A **47**: 1858-1859.

Klenz, U., M. Saleem, M. C. Meyer and H. Galla (2008). "Influence of Lipid Saturation Grade and Headgroup Charge: A Refined Lung Surfactant Adsorption Model." Biophys J **95**(2): 699-709.

Knells, G., M. K. Ahmed, R. M. Das, M. R. Oulton, H. H. Mantsch and J. E. Scott (1995). "Fourier-transform infrared spectroscopic analysis of rabbit lung surfactant: subfraction-associated phospholipid and protein profiles." Chem Phys Lipids **77**(2): 193-201.

Knoll, A., T. Brockmeyer, R. Chevalier, K. Zscheppang, H. Nielsen and C. Dammann (2013). "Adult Rat Bone Marrow-Derived Stem Cells Promote Late Fetal Type II Cell Differentiation in a Co-Culture Model." Open Respir Med J **7**: 46-53.

Kohsa, K., H. Yamada and H. Sugihara (1996). "Influence of air exposure treatment on alveolar type II epithelial cells cultured on extracellular matrix." Cell Struct Funct **21**(1): 81-89.

Korfei, M., C. Ruppert, P. Mahavadi, I. Henneke, P. Markart, M. Koch, G. Lang, L. Fink, R.-M. Bohle, W. Seeger, T. E. Weaver and A. Guenther (2008). "Epithelial Endoplasmic Reticulum Stress and Apoptosis in Sporadic Idiopathic Pulmonary Fibrosis." American Journal of Respiratory and Critical Care Medicine **178**(8): 838-846.

Koval, M., C. Ward, M. K. Findley, S. Roser-Page, M. N. Helms and J. Roman (2010). "Extracellular matrix influences alveolar epithelial claudin expression and barrier function." Am J Respir Cell Mol Biol **42**(2): 172-180.

Koynova, R. and B. Tenchov (2013). "Transitions between lamellar and non-lamellar phases in membrane lipids and their physiological roles." OA Biochemistry **1**(1): 1-9.

Kramer, A., A. Wintergalen, M. Sieber, H. J. Galla, M. Amrein and R. Guckenberger (2000). "Distribution of the surfactant-associated protein C within a lung surfactant model film investigated by near-field optical microscopy." Biophys J **78**(1): 458-465.

Krol, S., M. Ross, M. Sieber, S. Kunneke, H. J. Galla and A. Janshoff (2000). "Formation of three-dimensional protein-lipid aggregates in monolayer films induced by surfactant protein B." Biophys J **79**(2): 904-918.

Kuroki, Y. and T. Akino (1991). "Pulmonary surfactant protein A (SP-A) specifically binds dipalmitoylphosphatidylcholine." J Biol Chem **266**(5): 3068-3073.

Ladenburger, A., M. Seehase, B. W. Kramer, W. Thomas, J. Wirbelauer, C. P. Speer and S. Kunzmann (2010). "Glucocorticoids potentiate IL-6-induced SP-B expression in H441 cells by enhancing the JAK-STAT signaling pathway." Am J Physiol Lung Cell Mol Physiol **299**(4): L578-584.

Lang, C. J., A. D. Postle, S. Orgeig, F. Possmayer, W. Bernhard, A. K. Panda, K. D. Jurgens, W. K. Milsom, K. Nag and C. B. Daniels (2005). "Dipalmitoylphosphatidylcholine is not the major surfactant phospholipid species in all mammals." Am J Physiol Regul Integr Comp Physiol **289**(5): R1426-1439.

Langman, C., S. Orgeig and C. B. Daniels (1996). “Alterations in composition and function of surfactant associated with torpor in Sminthopsis crassicaudata.” Am J Physiol **271**(2 Pt 2): R437-445.

Lankoff, A., W. J. Sandberg, A. Wegierek-Ciuk, H. Lisowska, M. Refsnes, B. Sartowska, P. E. Schwarze, S. Meczynska-Wielgosz, M. Wojewodzka and M. Kruszewski (2012). “The effect of agglomeration state of silver and titanium dioxide nanoparticles on cellular response of HepG2, A549 and THP-1 cells.” Toxicol Lett **208**(3): 197-213.

Lee, D. B. N., N. Jamgotchian, S. G. Allen, M. B. Abeles and H. J. Ward (2008). A lipid-protein hybrid model for tight junction.

Lehmann, A. D., N. Daum, M. Bur, C. M. Lehr, P. Gehr and B. M. Rothen-Rutishauser (2011). “An in vitro triple cell co-culture model with primary cells mimicking the human alveolar epithelial barrier.” Eur J Pharm Biopharm **77**(3): 398-406.

Lenz, A. G., E. Karg, B. Lentner, V. Dittrich, C. Brandenberger, B. Rothen-Rutishauser, H. Schulz, G. A. Ferron and O. Schmid (2009). “A dose-controlled system for air-liquid interface cell exposure and application to zinc oxide nanoparticles.” Part Fibre Toxicol **6**: 32.

Levenberg, S., N. F. Huang, E. Lavik, A. B. Rogers, J. Itskovitz-Eldor and R. Langer (2003). “Differentiation of human embryonic stem cells on three-dimensional polymer scaffolds.” Proc Natl Acad Sci U S A **100**(22): 12741-12746.

LeVine, A. M., J. Gwozdz, J. Stark, M. Bruno, J. Whitsett and T. Korfhagen (1999). “Surfactant protein-A enhances respiratory syncytial virus clearance in vivo.” The Journal of Clinical Investigation **103**(7): 1015-1021.

Levinson-Dushnik, M. and N. Benvenisty (1997). “Involvement of hepatocyte nuclear factor 3 in endoderm differentiation of embryonic stem cells.” Mol Cell Biol **17**(7): 3817-3822.

Lewis, R. N. and R. N. McElhaney (2013). “Membrane lipid phase transitions and phase organization studied by Fourier transform infrared spectroscopy.” Biochim Biophys Acta **1828**(10): 2347-2358.

Lieber, M., B. Smith, A. Szakal, W. Nelson-Rees and G. Todaro (1976). “A continuous tumor-cell line from a human lung carcinoma with properties of type II alveolar epithelial cells.” Int J Cancer **17**(1): 62-70.

Limbach, L. K., Y. Li, R. N. Grass, T. J. Brunner, M. A. Hintermann, M. Muller, D. Gunther and W. J. Stark (2005). “Oxide nanoparticle uptake in human lung fibroblasts: effects of particle size, agglomeration, and diffusion at low concentrations.” Environ Sci Technol **39**(23): 9370-9376.

Liu, F. Y., Z. Shao, D. O. Kildsig and A. K. Mitra (1993). “Pulmonary delivery of free and liposomal insulin.” Pharm Res **10**(2): 228-232.

Livak, K. J. and T. D. Schmittgen (2001). “Analysis of relative gene expression data using real-time quantitative PCR and the 2(-Delta Delta C(T)) Method.” Methods **25**(4): 402-408.

Loira-Pastoriza, C., J. Todoroff and R. Vanbever (2014). “Delivery strategies for sustained drug release in the lungs.” Adv Drug Deliv Rev **75c**: 81-91.

López-Rodríguez, E., A. Cruz, R. P. Richter, H. W. Taeusch and J. Pérez-Gil (2013). “Transient exposure of pulmonary surfactant to hyaluronan promotes structural and compositional transformations into a highly active state.” J Biol Chem **288**(41): 29872-29881.

López-Rodríguez, E., M. Echaide, A. Cruz, H. W. Taeusch and J. Pérez-Gil (2011). “Meconium impairs pulmonary surfactant by a combined action of cholesterol and bile acids.” Biophys J **100**(3): 646-655.

López-Rodríguez, E., O. L. Ospina, M. Echaide, H. W. Taeusch and J. Pérez-Gil (2012). “Exposure to polymers reverses inhibition of pulmonary surfactant by serum, meconium, or cholesterol in the captive bubble surfactometer.” Biophys J **103**(7): 1451-1459.

López-Rodríguez, E. and J. Pérez-Gil (2014). “Structure-function relationships in pulmonary surfactant membranes: from biophysics to therapy.” Biochim Biophys Acta **1838**(6): 1568-1585.

Lotta, T. I., J. A. Virtanen and P. K. Kinnunen (1988). “Fourier transform infrared study on the thermotropic behaviour of fully hydrated 1-palmitoyl-2-[10-(pyren-1-y) decanoyl]-sn-glycero-3-phosphatidylcholine.” Chem Phys Lipids **46**(1): 13-23.

Lowry, O. H., N. J. Rosebrough, A. L. Farr and R. J. Randall (1951). “Protein measurement with the Folin phenol reagent.” J Biol Chem **193**(1): 265-275.

Lucic, V., F. Forster and W. Baumeister (2005). “Structural studies by electron tomography: from cells to molecules.” Annu Rev Biochem **74**: 833-865.

Luzzati, V. (1997). “Biological significance of lipid polymorphism: the cubic phases.” Curr Opin Struct Biol **7**(5): 661-668.

Luzzati, V., T. Gulik-Krzywicki and A. Tardieu (1968). “Polymorphism of Lecithins.” Nature **218**(5146): 1031-1034.

Lwebuga-Mukasa, J. S., G. Thulin, J. A. Madri, C. Barrett and J. B. Warshaw (1984). “An acellular human amnionic membrane model for in vitro culture of type II pneumocytes: the role of the basement membrane in cell morphology and function.” J Cell Physiol **121**(1): 215-225.

Ma, N., H. Gai, J. Mei, F. B. Ding, C. R. Bao, D. M. Nguyen and H. Zhong (2011). “Bone marrow mesenchymal stem cells can differentiate into type II alveolar epithelial cells in vitro.” Cell Biol Int **35**(12): 1261-1266.

MacDonald, R. C. and S. A. Simon (1987). “Lipid monolayer states and their relationships to bilayers.” Proc Natl Acad Sci U S A **84**(12): 4089-4093.

Macias, M. I., J. Grande, A. Moreno, I. Dominguez, R. Bornstein and A. I. Flores (2010). “Isolation and characterization of true mesenchymal stem cells derived from human term decidua capable of multilineage differentiation into all 3 embryonic layers.” Am J Obstet Gynecol **203**(5): 8.

Magoon, M. W., J. R. Wright, A. Baritussio, M. C. Williams, J. Goerke, B. J. Benson, R. L. Hamilton and J. A. Clements (1983). “Subfractionation of lung surfactant. Implications for metabolism and surface activity.” Biochim Biophys Acta **750**(1): 18-31.

Mamchaoui, K. and G. Saumon (2000). “A method for measuring the oxygen consumption of intact cell monolayers.” Am J Physiol Lung Cell Mol Physiol **278**(4): L858-863.

Marcus, A. J. and D. Woodbury (2008). “Fetal stem cells from extra-embryonic tissues: do not discard.” J Cell Mol Med **12**(3): 730-742.

Markart, P., C. Ruppert, M. Wygrecka, T. Colaris, B. Dahal, D. Walmrath, H. Harbach, J. Wilhelm, W. Seeger, R. Schmidt and A. Guenther (2007). “Patients with ARDS show improvement but not normalisation of alveolar surface activity with surfactant treatment: putative role of neutral lipids.” Thorax **62**(7): 588-594.

Marsh, D. (2012). “Thermodynamics of phospholipid self-assembly.” Biophys J **102**(5): 1079-1087.

Mason, R. J., M. C. Lewis, K. E. Edeen, K. McCormick-Shannon, L. D. Nielsen and J. M. Shannon (2002). “Maintenance of surfactant protein A and D secretion by rat alveolar type II cells in vitro.” Am J Physiol Lung Cell Mol Physiol **282**(2): L249-258.

Mason, R. J. and D. R. Voelker (1998). “Regulatory mechanisms of surfactant secretion.” Biochim Biophys Acta **1408**(2-3): 226-240.

Mason, R. J. and M. C. Williams (1977). “Type II alveolar cell. Defender of the alveolus.” Am Rev Respir Dis **115**(6 Pt 2): 81-91.

Mason, R. J. and M. C. Williams (1980). “Phospholipid composition and ultrastructure of A549 cells and other cultured pulmonary epithelial cells of presumed type II cell origin.” Biochim Biophys Acta **617**(1): 36-50.

Matikainen, T. and J. Laine (2005). “Placenta—an alternative source of stem cells.” Toxicology and Applied Pharmacology **207**(2, Supplement): 544-549.

Mayhew, T. M., C. Muhlfeld, D. Vanhecke and M. Ochs (2009). “A review of recent methods for efficiently quantifying immunogold and other nanoparticles using TEM sections through cells, tissues and organs.” Ann Anat **191**(2): 153-170.

McCormack, F. X. and J. A. Whitsett (2002). “The pulmonary collectins, SP-A and SP-D, orchestrate innate immunity in the lung.” J Clin Invest **109**(6): 707-712.

Mendelson, C. R. and V. Boggaram (1990). “Hormonal and developmental regulation of pulmonary surfactant synthesis in fetal lung.” Baillieres Clin Endocrinol Metab **4**(2): 351-378.

Mendelson, C. R. and V. Boggaram (1991). “Hormonal control of the surfactant system in fetal lung.” Annu Rev Physiol **53**: 415-440.

Miklavc, P., N. Mair, O. H. Wittekindt, T. Haller, P. Dietl, E. Felder, M. Timmler and M. Frick (2011). “Fusion-activated Ca2+ entry via vesicular P2X4 receptors promotes fusion pore opening and exocytotic content release in pneumocytes.” Proc Natl Acad Sci U S A **108**(35): 14503-14508.

Miles, P. R., L. Bowman, J. Tucker, M. J. Reasor and J. R. Wright (1986). “Alterations in rat alveolar surfactant phospholipids and proteins induced by administration of chlorphentermine.” Biochim Biophys Acta **877**(1): 167-178.

Miyamura, K., R. Malhotra, H. J. Hoppe, K. B. Reid, P. J. Phizackerley, P. Macpherson and A. Lopez Bernal (1994). “Surfactant proteins A (SP-A) and D (SP-D): levels in human amniotic fluid and localization in the fetal membranes.” Biochim Biophys Acta **1210**(3): 303-307.

Miyamura, K., R. Malhotra, H. J. Hoppe, K. B. Reid, P. J. Phizackerley, P. Macpherson and A. Lopez Bernal (1994). “Surfactant proteins A (SP-A) and D (SP-D): levels in human amniotic fluid and localization in the fetal membranes.” Biochim Biophys Acta **20**(3): 303-307.

Moodley, Y., S. Ilancheran, C. Samuel, V. Vaghjiani, D. Atienza, E. D. Williams, G. Jenkin, E. Wallace, A. Trounson and U. Manuelpillai (2010). “Human amnion epithelial cell transplantation abrogates lung fibrosis and augments repair.” Am J Respir Crit Care Med **182**(5): 643-651.

Moreno-Herrero, F., J. Colchero, J. Gomez-Herrero and A. M. Baro (2004). “Atomic force microscopy contact, tapping, and jumping modes for imaging biological samples in liquids.” Phys Rev E Stat Nonlin Soft Matter Phys **69**(3 Pt 1): 031915.

Mosmann, T. (1983). “Rapid colorimetric assay for cellular growth and survival: application to proliferation and cytotoxicity assays.” J Immunol Methods **65**(1-2): 55-63.

Nafee, N., M. Schneider, U. F. Schaefer and C. M. Lehr (2009). “Relevance of the colloidal stability of chitosan/PLGA nanoparticles on their cytotoxicity profile.” Int J Pharm **381**(2): 130-139.

Nag, K., C. Boland, N. Rich and K. M. Keough (1991). “Epifluorescence microscopic observation of monolayers of dipalmitoylphosphatidylcholine: dependence of domain size on compression rates.” Biochim Biophys Acta **1068**(2): 157-160.

Nag, K., J. G. Munro, S. A. Hearn, J. Rasmusson, N. O. Petersen and F. Possmayer (1999). “Correlated atomic force and transmission electron microscopy of nanotubular structures in pulmonary surfactant.” J Struct Biol **126**(1): 1-15.

Newman, G. E., P. J. Phizackerley, A. Lopez Bernal, G. R. Noble and A. C. Willis (1991). “Adsorption of fetal surfactant protein SP-B on the human amnion at term and on amniocytes incubated with fetal surfactant in vitro.” Reprod Fertil Dev **3**(4): 421-430.

Nicholas, T. E., J. H. Power and H. A. Barr (1982). “The pulmonary consequences of a deep breath.” Respir Physiol **49**(3): 315-324.

Ning, J., Z. L. Yu, L. H. Hu, C. Wang, X. K. Huo, S. Deng, J. Hou, J. J. Wu, G. B. Ge, X. C. Ma and L. Yang (2015). “Characterization of phase I metabolism of resibufogenin and evaluation of the metabolic effects on its antitumor activity and toxicity.” Drug Metab Dispos **43**(3): 299-308.

Nogee, L. M., G. Garnier, H. C. Dietz, L. Singer, A. M. Murphy, D. E. deMello and H. R. Colten (1994). "A mutation in the surfactant protein B gene responsible for fatal neonatal respiratory disease in multiple kindreds." The Journal of Clinical Investigation **93**(4): 1860-1863.

Ochs, M. (2010). "The closer we look the more we see? Quantitative microscopic analysis of the pulmonary surfactant system." Cell Physiol Biochem **25**(1): 27-40.

Ochs, M., G. Johnen, K. M. Muller, T. Wahlers, S. Hawgood, J. Richter and F. Brasch (2002). "Intracellular and intraalveolar localization of surfactant protein A (SP-A) in the parenchymal region of the human lung." Am J Respir Cell Mol Biol **26**(1): 91-98.

Ochs, M., J. R. Nyengaard, A. Jung, L. Knudsen, M. Voigt, T. Wahlers, J. Richter and H. J. Gundersen (2004). "The number of alveoli in the human lung." Am J Respir Crit Care Med **169**(1): 120-124.

Okamoto, K., S. Miyoshi, M. Toyoda, N. Hida, Y. Ikegami, H. Makino, N. Nishiyama, H. Tsuji, C. H. Cui, K. Segawa, T. Uyama, D. Kami, K. Miyado, H. Asada, K. Matsumoto, H. Saito, Y. Yoshimura, S. Ogawa, R. Aeba, R. Yozu and A. Umezawa (2007). "'Working' cardiomyocytes exhibiting plateau action potentials from human placenta-derived extraembryonic mesodermal cells." Exp Cell Res **313**(12): 2550-2562.

Olmeda, B., B. García-Álvarez and J. Pérez-Gil (2013). "Structure-function correlations of pulmonary surfactant protein SP-B and the saposin-like family of proteins." Eur Biophys J **42**(2-3): 209-222.

Olmeda, B., L. Villén, A. Cruz, G. Orellana and J. Pérez-Gil (2010). "Pulmonary surfactant layers accelerate O(2) diffusion through the air-water interface." Biochim Biophys Acta **1798**(6): 1281-1284.

Orgeig, S., W. Bernhard, S. C. Biswas, C. B. Daniels, S. B. Hall, S. K. Hetz, C. J. Lang, J. N. Maina, A. K. Panda, J. Pérez-Gil, F. Possmayer, R. A. Veldhuizen and W. Yan (2007). "The anatomy, physics, and physiology of gas exchange surfaces: is there a universal function for pulmonary surfactant in animal respiratory structures?" Integr Comp Biol **47**(4): 610-627.

Orgeig, S. and C. B. Daniels (2001). "The roles of cholesterol in pulmonary surfactant: insights from comparative and evolutionary studies." Comp Biochem Physiol A Mol Integr Physiol **129**(1): 75-89.

Orgeig, S., C. B. Daniels, S. D. Johnston and L. C. Sullivan (2003). "The pattern of surfactant cholesterol during vertebrate evolution and development: does ontogeny recapitulate phylogeny?" Reprod Fertil Dev **15**(1-2): 55-73.

Oshika, E., S. Liu, L. P. Ung, G. Singh, H. Shinozuka, G. K. Michalopoulos and S. L. Katyal (1998). "Glucocorticoid-induced effects on pattern formation and epithelial cell differentiation in early embryonic rat lungs." Pediatr Res **43**(3): 305-314.

Oulton, M., J. MacDonald, D. T. Janigan and G. T. Faulkner (1993). "Mouse alveolar surfactant: characterization of subtypes prepared by differential centrifugation." Lipids **28**(8): 715-720.

Owens, D. E., 3rd and N. A. Peppas (2006). "Opsonization, biodistribution, and pharmacokinetics of polymeric nanoparticles." Int J Pharm **307**(1): 93-102.

Palaniyar, N., R. A. Ridsdale, S. A. Hearn, F. Possmayer and G. Harauz (1999). "Formation of membrane lattice structures and their specific interactions with surfactant protein A." Am J Physiol **276**(4 Pt 1): L642-649.

Panyam, J. and V. Labhasetwar (2004). "Sustained cytoplasmic delivery of drugs with intracellular receptors using biodegradable nanoparticles." Mol Pharm **1**(1): 77-84.

Parasassi, T., G. De Stasio, A. d'Ubaldo and E. Gratton (1990). "Phase fluctuation in phospholipid membranes revealed by Laurdan fluorescence." Biophys J **57**(6): 1179-1186.

Parasassi, T., G. De Stasio, G. Ravagnan, R. M. Rusch and E. Gratton (1991). "Quantitation of lipid phases in phospholipid vesicles by the generalized polarization of Laurdan fluorescence." Biophys J **60**(1): 179-189.

Park, E. J., J. Yi, Y. Kim, K. Choi and K. Park (2010). “Silver nanoparticles induce cytotoxicity by a Trojan-horse type mechanism.” Toxicol In Vitro **24**(3): 872-878.

Parolini, O., F. Alviano, G. P. Bagnara, G. Bilic, H. J. Buhring, M. Evangelista, S. Hennerbichler, B. Liu, M. Magatti, N. Mao, T. Miki, F. Marongiu, H. Nakajima, T. Nikaido, C. B. Portmann-Lanz, V. Sankar, M. Soncini, G. Stadler, D. Surbek, T. A. Takahashi, H. Redl, N. Sakuragawa, S. Wolbank, S. Zeisberger, A. Zisch and S. C. Strom (2008). “Concise review: isolation and characterization of cells from human term placenta: outcome of the first international Workshop on Placenta Derived Stem Cells.” Stem Cells **26**(2): 300-311.

Parra, E., A. Alcaraz, A. Cruz, V. M. Aguilella and J. Pérez-Gil (2013). “Hydrophobic pulmonary surfactant proteins SP-B and SP-C induce pore formation in planar lipid membranes: evidence for proteolipid pores.” Biophys J **104**(1): 146-155.

Parra, E., L. H. Moleiro, I. Lopez-Montero, A. Cruz, F. Monroy and J. Pérez-Gil (2011). “A combined action of pulmonary surfactant proteins SP-B and SP-C modulates permeability and dynamics of phospholipid membranes.” Biochem J **438**(3): 555-564.

Parra, E. and J. Pérez-Gil (2015). “Composition, structure and mechanical properties define performance of pulmonary surfactant membranes and films.” Chem Phys Lipids **185c**: 153-175.

Pascarelli, N. A., E. Moretti, G. Terzuoli, A. Lamboglia, T. Renieri, A. Fioravanti and G. Collodel (2013). “Effects of gold and silver nanoparticles in cultured human osteoarthritic chondrocytes.” J Appl Toxicol **33**(12): 1506-1513.

Pattle, R. E. (1955). “Properties, function and origin of the alveolar lining layer.” Nature **175**(4469): 1125-1126.

Pattle, R. E. and L. C. Thomas (1961). “Lipoprotein composition of the film lining the lung.” Nature **189**: 844.

Patton, J. S. and P. R. Byron (2007). “Inhaling medicines: delivering drugs to the body through the lungs.” Nat Rev Drug Discov **6**(1): 67-74.

Paur, H.-R., F. R. Cassee, J. Teeguarden, H. Fissan, S. Diabate, M. Aufderheide, W. G. Kreyling, O. Hänninen, G. Kasper, M. Riediker, B. Rothen-Rutishauser and O. Schmid (2011). “In-vitro cell exposure studies for the assessment of nanoparticle toxicity in the lung—A dialog between aerosol science and biology.” Journal of Aerosol Science **42**(10): 668-692.

Pereiro, E. and F. Chichón (2014). “Cryo-Soft X-ray Tomography of the Cell. In: eLS. John Wiley & Sons, Ltd: Chichester.”.

Pérez-Gil, J. (2008). “Properly interpreting lipid-protein specificities in pulmonary surfactant.” Biophys J **94**(4): 1542-1543; discussion 1544.

Pérez-Gil, J. (2008). “Structure of pulmonary surfactant membranes and films: the role of proteins and lipid-protein interactions.” Biochim Biophys Acta **1778**(7-8): 1676-1695.

Pérez-Gil, J. (2010). “El sistema surfactante pulmonar.” Investigación y Ciencia **401**: 38-45.

Pérez-Gil, J., C. Casals and D. Marsh (1995). “Interactions of hydrophobic lung surfactant proteins SP-B and SP-C with dipalmitoylphosphatidylcholine and dipalmitoylphosphatidylglycerol bilayers studied by electron spin resonance spectroscopy.” Biochemistry **34**(12): 3964-3971.

Pérez-Gil, J., A. Cruz and C. Casals (1993). “Solubility of hydrophobic surfactant proteins in organic solvent/water mixtures. Structural studies on SP-B and SP-C in aqueous organic solvents and lipids.” Biochim Biophys Acta **1168**(3): 261-270.

Pérez-Gil, J. and K. M. Keough (1998). “Interfacial properties of surfactant proteins.” Biochim Biophys Acta **1408**(2-3): 203-217.

Pérez-Gil, J., J. Tucker, G. Simatos and K. M. Keough (1992). “Interfacial adsorption of simple lipid mixtures combined with hydrophobic surfactant protein from pig lung.” Biochem Cell Biol **70**(5): 332-338.

Pérez-Gil, J. and T. E. Weaver (2010). “Pulmonary surfactant pathophysiology: current models and open questions.” Physiology (Bethesda) **25**(3): 132-141.

Perkins, W. R., R. B. Dause, R. A. Parente, S. R. Minchey, K. C. Neuman, S. M. Gruner, T. F. Taraschi and A. S. Janoff (1996). “Role of lipid polymorphism in pulmonary surfactant.” Science **273**(5273): 330-332.

Phua, J., J. R. Badia, N. K. J. Adhikari, J. O. Friedrich, R. A. Fowler, J. M. Singh, D. C. Scales, D. R. Stather, A. Li, A. Jones, D. J. Gattas, D. Hallett, G. Tomlinson, T. E. Stewart and N. D. Ferguson (2009). “Has Mortality from Acute Respiratory Distress Syndrome Decreased over Time?” American Journal of Respiratory and Critical Care Medicine **179**(3): 220-227.

Picardi, M. V., A. Cruz, G. Orellana and J. Pérez-Gil (2011). “Phospholipid packing and hydration in pulmonary surfactant membranes and films as sensed by LAURDAN.” Biochim Biophys Acta **1808**(3): 696-705.

Pipino, C., P. Shangaris, E. Resca, S. Zia, J. Deprest, N. J. Sebire, A. L. David, P. V. Guillot and P. De Coppi (2013). “Placenta as a reservoir of stem cells: an underutilized resource?” Br Med Bull **105**: 43-68.

Pomorski, T. and A. K. Menon (2006). “Lipid flippases and their biological functions.” Cell Mol Life Sci **63**(24): 2908-2921.

Portmann-Lanz, C. B., A. Schoeberlein, A. Huber, R. Sager, A. Malek, W. Holzgreve and D. V. Surbek (2006). “Placental mesenchymal stem cells as potential autologous graft for pre- and perinatal neuroregeneration.” Am J Obstet Gynecol **194**(3): 664-673.

Poulain, F. R., J. Akiyama, L. Allen, C. Brown, R. Chang, J. Goerke, L. Dobbs and S. Hawgood (1999). “Ultrastructure of phospholipid mixtures reconstituted with surfactant proteins B and D.” Am J Respir Cell Mol Biol **20**(5): 1049-1058.

Poulain, F. R., L. Allen, M. C. Williams, R. L. Hamilton and S. Hawgood (1992). “Effects of surfactant apolipoproteins on liposome structure: implications for tubular myelin formation.” Am J Physiol **262**(6 Pt 1): L730-739.

Pryhuber, G. S., W. M. Hull, I. Fink, M. J. McMahan and J. A. Whitsett (1991). “Ontogeny of surfactant proteins A and B in human amniotic fluid as indices of fetal lung maturity.” Pediatr Res **30**(6): 597-605.

Puff, N. and M. I. Angelova (2006). “Chapter 7 Lipid Vesicles - Development and Applications for Studing Membrane Heterogeneity and Interactions.” Advances in Planar Lipid Bilayers and Liposomes. A. L. Liu, Academic Press **5**: 173-228.

Putman, E., L. A. Creuwels, L. M. van Golde and H. P. Haagsman (1996). “Surface properties, morphology and protein composition of pulmonary surfactant subtypes.” Biochem J **320 (Pt 2)**: 599-605.

Radmacher, M., J. P. Cleveland, M. Fritz, H. G. Hansma and P. K. Hansma (1994). “Mapping interaction forces with the atomic force microscope.” Biophys J **66**(6): 2159-2165.

Rannels, D. E. and S. R. Rannels (1989). “Influence of the extracellular matrix on type 2 cell differentiation.” Chest **96**(1): 165-173.

Ravasio, A., A. Cruz, J. Pérez-Gil and T. Haller (2008). “High-throughput evaluation of pulmonary surfactant adsorption and surface film formation.” J Lipid Res **49**(11): 2479-2488.

Ravasio, A., B. Olmeda, C. Bertocchi, T. Haller and J. Pérez-Gil (2010). “Lamellar bodies form solid three-dimensional films at the respiratory air-liquid interface.” J Biol Chem **285**(36): 28174-28182.

Ravi Kumar, M. N., U. Bakowsky and C. M. Lehr (2004). “Preparation and characterization of cationic PLGA nanospheres as DNA carriers.” Biomaterials **25**(10): 1771-1777.

Richardson, S. C., H. V. Kolbe and R. Duncan (1999). “Potential of low molecular mass chitosan as a DNA delivery system: biocompatibility, body distribution and ability to complex and protect DNA.” Int J Pharm **178**(2): 231-243.

Ridsdale, R., C. L. Na, Y. Xu, K. D. Greis and T. Weaver (2011). “Comparative proteomic analysis of lung lamellar bodies and lysosome-related organelles.” PLoS One **6**(1): e16482.

Rippon, H. J., J. M. Polak, M. Qin and A. E. Bishop (2006). “Derivation of distal lung epithelial progenitors from murine embryonic stem cells using a novel three-step differentiation protocol.” Stem Cells **24**(5): 1389-1398.

Roe, D., B. Karandikar, N. Bonn-Savage, B. Gibbins and J. B. Roullet (2008). “Antimicrobial surface functionalization of plastic catheters by silver nanoparticles.” J Antimicrob Chemother **61**(4): 869-876.

Roldan, N., E. Goormaghtigh, J. Pérez-Gil and B. García-Álvarez (2015). “Palmitoylation as a key factor to modulate SP-C-lipid interactions in lung surfactant membrane multilayers.” Biochim Biophys Acta **1848**(1 Pt A): 184-191.

Roper, J. M., R. J. Staversky, J. N. Finkelstein, P. C. Keng and M. A. O’Reilly (2003). “Identification and isolation of mouse type II cells on the basis of intrinsic expression of enhanced green fluorescent protein.” Am J Physiol Lung Cell Mol Physiol **285**(3): L691-700.

Ross, M., S. Krol, A. Janshoff and H. J. Galla (2002). “Kinetics of phospholipid insertion into monolayers containing the lung surfactant proteins SP-B or SP-C.” Eur Biophys J **31**(1): 52-61.

Roszell, B., M. J. Mondrinos, A. Seaton, D. M. Simons, S. H. Koutzaki, G. H. Fong, P. I. Lelkes and C. M. Finck (2009). “Efficient derivation of alveolar type II cells from embryonic stem cells for in vivo application.” Tissue Eng Part A **15**(11): 3351-3365.

Rothen-Rutishauser, B., S. D. Kramer, A. Braun, M. Gunthert and H. Wunderli-Allenspach (1998). “MDCK cell cultures as an epithelial in vitro model: cytoskeleton and tight junctions as indicators for the definition of age-related stages by confocal microscopy.” Pharm Res **15**(7): 964-971.

Rothen-Rutishauser, B. M., S. G. Kiama and P. Gehr (2005). “A three-dimensional cellular model of the human respiratory tract to study the interaction with particles.” Am J Respir Cell Mol Biol **32**(4): 281-289.

Rouser, G., S. Fkeischer and A. Yamamoto (1970). “Two dimensional then layer chromatographic separation of polar lipids and determination of phospholipids by phosphorus analysis of spots.” Lipids **5**(5): 494-496.

Rouser, G., A. N. Siakotos and S. Fleischer (1966). “Quantitative analysis of phospholipids by thin-layer chromatography and phosphorus analysis of spots.” Lipids **1**(1): 85-86.

Ruano, M. L., J. Pérez-Gil and C. Casals (1998). “Effect of acidic pH on the structure and lipid binding properties of porcine surfactant protein A. Potential role of acidification along its exocytic pathway.” J Biol Chem **273**(24): 15183-15191.

Russo, S. J., W. Wang, C. A. Lomax and M. F. Beers (1999). “Structural requirements for intracellular targeting of SP-C proprotein.” Am J Physiol **277**(5 Pt 1): L1034-1044.

Ryan, M. A., X. Qi, A. G. Serrano, M. Ikegami, J. Pérez-Gil, J. Johansson and T. E. Weaver (2005). “Mapping and analysis of the lytic and fusogenic domains of surfactant protein B.” Biochemistry **44**(3): 861-872.

Sadava, D. E., H. C. Heller and D. Hillis (2012). Life: The Science of Biology; 8th edition, Worth Publ Inc.

Saenz, A., O. Cañadas, L. A. Bagatolli, F. Sanchez-Barbero, M. E. Johnson and C. Casals (2007). “Effect of surfactant protein A on the physical properties and surface activity of KL4-surfactant.” Biophys J **92**(2): 482-492.

Sakagami, M. (2006). “In vivo, in vitro and ex vivo models to assess pulmonary absorption and disposition of inhaled therapeutics for systemic delivery.” Adv Drug Deliv Rev **58**(9-10): 1030-1060.

Salmona, M., M. Donnini, L. Perin, L. Diomede, M. Romano, M. G. Marini, M. T. Tacconi and M. Luisetti (1992). “A novel pharmacological approach for paraquat poisoning in rat and A549 cell line using ambroxol, a lung surfactant synthesis inducer.” Food Chem Toxicol **30**(9): 789-794.

Salomon, J. J. and C. Ehrhardt (2012). “Organic cation transporters in the blood-air barrier: expression and implications for pulmonary drug delivery.” Ther Deliv **3**(6): 735-747.

Salomon, J. J., S. Endter, G. Tachon, F. Falson, S. T. Buckley and C. Ehrhardt (2012). “Transport of the fluorescent organic cation 4-(4-(dimethylamino)styryl)-N-methylpyridinium iodide (ASP+) in human respiratory epithelial cells.” Eur J Pharm Biopharm **81**(2): 351-359.

Salomon, J. J., V. E. Muchitsch, J. C. Gausterer, E. Schwagerus, H. Huwer, N. Daum, C. M. Lehr and C. Ehrhardt (2014). “The Cell Line NCl-H441 Is a Useful in Vitro Model for Transport Studies of Human Distal Lung Epithelial Barrier.” Mol Pharm.

Samadikuchaksaraei, A. and A. E. Bishop (2006). “Derivation and characterization of alveolar epithelial cells from murine embryonic stem cells in vitro.” Methods Mol Biol **330**: 233-248.

Samadikuchaksaraei, A., S. Cohen, K. Isaac, H. J. Rippon, J. M. Polak, R. C. Bielby and A. E. Bishop (2006). “Derivation of distal airway epithelium from human embryonic stem cells.” Tissue Eng **12**(4): 867-875.

Sánchez, S. A., M. A. Tricerri, G. Gunther and E. Gratton (2007). “Laurdan Generalized Polarization: from cuvette to microscope.” Modern Research and Educational Topics in Microscopy.

Sannes, P. L. (1991). “Structural and functional relationships between type II pneumocytes and components of extracellular matrices.” Exp Lung Res **17**(4): 639-659.

Sano, H. and Y. Kuroki (2005). “The lung collectins, SP-A and SP-D, modulate pulmonary innate immunity.” Mol Immunol **42**(3): 279-287.

Santander-Ortega, M. J., D. Bastos-González and J. L. Ortega-Vinuesa (2007). “Electrophoretic mobility and colloidal stability of PLGA particles coated with IgG.” Colloids Surf B Biointerfaces **60**(1): 80-88.

Sati, L., Y. Seval-Celik and R. Demir (2007). “Lung surfactant proteins in the early human placenta.” Histochem Cell Biol **133**(1): 85-93.

Scanlon V.C. and S. T. (2015). Essentials of Anatomy and Physiology, 7th edition, F.A. Davis Company.

Schmeckebier, S., C. Mauritz, K. Katsirntaki, M. Sgodda, V. Puppe, J. Duerr, S. C. Schubert, A. Schmiedl, Q. Lin, J. Palecek, G. Draeger, M. Ochs, M. Zenke, T. Cantz, M. A. Mall and U. Martin (2013). “Keratinocyte growth factor and dexamethasone plus elevated cAMP levels synergistically support pluripotent stem cell differentiation into alveolar epithelial type II cells.” Tissue Eng Part A **19**(7-8): 938-951.

Schneider, G. (1998). “Cryo X-ray microscopy with high spatial resolution in amplitude and phase contrast.” Ultramicroscopy **75**(2): 85-104.

Schneider, G., P. Guttmann, S. Heim, S. Rehbein, F. Mueller, K. Nagashima, J. B. Heymann, W. G. Muller and J. G. McNally (2010). “Three-dimensional cellular ultrastructure resolved by X-ray microscopy.” Nat Meth **7**(12): 985-987.

Schoel, W. M., S. Schurch and J. Goerke (1994). “The captive bubble method for the evaluation of pulmonary surfactant: surface tension, area, and volume calculations.” Biochim Biophys Acta **1200**(3): 281-290.

Schurch, D., O. L. Ospina, A. Cruz and J. Pérez-Gil (2010). "Combined and independent action of proteins SP-B and SP-C in the surface behavior and mechanical stability of pulmonary surfactant films." Biophys J **99**(10): 3290-3299.

Schurch, S., H. Bachofen, J. Goerke and F. Possmayer (1989). "A captive bubble method reproduces the in situ behavior of lung surfactant monolayers." J Appl Physiol (1985) **67**(6): 2389-2396.

Schurch, S., F. H. Green and H. Bachofen (1998). "Formation and structure of surface films: captive bubble surfactometry." Biochim Biophys Acta **1408**(2-3): 180-202.

Serrano, A. G. and J. Pérez-Gil (2006). "Protein-lipid interactions and surface activity in the pulmonary surfactant system." Chem Phys Lipids **141**(1-2): 105-118.

Shapiro, D. L., L. L. Nardone, S. A. Rooney, E. K. Motoyama and J. L. Munoz (1978). "Phospholipid biosynthesis and secretion by a cell line (A549) which resembles type II aleveolar epithelial cells." Biochim Biophys Acta **530**(2): 197-207.

Shipley, G. G., L. S. Avecilla and D. M. Small (1974). "Phase behavior and structure of aqueous dispersions of sphingomyelin." Journal of Lipid Research **15**(2): 124-131.

Shulenin, S., L. M. Nogee, T. Annilo, S. E. Wert, J. A. Whitsett and M. Dean (2004). "ABCA3 Gene Mutations in Newborns with Fatal Surfactant Deficiency." New England Journal of Medicine **350**(13): 1296-1303.

Singer, W., M. Frick, T. Haller, S. Bernet, M. Ritsch-Marte and P. Dietl (2003). "Mechanical forces impeding exocytotic surfactant release revealed by optical tweezers." Biophys J **84**(2 Pt 1): 1344-1351.

Siti-Ismail, N., A. Samadikuchaksaraei, A. E. Bishop, J. M. Polak and A. Mantalaris (2012). "Development of a novel three-dimensional, automatable and integrated bioprocess for the differentiation of embryonic stem cells into pulmonary alveolar cells in a rotating vessel bioreactor system." Tissue Eng Part C Methods **18**(4): 263-272.

Smith, B. T. (1977). "Cell line A549: a model system for the study of alveolar type II cell function." Am Rev Respir Dis **115**(2): 285-293.

Soncini, M., E. Vertua, L. Gibelli, F. Zorzi, M. Denegri, A. Albertini, G. S. Wengler and O. Parolini (2007). "Isolation and characterization of mesenchymal cells from human fetal membranes." J Tissue Eng Regen Med **1**(4): 296-305.

Spain, C. L., R. Silbajoris and S. L. Young (1987). "Alterations of surfactant pools in fetal and newborn rat lungs." Pediatr Res **21**(1): 5-9.

Spitalieri, P., M. C. Quitadamo, A. Orlandi, L. Guerra, E. Giardina, V. Casavola, G. Novelli, C. Saltini and F. Sangiuolo (2012). "Rescue of murine silica-induced lung injury and fibrosis by human embryonic stem cells." Eur Respir J **39**(2): 446-457.

Spragg, R. G., F. J. Taut, J. F. Lewis, P. Schenk, C. Ruppert, N. Dean, K. Krell, A. Karabinis and A. Gunther (2011). "Recombinant surfactant protein C-based surfactant for patients with severe direct lung injury." Am J Respir Crit Care Med **183**(8): 1055-1061.

Stahlman, M. T., V. Besnard, S. E. Wert, T. E. Weaver, S. Dingle, Y. Xu, K. von Zychlin, S. J. Olson and J. A. Whitsett (2007). "Expression of ABCA3 in developing lung and other tissues." J Histochem Cytochem **55**(1): 71-83.

Stahlman, M. T., M. E. Gray and J. A. Whitsett (1992). "The ontogeny and distribution of surfactant protein B in human fetuses and newborns." J Histochem Cytochem **40**(10): 1471-1480.

Stahlman, M. T., M. P. Gray, M. W. Falconieri, J. A. Whitsett and T. E. Weaver (2000). "Lamellar body formation in normal and surfactant protein B-deficient fetal mice." Lab Invest **80**(3): 395-403.

Steimer, A., M. Laue, H. Franke, E. Haltner-Ukomado and C. M. Lehr (2006). “Porcine alveolar epithelial cells in primary culture: morphological, bioelectrical and immunocytochemical characterization.” Pharm Res **23**(9): 2078-2093.

Stentebjerg-Andersen, A., I. V. Notlevsen, B. Brodin and C. U. Nielsen (2011). “Calu-3 cells grown under AIC and LCC conditions: implications for dipeptide uptake and transepithelial transport of substances.” Eur J Pharm Biopharm **78**(1): 19-26.

Su, W. Y., B. J. Day, B. H. Kang, J. D. Crapo, Y. C. Huang and L. Y. Chang (1996). “Lung epithelial cell-released nitric oxide protects against PMN-mediated cell injury.” Am J Physiol **271**(4 Pt 1): L581-586.

Sugihara, H., S. Toda, S. Miyabara, C. Fujiyama and N. Yonemitsu (1993). “Reconstruction of alveolus-like structure from alveolar type II epithelial cells in three-dimensional collagen gel matrix culture.” Am J Pathol **142**(3): 783-792.

Suliman, Y. A., D. Ali, S. Alarifi, A. H. Harrath, L. Mansour and S. H. Alwasel (2013). “Evaluation of cytotoxic, oxidative stress, proinflammatory and genotoxic effect of silver nanoparticles in human lung epithelial cells.” Environ Toxicol.

Sun, K., D. Brockman, B. Campos, B. Pitzer and L. Myatt (2006). “Induction of surfactant protein A expression by cortisol facilitates prostaglandin synthesis in human chorionic trophoblasts.” J Clin Endocrinol Metab **91**(12): 4988-4994.

Sung, J. C., B. L. Pulliam and D. A. Edwards (2007). “Nanoparticles for drug delivery to the lungs.” Trends Biotechnol **25**(12): 563-570.

Suri, L. N., L. McCaig, M. V. Picardi, O. L. Ospina, R. A. Veldhuizen, J. F. Staples, F. Possmayer, L. J. Yao, J. Pérez-Gil and S. Orgeig (2012). “Adaptation to low body temperature influences pulmonary surfactant composition thereby increasing fluidity while maintaining appropriately ordered membrane structure and surface activity.” Biochim Biophys Acta **1818**(7): 1581-1589.

Suzuki, Y., Y. Fujita and K. Kogishi (1989). “Reconstitution of tubular myelin from synthetic lipids and proteins associated with pig pulmonary surfactant.” Am Rev Respir Dis **140**(1): 75-81.

Swain, R. J., S. J. Kemp, P. Goldstraw, T. D. Tetley and M. M. Stevens (2010). “Assessment of cell line models of primary human cells by Raman spectral phenotyping.” Biophys J **98**(8): 1703-1711.

Taeusch, H. W., J. Bernardino de la Serna, J. Pérez-Gil, C. Alonso and J. A. Zasadzinski (2005). “Inactivation of pulmonary surfactant due to serum-inhibited adsorption and reversal by hydrophilic polymers: experimental.” Biophys J **89**(3): 1769-1779.

Taneva, S. and K. M. Keough (1994). “Pulmonary surfactant proteins SP-B and SP-C in spread monolayers at the air-water interface: II. Monolayers of pulmonary surfactant protein SP-C and phospholipids.” Biophys J **66**(4): 1149-1157.

Tate, M. W., E. F. Eikenberry, D. C. Turner, E. Shyamsunder and S. M. Gruner (1991). “Nonbilayer phases of membrane lipids.” Chem Phys Lipids **57**(2-3): 147-164.

Thet, L. A., L. Clerch, G. D. Massaro and D. Massaro (1979). “Changes in sedimentation of surfactant in ventilated excised rat lungs. Physical alterations in surfactant associated with the development and reversal of atelectasis.” J Clin Invest **64**(2): 600-608.

Tinazli, A., J. Piehler, M. Beuttler, R. Guckenberger and R. Tampe (2007). “Native protein nanolithography that can write, read and erase.” Nat Nanotechnol **2**(4): 220-225.

Ueda, T., M. Ikegami and A. Jobe (1994). “Surfactant subtypes. In vitro conversion, in vivo function, and effects of serum proteins.” Am J Respir Crit Care Med **149**(5): 1254-1259.

Ueno, T., S. Linder, C. L. Na, W. R. Rice, J. Johansson and T. E. Weaver (2004). “Processing of pulmonary surfactant protein B by napsin and cathepsin H.” J Biol Chem **279**(16): 16178-16184.

van den Brink-van der Laan, E., J. A. Killian and B. de Kruijff (2004). “Nonbilayer lipids affect peripheral and integral membrane proteins via changes in the lateral pressure profile.” Biochim Biophys Acta **1666**(1-2): 275-288.

Van Haute, L., G. De Block, I. Liebaers, K. Sermon and M. De Rycke (2009). “Generation of lung epithelial-like tissue from human embryonic stem cells.” Respir Res **10**: 105.

van Meer, G., D. R. Voelker and G. W. Feigenson (2008). “Membrane lipids: where they are and how they behave.” Nat Rev Mol Cell Biol **9**(2): 112-124.

Van Vranken, B. E., H. J. Rippon, A. Samadikuchaksaraei, A. O. Trounson and A. E. Bishop (2007). “The differentiation of distal lung epithelium from embryonic stem cells.” Curr Protoc Stem Cell Biol **Chapter 1**: Unit 1G.1.

Vandenbussche, G., A. Clercx, T. Curstedt, J. Johansson, H. Jornvall and J. M. Ruysschaert (1992). “Structure and orientation of the surfactant-associated protein C in a lipid bilayer.” Eur J Biochem **203**(1-2): 201-209.

Vanderbilt, J. N., R. F. González, L. Allen, A. Gillespie, D. Leaffer, W. B. Dean, C. Chapin and L. G. Dobbs (2015). “High Efficiency Type II Cell EGFP Expression Facilitates Cellular Identification, Tracking, and Isolation.” Am J Respir Cell Mol Biol.

Vanhecke, D., G. Herrmann, W. Graber, T. Hillmann-Marti, C. Muhlfeld, D. Studer and M. Ochs (2010). “Lamellar body ultrastructure revisited: high-pressure freezing and cryo-electron microscopy of vitreous sections.” Histochem Cell Biol **134**(4): 319-326.

Vegh, I., M. Grau, M. Gracia, J. Grande, P. de la Torre and A. I. Flores (2013). “Decidua mesenchymal stem cells migrated toward mammary tumors in vitro and in vivo affecting tumor growth and tumor development.” Cancer Gene Ther **20**(1): 8-16.

Veldhuizen, E. J. and H. P. Haagsman (2000). “Role of pulmonary surfactant components in surface film formation and dynamics.” Biochim Biophys Acta **1467**(2): 255-270.

Veldhuizen, R., K. Nag, S. Orgeig and F. Possmayer (1998). “The role of lipids in pulmonary surfactant.” Biochim Biophys Acta **1408**(2-3): 90-108.

Veldhuizen, R. A., S. A. Hearn, J. F. Lewis and F. Possmayer (1994). “Surface-area cycling of different surfactant preparations: SP-A and SP-B are essential for large-aggregate integrity.” Biochem J **300 (Pt 2)**: 519-524.

Veldhuizen, R. A., K. Inchley, S. A. Hearn, J. F. Lewis and F. Possmayer (1993). “Degradation of surfactant-associated protein B (SP-B) during in vitro conversion of large to small surfactant aggregates.” Biochem J **295 (Pt 1)**: 141-147.

Voisin, C., C. Aerts, E. Jakubczk and A. B. Tonnel (1977). “La culture cellulaire en phase gazeuse. Un nouveau modele experimental d’etude in vitro des activites des macrophages alveolaires.” Bull Eur Physiopathol Respir **13**(1): 69-82.

Voisin, C., C. Aerts, A. B. Tonnel, J. L. Houdret and P. Ramon (1975). “Survival in gazeous phase and reconstitution “in vitro” of the natural microenvironment of alveolar macrophages.” Pathol Biol (Paris) **23**(6): 453-459.

von Neegaard, K. (1929). “Neue Auffasungen über einen Grundbegriff der Atemmechanik.” Z. Gesamte. Exp. Med. **66**: 373-394.

Voorhout, W. F., T. Veenendaal, H. P. Haagsman, A. J. Verkleij, L. M. van Golde and H. J. Geuze (1991). “Surfactant protein A is localized at the corners of the pulmonary tubular myelin lattice.” J Histochem Cytochem **39**(10): 1331-1336.

Wallach, D. F., S. P. Verma and J. Fookson (1979). “Application of laser Raman and infrared spectroscopy to the analysis of membrane structure.” Biochim Biophys Acta **559**(2-3): 153-208.

Wan, H., H. L. Winton, C. Soeller, G. A. Stewart, P. J. Thompson, D. C. Gruenert, M. B. Cannell, D. R. Garrod and C. Robinson (2000). "Tight junction properties of the immortalized human bronchial epithelial cell lines Calu-3 and 16HBE14o." Eur Respir J **15**(6): 1058-1068.

Wan, H., Y. Xu, M. Ikegami, M. T. Stahlman, K. H. Kaestner, S. L. Ang and J. A. Whitsett (2004). "Foxa2 is required for transition to air breathing at birth." Proc Natl Acad Sci U S A **101**(40): 14449-14454.

Wang, D., D. L. Haviland, A. R. Burns, E. Zsigmond and R. A. Wetsel (2007). "A pure population of lung alveolar epithelial type II cells derived from human embryonic stem cells." Proc Natl Acad Sci U S A **104**(11): 4449-4454.

Wang, G., B. A. Bunnell, R. G. Painter, B. C. Quiniones, S. Tom, N. A. Lanson, Jr., J. L. Spees, D. Bertucci, A. Peister, D. J. Weiss, V. G. Valentine, D. J. Prockop and J. K. Kolls (2005). "Adult stem cells from bone marrow stroma differentiate into airway epithelial cells: potential therapy for cystic fibrosis." Proc Natl Acad Sci U S A **102**(1): 186-191.

Wang, P., N. R. Chintagari, J. Narayanaperumal, S. Ayalew, S. Hartson and L. Liu (2008). "Proteomic analysis of lamellar bodies isolated from rat lungs." BMC Cell Biol **9**: 34.

Wang, Y. Y., X. Z. Li and L. B. Wang (2013). "Therapeutic implications of mesenchymal stem cells in acute lung injury/acute respiratory distress syndrome." Stem Cell Res Ther **4**(3): 45.

Weaver, T. E. (1998). "Synthesis, processing and secretion of surfactant proteins B and C." Biochimica et Biophysica Acta (BBA) - Molecular Basis of Disease **1408**(2–3): 173-179.

Weaver, T. E. and J. J. Conkright (2001). "Function of surfactant proteins B and C." Annu Rev Physiol **63**: 555-578.

Weaver, T. E. and J. A. Whitsett (1991). "Function and regulation of expression of pulmonary surfactant-associated proteins." Biochem J **273(Pt 2)**: 249-264.

Weber, G. and F. J. Farris (1979). "Synthesis and spectral properties of a hydrophobic fluorescent probe: 6-propionyl-2-(dimethylamino)naphthalene." Biochemistry **18**(14): 3075-3078.

Weibel, E. R., G. S. Kistler and G. Tondury (1966). "A stereologic electron microscope study of "tubular myelin figures" in alveolar fluids of rat lungs." Z Zellforsch Mikrosk Anat **69**: 418-427.

Weiss, B., U. F. Schaefer, J. Zapp, A. Lamprecht, A. Stallmach and C. M. Lehr (2006). "Nanoparticles made of fluorescence-labelled Poly(L-lactide-co-glycolide): preparation, stability, and biocompatibility." J Nanosci Nanotechnol **6**(9-10): 3048-3056.

Wert, S. E., M. Yoshida, A. M. LeVine, M. Ikegami, T. Jones, G. F. Ross, J. H. Fisher, T. R. Korfhagen and J. A. Whitsett (2000). "Increased metalloproteinase activity, oxidant production, and emphysema in surfactant protein D gene-inactivated mice." Proc Natl Acad Sci U S A **97**(11): 5972-5977.

Whitcutt, M. J., K. B. Adler and R. Wu (1988). "A biphasic chamber system for maintaining polarity of differentiation of cultured respiratory tract epithelial cells." In Vitro Cell Dev Biol **24**(5): 420-428.

Widmaier, E. P., H. Raff and K. T. Strang (2014). Vander's Human Physiology. 13th edition, Mc Graw Hill.

Wierzbicka-Patynowski, I. and J. E. Schwarzbauer (2003). "The ins and outs of fibronectin matrix assembly." J Cell Sci **116**(Pt 16): 3269-3276.

Williams, G. D., J. Christodoulou, J. Stack, P. Symons, S. E. Wert, M. J. Murrell, Nogee and Lm (1999). "Surfactant protein B deficiency: Clinical, histological and molecular evaluation." Journal of Paediatrics and Child Health **35**(2): 214-220.

Williams, M. C. (1977). "Conversion of lamellar body membranes into tubular myelin in alveoli of fetal rat lungs." J Cell Biol **72**(2): 260-277.

Winkler, M. E., C. Mauritz, S. Groos, A. Kispert, S. Menke, A. Hoffmann, I. Gruh, K. Schwanke, A. Haverich and U. Martin (2008). “Serum-free differentiation of murine embryonic stem cells into alveolar type II epithelial cells.” Cloning Stem Cells **10**(1): 49-64.

Wong, A. P., A. E. Dutly, A. Sacher, H. Lee, D. M. Hwang, M. Liu, S. Keshavjee, J. Hu and T. K. Waddell (2007). “Targeted cell replacement with bone marrow cells for airway epithelial regeneration.” Am J Physiol Lung Cell Mol Physiol **293**(3): 6.

Wong, A. P., A. Keating, W. Y. Lu, P. Duchesneau, X. Wang, A. Sacher, J. Hu and T. K. Waddell (2009). “Identification of a bone marrow-derived epithelial-like population capable of repopulating injured mouse airway epithelium.” J Clin Invest **119**(2): 336-348.

Wong, A. P. and J. Rossant (2013). “Generation of Lung Epithelium from Pluripotent Stem Cells.” Curr Pathobiol Rep **1**(2): 137-145.

Wright, J. R. (1990). “Clearance and recycling of pulmonary surfactant.” Am J Physiol **259**(2 Pt 1): L1-12.

Wright, J. R. (2003). “Pulmonary surfactant: a front line of lung host defense.” J Clin Invest **111**(10): 1453-1455.

Wright, J. R. (2005). “Immunoregulatory functions of surfactant proteins.” Nat Rev Immunol **5**(1): 58-68.

Wright, J. R. and J. A. Clements (1987). “Metabolism and turnover of lung surfactant.” Am Rev Respir Dis **136**(2): 426-444.

Wright, J. R. and L. G. Dobbs (1991). “Regulation of pulmonary surfactant secretion and clearance.” Annu Rev Physiol **53**: 395-414.

Wu, H., A. Kuzmenko, S. Wan, L. Schaffer, A. Weiss, J. H. Fisher, K. S. Kim and F. X. McCormack (2003). “Surfactant proteins A and D inhibit the growth of Gram-negative bacteria by increasing membrane permeability.” The Journal of Clinical Investigation **111**(10): 1589-1602.

Wu, X. S. (2004). “Synthesis, characterization, biodegradation, and drug delivery application of biodegradable lactic/glycolic acid polymers: Part III. Drug delivery application.” Artif Cells Blood Substit Immobil Biotechnol **32**(4): 575-591.

Yamaya, M., W. E. Finkbeiner, S. Y. Chun and J. H. Widdicombe (1992). “Differentiated structure and function of cultures from human tracheal epithelium.” Am J Physiol **262**(6 Pt 1): L713-724.

Yang, M. Y., M. B. Hilton, S. Seaman, D. C. Haines, K. Nagashima, C. M. Burks, L. Tessarollo, P. T. Ivanova, H. A. Brown, T. M. Umstead, J. Floros, Z. C. Chroneos and B. St Croix (2013). “Essential regulation of lung surfactant homeostasis by the orphan G protein-coupled receptor GPR116.” Cell Rep **3**(5): 1457-1464.

Yim, E. K. and K. W. Leong (2005). “Proliferation and differentiation of human embryonic germ cell derivatives in bioactive polymeric fibrous scaffold.” J Biomater Sci Polym Ed **16**(10): 1193-1217.

Zeniou-Meyer, M., N. Zabari, U. Ashery, S. Chasserot-Golaz, A. M. Haeberle, V. Demais, Y. Bailly, I. Gottfried, H. Nakanishi, A. M. Neiman, G. Du, M. A. Frohman, M. F. Bader and N. Vitale (2007). “Phospholipase D1 production of phosphatidic acid at the plasma membrane promotes exocytosis of large dense-core granules at a late stage.” J Biol Chem **282**(30): 21746-21757.

Zhou, L., L. Lim, R. H. Costa and J. A. Whitsett (1996). “Thyroid transcription factor-1, hepatocyte nuclear factor-3beta, surfactant protein B, C, and Clara cell secretory protein in developing mouse lung.” J Histochem Cytochem **44**(10): 1183-1193.

Zuo, Y. Y., R. A. Veldhuizen, A. W. Neumann, N. O. Petersen and F. Possmayer (2008). “Current perspectives in pulmonary surfactant--inhibition, enhancement and evaluation.” Biochim Biophys Acta **1778**(10): 1947-1977.

Web pages

Cbmn.u-bordeaux.fr [Internet]. Pessac, 2014. [Updated 07/05/2015; Cited 12/01/15]. Available at www.cbmn.u-bordeaux.fr

Cells.es [Internet]. Barcelona, 2014. [Updated 07/05/2015; Cited 12/01/15]. Available at http://www.cells.es/

Confluence.aps.anl.gov [Internet]. Sidney, 2015. [Updated 07/05/2015; Cited 23/01/15]. Available at https://confluence.aps.anl.gov

Diamond.ac.uk [Internet]. Oxford, 2014. [Updated 07/05/2015; Cited 21/01/15]. Available at http://www.diamond.ac.uk/

E-shop.vitaris.com [Internet]. Baar, 2014. [Updated 07/05/2015; Cited 09/01/15]. Available at www.e-shop.vitaris.com.

Eandkscientific.com [Internet]. California, 2015. [Updated 07/05/2015; Cited 15/01/15]. Available at www.eandkscientific.com

Particlesciences.com [Internet]. Philadelphia, 2015. [Updated 07/05/2015; Cited 08/01/15]. Available at www.particlesciences.com.

Pharmaceutical-int.com [Internet]. Exeter, 2015. [Updated 07/05/2015; Cited 28/01/15]. Available at www.pharmaceutical-int.com

Wpiinc.com [Internet]. Sarasota, 2014. [Updated 07/05/2015; Cited 25/01/15]. Available at www.wpiinc.com